Discovery of a novel microtubule-associated protein that plays a multifaceted role in primary cilia and midbodies

Dissertation

zur Erlangung des Grades eines

Doktors der Naturwissenschaften

Dr. rer. nat.

Institute of Medical Biochemistry and Molecular Biology
Center for Molecular Signaling
Saarland University School of Medicine

Valerie Chaumet
born 20.04.1994 in Titisee-Neustadt (Baden-Württemberg)
Matriculation Number: 2571469

Tag der Promotion: 11.12.2025
Dekan: Prof. Dr. M. Hannig
Berichterstatter/-in: Prof. D. Mick
Prof. R. Lancaster

Acknowledgments

I dedicate this work to my family and friends and Felix who supported, accompanied, and encouraged me during this time and thus contributed to the completion of this thesis.

I thank everyone who helped me finalize this work.
I thank Burak, because promises are meant to be kept.
I thank my colleagues and everyone who contributed to a positive working environment and made Homburg a better place. ;)

Last but not least, I also thank my colleagues who contributed to this work through experiments, brainstorming, or other forms of support.

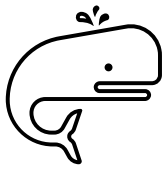

« Diss Johr pagge mas »

(source unknown)

Table of Contents

Summary

The primary cilium is a microtubule-based organelle that serves as a signaling hub in nearly all vertebrate cells. Through changes in the ciliary proteome, it regulates downstream signaling processes important for cell-cell communication, development and tissue homeostasis. Defects in its structure or signaling function can lead to diseases, called ciliopathies. The cilium formation itself is linked to the cell cycle as it is templated by the mother centriole. Additionally, cilium formation requires a controlled coordination of microtubules (MTs), the actin cytoskeleton and vesicle trafficking. Emerging links of microtubule associated proteins (MAPs) contributing to the structural and functional integrity of cilia were drawn. Many ciliary MAPs do not exclusively localize to primary cilia but also other MT-based structures, such as centrioles. Besides the mother centriole as ciliary templating structure, also midbodies were linked to cilium formation. Given the broad disease spectrum of ciliopathies related to ciliary proteins, studying MAPs is crucial, as they influence not only cilia but also other cellular MT networks, centrioles and spindle structures.

In this study I characterized a novel ciliary protein, FCAP33, which was identified through a proteomic screen of primary cilia in murine inner medullary collecting duct cells (IMCD3) cells. Microscopy revealed the localization of FCAP33 to primary cilia, basal bodies, centrioles, midbodies and the mitotic spindle. This suggested a role in MT-based structures beyond primary cilia. Further imaging-based approaches demonstrated its ability to bind to preformed MTs indicating its role as a MAP rather than being a MT inner binding protein. The microtubule association was also confirmed to the ciliary axoneme, where it potentially fulfills a stabilizing role. Additionally, FCAP33 appeared as a static component with limited mobility within the primary cilium in live cell photobleaching experiments. Functional studies revealed that overexpressed full-length FCAP33 promotes ciliary elongation whereas the overexpression of the N-terminal part of FCAP33 had a dominant negative effect, leading to shorter cilia and lower ciliation rates. Immunofluorescence and pull-down assays of full-length and short variants indicate that FCAP33 forms redox-sensitive oligomers *via* its N-terminus, which also plays a role in oligomerization and MT binding whereas the C-terminus might be involved in regulatory functions. This hypothesis can be supported by *in silico* and structural analysis of the protein. Beyond a ciliary localization FCAP33 also localizes to midbodies including the stem body region and the midbody remnant.

This study introduces FCAP33 as a novel ciliary MAP with multifaceted roles in MT-based organelles by potentially regulating ciliogenesis and MT stability.

Zusammenfassung

Das primäre Zilium ist ein auf Mikrotubuli basiertes Zellorganell, das in fast allen Wirbetlierzellen als Signalvermittlungszentrum gilt. Durch Veränderungen des ziliären Proteoms reguliert es nachgeschaltete Signalprozesse, die für Kommunikation, Entwicklung und Gewebehomöostase wichtig sind. Defekte in seiner Struktur oder Signalfunktion können zu Krankheiten führen, die als Ziliopathien bezeichnet werden. Die Zilienbildung selbst ist mit dem Zellzyklus verknüpft, da sie von der Mutterzentriole gesteuert wird. Darüber hinaus erfordert die Zilienbildung eine kontrollierte Koordination von Mikrotubuli (MT), des Aktinzytoskeletts und des Vesikeltransports. Es wurden neue Verbindungen zwischen Mikrotubuli assoziierten Proteinen (MAPs) und Zilien hergestellt, die zur strukturellen und funktionellen Integrität von Zilien beitragen. Viele ziliare MAPs sind nicht ausschließlich in primären Zilien lokalisiert, sondern auch in anderen MT-basierten Strukturen, wie z.B. Zentriolen. Neben der Mutterzentriole als ziliäre Grundstruktur wurden auch Midbodies mit der Zilienbildung in Verbindung gebracht. Angesichts des breiten Krankheitsspektrums von Ziliopathien, die mit ziliären Proteinen zusammenhängen, ist die Untersuchung von MAPs von entscheidender Bedeutung, da sie nicht nur Zilien, sondern auch andere zelluläre MT-Netzwerke, Zentriolen und Spindelstrukturen beeinflussen. In dieser Studie charakterisierte ich ein neuartiges Zilienprotein FCAP33, das durch ein proteomisches Screening von primären Zilien in mIMCD3-Zellen identifiziert wurde. Mikroskopie zeigte die Lokalisierung von FCAP33 in primären Zilien, ziliären Basalkörpern, Zentriolen, Midbodies und der mitotischen Spindel. Dies deutet über die primären Zilien hinaus auf eine Rolle in MT-basierten Strukturen hin. Weitere bildgebende Verfahren zeigten die Fähigkeit von FCAP33, an bereits gebildete MTs zu binden, was auf seine Rolle als MAP und nicht als MT-Innenbindungsprotein hinweist. Die Mikrotubuli-Assoziation wurde auch im Axonem der Zilien bestätigt, wo es möglicherweise eine stabilisierende Rolle spielt. Darüber hinaus ist FCAP33 eine eher statische Komponente, die in Live-Cell-Photobleaching Experimenten nicht mobil im Zilium transportiert wird. Funktionelle Studien ergaben, dass überexprimiertes FCAP33 in voller Länge die ziliare Elongation fördert, während die Überexpression des N-terminalen Teils von FCAP33 einen dominant negativen Effekt hatte, der zu kürzeren Zilien und niedrigeren Ziliationsraten führte. Immunfluoreszenz und Pull-Down Versuche von Volllängen- und Kurzvarianten deuten darauf hin, dass FCAP33 redox-empfindliche Oligomere bildet, durch den N-terminus, der ebenso eine Rolle bei der Oligomerisierung und MT-Bindung spielt, während der C-terminus an regulatorischen Funktionen beteiligt sein könnte. Diese Hypothese

kann durch *in silico* und strukturelle Analysen des Proteins gestützt werden. In dieser Studie wird FCAP33 als ein neuartiges ziliäres MAP vorgestellt, mit vielfältigen Funktionen in MT-basierten Organellen, durch die mögliche Regulation der Ziliogenese und der MT-Stabilität.

List of Figures

List of Tables

Abbreviations

%	percent
°C	degree Celsius
x g	times gravity, relative centrigfugal force
µg	microgram
µm	micrometer
µM	micromolar
mM	millimolar
3T3	3-day transfer, inoculum 3×10^5 cells (3T3 Swiss albino fibroblast cell line)
AF488	Alexa Fluor 488 conjugate
AF555	Alexa Fluor 555 conjugate
AF647	Alexa Fluor 647 conjugate
ANOVA	single factor analysis of variance
APEX	ascorbate peroxidase
APS	Ammonium persulfate
ARL13b	ADP ribosylation factor-like protein 13
att	bacteriophage recombination sites
attL	“left” attachment site
attR	“right” attachment site
BBS	Bardet Biedl syndrome
BBSome	Bardet Biedl syndrome-associated protein complex
BSA	bovine serum albumin

cDNA	complementary DNA
cilia-APEX	engineered ascorbate peroxidase 2 localized to primary cilia
CMV	human cytomegalovirus promoter
ΔCMV	truncated CMV
CatN	catalog number
CO_2	carbon dioxide
dH_2O	distilled water
DMEM	Dulbecco's Modified Eagle's Medium
DMEM	F-12 Dulbecco's Modified Eagle's Medium/Ham's Nutrient Mixture F-12 1:1 mix
DDM	N-Dodecyl-beta-D-maltosidase
dNTPs	deoxynucleoside triphosphates
DMSO	Dimethyl sulfoxide
DNA	deoxyribonucleic acid
DTT	dithiothreitol
E. coli	Escherichia coli
e.g.	exempli gratia
EDTA	ethylenediaminetetraacetic acid
EGTA	triethylene glycol diamine tetraacetic acid
EtOH	ethanol
FBS	fetal bovine serum
f.c.	final concentration
fwd	forward (5'-3' strand)
GFP	green fluorescent protein
h	hour(s)
HCl	hydrogen chloride
HEK	human embryonic kidney cell line 293T
H_2O	water
H_2O_2	hydrogen peroxide
IF	immunofluorescence
IFT	intraflagellar transport
IMCD3	inner medullary collecting duct clone 3
kDa	kilodalton
KO	knock-out

L	Liter
M	molar
MeOH	methanol
MG132	Z-L-Leu-D-Leu-L-Leu-al Peptidaldehyd-Proteasom-Inhibitor
min	minute(s)
ml	milliliters
mol	mole
MOPS	3-(N-morpholino)propanesulfonic acid
MS	mass spectrometry
NaCl	sodium chloride
NaOH	sodium hydroxide
ng	nanogram
NPHP3	nephrocystin 3
PAGE	polyacrylamide gel electrophoresis
PBS	Dulbecco's phosphate buffered saline
PCR	polymerase chain reaction
PFA	paraformaldehyde
pH	potentia hydrogenii
PIC	protease inhibitor cocktail
PMSF	phenylmethylsulfonyl fluoride
Puro	puromycin
rev	reverse (3'-5' strand)
RFU	relative fluorescence units
RNA	ribonucleic acid
RPE	retinal pigment epithelium
RPM	revolutions per minute, centrifuge rotor speed
RT	room temperature
s	second(s)
SAG	Smoothened antagonist
SD	standard deviation
SDS	sodium dodecyl sulfate
SHH	Sonic hedgehog protein
Tab.	table
TBS	tris buffered saline

TBS-T	tris buffered saline with Tween20
TEMED	Tetramethylethylenediamine
TZ	transition zone
U-ExM	ultrastructure expansion microscopy
v/v	volume per volume
WB	Western blot
WT	wild type
w/v	weight per volume

Introduction

The primary cilium

Cilia are antenna-like microtubule-based structures that protrude from the cell surface and are surrounded by a ciliary membrane which is continuous with the cellular plasma membrane (Satir and Christensen, 2007). These organelles can essentially be classified into two different categories: motile and non-motile cilia or primary cilia (Singla and Reiter, 2006). Motile cilia are mainly found on multiciliated cells, e.g. cells of the airway epithelium, where ciliary beating enables mucus clearance. This is possible because of their axonemal structure. The axoneme is the microtubule (MT)-based core, that is composed of 9 microtubule doublets and a central pair of microtubules (Gibbons, 1961; Nicastro et al., 2006). Dynein arms linked to the nine MT doublets allow ciliary beating (Nicastro et al., 2006). Motile cilia can also be found on single cell organisms like *Chlamydomonas reinhardtii* or specified cells like sperm cells, where they are used for locomotion (Kozminski et al., 1993; Mitchell, 2007). Motile cilia potentially evolved from single-cell organisms that developed flagella for movement. Additionally, intraflagellar transport (IFT) proteins are highly conserved and involved in flagellum and sensory receptor assembly in these organisms (Kozminski et al., 1993; Mitchell, 2007). Primary cilia are non-motile cilia that are known for their distinct signaling function (Pazour and Witman, 2003; Singla and Reiter, 2006; Eggenschwiler and Anderson, 2007; Berbari et al., 2009; Mill et al., 2023). The core axoneme structure is built by nine MT doublets, lacking the central pair and the dynein arms, which makes them immotile (Satir and Christensen, 2007). They act as signaling hubs and have diverse functions in different organs and cell types. Primary cilia are important for a broad range of signal transduction: from neuronal cell fate decision during embryonal development (Sonic Hedgehog signaling) to the regulation of planar cell polarity, signal transduction in kidney epithelia and retinal photoreceptor cells (Goetz and Anderson, 2010; Reiter and Leroux, 2017). Primary cilia are found on almost all vertebrate cells and their involvements in various signaling pathways during development and in adult homeostasis makes them versatile but also susceptible to a broad spectrum of diseases, called ciliopathies (Badano et al., 2006; Hildebrandt et al., 2011; Reiter and Leroux, 2017; Mill et al., 2023).

Ciliopathies

Primary cilia are very small and therefore restricted in space, which leads to a content highly enriched in several proteins, like G protein coupled receptors (GPCRs), ion channels and second messengers (Seeley and Nachury, 2010; Wheway et al., 2018; Nachury and Mick, 2019). Therefore, the primary cilium provides perfect environment for these "signal transducers" to be able to fulfill their signaling function (Singla and Reiter, 2006; Goetz and Anderson, 2010). Ligand binding to GPCRs or other internal and external signaling events can lead to signal cascades inducing the transport of proteins into and out of the cilium by IFTs (Pedersen and Rosenbaum, 2008; Berbari et al., 2009). There are many known genetic mutations in ciliary proteins leading to diverse and severe diseases (Badano et al., 2006; Hildebrandt et al., 2011; Reiter and Leroux, 2017; Mill et al., 2023). Main protein complexes of the primary cilium were termed after their disease associations, like: BBSome proteins involved in Bardet-Biedl syndrome (Jin et al., 2010; Nachury et al., 2010), Nephronophthisis first associated with mutations in the so called NPHP proteins and the Meckel syndrome linked to mutations in MKS proteins(Otto et al., 2003; Dawe et al., 2007; Sang et al., 2011). Many more ciliopathies are known to this day with many of them even having different phenotypes. Additionally, mutations in the same gene can manifest different diseases (Reiter and Leroux, 2017; Mill et al., 2023).

The diversity of ciliopathies occurs since mutations can lead to structural defects or even the absence of cilia, but also to defects in signal transduction. This can have an effect at the cellular level but also at the organ level, e.g. impaired signal transduction leads to incorrect cell fate decisions or cell proliferation, i.e. to tumors or cysts (polycystic kidney disease, most common) (Han and Alvarez-Buylla, 2010; Hildebrandt et al., 2011; Mill et al., 2023). In the specialized primary cilia of the retina, structural defects can lead to blindness. In other cell types, defects in primary cilia can disrupt metabolic pathways such as the insulin pathway (Gerdes et al., 2014; May-Simera et al., 2018; Wheway et al., 2018; Chen et al., 2020). For this reason, it is important to know and study the components of the primary cilium in detail and to understand their differences in diverse cell types and organisms to better understand and treat ciliopathies.

Primary cilium formation – a centriole dependent structure

As beforementioned, the core structure of primary cilia is the so-called axoneme which originates from nine microtubule (MT) doublets (Sorokin, 1968; Nicastro et al., 2006; Satir and Christensen, 2007). The MT doublets originate from the basal body which is templated by

a modified mother centriole. Therefore, the primary cilium is a structure tightly linked to the cell cycle (Seeley and Nachury, 2010; Nigg and Stearns, 2011; Izawa et al., 2015; Breslow and Holland, 2019).

All types of primary cilia originate from the basal body (BB). The basal body is the mother centriole, still connected to its daughter centriole and released after mitosis during cell cycle (Breslow and Holland, 2019). The mother centriole is built by nine MT triplets, that are each connected by an AC linker between the C tubule of one triplet and the A tubule of the next triplet (Wang and Stearns, 2017; Breslow and Holland, 2019). The nine distal appendages connected to each triplet at the distal end of the centriole (transition fibers) serve as anchoring base of the BB to the plasma membrane. The distal end of the centriole emerges into the nine MT doublet forming the core structure of the primary cilium, ciliary axoneme (Kobayashi and Dynlacht, 2011; Tanos et al., 2013). Distal from the ciliary base and the so-called transition zone, the MT doublets develop into MT singlets, with the b tubules varying in length (Brown and Zhang, 2020; Mill et al., 2023). The axoneme serves as tracks for protein trafficking along the MTs, which allows the transport of signaling components into and out of the cilium. The axoneme is surrounded by the ciliary membrane, which is formed by a continuous protrusion of the plasma membrane. This creates a unique cell organelle, that is not completely enclosed by a membrane but open towards the cell body, which allows diffusion of small molecules and particles (Pedersen and Rosenbaum, 2008; Seeley and Nachury, 2010; Garcia-Gonzalo and Reiter, 2017). To generate a barrier and separate the ciliary compartment from the cell body, the transition zone (TZ) is formed. Electron dense protein fibers, called Y-links connect the axoneme to the ciliary membrane distal from the basal body, forming a gating structure, which makes the ciliary compartment distinct from the cell plasma (Reiter et al., 2012; Garcia-Gonzalo and Reiter, 2017). Proteins and large cargoes are actively transported through the transition zone by intraflagellar proteins (IFTs) that form oligomers and traffic along the MT of the axoneme, serving as “trains”. The IFT trains, composed of several copies of the IFT-A and the IFT-B complexes can move towards the tip (anterograde) with the motor protein kinesin 2. At the primary cilium tip the trains are rearranged and transported out of the cilium (retrograde) by the help of dynein 2, another motor protein. In addition to the IFT transport system the BBSome complex mediates the exit of membrane proteins from primary cilia (Rosenbaum and Witman, 2002; Vale, 2003; Jin et al., 2010; Nachury et al., 2010). The subdistal appendages help anchoring the BB in the cell and serve as microtubule organizing center (MTOC) which facilitates transport of vesicles and proteins to the primary cilium. The daughter centriole stays connected to the BB throughout ciliation, which controls proper

positioning and together forms the centrosome (Kobayashi and Dynlacht, 2011; Nigg and Stearns, 2011; Pedersen et al., 2012). The primary cilia formation process or ciliation follows two different pathways dependent on different cell types (Sorokin, 1968; Goetz and Anderson, 2010). The intracellular and the extracellular pathway. In the intracellular pathway, the primary cilium formation is initiated in the cell. Ciliary vesicles dock to the distal appendages of the mother centriole, releasing a distal cap, that prevents MTs from growing (Kobayashi and Dynlacht, 2011; Garcia-Gonzalo and Reiter, 2012). The removal of the cap complex gives rise to the axonemal elongation of the MT doublets still enclosed by the ciliary vesicle. This vesicle can then dock and fuse with the plasma membrane, allowing for TZ formation and further axoneme elongation ultimately leading to cilium formation (Goetz and Anderson, 2010; Garcia-Gonzalo and Reiter, 2012). The fusion of the ciliary vesicle with the membrane leads to an invagination of the ciliary membrane, called ciliary pocket (Pedersen et al., 2012). This route is used by fibroblasts and retinal epithelial cells (Sorokin, 1968; Goetz and Anderson, 2010).

In the extracellular pathway the mother centriole directly docks to the plasma membrane via its distal appendages (Nigg and Stearns, 2011; Garcia-Gonzalo and Reiter, 2012). The protein complex capping structure that prevents MT growing at the distal end of the centriole is removed, allowing axonemal growth and cilium formation. For example, kidney epithelium cells use this cilium formation process (Sorokin, 1968; Goetz and Anderson, 2010; Garcia-Gonzalo and Reiter, 2012) (Figure 1).

Centriole biogenesis and cilium formation during the cell cycle

The biogenesis of primary cilia and centrioles is regulated during the cell cycle. The cell cycle has four major phases: The G_1 phase, where the cell prepares for division, the S phase, the DNA synthesis phase where the replication of DNA begins, the G_2 stage, where the DNA condenses and is prepared for division, and the M phase where the actual mitosis, cell division, takes place. In G1 a cell contains two mature centrioles. The mature parent centriole, also termed mother centriole which has distal and subdistal appendages (Fırat-Karalar and Stearns, 2014). The mother centriole is linked to the daughter centriole (the second mature centriole) by a linker region. The daughter centriole lacks distal appendages and is connected to its mother via a flexible linker (Fırat-Karalar and Stearns, 2014; Breslow and Holland, 2019). In the S phase, when the genetic material is condensed and prepared for duplication, centrioles start their duplication process to build two independent centrosomes for chromatid separation (Schöckel et al., 2011; Nigg and Holland, 2018). Each of the parent centrioles assembles a new

procentriole orthogonally at the proximal end. The formation of the procentrioles is templated by the recruiting of specific proteins like SAS6m PLK4 and STIL that initiate the assembly of the cartwheel, which forms the ring like structural base for procentriole formation (Nigg and Holland, 2018; Breslow and Holland, 2019). After cartwheel assembly (a process called engagement), the newly formed procentrioles start to elongate and cells move on into G2 phase. To prepare for mitotic spindle formation, the newly formed centriole pair matures and starts to build pericentriolar material (PCM). At the end of mitosis, the cartwheel is removed from the procentriole and the centriole pair, which leads to disengagement and the parent centriole (mother) is released for duplication in a new cell cycle (Schöckel et al., 2011; Fırat-Karalar and Stearns, 2014; Breslow and Holland, 2019). The procentriole is converted into a mature daughter centriole. This process is called centriole-to-centrosome conversion. During this conversion the procentriole can recruit pericentriolar material, needed for duplication (Fırat-Karalar and Stearns, 2014; Joukov and De Nicolo, 2019). The appendages of the mother centriole get modified and disassembled during mitosis and reform during G1 phase on the mature parent centriole. In non-dividing cells, this mother centriole can migrate to the cell membrane and initiate primary cilium formation by templating the basal body. As the centriole is needed for a new mitotic process, the primary cilium has to be disassembled before mitotic entry of the cell (Fırat-Karalar and Stearns, 2014; Breslow and Holland, 2019; Joukov and De Nicolo, 2019) **(**Figure 1 B).

To study primary cilia in the lab. We can make use of the cell cycle dependent ciliation. Ciliation can be initiated by forcing cells to stay in a non-dividing state, which can be achieved by serum-starving cells, meaning culturing them in medium deprived from growth factors.

Spindle and midbody formation during mitosis

Centriole biogenesis is important for cell division especially in the centrioles-to-centrosome conversion in S-phase (see also above). The centriole pair (consisting of mother centriole MC and daughter centriole DC) disengages and each, MC and DC, develop a new procentriole to duplicate and to finally form two new centrosomes (Fırat-Karalar and Stearns, 2014; Fu et al., 2015). Before mitosis (actual division phase) starts, centrosomes form microtubule (MT) asters, which are pushed away by motor proteins. When the nuclear envelope collapses, centrosome MTs attach to kinetochores of chromosome and spindle formation is thus initiated. Centrosomes are now the hub for mitosis (Haren et al., 2006; Debec et al., 2010). However, there are organisms/cells that can form a spindle independent of centrosomes but they need a

microtubule organizing center (MTOC) available to initiate spindle formation (Khodjakov et al., 2000; Debec et al., 2010; Meunier and Vernos, 2016).

Mitosis is the term for the actual separation of the duplicated genetic material in the cell. Mitosis itself can be more precisely separated further in distinct steps: Prophase/Prometaphase, Metaphase, Anaphase and Telophase.

In Prophase/Prometaphase the mitotic nuclear envelope collapses, such that spindle fibers can connect to the chromosomes for division of their chromatids (Beaudouin et al., 2002). At the same time the mitotic spindle forms, a microtubule (MT)-based structure that will bind to centromeres of the chromosomes and initiate separation of genetic material into two new cells (Prosser and Pelletier, 2017). In metaphase, the mitotic spindle consists of kinetochore fibers, astral fibers and interpolar microtubules. Chromosomes align along the metaphase plate and spindles attach to the centromeres (Desai and Mitchison, 1997; Cheeseman and Desai, 2008). In anaphase, the central spindle is formed. The central spindle is built by antiparallel MTs which overlap at the center between the two dividing cells. Its formation requires kinesin motor proteins, microtubule associated proteins (MAPs) and protein kinases (Glotzer, 2001; White and Glotzer, 2012). The central components are: Centralspindlin (a complex that contains kinesin and Rho GTPase-activating protein subunits), the microtubule-bundling protein regulator of cytokinesis 1 (PRC1) and the chromosome passenger complex (CPC) (Fededa and Gerlich, 2012; White and Glotzer, 2012).

PRC1 binds antiparallel MTs which is only active in its dimerized state during anaphase. Centralspindlin, another protein complex that involves the kinesin motor protein MKLP1/KIF23 and Rho-family GTPase activating protein (GAP) CYK-4/MgcRacGAP also binds to the central spindle as clusters, being able to travel along MTs towards the plus ends and accumulate at the central region (Fededa and Gerlich, 2012). Centralspindlin targeting is mediated by MKLP1, which is inhibited by CDK1 (Cyclin-dependent kinase 1) phosphorylation of its motor domain (similar to PRC1 inhibition by CDK1 mediated phosphorylation) but activated by Aurora B mediated phosphorylation in anaphase (Guse et al., 2005). Aurora B mediated activation of MKLP1 leads to clustering of Centralspindlin by triggering its release from the inhibitory protein 14-3-3 (Glotzer, 2001; Fededa and Gerlich, 2012). The chromosomal passenger complex (CPC) is the third essential complex for central spindle formation. It first localizes to centromeres for attachment of chromosomes to the spindle, then it relocates to the spindle and phosphoregulates PRC1 and MKLP1 and might mediate MT bundling; and it directly contributes to the formation of the actomyosin ring (Vázquez-Novelle and Petronczki, 2010). The actomyosin or contractile ring is necessary for

the cytokinetic furrow ingression which leads to the separation of the emerging sister cells at the end of mitosis. Actin and myosin act together in a dynamic manner to contribute to contractile forces (Glotzer, 2001; Albertson et al., 2008; Fededa and Gerlich, 2012; Wu et al., 2018). The final stage of mitosis is the abscission of the newly generated sister cells that are still connected by the intercellular bridge. The intercellular bridge contains dens antiparallel MTs that overlap in the middle region, termed midbody. The intercellular bridge/midbody consists of more than 100 proteins, for some of which the functions of some still need to be elucidated. Abscission is promoted by the removal of cytoskeletal structure from the intercellular bridge, constriction of cell cortex and membrane fission (Gromley et al., 2005; Morita et al., 2007; Fededa and Gerlich, 2012; Andrade and Echard, 2022). After furrowing Golgi- and endosome-derived vesicles accumulate at regions close to the midbody. Vesicles in the bridge fuse with the plasma membrane and vesicle-targeting and tethering components induce abscission (Gromley et al., 2005; Morita et al., 2007). Additionally, cytoskeletal structures have to be removed which involves the 14-3-3 complex and other factors for the removal of actin (Fededa and Gerlich, 2012; Andrade and Echard, 2022). Components of the so called ESCRT complex together with spastin lead to the separation of bundled MTs. The leftover midbody structure can have different functions as it can be released to the extracellular medium, can be degraded or it can persist in the cytoplasm (Morita et al., 2007; Andrade and Echard, 2022).

Central spindle MTs are highly stabilized through microtubule-associated proteins and central spindle MTs regulate the furrow formation and completion of cytokinesis. They form the intercellular bridge and its leftovers after abscission are called midbodies (Gromley et al., 2005; Morita et al., 2007; Fededa and Gerlich, 2012; Andrade and Echard, 2022).

Microtubules – MAPs and PTMs in cilia and cell division

Primary cilia, centrioles, the mitotic spindle, the central spindle and the midbodies are all dynamically linked to the cell cycle. But even more important, they do all share their main core structure because all these structures are formed by microtubules (MTs). In the different structures, MTs play important roles in the formation of tracks for intracellular transport, chromosome separation or cell polarity formation of the basal body.

The core structure of a MT is built by tubulin heterodimers consisting of a α- and ß-tubulin, which was first identified by Weisenberg et al 1968 (Weisenberg et al., 1968). Weisenberg also discovered, that ß-tubulin hydrolyzes GTP during MT polymerization which leads to a dynamic

instability that allows a switch between polymerization (growth) and depolymerization (shrinkage or catastrophe) (Weisenberg et al., 1968; Inoué and Salmon, 1995). Alpha-tubulin is GTP bound, which is non-exchangable, but ß-tubulin has an exchangeable GTP site, where GTP can be hydrolyzed and nucleotide exchange can happen. GTP-bound tubulin can be added to growing MT ends (plus-ends) and form a protective cap. The plus end is the faster growing side having the exposed "N-domain" with the exchangeable GTP site compared to the minus-end with α-tubulin exposed without the domain (Desai and Mitchison, 1997; Cleary and Hancock, 2021).

MTs are usually modified by post translational modifications (PTMs). Additionally, microtubule associated proteins (MAPs) play crucial roles in regulating MT dynamics, stability, interaction with other cellular structures (e.g. actin) and for transport of cargoes along MT tracks (Janke, 2014; Bodakuntla et al., 2019, 2020). MAPs can mediate protein trafficking (cilium), recruitment of proteins or tubulin-modifying enzymes for post-translation modification. Dynein and Kinesin facilitate the transport of cargoes along MTs. Dynein moves towards the minus end, whereas Kinesin moves towards the plus end. This allows directional transport, along MTs such as the primary cilium axoneme (Vale, 2003; Stepanek and Pigino, 2016; Nakayama and Katoh, 2018; Ma et al., 2023). MT growth and catastrophe (important for axonemal maintenance and cell division) is mediated by polymerization and depolymerization at MT plus ends (+TIP). EB proteins, another group of MAPs, are +TIP proteins and regulate MT growth and dynamics (Akhmanova and Steinmetz, 2015). Known ciliary MAPs are: CEP104, CSPP1, TOGARAM-1, ARMC9 and CCDC66. It is of note, that their localization is not restricted to primary cilia, but they also localize to other MT-based structures. They have been linked to ciliopathy phenotypes proposing these MAPs as an additional ciliary ciliopathy module (Reiter and Leroux, 2017; Wheway et al., 2018; Conkar and Firat-Karalar, 2021). Loss-of-function studies showed ciliogenesis and cilia length defects (Conkar and Firat-Karalar, 2021). ARMC9 and TOGARAM-1 deficient patients showed deficiencies in the microtubule PTMs: acetylation and glutamylation (Gadadhar et al., 2017; Conkar and Firat-Karalar, 2021). CEP104 and TOGARAM-1 carry a TOG domain, which can bind to tubulin dimers as described for the well characterized MAP, XMAP215 (Conkar and Firat-Karalar, 2021). XMAP215 promotes polymerization and dynamics in mitotic spindles (Kerssemakers et al., 2006; Brouhard et al., 2008). Additionally, CEP104 localizes to the tips of microtubules, where it regulates MT/ciliary length (Frikstad et al., 2019; Ryniawec et al., 2023). CCDC66, ARMC9 and CSPP1 do not have domains that are homologous to any known MT binding domains. The

specific function of these ciliary MAPs is still under investigation, but the proposed mechanisms are regulation of plus end dynamics of axoneme, regulation of signaling response

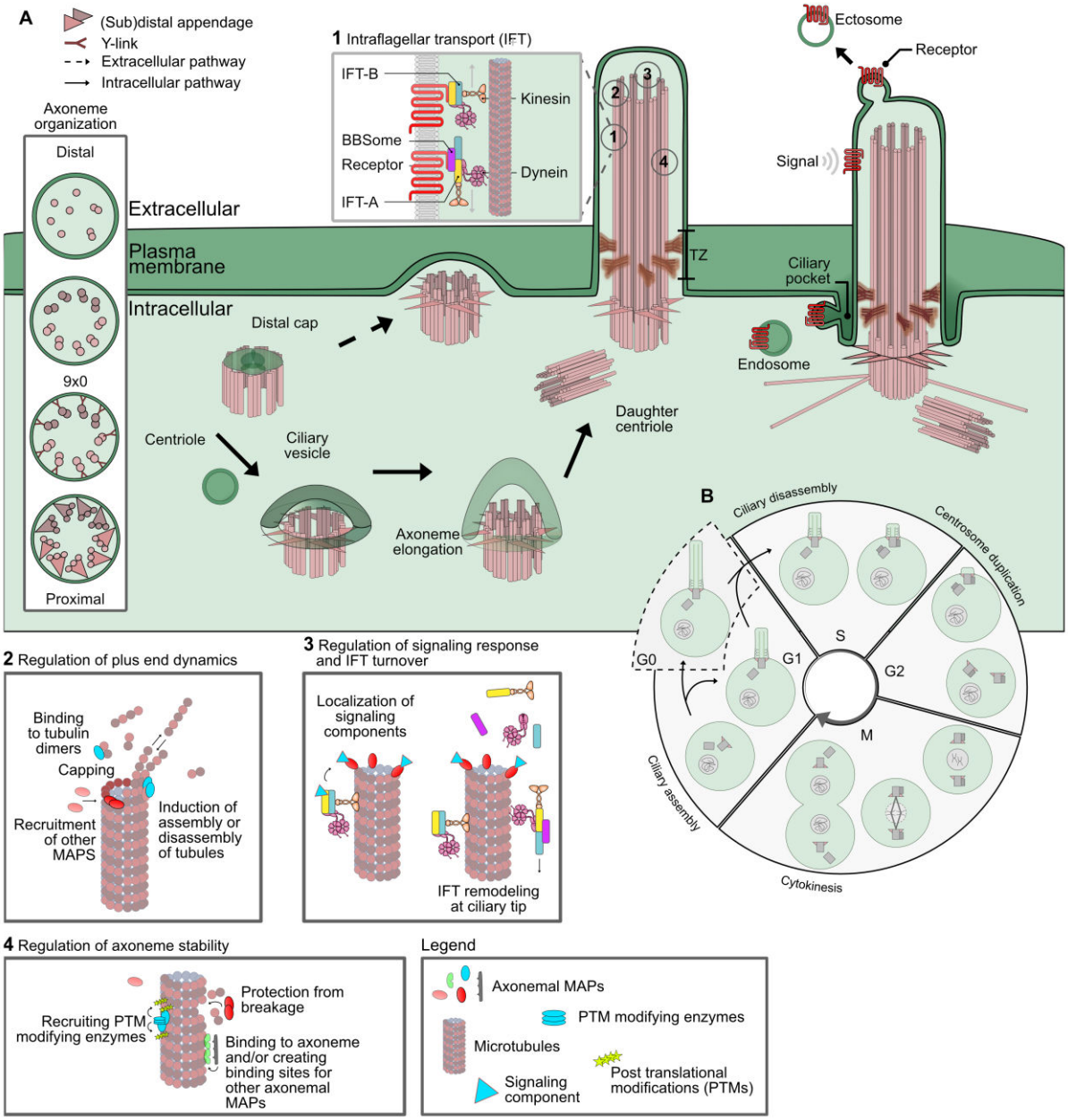

Figure 1: Intra- and Extracellular Pathway of cilium assembly, the link of the primary cilium to the cell cycle and the role of ciliary microtubule-associated proteins

(A) Cilium assembly through the extracellular and intracellular route and the role of microtubule-associated proteins (MAPs) (1-4) in primary cilia. Cilium assembly depends on the cell type. In the intracellular pathway, ciliary vesicles dock to the mother centriole (MC), forming a ciliary sheath and initiating axoneme growth. Distal appendages of the MC dock to the membrane and Y-links (transition fibers) connect to the ciliary membrane forming the transition zone (TZ). The fusion of the sheath in the intracellular pathway leads to the formation of cilia pockets. In the extracellular pathway the MC directly docks to the membrane via the distal appendages, which initiates ciliation. MTs form the axoneme, the scaffold structure for transport of ciliary proteins, mediated by intraflagellar transport-proteins (IFTs). (1) Regulation of ciliary transport. IFT and Bardet-Biedl Syndrome (BBSome) complexes for transport of proteins into cilium and out of the cilium. Proteins transported involve signaling components and structural components (tubulin dimers). Transport is mediated by the motor proteins dynein (retrograde) and kinesin (anterograde) and might be optimized/influenced by MAPs and MAPs can act as signaling components.

(2) Regulation of plus end dynamics. Axonemal MAPs influence MT length by: MT capping which prevents MT elongation, specific MAPs specifically influence A and B tubule lengths; regulating assembly and disassembly of MTs, by binding to MT plus end and initiation of (de-)polymerization processes e.g. required fro ciliary disassembly; serving as scaffold for the recruitment of further MAPs. (3) Regulation of ciliary signaling and IFT transport. At the ciliary tip IFTs are remodeled and Hedgehog pathway is activated. MAPs potentially are involved in IFT turnover and creating binding sites for signal molecules. (4) Regulation of axoneme stability by MT modification through PTMs like: acetylation, polyglutamylation, polyglycylation and (de-)tyrosination mediated by tubulin-modifying enzymes. MAPs can inhibit MT breakage or recruit factors that stabilize MTs. (Conkar and Firat-Karalar, 2021) (B) Simplified scheme of cell cycle and its link to primary cilia formation. In G1 a cell contains two mature centrioles. The mature parent centriole, mother centriole (MC) with (sub)distal appendages. The MC is linked to the daughter centriole (DC) via a flexible linker. In the S phase, DNA is prepared for duplication, centrioles start their duplication process to build two independent centrosomes for chromatid separation. Each of the parent centrioles assembles a new procentriole which initiates cartwheel assembly (needed for procentriole formation). Procentrioles start to elongate, and cells move to G2 phase to prepare for mitotic spindle formation. Centriole pairs mature. In the end of mitosis cartwheel is removed from procentriole and centriole pair, MC is released for a new cell cycle. The mitosis phase (M) itself is further separated in several phases and is the process auf actual duplication and separation of the genetic material (see "Centrioles give rise to mitotic spindle and midbody formation during mitosis"). Adapted from Sroka (Sroka, n.d.) and Conkar and Firat-Karalar (Conkar and Firat-Karalar, 2021).

and IFT turnover at ciliary tip, regulation of axoneme stability and the regulation of transport complexes (Conkar and Firat-Karalar, 2021). (Figure 1 A1-4)

FCAP33 – a previously unknown ciliary protein

FCAP33 short for Found in Cilia APEX Proteome 33 kDa is a protein that was found in the primary cilia proteome of murine inner medullary collecting duct (IMCD3) cells using the APEX2-based system. In brief, the ascorbate peroxidase (APEX) allows the biotinylation of proteins in its proximity by adding biotin tyramide and hydrogen peroxide (Mick et al., 2015; May et al., 2021). After labeling, cells are lysed and the biotinylated proteins can be isolated by subsequent streptavidin chromatography and analyzed by mass spectrometry (MS). Using IMCD3-APEX2 cells, FCAP33 was found to be highly enriched in IMCD3 cells (unpublished Data). The APEX2 system was further developed and optimized by Sroka et al (Sroka et al., 2025). The improved setup is similarly based on the APEX driven reaction but uses locally produced hydrogen peroxide which makes it less toxic. Several improvements of the iAPEX system (for details see Sroka et al. 2025 (Sroka et al., 2025)) also lead to more robust and specific labeling. The improved setup revealed several new ciliary candidates, confirming the unknown protein C7orf57 (Gm11992), which we termed FCAP33 (**F**ound in **C**ilia **A**PEX **P**roteome with a size of **33** kDa) (Sroka et al., 2025).

FCAP33 is part of the cilia APEX proteome, but with low abundance. The peptide count of FCAP33 in the iAPEX MS dataset was 8. Compared to some known proteins of the IFT machinery, FCAP33 was less abundant (IFT80,40 peptides IFT81,41 peptides and IFT172 81 peptides) but some proteins of the IFT machinery were even less enriched (IFT20, 20 peptides; IFT43, 3 peptides), when compared to the control. MAP4 a microtubule associated protein found in primary cilia had 49 unique peptides, but MAP6 only 5 and the microtubule-actin crosslinking factor 1 MACF1 had 118 unique peptide counts.

In comparison to other known proteins of the primary cilia proteome of IMCD3 cells, FCAP33 seems less abundant from the MS data but its enrichment is highly specific as it was not detected in the control (Sroka et al., 2025, and unpublished data). To date, FCAP33 is a novel, not yet described ciliary protein.

Aim of the study

The aim of this study was to characterize the newly identified protein FCAP33, which was not previously detected in primary cilia of any cell type. FCAP33 was discovered through a proteomic screen of primary cilia from murine IMCD3 cells.

The primary cilium is an MT-based organelle that plays a critical role in vertebrate cells by serving as a signaling hub (Goetz and Anderson, 2010; Garcia-Gonzalo and Reiter, 2012). Through changes in the ciliary proteome, it regulates key signaling pathways important for development, tissue homeostasis and intercellular communication (Garcia-Gonzalo and Reiter, 2012). Disruptions in ciliary structure or functions are linked to ciliopathies (Breslow and Holland, 2019; Joukov and De Nicolo, 2019). The cilium formation is tightly linked to the cell cycle, being templated by the mother centriole (Sorokin, 1968; Fırat-Karalar and Stearns, 2014). This process of cilium formation relies on a coordinated interaction between microtubules, the actin cytoskeleton and vesicle trafficking which involves the action of microtubule-associated proteins (MAPs) making them of special interest for research in the context of primary cilia (Akhmanova and Steinmetz, 2015; Stepanek and Pigino, 2016; Conkar and Firat-Karalar, 2021). Recent studies have identified many MAPs, that are not exclusively localized to the cilium but also associate with other MT-based structures such as centrioles, midbodies and the mitotic spindle (Frikstad et al., 2019; Conkar and Firat-Karalar, 2021; Ryniawec et al., 2023).

This raises several key questions to investigate the role of FCAP33 in this study:

Is FCAP33 a *bona fide* ciliary protein? What is the molecular function of FCAP33? Does FCAP33 play a unique role in primary cilia, or does it have more general functions in other MT-based organelles?

By addressing these questions, this study will gain insights into the potential function of the previously unknown protein FCAP33.

Methods

Ultrastructure Expansion microscopy

Ultrastructure Expansion microscopy (U-ExM) is a method, based on crosslinking structures within an agarose gel, followed by enlarging the structure within the gel. This increases artificially the resolution of the structure by keeping the original dimensions. In this work, standard expansion yielding to an enlargement of the sample of 4 x was used.

Cells were seeded as for standard immunofluorescence (IF) (see methods, immunofluorescence) (50'000 cells/24-well for IMCD3 cell lines).

On Day 0 all solutions were prepared: 38% sodium acrylate (stored at -20 °C), the Monomer solution (stored at -20 °C), the Denaturation buffer (kept at RT). The Monomer solution was frozen in working aliquots of 90 µl (for 2 coverslips). Cells were starved for ciliation on Day 0. On Day 1, cells are crosslinked, gelified, denatured, expanded (1st round), shrank, and incubated in primary antibody overnight. For crosslinking prevention, the crosslinking solution was prepared freshly: 1,4 % formaldehyde and 2% acrylamide in 1x PBS. Pre-fixation with 4 % PFA as for standard IF is not needed, as the crosslinking includes fixation by formaldehyde. For specified antibodies, cells were fixed for 5-10 min in ice-cold methanol at -20 °C prior to the crosslinking step. Coverslips with cells were placed in a fresh 24-well plate with 1 mL of crosslinking solution per coverslip. Empty wells are filled up with water to prevent evaporation, and the plate was sealed with parafilm. Crosslinking was performed for 5h at 37°C while gently shaking (50-60 rpm, bacterial shaker). During crosslinked, a humid chamber was prepared and cooled down at -20 °C. Wet papers, were placed on the bottom of a 15-cm cell culture dish and covered by parafilm. For the Gelation, the humid chamber, as well as stocks of TEMED, APS and the monomer solution were placed on ice. 2 coverslips were put on a kimwipe paper, 5 µl of 10 % TEMED and APS were added to 90 µl Monomer solution and vortexed. 2 drops of 35 µl final Monomer solution were added on the parafilm in the humid chamber, and coverslips were rapidly dropped on the drop of Monomer solution, with the cells

facing the solution. The gels with the coverslip were incubated in the humid chamber at 37 °C for 1 hour. The gelation was followed by the denaturation step. For this, coverslips with the gels attached were transferred into 6 -well plated with the coverslips (CS) at the bottom and the gel on top and filled with 1 ml of denaturation buffer. After 15 min of shaking at RT gels detached from the CS and were transferred into a 1,5 ml tube filled with 1,5 mL fresh denaturation buffer. Gels were incubated for 1,5 hours at 95 °C. After denaturation, gels were transferred into 250 ml beakers with ddH2O and gently shook for 30 min. The first round of expansion was done for 30 min with 2-3 changes of water on an orbital shaker) After the expansion the sizes of the gel were measured and divided by the size of the CS. This gives an expansion factor of 4 x for all experiments. For antibody staining, gels must be shrunk again, which is reached by washing the gels in 1 x PBS for 30 min (110-120 rpm). For antibody staining, PBS-BSA 2% was prepared freshly from a filtered 10 % BSA stock solution. A gel piece was cut and transferred into a 24-well plate for antibody staining. 200 µl of antibody diluted in PBS-BSA 2% was added to each well and incubated overnight in the coldroom on an orbital shaker. For expansion, double the concentrations of the standard IF procedure was used.

Next day, on Day 2, gels were washed in the 24-well plate with PBS + 0,1 % Tween, 3 x for 10 min at RT. Secondary antibody staining was done in 200 µl of PBS-BSA 2% with secondary antibodies ad 27 ° C for 2 h and 30 min with agitation and covered from light. Gels were washed again with PBS + 0,1 % Tween, 3 x for 10 min at RT and protected from light. For the second round of expansion, stained gel pieces were transferred to a 6-well plate and washed at least twice in ddH2O for 30 min. The second wash can be done overnight. Gels can be kept in water until imaging. For imaging, pre-coated poly-D-Lysine CS were used. 24 mm imaging CS were incubated in 100 µg/mL poly-D-Lysine solution for 45 min at 37°C. Coated 24 mm CS were washed trice in ddH2O and dried. Coated imaging CS can be stored in the fridge for several days.

To confirm the correct side of the gel, a gel piece was cut and imaged on an uncoated 24 mm CS. When the correct side was confirmed, gels were imaged with the coated 24 mm CS to prevent the geld from sliding while performing z-stack imaging. Imaging was done with the Confocal microscope LSM900 and the super resolution (SR) Airy Scan method. Optimized protocol from (Gambarotto et al., 2021).

Immunofluorescence

Immunofluorescence (IF) microscopy is a common method to localize proteins, RNAs, DNAs or organelles within cells or tissues. To investigate primary cilia, cells were seeded on 12 mm 1.5 mm thick coverslips (CS), placed in a 24-well plate. Cells were counted and 50'000 cells were seeded if IMCD3 cells were used. After 24 hours of growth cells were starved to induce ciliation. For standard IF, cells were covered and fixed with 4 % PFA for 10-15 min at RT. After fixation, cells can be stored at 4 °C when washed thoroughly and kept in 1 x PBS. Depending on antibody staining, PFA fixation followed washing of the CS with PBS. When PFA was removed, cells were additionally fixed/permeabilized by putting the coverslips for 5 min pre-cooled MeOH at -20 °C. After fixation/permeabilization, CS were transferred into to "staining chamber", a parafilm coated cell culture dish, encoated with aluminum foil, to protect CS from light. In the chamber, CS were placed with cells, facing upwards for following procedures. CS were always blocked at RT with 100 µl blocking buffer (BB) containing 0,1 % triton. Primary antibody mixes were prepared in BB. Blocking buffer was aspirated and CS were washed once with 1 x PBS before adding the primary antibody mix. 40 µl was added per CS when incubated 1 h at RT and 50 µl antibody mix was added per CS when incubated ON. For ON incubation, wet papers were added to the staining chamber to prevent CS from drying out. Incubation with primary antibodies was followed by 3 washes with 1x PBS 5-10 min at RT. Secondary antibody dilutions were prepared in BB and 40 µl were added to each CS for 30 min at RT. If nuclei staining with Hoechst was done, secondary antibody staining was followed by incubating CS 10 min with Hoechst. If staining procedures were finalized, CS were again washed 3 times with 1 x PBS and mounted with Fluoromount G by putting the CS on a glass side, with the cells facing the glass slide.

Standard IF imaging was performed with the Inverted Microscope Leica DMi8 from Leica Microsystems using the Las X Life Science Microscope Software. Stacks were taken by setting the focus plane and stacks of 0,5 µm with 10 slices. The range was calculated by the software with the focus plane at the center of the stack.

Microscopy Image analysis

Image analysis was done using the open-source software Fiji (Image J). Cilia intensities were measured by using the Cilia Q Plugin in Fiji, developed and published by Hansen et al., 2021. Cilium masks were done using the ARL13b signal if not stated differently and an appropriate threshold method was chosen. If the channel was adapted for masking cilia, this will be mentioned in the results section.

Ciliation rates were quantified by using a macro (Tommy Sroka) that automatically counts nuclei and cilia. This is done by masking nuclei via nucleus stain and the same for cilia, like the cilium mask in Cilia Q.

Demembranation

To investigate if proteins localize to the cell membrane and/or ciliary membrane, permeabilization of the cell membrane was induced and followed by investigation with immunofluorescence. Proteins that would localize to the cell or ciliary membrane should only be visible in the buffer control, but not in permeabilized cells. For cilia membrane proteins, cells were seeded and ciliation was induced as described. Cells were either treated with PHEM (cytoskeleton) buffer only for 30s or 60s as positive control. The reaction was stopped by PFA fixation with 4 % PFA at RT. Demembranation was induced by adding 30 s or 60 s 0,5 % triton in 1x PHEM buffer prior to fixation. Staining with the ciliary membrane marker ARL13b confirmed the absence (+ 0,5 % triton) or presence (control) of the ciliary membrane. Staining of the axoneme with AcTUB confirmed the intact core structure or the primary cilium after treatment with 0,5 % triton.

Transient transfection

For transfection, 250’000 cells were seeded per 6-well one day prior to transfection. The day after seeding, cells were transfected using the JetPrime reagents and 2 µg of DNA. DNA was mixed well, and 2 µg were added to 200 µl of JetPrime buffer and the mix was vortexed for 10 s. 4 µl of JetPrime reagent were added to the buffer with the DNA. The mix was vortexed for 1 s and incubated for 10 min at RT and dropwise added to the cells, afterwards. After 4 hours of incubation under cell culture conditions, the medium was replaced for fresh culture medium. Next day, cells could be used for further experiments.

Creation of stable cell lines using the FlipIn system

In this work, all stable cell lines created were done, using IMCD3 cells containing the FlipIn locus for easy and controlled transfection and gene expression. The parental IMCD3 FlipIn cell line (IMCD3 WT) contains FRT sites, which are the target site for the FLP recombinase. FLP-mediated recombination allows the recombination of a gene of interest (GOI) from a plasmid (GOI between FRT sites) into the FRT sites of the IMCD3 cells genome.

For this, the FLP-recombinase encoding plasmid (pOG44) is transfected into the cells together with the plasmid, encoding the GOI between the FRT sites and an antibiotic resistance for antibiotic selection pressure (Szczesny et al., 2018).

For transfection, 250'000 cells were seeded per 6-well one day prior to transfection. The day after seeding, cells were transfected using the JetPrime reagents and 2,4 µg of total DNA. Plasmid-DNA was mixed well, and 0,8 µg were added to 200 µl of JetPrime buffer. 0,6 µg pOG44 was added to the buffer and Plasmid-DNA and the mix was vortexed for 10 s. 4,8 µl of JetPrime reagent were added to the Buffer with the DNA. The mix was vortexed for 1 s incubated for 10 min at RT and dropwise added to the cells, afterwards. After 4 hours of incubation under standard cell culture conditions, the medium was replaced for fresh culture medium. Next day, cells could be used for further experiments. Cell culture medium with antibiotics was prepared. The antibiotics were selected respective to the antibiotic resistance encoded in the plasmid that was transfected. Only cells expressing plasmid are resistant to the antibiotic and should survive.

To reach survival of single cell (cell clones), one 6-well was resuspended in 6 ml culture medium with antibiotics. 4 ml of resuspended cells were added to a 15-cm dish containing antibiotic medium and 1 ml of resuspended cells were added to a 15-cm dish containing medium with antibiotics. The remaining 1 ml of cells was added back into the 6-well and filled up with 1 ml of cell culture medium with antibiotics (cell pool).

After 2 weeks of selective antibiotic pressure culture, single cell clones were picked using cloning rings. This allows to separately trypsinize single cell clones. After transferring to six wells, antibiotic pressure was stopped, switching to standard cell culture medium. Confluent cells were frozen and further analyzed by IF (or western blot).

Genomic DNA extraction

Genomic DNA (gDNA) was extracted from cells, to characterize potential knockout or Crispr cell lines. For this, cells were seeded in 6-well plates. Confluent cells were pelleted: cells were trypsinized and resuspended in cell culture medium. The cell suspension was centrifuged at 200 x g for 5-10 min (Centrifuge 5804 R, Eppendorf). Medium was aspirated and pellet was resuspended in 1 x PBS. Cells were centrifuged as before; PBS was aspirated and cells were resuspended in 1 x PBS again and counted. 10'000 cells were resuspended in 15 µl freshly prepared PKT-20 lysis buffer. Samples were heated for 60 min at 50 °C and 15 min at 95 °C.

Western blot

Western blotting (WB) is used to transfer proteins separated by charge and mass in SDS-PAGE (Sodium Dodecyl Sulfate Polyacrylamide Gel Electrophoresis (SDS-PAGE) to a membrane (Towbin et al., 1979; Burnette, 1981).

Dependent on the chosen method, western blot can be quantitative (using fluoresce) or semi-quantitative (chemiluminescence detection, based on peroxidase) but in both cases yields to higher sensitivity in detection compared to Coomassie staining or similar methods.

For quantitative WB, proteins are transferred to nitrocellulose, which needs to be activated in transfer buffer. When performing a semi-quantitative WB, a polyvinylidene fluoridine (PVDF) membrane us used. The PVDF membrane has to be activated with EtOH and equilibrated in transfer buffer before use. The transfer of the proteins in the gel on the membrane was done, using a standard wet blot system. If not noted differently, standard transfer was performed for 60 min, at 100 V, on ice. After transferring, membranes were directly blocked using 5% milk in 1 x TBS for 30 min or used for total protein staining: Nitrocellulose membranes could be used for staining of the total protein, using LI-COR® staining solution and standard LI-COR® protocol. If total protein staining was performed, it continued with the blocking step afterwards. After a short wash with TBS, membranes were incubated in primary antibody overnight, in the cold room, while shaking. After multiple washing steps with 1x TBS with Tween (TBS-T). When using PVDF, TBS-T was used with 0,05% Tween. For nitrocellulose membranes, 0,1 % Tween was used. After washing, membranes were incubated for 30 – 60 min in secondary antibodies. For semi-quantitative HRP blots using PVDF, secondary antibodies against rabbit or mouse coupled to horseradish-peroxidase (HRP) were used. For quantitative analysis on nitrocellulose, fluorescently labeled secondary antibodies were used and membranes were covered from light until imaging. After incubating the membranes were washed twice in respective TBS-T buffer. A final washing step with TBS was performed. The fluorescently labeled nitrocellulose was imaged using the LI-COR Oddysey® DLx imager. The HRP-mediated PVDF imaging is based on chemiluminescence. Therefore, membranes hat to be incubated in developer solution (SuperSignal™ West Pico Plus) containing a substrate (luminol) for HRP to produce a detectable light signal. Afterwards, light signals were detected, using the Amersham™ ImageQuant device. Membrane images were edited in Image Studio™ Lite or Fiji and figures were made using Affinity Designer.

Sodium Dodecyl Sulfate Polyacrylamide Gel Electrophoresis (SDS-PAGE)

SDS-PAGE was performed to separate proteins from cell lysates or chromatography samples by negative charge and protein mass. In this work either self-made Bis-Tris gels or commercially available Bis-Tris gradient gels (4 – 12%, Invitrogen) were used. Selfmade gels contained a stacking gel with 4,5% acrylamide and a separating gel containing 10 % acrylamide:

Ingredients	Running Gel (10%)	Stacking Gel (4.50%)
Acrylamide (30%)	30	4.5
Bis-Tris buffer (3×)	30	10
dH2O	30	15.5
APS	0.45	0.3
TEMED	0.045	0.03

Protein samples were prepared with 1x Laemmli buffer, containing SDS, unfolding the protein structure and adding a negative charge. Additionally, protein samples containing 1x Laemmli were boiled at 95 °C for 5-10 min. Dependent on experimental setup, samples were additionally supplemented with 100 mM DTT. Gels were run in 1 x MOPS buffer. After 10 min running at 100 V, gels were run at 120-140 V until the blue running front reached the end of the gel. SDS-PAGE gels were used for further Western blotting.

Bicinchonic assay (BCA-Assay)

Protein concentrations were measured using the BCA (Thermo Fisher) assay. It is based on the Biuret reaction, the reduction of Cu^{+2} to Cu^{+1} by protein in an alkaline medium combined with a reagent containing bicinchonic acid. This leads to a purple-colored reaction product, measurable at 562 nm (Smith et al., 1985). The assay was performed according to the manufacturers protocol in a 96-well plate format. Incubation was done for 30 min at 37 °C before measuring using the TECAN Reader Spark® 10 M microplate reader and the Spark® Control software from TECAN.

Immunoprecipitation (IP)

Immunoprecipitation is based on the binding of a proteinaceous antigen in solution by an antibody or nanobody. This is followed by purification of the antigen-antibody complex, as the antibody is attached to a matrix (agarose). This technique allows the specific isolation of a protein (complex) of interest out of a cell lysate. If interacting proteins are isolated with the protein of detection, it is referred to as Co-IP. Different methods can be used to pull down the antigen from the matrix: enzymatic digestion, competitive elution, detergent pull-down or pH mediated pull down.

For all different types of chromatograhies, cells were lysed in 1 x solubilization buffer (SB) with 0,6 % DDM (see table). Cell lysates were cleared from insoluble fractions and nuclei via centrifugation and the protein concentration of the cleared cell lysates was measured, using the BCA assay. Samples were adjusted to same protein concentrations in all samples within one experiment. Adjusted lysates were used as Inputs for the IP and 50- 100 µl of Input samples were taken for further analyses. Sample preparation and IP experiments were performed on ice. Dependent in the method of IP and the protein concentration, the amount of Sepharose beads (= matrix) was adjusted. IPs were performed using Mobicol „F“columns (fixed outlet plug, inserted 35 µm filter, small columns) from MoBiTec. Beads were added to the Mobicols with a cut pipet tip. For all IPs, the bead material was washed with 2 x SB and equilibrated with 1 x SB + 0,6 % DDM prior to use. Washing and equilibration steps were performed by adding 500 µl of buffer and centrifuging the Mobicols at 200 x g for 30 seconds.

In this work four setups for IP were used.

Anti-GFP IP with protease elution

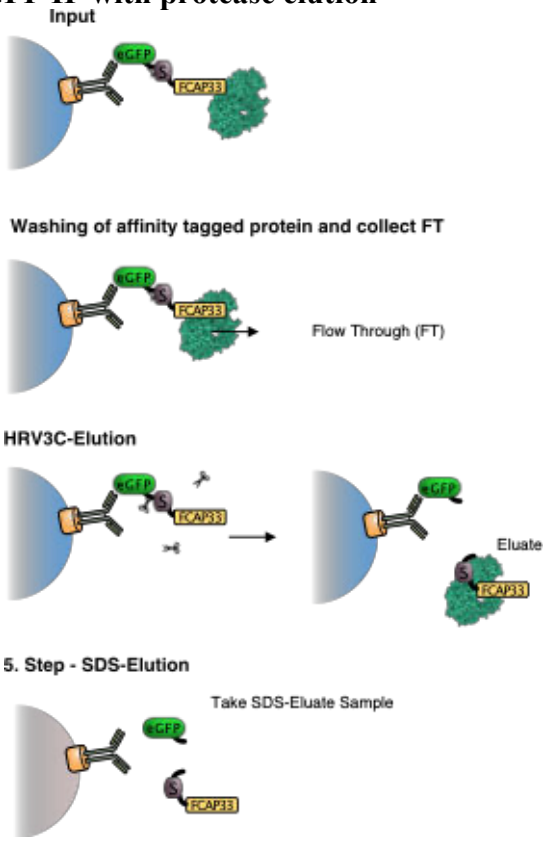

LAP-tagged proteins or GFP-tagged proteins were purified by using anti-GFP Sepharose. Cell lysates, containing GFP-tagged (LAP-tagged) proteins were subjected to GFP-beads and incubated for 1h in a heads-on shaker at 8 °C. After binding, the unbound material, referred to as flow-through (FT) was spun out, and a FT sample was collected. The GFP matrix was washed 9 times with 1 x SB (no PIC) + 0,05% DDM. The LAP tag consists of a GFP, an HRV3C cleavage site and the S-tag. Therefore, the elution of purified LAP-tagged proteins was done, by HRV3C protease cleavage. After washing, Mobicols were closed from the bottom, and 1 x SB (no PIC) + 0,05% DDM + HRV3C protease was added. 1 x volumes depending on the volume of bead material was used and elution was performed ON in the cold-room in a heads-on shaker. After ON-incubation, first elution was collected by centrifuging at 200 x g for 30 s. 1 x bead volume of 1 x SB (no PIC) + 0,05% DDM was added again and centrifuged at 300 x g for 1 min (Centrifuge 5424 R, Eppendorf). The final elution volume was 2 x bead volume. After elution of GFP-tagged proteins (and interaction partners), the bead material was incubated with 1 x Laemmli buffer, diluted in 1 x SB (no PIC) + 0,05% DDM, and boiled for 5 min at 95°C. This SDS-elution was centrifuged for 2 min at 300 x g (Centrifuge 5424 R, Eppendorf). The SDS in the Laemmli buffer and the heating leads to a removal of all material still bound to the bead material. In the case of the

GFP-IP using protease cleavage, GFP should remain on the beads and only be removed upon SDS-elution. For analysis on SDS-PAGE followed by WB, the Input sample, FT sample and an eluate sample were prepared with 1 x Laemmli final concentration and boiled for 95 °C for 5-10 min as done for the SDS Samples.

Anti S-peptide IP

This method was only used after GFP-IP. The eluate after GFP-IP should contain all proteins, still tagged to the s-tag (remaining part of the LAP-tag) and its interaction partners. To further purify and enrich these proteins for mass spectrometry, the GFP-elution fractions were subjected to s-protein agarose. Washing, equilibration, binding and washing after binding was performed as described. Elution was directly done in 2 x MS grade sample buffer. Done by Sabrina Ehr.

ALFA-IP with competitive elution

The ALFA IP was done as described above until the washing of the bead material. Binding and following steps were done at RT as ALFA-PE (optimized for RT) were used. The ALFA-tagged proteins were eluted by competitive elution. For competitive elution, columns were closed and 1 x SB with 0.05 % DDM and 2 % v/v ALFA-peptide was added to the beads using 2 x bead volume. Closed columns were shake for 20 min at 1000 rpm. The elution fraction was centrifuged out for 2 min at 300 x g (Centrifuge 5424 R, Eppendorf). The ALFA elution was followed by a SDS elution as described above.

FCAP33-IP with competitive elution

Performed as described for ALFA-IP. Bead material was self-made by David Mick by coupling the FCAP33 antibody (Martin Jung) to protein A Agarose (Coupling of antibodies to Protein A Agarose). This allowed pull was done with FLAG peptide (Martin Jung) 120 µg/mL final concentration in 1 x SB with 0.05 % DDM.

Coupling of antibodies to Protein-A Agarose

Protein-A-Sepharose (500 µl) was added to a column and washed twice with 5 ml 0.1 M KPi by centrifuging at 100 x g for 30 s. The antibody serum (FCAP33 – 1706) was diluted 1:3 in KPi buffer, to a final volume of 4 mL. The antibody dilution was incubated with the beads for 1h at RT while mixing. The unbound material was removed by spinning down the Agarose. Agarose was washed in the column twice with 0.1 M sodium borate. A DMP solution was prepared using 5 mg/ml DMP in 0.1 M sodium borate buffer. The column was closed from the bottom and 3.5 mL of DMP solution was added and the column was closed from the top to

incubate for 30 min at RT. The DMP solution was spun out and the column was washed in 1 M Tris. After, the column was incubated for 2 hours with 5 ml 1 M Tris. For storage, Tris was removed by spinning and the beads were washed 3 times with TBS. Finally, beads were transferred and stored in a tube in 1 x TBS with 2 mM azide as preservative.

CRISPR-Cas9 mediated Genome Editing

Clustered regularly interspaced short palindromic repeats (CRISPR)-Cas is a microbial adaptive immune system that uses RNA-guided nucleases, to cleave genetic elements (Ran et al). Today, CRISPR-Cas9, consisting of the nuclease Cas9 and a sgRNA, is commonly used to generate gene knockouts for scientific purposes. The single guide RNA (sgRNA) is a 20-nucleotide sequence directed to a target gene by complementarity to the target gene, upstream of the PAM sequence. The binding of the sgRNA to the target initiates the Cas9 mediated double strand break of the DNA. The resulting mechanisms are prone to mistakes and can lead to random indel or deletion mutations at the site of repair. These mutations in the DNA sequence can cause mutagenesis and therefore defective gene expression and or defective proteins up to nearly transcriptional silencing (Ran et al., 2013).

Sequences for sgRNA targeting were designed using Chopchop (https://chopchop.cbu.uib.no). Two sgRNAs were selected, either targeting Exon 2 or Exon 4 of a total of 7 Exons.

r1 – Exon 2
5’ caccgCAGAACGCTTCACAGGTAGG 3’ (forward)
5’ aaacCCTACCTGTGAAGCGTTCTGC 3’ (reverse)

r2 – Exon 4
5’ caccgTTCAACCCCGATCAGGCCAA 3’ (forward)
5’ aaacTTGGCCTGATCGGGGTTGAAC 3’ (reverse)

Phosphorylation and annealing of the oligos were done and the annealed oligos were cloned into the pSpCas9 (BB)-1A-GFP vector. The fluorescent GFP is used as selection marker to only select for cells expressing the Cas9 plasmid. The Cas9 plasmid was transfected using the JetPrime Kit and transfection was performed as described in section xx, transient transfection. Single GFP-expressing cells and pools were sorted (Lab of Prof. Dr. Daniela Yildiz, PZMS,

Homburg). Design of sgRNAs and cloning was done by Lea Sanwald. Transfection and sorting were done by Lea Sanwald and Dr. Avishek Prasai.
Single cells and pools were cultured, and growing cells were tested by immunofluorescence and sequencing of genomic DNA.

Amplification PCR for genomic DNA

15 µl genomic DNA
2,5 µl forward primer
2,5 µl reverse primer
25 µl Q5® High-Fidelity 2 x Master Mix
5 µl water

98 °C 30s
98 °C 10s
67 °C 30 s | 30 cycles
72 °C 30 s
72 °C 2 min

r1 – Exon 2 PCR primer:
5’ CTGAGACATCTGAGATGTGGTC 3’ (forward)
5’ CTGAGACATCTGAGATGTGGTC 3’ (reverse)
Primers also used for sequencing.

r2 - Exon 4 PCR primer:
5’ CTGTTGTTCTGGGGATCCTG 3’ (forward)
5’ AAGCAGACGCAGATGATGGC 3’ (reverse)
Additional sequencing primer: 5’ gagactatagagggagggagc 3’ (forward)
Primer design was done by me, gDNA extractions and following PCRs were done by Sabine Plant and me.
The PCR was loaded on an 0.8 % agarose gel and the product was purified using the silica membrane-based NucleoSpin® Gel and PCR Clean-up Kit according to the manufacturer’s instructions (Machery-Nagel).

siRNA mediated Knockdown

Instead of creating conditional knockout cell lines using CRISPR-Cas9, gene silencing can also be achieved by the expression of small interfering RNAs (siRNA). The 21-25 nucleotide long siRNAs are the signature of any homology-dependent RNA-silencing event (Agrawal et al., 2003). Therefore, 21-nucleotide long siRNA duplexes can efficiently be used for gene suppression (Elbashir et al., 2001) in mammalian cells.

For transfection with siRNAs, 250'000 cells were seeded per 6-well one day prior to transfection. The day after seeding, cells were transfected using the RNAiMAX reagents and 6 µl of siRNA (10 µM stock). siRNA was mixed with 150 µl of Opti-MEM medium in a xxx tube be carefully pipetting up and down. Three times the siRNA volume was used for Lipofectamine RNAiMAX reagent. 18 µl of Lipofectamine RNAiMAX reagent was mixed with 150 µl of Opti-MEM. Both mixes were combined in one tube, incubated for 5 min at R and dropwise added to the cells. Cells were cultured under standard cell culture conditions for 24 h prior to use. Ratios of siRNA and RNAiMAX reagent were kept the same, also for smaller scale experiments. For WB experiments, cells were transfected in a 6-well format, according to the protocol, solubilized in 1 x SB with 0.6 DDM and TCA precipitation was performed.

RNAs were designed and used by GeneGlobe: Mm_RP23-219P13.3_2 FlexiTube siRNA and scrambled siRNA from the same manufacturer was used as control.

Fluorescence Recovery After Photobleaching (FRAP)

To investigate the kinetics of a component through a tissue or cell, fluorescence recovery after photobleaching (FRAP) experiments were performed.

Cells were seeded in 6-well plates on 25 mm 1.5 H coverslips, two days in advance of the experiment. After 24 h of growth, cells were starved for 24 h to induce ciliation.

For imaging the Zeiss LSM880 microscope was used with a 63 x oil objective. For imaging, coverslips were placed in a ring holder, and filled with 500-800 µl cell culture medium, without phenol red. The coverslips were cleaned from the bottom side, and immersion oil (Immersol^{TM} 518 F) was used for imaging. Imaging was done in a dark room without heating chamber or CO_2 supply.

Photobleaching was done with 100% laser power as fast as possible with 8 iterations in the 488 nm channel in confocal mode. Time series for signal recovery in the green channel were done in 1 min or 30 s intervals for FCAP33^{cLAP} and FCAP33^{NG} cells. Control experiments were performed with SSTR3^{NG} and FCAP33^{NG} cells with recovery intervals as fast as possible.

Recovery imaging in the green channel at 488 nm wavelength was done with 4,8 % laser intensity. Pinhole settings varied between the day of experiments between 36 and 37, Master Gain between 600-750 and Digital Gain between 1.2 and 1.24 for the 488 nm channel. As recovery analysis is normalized within itself by referencing signal intensities to timepoint zero, before bleaching, different imaging settings should not interfere with the results of the experiments. Additional imaging for fluorescent signals at 555 nm or 647 nm differed between experiments. Laser settings were kept for all experiments at 3% at 555 nm and 12,5 % at 647 nm and Digital Gain for both channels at 1. Pinholes varied for both channels between 36,5 - 38 and the Master Gain between 600 -700. If z-stacks were done before the bleaching event and at the end of the time series, maximum projections are represented. Z-stack settings were: 3 planes, with 0,35 µm intervals.

FRAP analysis

FRAP analysis was done using Image J (Fiji). For recovery line plots, images were bleach corrected using the histogram matching method of the bleach correction tool in Fiji. Cilium or midbody ROIs were defined. For creating and analyzing recovery plots “Plot Z-axis profile” in Fiji was used. Lists of created plots were saved and further processed in Excel. For combining and comparing several spectra of one experiment normalization was performed. For each cilium/midbody, the maximum intensity was set to 100 % (a value before bleaching) and all the other values are calculated as % of the maximum. Lists were further processed in GraphPad Prism where standard errors were calculated, and Graphs were visualized.
Additionally, ROIs were of the same cilia and midbodies to generate line plots of the ROIs before bleaching, after bleaching and at the end of the time series, named “recovery”. Plots were done, using the plot tool of ImageJ and lists were used to generate graphs with GraphPad Prism. For line plots the highest value was set to 100% and all other intensities were calculated as % of the maximum value. Figures show representative images for each FRAP condition.

Impedance measurements – xCELLigence

Impedance measurements were performed using the xCELLigence system from Agilent. RTCA E-plates were used to measure “cell behavior” over time. The xCELLigence instrument is placed in a CO_2 cell culture incubator and allows the measurement of impedance by the use of “E-plates”. These 96-well plates, have gold electrodes on the bottom of each well to measure the electron flow between the two electrodes (bottom figure, left). Adherent, growing cells cover the electrodes, and therefore impair the flow current. The impedance is measured and

represented in the standardized Cell Index (CI) over time (bottom figure, right) (Luong et al., 2021). Impedance measurements are often used to investigate the cells behavior upon drug treatment or to study knockout and knockdown cell lines.

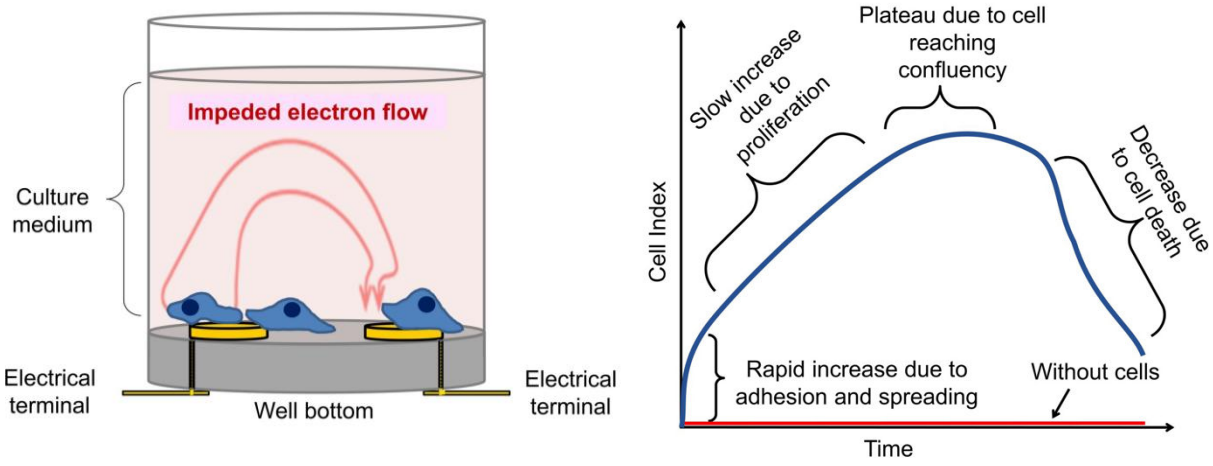

Mass Spectrometry

The mass spectrometric measurements were performed by Dr. C. Fecher-Trost (MS Core Facility of Saarland University, Institute of Experimental and Clinical Pharmacology and Toxicology, PZMS) using an Orbitrap Eclipse™ Tribrid Mass Spectrometer (Thermo Scientific™). For this, proteins were digested in-gel with trypsin (Diener et al. 2024), and the resulting tryptic peptides were analyzed via nano-LC-ESI-MS/MS using the following equipment: an Ultimate 3000 RSLC nano chromatography system equipped with an Ultimate 3000 RS autosampler, coupled with a Thermo Easy-nanoLC and a Thermo Scientific Orbitrap Eclipse Tribrid Mass Spectrometer (Thermo Scientific). Peptides were separated over a 120-minute gradient generated using buffer A (water and 0.1% formic acid) and buffer B (90% acetonitrile and 0.1% formic acid) at a flow rate of 300 nl/min: 0–5 min 4% B, 5–80 min 31% B, 80–95 min 50% B, 95–100 min 90% B, 100–105 min 90% B, 105–106 min 4% B, and 106–120 min 4% B.

Peptides were concentrated on a C18 trap column (75 µm × 2 cm, Acclaim PepMap100C18, 3 µm, Thermo Scientific) and separated on a reverse-phase column (nanoViper Acclaim PepMap capillary column, C18; 2 µm; 75 µm × 50 cm, Thermo Scientific). The eluate was ionized using a coated emitter (PicoTipEmitter, 30 µm, New Objective, Woburn, MA, USA, ionization energy: 2.4 keV) and introduced into the mass spectrometer. MS1 peptide spectra were acquired using an Orbitrap analyzer (instrument settings: R = 120k, RF lens = 30%, mass/charge range: m/z = 375‑1500, MaxIT: auto, intensity threshold: 10^4). Dynamic

exclusion of the 10 most abundant peptides was applied for 60 seconds. MS2 spectra were recorded in the linear ion trap (isolation mode: quadrupole, isolation window: 1.2, activation: HCD, HCD collision energy: 30%, scan rate: rapid, data type: centroid). (Text written by Dr. C. Fecher-Trost)

Primary Analysis of Mass Spectrometry Raw Data

Peptide and fragment spectra were analyzed using the PEAKS software (PEAKS Studio 10.6, Bioinformatics Solutions Inc., Canada). Fragment ions were matched against an extended mouse SwissProt protein database (version 2024_03), assuming the following mass tolerances: peptide: 10 ppm, peptide fragment: 0.7 Da. The workflow included: tryptic enzymatic digestion allowing for up to three missed cleavage sites, carbamidomethylation of cysteine (fixed modification), and deamidation of asparagine and glutamine, acetylation of lysine, and oxidation of methionine (variable modifications). Fractions belonging to the same sample were combined for analysis. For significant protein identification, the FDR (false discovery rate) filter was set to a maximum of 1% and 5% for protein and peptide probability, respectively.
(Text written by Dr. C. Fecher-Trost (Diener et al., 2023))

For the purpose of this work, I only used hits with a peptide threshold of 0.5 % and a minimum number of 2 peptides. To calculate the fold change, the number spectrum counts of the sample was divided by the number of spectra of the respective control. Only hits, that had an enrichment higher than 2 were used for comparison analyses. To calculate the fold change, values being 0 were imputed by setting them to 0.1. For VENN analysis the open-source software BioVENN was used. Networks and enrichment plots were done using the open-source software STRINGdb.

In vitro microtubule binding assay

The potential binding of microtubule associated proteins (MAP) can be assessed by an in vitro cell lysate-based assay. Binding of the MAPs to growing MTs can be followed by TIRF or steady-state microscopy. In our setup, steady-state images were conducted with the LSM900 confocal microscope.

The assay was performed in the Lab of Jun.-Prof. Laura Aradilla Zapata (Biophysics of the Cytoskeleton, University of Saarbrücken) by the PhD student Dyuthi Sreekumar. She performed the assay as described by Jijumon et al (Jijumon et al., 2022). HEK293T cells were seeded in two 6 wells (0.6×10^6 cells per well) to 40-50 % confluency before transfection. 4

µg DNA were transfected using jetPEI. The DNA was mixed with 250 µl of serum free medium and 6-8 µl of jetPEI were mixed with 250 µl serum free medium. Plasmid DNA was the same as used for the generation of stable IMCD3 cell lines and the DNA and HEK293T cells were provided by our lab. Both mixes (DNA and jetPEI) were combined, incubated for 20 min and added dropwise to the cells. Transfection efficiency was checked after 48 hours. Cell lysates were prepared as described before (Jijumon et al., 2022). The last centrifugation step was done in a 70Ti rotor for 30 min at 19'200 rpm and 4 °C. The MT binding assay and the imaging was done by Dyuthi Sreekumar.

Cloning

In this work, different plasmids were cloned to generate tagged variants of the protein of interest. For this, existing plasmids with existing tags in the lab were used, to generate new plasmids. Sabine Plant assisted in performing PCR and other cloning reactions.

Agarose Gel Electrophoresis

Control digests, PCR products and other DNA probes were analyzed or purified from 0.8 – 1 % Agarose gels. 0.8 – 1 % agarose powder was boiled in 1 x TAE in a microwave until agarose powder was solved. When the agarose solution was cooled down, 2 µl of pegGREEN DNA dye was added to 50 ml of 0.8 -1 % agarose. DNA samples were run in 1 x TAE at 80 V for 40 min.

Cloning strategies

Different cloning strategies were used. Gibson cloning, gateway cloning and classical cloning by restriction digestion of the insert and the backbone with the same enzymes, followed by ligation of the two products.

Classical cloning

If enzymatic restriction digests were performed, enzymes were used from NEB together with the respective cutting buffers according to the NEB protocol. Optimal temperatures for digestions were also set according to NEBs temperature recommendations. Usually, a DNA sequence of interest was cut from a plasmid, or a PCR product (insert), and pasted into a plasmid of destination (backbone), digests with the same plasmids. This creates sticky ends, which gives rise to the correct orientation of the insert into the backbone. Optionally, rSAP

(Shrimp alkaline phosphatase, NEB) was added to the digested backbone to prevent re-ligation of the backbone without insert.

Polymerase Chain reaction with Q5

PCR reactions were performed using Q5 PCR mix from NEB:

40-50 ng plasmid DNA
1,25 µl forward primer
1,25 µl reverse primer
11,25 µl Q5® High-Fidelity 2 x Master Mix
x µl water up to 22,5 µl total reaction

98 °C 5 min
98 °C 30s
52 °C 30 s | 30 cycles
72 °C 30 s
72 °C 5 min

PCRs were either loaded on an 0.8 % agarose gel and the product was purified using the silica membrane-based NucleoSpin® Gel and PCR Clean-up Kit according to the manufacturer's instructions (Machery-Nagel) or the PCR clean-up Kit from NEB (T1030) was used.

Ligation Classical Cloning

Ingredient	Volume (µl)
DNA (e.g., annealed oligos, PCR product)	1
Pre-digested plasmid (10 ng/µl)	1
2x Quick Ligase Buffer	2,5
NEB Quick Ligase	0.5

Quick Ligation was performed according to the manufacturers protocol. 5 µl of Ligation mix was used for the transformation of 50 µl competent cells.

Gateway Cloning

For LR cloning the Invitrogen™ Gateway™ LR Clonase™ II enzyme mix was used. It catalyzes the recombination between an entry vector (gene between attL sites) and a destination vector (arttR sites).

Ingredient	Volume (µl)
Backbone	1 (75 ng)
Insert	1 (75 ng)
1 x TE buffer	4
LR Clonase mix	1

The whole mix was used for the transformation of 50 µl competent cells.

Gibson Assembly

Gibson assembly is a method used to seamlessly join DNA fragments together by the use of a 5' exonuclease, a DNA polymerase and DNA ligase in the Gibson mix (Gibson et al). This method can be used to bring a PCR product into a destination vector. The PCR product is designed with overhangs, being complementary to the destination vector. A destination vector is cut with a single-cutting enzyme. The PCR primers have overlapping base pairs, complementary to both sites of the restriction site. This allows to ligation of the PCR product into the destination vector using the Gibson assembly.
The PCR was loaded on an 0.8 % agarose gel and the product was purified using the silica membrane-based NucleoSpin® Gel and PCR Clean-up Kit according to the manufacturer's instructions (Machery-Nagel).

Ingredient	**Volume (µl)**
Gibson mix (NEB)	5
PCR plasmid	1

Digested Backbone	1

The whole mix was used for the transformation of 50 µl competent cells.

Bacterial Transformation

Foreign DNA can be taken up and replicated by competent cells. This has become a common method in molecular genetics with Escherichia Coli as a universal host organism for molecular cloning (Hanahan et al.). *E.coli* cells are chemically modified to competently take up DNA, mediated by an additional heat-shock (Mandel et al., Hanahan et al). Cells are thawed on ice and 10-20 % v/v was added to the *E.coli* cells (7 µl mix of Gibson, 6 µl LR mix to 50 µl of competent cells). Cells were incubated on ice for 15 min. Heat-shock was performed after incubation on ice for 45 s at 42 °C. After heat-shock, cells were cooled down for 2 min on ice. LB-Medium was added to the *E.coli* (250 – 500ml) and incubated at 1000 rpm for 1 h at 37°C in a 1,5 ml reaction tube. The culture was streaked on an LB-plate with antibiotics for ON incubation at 37 °C. Usually the plasmid of interest expresses an antibiotic resistance gene for selection for cells expressing the plasmids. According to this, antibiotics was added to the LB-plates, before pouring. Upon ON incubation of the transformed *E.coli* on LB plates, colonies were selected and liquid LB-medium with the same antibiotics was inoculated with a single colony.

Plasmid Isolation

To screen DNA via sequencing after cloning or to reproduce plasmid DNA, DNA has to be isolated from *E.coli* after efficient bacterial transformation. 5 ml antibiotic LB-cultures of single colonies (see transformation) were grown over night at 37 °C at 180 rpm in a bacterial shaker. Extraction and purification of plasmid DNA was done using NucleoSpin® Plasmid Kit according to the manufacturer's instructions (Macherey-Nagel). Centrifuging steps in 1.5 mL Tubes were done in a Centrifuge 5424 R from Eppendorf.

Sequencing

Sequencing of PCR products and plasmids was done using MicroSynth Seqlab (https://www.microsynth.com/home-de.html). Sequences were analyzed with open software source Benchling using MAFFT v7 algorithm and the software ApE for manual alaysis of sequences. Benchling does not align sequences under a certain threshold of quality. These parts

of sequences were manually "analyzed" using ApE, without an alignment and just checking chromatograms.

Statistics

Statistics was done using GraphPad Prism 10 Version 10.4.1. One-way ANOVA analysis was done and a Dunnett's multiple comparison between the WT or control group and the groups to compare was run. Therefore, the mean values of each group are calculated together with their confidence intervals (CI). If 95% CI range does not include 0, the difference is statistically significant. The p value was set to 0.05 as a threshold. Meaning if 95% CI ranges around 0 and $p < 0.05$, there is as statistical significance of the means of the tested group when compared to the control group. Prism interprets the p-Values as:

$p \leq 0.0001$ Extremely significant****

$p \leq 0.001$ Very significant***

$p \leq 0.01$ Significant**

$p \leq 0.05$ Moderately significant*

$p > 0.05$ Not significant ns

(https://www.graphpad.com/guides/prism/latest/user-guide/index.htm)

If not stated in graphs, no significance was calculated and might not be indicated. Additionally, if experimental groups are rather small, highly significant results should be regarded with caution.

3D spheroids

Mouse IMCD3 cells can be used to generate epithelial spheroids. This 3D cell culture model was described and published by Giles et al., 2014. Lea Sanwald performed 3D culture assays following the published protocol (Giles et al., 2014).

Trichloroacetic acid (TCA) Precipitation

To “enrich” proteins in a sample and to overcome detection-limits, when having small sample volumes or low-expressing proteins, precipitation can be used. Here, we used trichloroacetic (TCA) acid to precipitate proteins from the sample and reconstitute the precipitate in a smaller sample volume. This leads to an enrichment of the content within the sample.

Samples were adjusted to ~0.5% Triton-X100 and chilled on ice. TCA was added to a final concentration of 15% of the sample volume. Samples were mixed well and incubated for 30 min on ice. The precipitate was collected by centrifugation at 13.000 rpm for 5 min in a cold

centrifuge (Centrifuge 5424 R, Eppendorf). The supernatant was removed, and the oily pellet was washed by addition of 1 ml ice-cold acetone. The acetone was removed after another centrifugation step. Afterwards, the pellet was air-dried until it no longer smelled of acetone. The protein containing pellet was directly resuspended in 1x Laemmli buffer and sonicated in six cycles of 10 s. Each cycle was performed with 5 s sonication pulses followed by 5 s breaks. Performed together with Shanli S. Tarrah.

In vitro translation (IVT) assay

Rabbit reticulocyte lysate can be used as a mammalian cell-free system for the expression of proteins. This allows even for the expression of proteins that would be toxic to cells or *E.coli*. Monika Lerner from AG Schrul used the TNT T7 coupled Reticulocyte Lysate System from Promega L4610 to perform the assay according to the standard protocol.

Ammonium sulfate precipitation

For the precipitation of proteins using ammonium sulfate, a saturated solution of ammonium sulfate $(NH_4)_2SO_4$ is used. The high salt concentration reduces solubility of proteins, which leads to precipitation.

The method was used for the precipitation for the samples of the IVT-assay. 7 µl of IVT samples were supplied with 23 µl water. 60 µl saturated ammonium sulfate (2 x samples volume) was added and vortexed. The mixture was incubated for 30 min on ice. After incubation, samples were centrifuged for 10 min at 13'000 x g at 4 ° C (Centrifuge 5424 R, Eppendorf). The supernatant was discarded, and the remaining pellet resuspended in 30 µl of water. 60 µl of 96% ethanol was added, incubated for 15 min on ice and the suspension was centrifuged as before. Most of the ethanol was reduced and then air dried at RT. 15 µl of 1 x Laemmli buffer with DTT was added and samples were boiled for 95 °C.

Real Time Quantitative PCR (RT-qPCR)

qPCR was used to investigate mRNA expression levels of a gene of interest.

Cells were seeded in 6 wells with 250'000 cells per well. If knockdown was performed, siRNA treatment was performed as described before. Two 6-wells were seeded per cell line of interest. After one day of growth, cells were pelleted, shock frozen with liquid nitrogen and stored at -80 °C until use.

Pelleting cells

Cells were trypsinized and resuspended in cell culture medium. The cell suspension was centrifuged down at 200 x g for 5-10 min in a cold centrifuge (Centrifuge 5804 R, Eppendorf). Medium was aspirated and pellet was resuspended in 1 x PBS. Cells were centrifuged as before in a cold centrifuge. Cells were resuspended in PBS again, transferred to a 1.5-mL tube and centrifuged for 30 min at 600 x g (Centrifuge 5424 R, Eppendorf).

mRNA Isolation

Messenger RNA (mRNA) Isolation was done with the RNeasy Mini Kit or miRNeasy Tissue/Cells Advanced Kit from Qiagen. Both Kits are suitable for the isolation of mRNA from cells. Pellets of 2 pooled 6 wells were homogenized in 450 RLT buffer and processed according to the manufacturer's protocol. mRNA levels were measured with a NanoDrop device.

Reverse transcription – Synthesis of cDNA

To perform qPCR, the isolated mRNA must be transcribed into cDNA. Reverse Transcription was done, using the QuantiTect Reverse Transcription Kit and following the QuantiTect Reverse Transcription Kit Handbook from Qiagen.

Reverse Transcriptase quantitative Polymerase Chain Reaction (RT-qPCR)

PCR was done using QunatiTect SYBR Green Assay and QuantStudio ™ 3 Real-Time PCR system (Thermo Fisher Scientific Inc., Waltham, USA) and software at the Institute for Human Genetics together with Dr. rer. nat. Nicole Ludwig.

Ingredient	Volume (µl)
2 x QuantiTect SYBR Green	10
1 x QuantiTect Primer Assay	2
RNAse free water	6
Template cDNA	2

PCR settings:

95 °C 15 min

94 °C 15 s
55 °C 30 s | 30 – 40 cycles
70 °C 30 s

Primers for FCAP33 were used from QuantiTect. GAPDH and Gli1 Primers were designed and a kind gift from Nicole Ludwig. Samples were done in Duplicates and NTC (No Template Controls) and RT – without the RT enzyme were also analyzed.

Cell Cycle analysis using Fluorescence Activated Cell Sorting (FACS)

FACS was used for cell cycle studies. To this end, cells were counted on the day of splitting 1-10 million cells were used for DNA staining using Hoechst DNA dye. The final number of cells were spun down for 5 min at 500 x g at 4 °C and washed in 500 µl PBS. For fixation, 4,5 ml of ice cold 70 % ethanol was added to 500 µl of 1-10 million cells, and slightly vortexed. Cells were incubated on ice for 2 hours. After 2 h supernatant was removed, and cells were taken up in 0.1 % triton in 1 x PBS containing 5 µg/ml Hoechst and eventually 100 µg/ml RNAse. Cells were incubated for at least 30 min on ice in buffer before proceeding to FACS. FACS was done at the CIPMM with the kind help of Dr. Dalia Ansary.

Antigen retrieval

Antibody staining can be improved by different methods. Detergents and heating can help do open up structures, such that antibody binding epitopes are easier accessible by antibodies. A possible way to do so is the antigen retrieval by using a basic Tris-HCl buffer containing 5 % urea (Shan-rong-Shi et al., 1996).
Cells were seeded as for standard immunofluorescence. Cells were fixed in 4 % PFA for 15 min at RT or with ice cold methanol at -20 °C for 5-10 min. Afterwards, cells were washed three times with 1 x PBS. 1 ml of pre-heated antigen retrieval buffer (95 ° C) was added to each well, and the plate was incubated at 95 °C for 10 min at 300- 500 rom (on a thermoshaker). Wells were again washed with PBS, 3 times. Immunofluorescence protocol was proceeded as described before, with the blocking step.

Cell culture

Cells were cultured in a cell culture incubator with 37 °C and 5% CO_2. Passaging of cell was done under sterile conditions under a laminar flow hood. For cell culture medium either DMEM or DMEM-F12 was used with 7,5 % FBS. Cells were cultured and passaged mainly in T-25, T-75 or 10 cm cell culture dished. Cells were usually split on Mondays, Wednesdays and Fridays, such that they were confluent on the day of splitting.

For most experiments, cells were counted using the Hirschmann™ counting chamber. Standard medium and trypsin volumes are listed below as well as standard cell numbers for seeding. To passage cells, cells were washed with 1 x PBS and the respective volume of trypsin (according to the surface of cell growth) was added. Cells with trypsin were incubated in the cell incubator until cells detached. Cells were resuspended in the with medium with the same volume as culture before. For standard passaging, 1:10 was transferred to a new dish during the week and 1:20 from Friday to Monday.

Ciliation was induced by synchronizing cells in a non-dividing state. Therefore, seeded cells were washed one with 1 x PBS and medium containing only 0.2 % of FBS was added for 24 h.

To freeze cells, cells were trypsinized as described and resuspended cells were pelleted at 200 x g. The cell pellet was resuspended in Bambanker. Usually a confluent 10-cm dish was used for 3 vials of cells. For one vial of cell 300 µl Bambanker freezing medium was used. Cells were frozen at -80 °C.

Table 1: Cell culture methods, definition of cell numbers for specific growth surfaces

Dish/ Plate	Growth area (cm2)	Seeding cell number	Medium volume (mL)	Trypsin volume (mL)
6 well	10	0.25×10^6	2	0.25
24 well	2	5×10^4	0.5	0.1
96 well	0.3	1.25×10^4	0.1-0.2	0.1
10 cm	78	1×10^6	10	1
15 cm	175	2.5×10^6	25	2.5
T-25	25	0.7×10^6	5	0.5
T-75	75	2.1×10^6	10	1

Table 2: Antibiotics and respective concentrations

Antibiotic	Stock Concentration (mg/ml)	Working Concentration (µg/ml)	Supplier/ CatN	Purpose
Ampicillin	100	100	Carl Roth K029.2	Bacterial Culture
Blasticidin S hydrochloride	10	4	Thermo Fisher A1113903	Cell Culture
Chloramphenicol	25	25	Carl Roth 3886.2	Bacterial Culture
Kanamycin sulfate	50	50	Fisher Scientific 11578676	Bacterial Culture
Penicillin-Streptomycin (100x)	10	100	Fisher Scientific 15140122	Cell Culture

Table 3: Primary Antibodies and specifications for usage

Antibody (clone)	Supplier/ CatN	Species	IgG	Clonality	Dilution IF	Dilution WB
AcTUB (6-11B-1)	Sigma-Aldrich (Merck) T7451	mouse	IgG2b	monoclonal	1:2000	1:2000
ALFA sdAb mouse-fc	NanoTag Biotechnologies N1582	camelid	IgG1	monoclonal	1:500	1:500
ARL13B	Proteintech 17711-1-AP	rabbit	IgG	polyclonal	1:1000	-
ARL13B	Clone N295B/66	mouse	IgG2a	monoclonal	1:1000	
FLAG (M2)	Sigma-Aldrich (Merck) F1804	mouse	IgG1	monoclonal	1:1000	1:1000
GAPDH (1E6D9)	Proteintech 60004-1-Ig	mouse	IgG2b	monoclonal	-	1:2000
GFP (3H9)	Proteintech (Chromotek) 3h9	rat	IgG2a	monoclonal	-	1:1000

GFP	self-made	rabbit	IgG	polyclonal	n.a.	1:500
FCAP33 Serum	self-made (Prof. Dr. Martin Jung)	rabbit	IgG	polyclonal	1:250-1:500	1:500
FLAG Serum	self-made (Prof. Dr. Martin Jung)	rabbit	IgG	polyclonal	-	1:500
Beta TUB	Abcam ab6046	rabbit	IgG	polyclonal	1:200	1:1000
Gamma TUB	Proteintech 66320-1-AP	mouse	IgG2a	monoclonal	1:5000	1:2000
Polyglutamylated TUB	GT335	mouse	IgG1	monoclonal	1:500	1:1000
Centrin	Millipore 20H5	mouse	IgG2a	monoclonal	1:1000	-
PRC1	Proteintech 15617-1-AP	rabbit	IgG	polyclonal	-	1:100
KIF23/MKLP1	Proteintech 28587-1-AP	rabbit	IgG	polyclonal	-	1:1000
ZO-1	Fisher Scientific 10129012 ZO1-1A12	rabbit	IgG	polyclonal	-	1:150
S-tag	Novagen® Merck 71549	mouse	IgG2b	monoclonal	1:1000	-
IFT88	Proteintech 60227-1-IG 4A4G5	rabbit	IgG	polyclonal	1:1000	-
FK2 Polyubiquitinylated proteins	Sigma, Anti-Ubiquitinylated proteins Antibody, clone FK2	mouse	IgG1	monoclonal	-	1:500
Beta Catenin	Proteintech 51067-2-AP	rabbit	IgG	polyclonal	-	1:100

Table 4: Secondary Antibodies and specifications for immunofluorescence

Antibody	**Supplier/ CatN**	**Host**	**Reactivity**	**Target Isotype**	**Dilution IF**

anti-mouse IgG1 Alexa Fluor™ 488	Thermo Fisher Scientific A-21121	goat	mouse	IgG1	1:500
anti-mouse IgG1 Cyanine3	Thermo Fisher Scientific M30010	goat	mouse	IgG1	1:500
anti-mouse IgG1 Cyanine5	Thermo Fisher Scientific A10524	donkey	mouse	IgG	1:500
anti-mouse IgG2a Alexa Fluor™ 488	Thermo Fisher Scientific A-21131	goat	mouse	IgG2a	1:500
anti -mouse IgG2a Alexa Fluor™ 555	Thermo Fisher Scientific A-21137	goat	mouse	IgG2a	1:500
anti -mouse IgG2a Alexa Fluor™ 647	Fisher Scientific A-21241	goat	mouse	IgG2a	1:500
anti -mouse IgG2b Alexa Fluor™647	Fisher Scientific A-21242	goat	mouse	IgG2b	1:500
anti-mouse IgG2b Alexa Fluor™ 488	Thermo Fisher Scientific A-21141	goat	mouse	IgG2b	1:500
anti-mouse IgG2b Alexa Fluor™ 555	Thermo Fisher Scientific A-21147	goat	mouse	IgG2b	1:500
anti-rabbit IgG Alexa Fluor™ 488	Thermo Fisher Scientific A-11008	donkey	rabbit	IgG	1:500
anti-rabbit IgG Alexa Fluor™ 647	Thermo Fisher Scientific A-21245	donkey	rabbit	IgG	1:500
anti-rabbit IgG Alexa Fluor™ plus555	Thermo Fisher Scientific A-31572	donkey	rabbit	IgG	1:500
Fluo-X2 anti-mNG Atto488	NanoTag Biotechnologies N3202-AT488-L	*Branchiostoma lance-olatume*	mNeon-Green	IgG2c	1:350

Phalloidin AF546	Fisher Scientific A22283	-	F-actin	-	1:400
SPY555 DNA	Tebu-bio SC201	-	DNA	-	2 x
SPY650 Tubulin	Tebu-bio SC503	-	Tubulin	-	2 x

Table 5: Secondary Antibodies and specifications for western blot

Antibody	**Supplier/ CatN**	**Host**	**Reactivity**	**Target Isotype**	**Dilution IF**
anti-rabbit IRDye® 800CW	LI-COR 926-32211	donkey	rabbit	IgG	- 1:10000
anti-rat IgG IRDye® 680RD	LI-COR 926-68073	goat	rabbit	IgG	- 1:10000
anti-mouse IRDye® 800 CW	LI-COR 926-32212	donkey	mouse	IgG	- 1:10000
anti-rat IgG IRDye® 800CW	LI-COR 926-32219	goat	rat	IgG	- 1:10000
anti-rabbit IgG HRP conjugate	Merck AP127P	goat	rabbit	IgG	- 1:2000

Table 6: Bacterial strains

Bacterial Strain	**Genotype**	**Supplier**
One Shot™ ccdB Survival™ 2 T1R Competent Cells	F*-mcrA Δ(mrr-hsdRMS-mcrBC) ϕ80lacZΔM15 ΔlacX74 recA1 araΔ39 Δ(ara-leu)7697 galU galK rpsL(Str) endA1 nupG fhuA::IS2	Thermo Fisher Scientific A10460
One Shot™ Mach1™ T1 Phage-Resistant Chemically Competent E. coli	F*- ϕ80(lacZ) Δ M15 ΔlacX74 hsdR(r*K*-, m*K*+) ΔrecA1398 endA1 tonA	Thermo Fisher Scientific C862003
XL1 Blue	recA1 end a1 gyrA96 thi-1hsdR17 supE44 relA1 lac [F' proAB laql^{q}ZΔM15 Tn10 (Tet^R)]	Stratagene (Anne Böwe)

Subcloning Efficiency™ DH5α Competent Cells	F*-ϕ80lacZΔM15 Δ (lacZYA-argF) U169 recA1 endA1 hsdR17(r*K*-, m*K*+) phoA supE44 thi-1 gyrA96 relA1	Thermo Fisher Scientific 18265017

Table 7: Buffers and solutions

Buffer/Solution	**Ingredients with final concentration**
Antigen retrieval buffer	100 mM Tris 5 % (v/v) Urea Adjust pH 9.5 water
APS	10 % APS in water
Blocking buffer (Immunofluorescence)	5% (v/v) Fetal bovine serum 3% (w/v) BSA 10% (v/v) PBS (10x) in water
BSA solution	10% (w/v) BSA In water Sterile filtered
Coomassie staining solution	40% (v/v) EtOH (100%) 10% (v/v) Glacial acetic acid 0.5% (w/v) Coomassie R in water
Coomassie Destaining solution	40% (v/v) EtOH (100%) 10% (v/v) Glacial acetic acid in water
DTT	1 M DTT in water
Denaturation buffer (Expansion)	200 mM SDS 200 mM NaCl 50 mM Tris, pH 9 (adjusted with HCL) in water
EDTA	500 mM EDTA in water (pH 8.0)
Hoechst	Stock solution: 10 mg/mL dH_2O Working solution: 2 µg/mL in 1xPBS

KPi buffer	For 0.1 M Potassium Phosphate: K_2HPO_4 1 M 80.2 mL KH_2PO_4 1 M 19.8 mL Add water to 1 L
Laemmli sample buffer (5x)	10% (w/v) SDS 50% (v/v) Glycerol 300 mM Tris/HCl (pH 6.8) 0.05% (w/v) Bromophenol blue in water
LICOR Revert Destaining solution	100 mM Sodium hydroxide 30% (v/v) MeOH (100%) in water
LICOR Revert Wash solution	6.7% (v/v) Glacial acetic acid 30% (v/v) MeOH (100%) in water
MG132	20 mM MG132
Monomer solution (Expansion)	19 % sodium acrylate 10 % AA 0,1 % BIS acrylamide 1 x PBS In water
MOPS (10x)	500 mM MOPS 500 mM Tris 1% (w/v) SDS 10.25 mM $Na_2EDTA*2H_2O$ in water (pH approx. 7.6)
NaCl	5 M NaCl In water
Nocodazole	10 mg/ml (30 mM) in water
PBS (10x)	27 mM KCl 18 mM KH_2PO_4 1369 mM NaCl 81 mM $Na_2HPO_4*2H_2O$ in water (pH 7.4 adjusted with HCl)
PFA (4%)	4% (v/v) PFA (16%) 10% (v/v) PBS (10x) in water

PHEM (4x)	60 mM PIPES 25 mM HEPES 10 mM EGTA 4 mM $MgSO_4$ pH7 with KOH
PKT-20 Lysis Buffer	10 mM Tris-HCl pH 8.0 10 µg/ml Proteinase K 2 mM EDTA pH 8.0 2 % Tween-20 in water
PMSF	200 mM PMSF in 100% EtOH
SAG	100 mM SAG in DMSO
SDS (10%)	10% (w/v) SDS in water
Sodium acrylate	38% sodium acrylate In water
Solubilization buffer (2x)	40 mM Tris-HCl pH 7,4 100 mM NaCl 20 % Glycerol 0,2 mM EDTA pH 8 dH_2O
Solubilization ALFA Elution buffer (1x)	2% (v/v) ALFA peptide (100x) in solubilization wash buffer (1x)
Solubilization (Lysis) buffer (1x)	1 x SB 0,6 % DDM 1 mM PMSF 1 x PIC (if no protease is used for elution) dH_2O
Solubilization wash buffer (1x)	1 x SB 0,05 % DDM 1 mM PMSF dH_2O
TAE buffer (50x)	500 mM Tris 5.7% (v/v) Glacial acetic acid (100%) 50 mM EDTA (500 mM, pH 8.0) in water
Tris/HCl	0.1 or 1 M Tris in water (pH 6.8, 7.5 or 8.5; all adjusted with HCl)

Triton X-100 (0.2%)	0.2% (v/v) Triton X-100 in water
Taxol (Paclitaxel)	10 mM in water
Transfer buffer (10x)	250 mM Tris 1920 mM Glycine in water (add 10% (v/v) EtOH (100%) when making 1x)
TBS (25x)	500 mM Tris/HCl 3.125 M NaCl in water (pH 7.5 adjusted with HCl)
TEMED	10% TEMED In water
Tris-HCl	1M Tris pH adjusted with HCl in water
Sodium Borate	1. M Sodium Borate pH adjusted to pH 9.0 in water

Table 8: Chemicals, Reagents, Solutions, Kits and Consumables

Chemicals, Reagents, Solutions, Kits, Consumables	**Supplier**
2-Propanol	VWR International 20842.323
10-cm Dish (Greiner CELLSTAR® dish, Tissue Culture Dish, diam. x H 100 mm x 20 mm)	Greiner Bio-One 664160
15-cm Dish (Greiner CELLSTAR® dish, diam. x H 145 mm x 20 mm)	Greiner Bio-One 639160
6-well Plate (Greiner CELLSTAR®, TC)	Greiner Bio-One 657160
24 well (Greiner CELLSTAR®, TC)	Greiner Bio-One 662160
Bovine Calf Serum	Sigma-Aldrich 12133C-500ML
BAMBANKER® serum-free cell freezing medium	Wako Chemicals 302-14681
Acrylamide	Carl Roth 7906.2
Acrylamide solution, 40%	Sigma-Aldrich A4058

ALFA peptide (#1787)	Martin Jung
ALFA Selector PE incl. ALFA elution peptide	Nano-Tag N1510
Alkyne-phenol	Hölzel Biotech HY-131442
APS (Ammonium peroxydisulphate)	Grüssing 10316250U
Ammonium sulfate >99,5% p.a.	Grüssing GmbH Analytica 101551000U
Bacto™ Agar soldifying agent	BD Diagnostics 214010
Bacto™ Yeast extract	BD Diagnostics 212720
Pierce™ BCA® Protein Assay Kits and Reagents	Fisher Scientific 10741395
BIS-TRIS Bis-(2-hydroxyethyl)-imino-tris-(hydroxymethyl)-methane	Carl Roth 9140.8
Bromophenol Blue sodium salt	SERVA 15375
BSA (Bovine Serum Albumin Fraction V, IgG free)	Carl Roth 3737.3
Carl Zeiss™ Immersol™ Immersion oil	Fisher Scientific 10539438
Counting chamber Hirschmann™	Fisher Scientific 10200872
Complete™ EDTA-free Protease Inhibitor Cocktail tablets	Sigma-Aldrich 5056489001
Coomassie Brilliant blue G 250	SERVA 35050
DDM (n-dodecyl--D-maltoside#9	Avanti Polar Lipids 850520P-5g
DMSO (Dimethylsufoxid)	Carl Roth 4720.1
DMP (dimethyl palmitate)	Thermo Scientific™ 21667 CAS 58537-94-3
dNTP Deoxynucleotide solution mix	New England Biolabs N0447S
DTT (1,4-Dithiothreitol)	Fisher Scientific 10578170
EDTA (Ethylenediaminetetraacetic acid disodium salt dihydrate)	Carl Roth 8043.2
EGTA (Ethylene Glycol Bis(-aminoethylether) tetraacetic acid)	Carl Roth 3054.1
Ethanol,99% denatured with 1% methyl ethyl ketone	BCD Chemie 10012343
Ethanol, absolute	Geyer 2273.1000
E-Plate 96 (xCELLIGENCE)	Agilent 5232368001
Formaldehyde solution, 36.5-38%	Sigma-Aldrich F8775

FBS (Gibco™ Fetal Bovine Serum, qualified, E.U.-approved, South America origin)	Fisher Scientific 11573397
FCAP33-Peptide (#1706)	Martin Jung
Fluoromount-G™ Befestigungsmedium	Invitrogen™ 15586276
Formaldehyde, 16%	Invitrogen™ 11586711
Formaldehyde	Polysciences 18814-20 (FA, 36.5-38%, F8775, SIGMA)
Formic acid	Thermo Fisher Scientific 85178
GFP Selector	NanoTag Biotechnologies N0310
Glacial acetic acid	Carl Roth 6755.1
Glycine Pufferan	Carl Roth 3908.3
Glyerol	Sigma-Aldrich G5516
Gibson Assembly® Master Mix	New England Biolabs E2611S
Gibco™ Bacto™ tryptone	Fisher Scientific 16279751
Gibco™ DMEM, high glucose, pyruvate	Fisher Scientific 11594486
Gibco™ DMEM/F-12, HEPES	Fisher Scientific 11594426
Gibco™ DMEM/F-12, HEPES	Fisher Scientific 11039021
Gibco™ TBS, pH 7.2	Fisher Scientific 11530546
Gibco™ Trypsin-EDTA (0.05%), phenol red	Fisher Scientific 11580626
HEPES	
Hoechst 33342	Fisher Scientific 1154876
Lipofectamine™ RNAiMAX Transfection Reagent	Thermo Scientific 13778150
Jetprime® DNA and siRNA transfection reagent	VWR International 101000046.
KIMTECH Precision Wipes	Kimberly-Clark 0511-7552
Macherey-Nagel™ NucleoBond™ Xtra Midi	Fisher Scientific 1279840
Macherey-Nagel™ NucleoSpin™ Plasmid Columns	Fisher Scientific 12353358
Macherey-Nagel™ NucleoSpin™ Gel- and PCR Cleanup	Fisher Scientific 12303368
Magnesiumchloride hexahydrate	Carl Roth 2189.2
Magnesium Sulfate Heptahydrate	Sigma-Aldrich M2773
MOPS (3-(N-Morpholino)-propane sulphonic acid)	Carl Roth 6979.3

Magnesium sulfate Heptahydrate ($MgSO_4$ * $7H_2O$)	SIGMA M-2773
MicroAmp™ Fast Optical 96-Well Reaction Plate with Barcode, 0.1 ml	Thermo Fisher Scientific Inc., Waltham, USA
MicroAmp™ Clear Adhesive Film	Thermo Fisher Scientific Inc., Waltham, USA
Monarch PCR and DNA Cleanup Kit	New England Biolabs (NEB) T1030
N,N'-Methylenebisacrylamide solution,for electrophoresis, 2% in H2O	Sigma-Aldrich M1533
Opti-MEM I Reduced-Serum Medium (1X)	Fisher Scientific 10149832
Parafilm	Carl Roth H666.1
PMSF (Phenylmethylsulfonylfluorid)	Carl Roth 6367.1
PIPES PUFFERAN ® ≥99 %	Carl Roth GmbH 9156.2
Potassium Chloride	Sigma-Aldrich P-9541
Potassium Phosphate K_2HPO_4 Dibasic	Grüssing GmbH 120321000
Potassium KH_2PO_4 Monobasic	Grüssing GmbH 120171000U
Protein-A-Agarose	Fisher Scientific 11836754
Poly-D-Lysine	Fisher Scientific A3890401
Potassium dihydrogen phosphate	Grüssing 120171000
Phusion Polymerase	M0530S
Peqlab peqGREEN DNA/RNA dye	VWR International 732-3196
QuantiTect SYBR Green PCR Kit	Qiagen 204143
QuantiTect Primer Assay Mm-Gm11992_2_SG	Qiagen 249900 Id: QT01553454
QuantiTect Reverse Transcription Kit	Qiagen 205311
Q5® High-Fidelity DNA Polymerase	New England Biolabs M0494S
Quick Ligation	New England Biolabs M2200S
Rneasy Mini Kit	Qiagen 74104
SAG (dihydrochloride Smoothened Agonist)	Sigma-Aldrich SML1314-1MG
SDS (Sodium dodecyl sulfate)	AppliChem A2572,1000
Sodium Borate	Riedel-de Haën 13573
Sodium azide	Carl Roth K305.1
Skimmed milk powder	Sucofin
Sodium acrylate	Sigma-Aldrich 408220

Sodium azide	Carl Roth K305.1
Sodium chloride	Fisher Scientific 10428420
Sodium hydroxide	Merck 6498
SuperSignal™ West Pico Plus Chemiluminescent Substrate	Fisher Scientific 34580
Taq DNA Ligase	M0208S
TCA (Trichloroacetic acid)	Carl Roth 8789.4
TEMED (Tetramethylethylendiamine)	Carl Roth 2367.1
Tricine	Sigma-Aldrich T-5816-25g
TRIS Pufferan	Carl Roth AE15.1
Triton-X100	Thermo Fisher Scientific A16046.AP
Tween® 20	Carl Roth 9127.2

Table 9: Cell lines

Cell line	Parental	Expression of	Reference
HEK 293 T wildtype (human) IMCD3 WT	HEK 293 T wildtype (human)	None	Pauline Schepsky
IMCD3 Flp-In™ wildtype (mouse)	IMCD3 Flp-In™ wildtype (mouse)	None	Mukhopadhyay 2010
NIH/3T3 Flp-In™ wildtype (mouse)	NIH/3T3 Flp-In™ wildtype (mouse)	None	ThermoFisher Scientific R76107
RPE FRT/To	RPE-1 Flp-In™ T-REx™	None	ATCC CRL-4000
$FCAP33^{FLAG}$-Pool1	IMCD3 Flp-In™	EF1α-Gm11992-Myc-DDK	This work
$\alpha TAT1^{-/-}$ $FCAP33^{FLAG}$-Pool1	$\alpha TAT1^{Crsipr}$	EF1α-Gm11992-Myc-DDK	This work
$\alpha TAT1^{-/-}$ $FCAP33^{FLAG}$-Pool2	$\alpha TAT1^{Crsipr}$	EF1α-Gm11992-Myc-DDK	This work
$\alpha TAT1^{-/-}$ $FCAP33^{FLAG}$-Pool3	$\alpha TAT1^{Crsipr}$	EF1α-Gm11992-Myc-DDK	This work

SSTR3^{NG}	IMCD3 Flip-In^{TM}	AP-SSTR3-NG	(Nager et al., 2017)
FCAP33^{FLAG}	IMCD3 Flp-In™	EF1α-Gm11992-Myc-DDK	This work, Tommy Sroka
FCAP33^{NG} (Pool2)	IMCD3 Flp-In™	pCMVΔ6-Gm11992-mNG-V5	This work
FCAP33$^{1-167}$-NG/ FCAP33^{NG} N-term	IMCD3 Flp-In™	pCMVΔ6-Gm11992$^{1-167}$-mNG-V5	This work
FCAP33$^{168-288}$-NG/ FCAP33^{NG} C-term	IMCD3 Flp-In™	pCMVΔ6-Gm11992$^{168-288}$-mNG-V5	This work
FCAP33^{cLAP}-(C6) (standard cell line)	IMCD3 Flp-In™	EF1α-Gm11992-eGFP	This work (for simplification usually referred to as FCAP33^{cLAP})
FCAP33^{cLAP}-Pool 4	FCAP33^{Crsipr}-C1	EF1α-Gm11992-eGFP	This work
FCAP33^{cLAP}Crispr-Pool 4	FCAP33^{Crsipr}-C1	EF1α-Gm11992-eGFP	This work
FCAP33^{cLAP}Crispr-C7	FCAP33^{Crsipr}-C1	EF1α-Gm11992-eGFP	This work
FCAP33$^{1-167}$-cLAP/ FCAP33^{cLAP}N-term C10	IMCD3 Flp-In™	EF1α- Gm11992$^{1-167}$-eGFP	This work, Sabrina Ehr
FCAP33$^{1-167}$-cLAP C11	IMCD3 Flp-In™	EF1α- Gm11992$^{1-167}$-eGFP	This work, Sabrina Ehr
FCAP33$^{1-167}$-cLAP C12	IMCD3 Flp-In™	EF1α- Gm11992$^{1-167}$-eGFP	This work, Sabrina Ehr
FCAP33$^{1-167}$-cLAP/ Pool1	IMCD3 Flp-In™	EF1α- Gm11992$^{1-167}$-eGFP	This work, Sabrina Ehr
FCAP33$^{1-167}$-cLAP/ pool2	IMCD3 Flp-In™	EF1α- Gm11992$^{1-167}$-eGFP	This work, Sabrina Ehr
FCAP33$^{168-288}$-cLAP/ FCAP33^{cLAP}C-term C27	IMCD3 Flp-In™	EF1α- Gm11992$^{168-288}$-eGFP	This work

FCAP33$^{168\text{-}288}$-cLAP C28	IMCD3 Flp-In™	EF1α- Gm11992$^{168\text{-}288}$-eGFP	This work
FCAP33$^{168\text{-}288}$-cLAP C29	IMCD3 Flp-In™	EF1α- Gm11992$^{168\text{-}288}$-eGFP	This work
FCAP33$^{168\text{-}288}$-cLAP pool 21	IMCD3 Flp-In™	EF1α- Gm11992$^{168\text{-}288}$-eGFP	This work
FCAP33$^{168\text{-}288}$-cLAP pool 22	IMCD3 Flp-In™	EF1α- Gm11992$^{168\text{-}288}$-eGFP	This work
FCAP33^{ALFA}	IMCD3 Flp-In™	pCMVΔ6-Gm11992-ALFA	This work, Patrick Schuster

Table 10: List of Crispr Cell Lines generated

KO/Crispr Cell line	Parental	CRISPR target	Comments	Reference
αTAT1$^{-/-}$	MEFs from αTAT1$^{-/-}$ mice	αTAT1		(Aguilar et al., 2014)
FCAP33^{Crsipr}-C1	IMCD3 Flp-In™	Gm11992 Exon 2	Sequence “breaks” (manual analysis with ApE) WT sequence overlay	This work, Lea Sanwald
FCAP33^{Crsipr}-C2	IMCD3 Flp-In™	Gm11992 Exon 2	1 allele WT sequence, mixed sequence	This work, Lea Sanwald
FCAP33^{Crsipr}-Pool1	IMCD3 Flp-In™	Gm11992 Exon 2	No clear sequence, overlay of several	This work, Lea Sanwald
FCAP33^{Crsipr}-C4	IMCD3 Flp-In™	Gm11992 Exon 2	C insertion, leads to frameshift	This work, Lea Sanwald
FCAP33^{Crsipr}-C6	IMCD3 Flp-In™	Gm11992 Exon 2	Sequence “breaks”	This work, Lea Sanwald
FCAP33^{Crsipr}-C7	IMCD3 Flp-In™	Gm11992 Exon 2	1 allele WT sequence, mixed sequence	This work, Lea Sanwald

FCAP33^{Crsipr}-C12	IMCD3 Flp-In™	Gm11992 Exon 4	1 allele most likely WT sequence, (manual analysis with ApE)	This work, Avishek Prasai
FCAP33^{Crsipr}-C16	IMCD3 Flp-In™	Gm11992 Exon 4	1 allele most likely WT sequence, (manual analysis with ApE)	This work, Avishek Prasai
FCAP33^{Crsipr}-C19	IMCD3 Flp-In™	Gm11992 Exon 4	No sequence yet	This work, Avishek Prasai
FCAP33^{Crsipr}-C22	IMCD3 Flp-In™	Gm11992 Exon 4	1 allele most likely WT sequence, (manual analysis with ApE)	This work, Avishek Prasai
FCAP33^{Crsipr}-P1-1	IMCD3 Flp-In™	Gm11992 Exon 4	WT Sequence	This work, Avishek Prasai
FCAP33^{Crsipr}-P1-2	IMCD3 Flp-In™	Gm11992 Exon 4	WT Sequence	This work, Avishek Prasai
FCAP33^{Crsipr}-P2-1	IMCD3 Flp-In™	Gm11992 Exon 4	WT Sequence	This work, Avishek Prasai
FCAP33^{Crsipr}-P2-2	IMCD3 Flp-In™	Gm11992 Exon 4	WT Sequence	This work, Avishek Prasai

Table 11: Primer

Name	**Direc-tion**	**Sequence 5'-3'**
oTS027	FWD	TACAAAAAAGCAGGCTCCACGCCACCATGAGGAACACCAGCAAG
oTS035	REV	tttgtacaagaaagctgggtgTGCTGGCGTTGATTCTGATG
p670	REV	tttgtacaagaaagctgggtgCTTCACATTTTCAAGCTCC
p759	FWD	tacaaaaaagcaggctccacgccaccATGAGAAAGGTGAAACTGCCAG
p757	FWD	agggtGTCGACttAGAAAGGTGAAACTGCCAG
p758	REV	ttGCGGCCGCTCACTTCACATTTTCAAGCTCC
oTS073	FWD	CTCCAGGGCTTCTGTACTCTGT
FCAP33_Exon2_rev	REV	CTGAGACATCTGAGATGTGGTC
FWD_r2_FCAP33_long	FWD	CTGTTGTTCTGGGGATCCTG
FWD_r2_FCAP33	FWD	gagactatagagggagggagc

REV_r2_FCAP33	REV	AAGCAGACGCAGATGATGGC
REV_r2_FCAP33_long	REV	GGGAGCAGAGAACTCAGATC

Plasmid Lab ID Personal ID	Description	Insert	Backbone	Method	Primer for PCR	Cells for cloning	Bacterial host	Bacterial Resistance	Mammalian Resistance	Reference
pDaM429 pTS023	FCAP33 (Gm11992) Entry vector	pENTR4-Kozak-Gm11992-NoStop	pENTR4	N.a.	N.a.	N.a.	Mach1	KanR	N.a.	Lab
pDaM442 pTS039	mNG-tag Destination vector	pEF5B-CMVΔ6-DEST-mNeongreen	pEF5B-CMVΔ6-DEST	N.a.	N.a.	N.a.	DB3.1	AmpR, CamR	BlastR	Tommy Sroka
pDaM447 pTS052	Destination FCAP33 full-length FLAG-tag	pEF5B-EF1alpha-Gm11992-Myc-DDK (FLAG)	pENTR4	N.a.		Mach1	DB3.1	AmpR	BlastR	Lab
pDaM611	Entry vector with attL sites	N.a.	pENTR4	N.a.	N.a.	N.a.	DB3.1	KanR	N.a.	Lab
pDaM655	LAP-tag Destination vector	cLAP (GFP-HRV3C-S-tag)	pEF5B/FRT/DEST	N.a.	N.a.	N.a.	DB3.1	AmpR, CamR	BlastR	Lab
pDaM681 pMN2412	CMVd6 Destination vector	N.a.	pEF5b CMVd6pro DEST	N.a.	N.a.	N.a.	DB3.1	AmpR, CamR	BlastR	Lab
pDaM737 pVC21	CMVΔ6-Gm11992-mNeongreen	FCAP33 (Gm11992) pTS023 (pDaM429)	pDaM438 (pTS032)	LR reaction pDaM433 with pDaM442/pTS039	N.a.	DB3.1	DB3.1	AmpR, CamR	BlastR	VC/Sabine Plant
pDaM797 pVC25	Entry full length FCAP33	FCAP33 (Gm11992) pTS023 (pDaM429) PCR Full length	pDaM611 pENTR4	Gibson with NcoI, XbaI digested pDaM611	oTS027 oTS035	DH5alpha	DB3.1	KanR	N.a.	VC/Sabine Plant
pDaM798 pVC26	Entry n-term FCAP33	FCAP33 (Gm11992) pTS023 (pDaM429) PCR n-term	pDaM611 pENTR4	Gibson with NcoI, XbaI digested pDaM611	oTS027 p670	DH5alpha	DB3.1	KanR	N.a.	VC/Sabine Plant
pDaM799 pVC27	Entry c-term FCAP33	FCAP33 (Gm11992) pTS023 (pDaM429) PCR c-term	pDaM611 pENTR4	Gibson with NcoI, XbaI digested pDaM611	p759 oTS035	DH5alpha	DB3.1	KanR	N.a.	VC/Sabine Plant
pDaM809 pVC30	Destination Full length FCAP33 cLAP-tag	FCAP33 (Gm11992) pTS023 (pDaM429)	pDaM655	LR reaction pDaM797/pVC25 with pDaM665	N.a.	Mach1	DB3.1	AmpR, CamR	BlastR	VC/Sabine Plant
pDaM827 pVC31	Destination n-term FCAP33 cLAP-tag	FCAP33 (Gm11992) PCR n-term pVC26	pDaM655	LR reaction pDaM798/pVC26 with pDaM665	N.a.	Mach1	DB3.1	AmpR, CamR	BlastR	VC/Sabine Plant
pDaM828 pVC32	Destination c-term FCAP33 cLAP-tag	FCAP33 (Gm11992) PCR c-term pVC27	pDaM655	LR reaction pDaM798/pVC27 with pDaM665	N.a.	Mach1	DB3.1	AmpR, CamR	BlastR	VC/Sabine Plant
pDaM878	Destination FCAP33 full-length ALFA-tag	FCAP33 (Gm11992) ALFA	pDaM681	LR reaction pDaM429 with pDaM681	N.a.	Mach1	DB3.1	AmpR, CamR	BlastR	Patrick Schuster
pDaM794 pVC22	Destination FCAP33 full-length mNG-tag	FCAP33 (Gm11992) from pVC25	pDaM442 (pTS039)	LR reaction pDaM797/pVC25 with pDaM442/pTS039	N.a.	XL1-blue	DB3.1	AmpR, CamR	BlastR	VC/Sabine Plant
pDaM795 pVC23	Destination FCAP33 n-term mNG-tag	FCAP33 (Gm11992) from pVC26	pDaM442 (pTS039)	LR reaction pDaM798/pVC26 with pDaM442/pTS039	N.a.	XL1-blue	DB3.1	AmpR, CamR	BlastR	VC/Sabine Plant
pDaM796 pVC24	Destination FCAP33 c-term mNG-tag	FCAP33 (Gm11992) from pVC27	pDaM442 (pTS039)	LR reaction pDaM799/pVC27 with pDaM442/pTS039	N.a.	XL1-blue	DB3.1	AmpR, CamR	BlastR	VC/Sabine Plant

Table 12: List of cloned plasmids

Results

FCAP33 was found in the proteome of primary cilia of mouse IMCD3 (IMCD3 WT) cells. This protein seemed to be a primary cilia specific protein, as it was not found in the control cell line. FCAP33 was highly enriched in a first proteomic dataset (APEX2 system, unpublished Data). FCAP33 could be confirmed as an enriched hit in the more sensitive iAPEX system, where the peptide count was even higher (8 peptides), making it an even more confident hit. To start this project and investigate this new ciliary protein, the localization of FCAP33 to primary cilia was assessed.

To confirm the localization of FCAP33 to primary cilia in IMCD3 cells, immunofluorescence (IF) experiments were performed with IMCD3 WT cells or IMCD3 cells stably expressing tagged FCAP33: (1) FCAP33^{FLAG}: FCAP33 fused to a FLAG-tag for IF staining and immunoprecipitation (IP), (2) FCAP33^{NG}: FCAP33 fused to a green fluorescent neon green protein (mNG) for live cell imaging, IF and IP, (3) FCAP33^{cLAP}: FCAP33 fused to a localization and purification (LAP) tag consisting of an S-tag, a cleavage site (HRV3C) and a green fluorescent protein (GFP), which can both be used for IP and for visualization. The GFP is suitable for live cell imaging and the protease cleavage site between the S-tag and the GFP allows for several IP methods. All tags are on the C-terminus of FCAP33. In this whole study, all cell lines stably expressing FCAP33 constructs were generated using the FlipIn system (see methods). The wildtype control cell line is always IMCD3 cells with FlipIn locus and will for simplification only be termed “IMCD3 WT”. Regarding this, all cell lines do express the endogenous FCAP33 as well as the fusion constructs, which results in overexpression of FCAP33 in these cells. If cell lines were generated in a non-wildtype background this will be indicated.

FCAP33 localizes to primary cilia

Ciliation was induced by serum-starvation and the localization of all different FCAP33 fusion constructs to primary cilia was confirmed. FCAP33^{NG} and FCAP33^{FLAG} colocalized with the ciliary membrane protein ADP-ribosylation factor like protein 13b (ARL13b) or the axonemal protein acetylated tubulin (AcTUB) as cilia marker. FCAP33^{FLAG} and FCAP33^{NG} were visualized by antibody staining (Figure 2 B and C). For FCAP33^{cLAP} the fluorescence of the green fluorescent protein (GFP) in the LAP tag was used for imaging.

To characterize the newly identified protein in mouse cells, an antibody against a small peptide in the mouse sequence of the protein was generated by Apl.-Prof. Martin Jung. Staining with

the antibody additionally confirmed FCAP33 localization in FCAP33^{NG} cells (Figure 2 B) but the signals in FCAP33^{FLAG} (Figure 2 C) seemed to be weaker.

Using the FCAP33 antibody to detect FCAP33 in WT cells, did not show specific signal of endogenous FCAP33 in primary cilia (Figure 2 A). Neither in IMCD3 cells or 3T3 cells (mouse cell line). Interestingly, antibody staining showed aggregate or condensate-like structures in the nucleus, that can also be detected in FCAP33^{NG} and FCAP33^{FLAG} cells but do not colocalize with antibody staining against mNG or FLAG. The structures within the nucleus resemble a nucleolus staining (Boisvert et al., 2007), but the lack of a nucleolus marker does not allow a confirmation of nucleolus localization (Figure 2 A).

Looking more deeply into these first IF images, it can be determined that there are structures, lacking ARL13b, between two nuclei, that contain FCAP33 or tag signal. These structures are so-called midbodies. FCAP33^{FLAG} (Figure 2 C) and FCAP33^{NG} (Figure 2 B, cycling cells) localize to these structures, which are indicated by arrows. Midbodies are remnants of the central spindle (see Introduction, Spindle and midbody formation during mitosis). In the middle of the midbody, antiparallel microtubules are densely packed (stem body) which makes these structures rarely accessible for antibody staining. The intrinsic neon green fluorescence of FCAP33^{NG} is also visible at these densely packed stem body structure (Figure 2 B, cycling cells). FCAP33 antibody staining additionally confirms the localization of the tagged proteins to the arms of the midbody (Figure 2 C, middle lane).

When performing IF experiments with the FCAP33^{NG} cells cilia appear longer than IMCD3 WT cilia. Yet, measuring cilia length in FCAP33^{NG} and comparing it to WT and FCAP33^{FLAG} did not show any statistically significant change in length between WT and the mNG tagged variant (Figure 2 D). This was also true for 3T3 WT cells. Even though the multiple comparison test using one-way ANOVA showed a significant difference between FCAP33^{FLAG} and WT cells, the length effect was only minor. Looking at the violin plots it can be noted that there is indeed a population with longer cilia in FCAP33^{NG} even though the mean length is not significantly different to WT (Figure 2 D left panel). Length measurements were made using ARL13b as cilia marker. In addition to the ciliary length, the ciliation rate was determined. Performing this analysis for six images and running again a multiple comparison test between

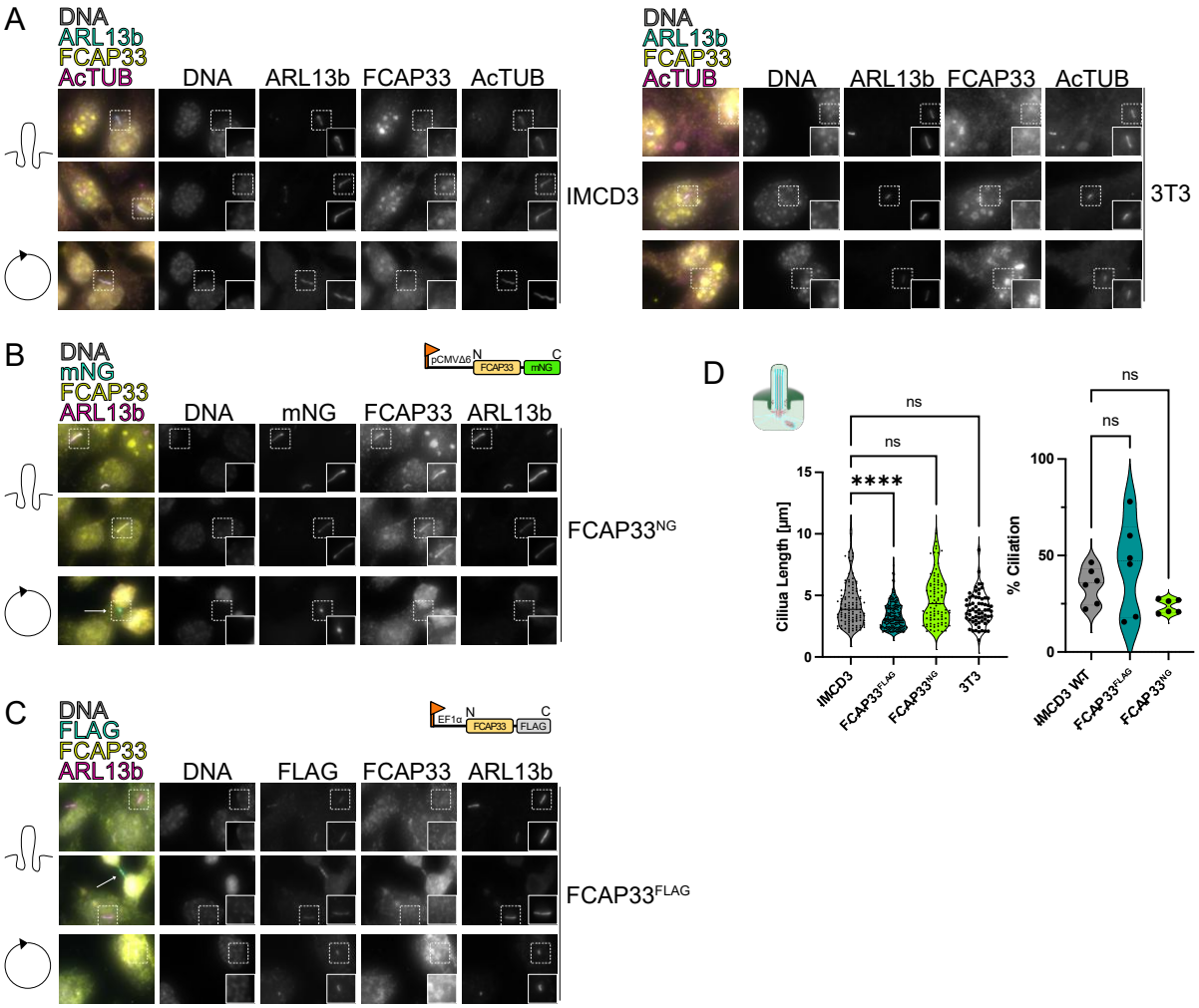

Figure 2: Localization of FCAP33 to primary cilia and midbody structures

(A) IF staining of IMCD3 WT and 3T3 cells. Staining for endogenous FCAP33 (yellow), acetylated tubulin (AcTUB) and ARL13b, cyan as cilia marker. (B + C) IF staining of tagged FCAP33. Staining for endogenous FCAP33 (yellow), ARL13b (magenta) as cilia marker and FLAG (cyan). NeonGreen was visualized by intrinsic fluorescence. Variants co-localize with ARL13b positive cilia and midbodies, shown by mNG fluorescence, FLAG staining and FCAP33 staining. (D) Cilium length measured using CiliaQ and ARL13b as cilium mask. Ciliation rate was measured by an automated tool to detect nuclear and cilia signal. Cilia over nuclei were quantified within one image and used to determine the ciliation rate.

IMCD3 WT and overexpressing cell lines, did show differences that were not statistically significant (Figure 2 D, right panel).

FCAP33 localizes to midbodies and co-localizes with different tubulin modifications

The signals of FCAP33 were not detectable in WT cells in primary cilia, and the signals of FCAP33^{FLAG} and the FCAP33^{NG} cell line were rather low. Therefore, a higher expressing FCAP33^{cLAP} cell lines was examined in IF. The expression of FCAP33^{NG} is promoted by a

weaker promotor commonly used for ciliary proteins, whereas the expression of FCAP33^{cLAP} is promoted a higher expressing promoter than FCAP33^{NG} (Figure 3, cartoons). Primary cilia localization of tagged FCAP33 was confirmed by co-localization with ARL13b (Figure 2) and AcTUB (Figure 3). In addition to the ciliary signal, FCAP33^{cLAP} and FCAP33^{NG} localized to midbodies (MBs) including the stem body (SB), also marked by AcTUB staining (Figure 3 A-C, indicated by green arrows). As midbodies are remnants of the spindle apparatus after cell cleavage, the association of FCAP33 with the spindle and spindle poles was investigated by staining with AcTUB, beta tubulin (bTUB, Figure 3 C) and gamma tubulin (gTUB, Figure 3 A). FCAP33^{cLAP} could be detected at spindle structures but with weak signals (Pink arrows Figure 3 A+C and indicated by midbody cartoons). FCAP33^{NG} did not show colocalization with the spindle markers (AcTUB and bTUB, Figure 3 C, spindle). In both cell lines there was no FCAP33 signal at the gTUB positive basal body or daughter centriole but a weak signal for FCAP33^{cLAP} (Figure 3 A) overlapping with the spindle fraction of gTUB (Figure 3 A + B, spindle). Interestingly, especially in FCAP33^{NG} cells it seemed, that FCAP33 accumulates at the opposite site of gTUB at the primary cilium tip in some cilia. Polyglutamylated tubulin (PolyTUB), a post translational modification of tubulin more prominently found at the ciliary base (He et al., 2017), co-localized with FCAP33 but the FCAP33 signal can be seen along the whole primary cilium (Figure 3 B). To validate the localization of FCAP33 to MB and SB structures, not only marked by tubulin staining, specific marker proteins were used to detect MBs in IF. Staining for MKLP1/KIF23 the kinesin like protein 23, which is a component of the Centralspindlin complex and a plus end directed motor enzyme that moves on antiparallel MTs. Therefore, it marks the SB region of the MB. Additionally, we used PRC1 (protein regulator of cytokinesis), which also crosslinks anti-parallel MTs and is essential for controlling the formation of the midzone and the successful cytokinesis (Introduction: Spindle and midbody formation during mitosis). Both proteins, KIF23 and PRC1 localized to parts of the SB and PRC1 also colocalized with AcTUB in the midbody arms. KIF23 has a SB surrounding pattern with FCAP33^{cLAP} localizing to the center of KIF23 (Figure 3 D). In our hands, PRC1 was rather localized to the MB arms, where it co-localized with FCAP33^{cLAP}. This confirmed the localization of FCAP33 to midbodies (Figure 3 D+E). Due to the available antibodies, which were all raised in rabbit, endogenous FCAP33 could not be stained in parallel to KIF23 and PRC1.

In summary, FCAP33 was confirmed to localize to the primary cilium in cells expressing tagged FCAP33. In these cells it also localized to midbodies and slightly to the spindle. In

addition to the uniform primary cilium distribution some cilia exhibited a ciliary tip signal in FCAP33^{NG} cells (Figure 3 A). The gamma tubulin staining (Figure 3 A) indicates the base of

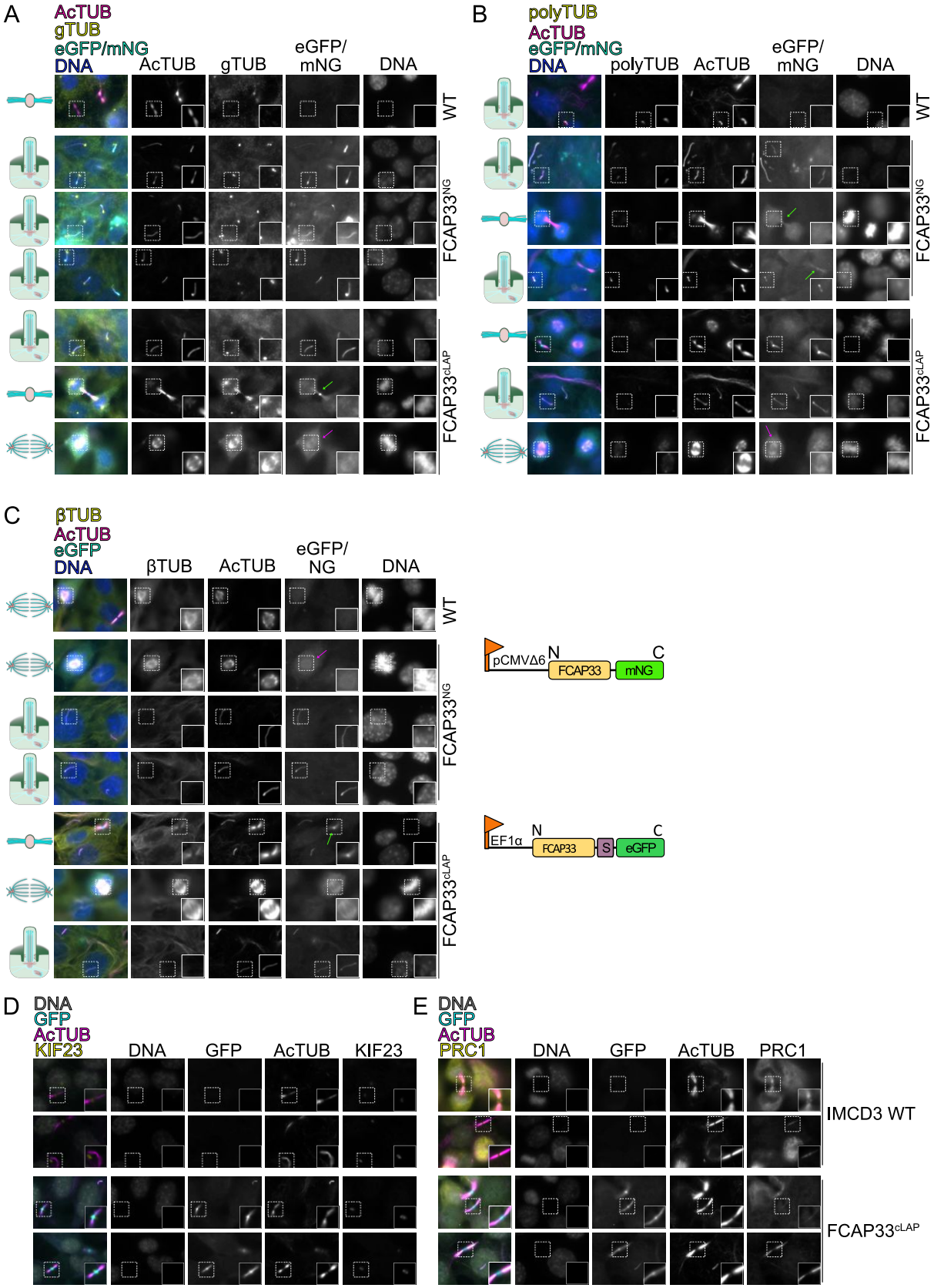

Figure 3: Co-localization of FCAP33 with different tubulin structures and tubulin modifications throughout the cell cycle.

Immunofluorescence images of tubulin modifications and midbody proteins for c-localization analysis. (A-C) FCAP33 is visualized by eGFP or mNG fluorescence and co-stained with

AcTUB (A) gamma tubulin (gTUB) or (B) polyglutamtylated tubulin (polyTUB) or (C) beta tubulin (ßTUB) as tubulin marker. DNA was stained for visualization of nuclei and dividing cells. (D+ E) IF Experiment performed by S. Ehr. FCAP33 is visualized by eGFP and co-stained with the midbody protein KIF23 (D) or PRC1 (E) and AcTUB as tubulin marker. Green arrows indicate stem body region; pink arrows indicate spindles.

the primary cilium. For some cilia, there is a stronger FCAP33 signal at the distal end distal end of the axoneme, not marked by gamma tubulin (Figure 3 A, FCAP33^{NG} cell line).

FCAP33 is expressed at low levels in IMCD3 cells and overexpression of FCAP33 induces cilium lengthening

From the proteomic study it was already expected that FCAP33 most likely is not present at high levels in primary cilia. As shown in Figure 2, FCAP33 could not be detected via antibody staining in IF IMCD3 WT cells (confirmed by M. Sc. student Shanli Seyed Tarrah).
Next, I wanted to confirm that the observed absence of endogenous FCAP33 in WT primary cilia is because of low levels of the protein and therefore due to detection limitations and not caused by the lack of the protein to localize to cilia in IMCD3 WT cells. To test this hypothesis and to indirectly test the specificity of the antibody, we performed knock down (KD) experiments using small inferring RNA (siRNA).

Using FCAP33 KD, we aimed to see a reduction of FCAP33 of either FCAP33^{FLAG} or FCAP33^{NG} by using the antibody in Immunofluorescence (IF) or Western Blot (WB) experiments as well as performing qPCR to test the reduction of FCAP33 on mRNA levels. Upon treatment of the different cell lines with siRNA, we could show, that in WB (Figure 4 A) and in IF (Figure 4 B) tagged FCAP33 was reduced even though FCAP33 could still not be detected in WT cells (Figure 4 A and 4 C) neither in WB, nor in IF (Figure 4 A and B). WB signals were also quantified and normalized to the GAPDH loading control (Figure 4 A, bar graph), which shows the lack of signal in IMCD3 WT and the reduction of FCAP33 in the tagged cell lines (FCAP33^{NG} and FCAP33^{FLAG}) using siRNA (siFCAP33) compared to the control (siCRTL) (Figure 4 A). Interestingly, we detected some higher molecular weight bands (at 185 kDa, red arrow and ~ 80 kDa), that were reduced upon siRNA treatment in all cell lines tested. This experiment, therefore, showed that indeed, we can visualize the reduction overexpressed FCAP33 using the FCAP33 antibody on WB and IF levels.
To further validate the reduction of FCAP33 using siRNA, RT-qPCR was used to investigate mRNA levels. This revealed a reduction in the relative expression (RQ value) of FCAP33 after KD (siFCAP33, light green) and no reduction in the control (siCRTL, light red) cells (Figure

4 D) compared to the IMCD3 WT (gray) control. Additionally, we detected massive levels of FCAP33 in FCAP33^{NG} cells compared to WT. Untreated IMCD3 WT and siCRTL cells showed similar levels of FCAP33 (Figure 4 D).

To investigate the role of FCAP33, we wanted to investigate if knocking out FCAP33 does lead to phenotypes in IMCD3 cells. In order to create stable cell lines lacking FCAP33 for future experiments, Lea Sanwald designed guide RNAs for CRISPR/Cas 9 mediated knockouts (KO) targeting either Exon 2 or Exon 4. After selecting IMCD3 cells efficiently transfected with the Crispr Cas plasmid, single clones or pools of IMCD3 cells expressing the Crispr plasmid were sorted. Only the IMCD3 WT cells where Exon 4 was targeted, recovered after sorting. We had two potential KO clones (FCAP33^{Crsipr}-C1 and FCAP33^{Crsipr}-C2) and one pool (FCAP33^{Crsipr}-Pool1) that could successfully be cultured. To validate if the knockout of FCAP33 was successful, genomic DNA (gDNA) was extracted from those cells, and sent for sequencing. Sequences were aligned to the WT sequence using the free software Benchling to check for a deletion or insertion or frameshift. For further analysis of whether the clones and the Pool to be a KO, the free open-source software TIDE (http://shinyapps.-datacurators.nl/tide/) was used. This software allows to compare the WT sequence to the potential KO sequences. Benchling alignments showed that FCAP33^{Crsipr}-C2 contained the the WT sequence which means that in this clone FCAP33 was not successfully deleted. The sequence of FCAP33^{Crsipr}-C1 breaks off in the region of the Crispr target sequence. For the FCAP33^{Crsipr}-Pool, sequence quality was too low to perform a proper alignment, which may reflect an expected mixed population of sequences. Even after several gDNA preparations this problem could not be solved. TIDE analysis confirmed the results that the alignment already showed. For FCAP33^{Crsipr}-C1 the confidence of alignment was high with $R^2 = 0.92$ and the best from all the sequences tested. Also, the predicted modification efficiency was the highest (92%) in this clone. It has to be taken into account, that for a diploid cell a percentage of 50% is expected per indel (TIDE). For C2 the confidence ($R^2 = 0.73$) and the predicted KO efficiency (12,5%) were lower, which is due to the fact that 60,3 % of the analyzed sequence does not show a deletion or inserting. Using TIDE for the analysis of pools does not give information about the specific indel of a specific allele.

Even though the detection of endogenous FCAP33 in IF was not successful, IF experiments were performed to see if knocking out the protein shows any phenotype in IMCD3 cells. Performing WB experiments using siRNA mediated KD of FCAP33 (siFCAP33) showed that we were not able to detect endogenous FCAP33 on WB (Figure 4 A, expected size 33 kDa) even after precipitation of the samples, confirming the low levels. We were able to show tagged

FCAP33 on WB and the reduced FCAP33 levels after siRNA treatment (Figure 4 A). The functional KD in the tagged cell lines was confirmed by IF (Figure 4 B). Again, staining of FCAP33 in WT cells did not show cilia specific signal (Figure 4 C, IMCD 3WT). This was also true for the potential FCAP33-KO (FCAP33^{Crispr}) cells. In the overexpressing cell lines (FCAP33^{NG} and FCAP33^{FLAG}) FCAP33 could be detected in primary cilia by antibody staining with FCAP33-specific antibodies (Figure 4 C). NG signals co-localized with FCAP33 in cilia. FLAG signals were not detectable, which might be due to inefficient staining or low levels. To investigate if reducing FCAP33 has an impact on cilium morphology I determined primary cilium length using CiliaQ and ARL13b as a cilia marker. There was no significant change in length between most of the different cell lines but FCAP33^{NG} had longer cilia than FCAP33^{Crsipr}-C1 (Figure 4 E, left panel). Though not being significant FCAP33^{NG} cells do have slightly longer cilia than WT cells (Figure 4 E, left panel). Quantifying cilium length manually by using AcTUB as a marker of the axoneme and comparing cilia length to the higher expressing FCAP33^{cLAP} cell lines, showed that overexpressing FCAP33 indeed increases axoneme length (Figure 4 F). I also created cell lines that stably express FCAP33^{cLAP} in the FCAP33^{Crsipr}-C1 cell line, referred to as FCAP33^{cLAP}Crispr. FCAP33^{cLAP}Crispr did not show longer cilia than WT cells, indicating that overexpressing FCAP33 may only induce elongation in the context of functional native protein.

Despite a reduction on mRNA levels (Figure 4 D, qPCR), quantifying the ciliation rate in FCAP33^{Crsipr}-C1 cells showed a for slightly less cilia but comparison analysis did not show statistically significant differences (Figure 4 E, right).

In summary the Crispr clone FCAP33^{Crsipr}-C1 was the most reliable cell line to study the effect of reduced FCAP33 in a stable cell line, so far. Additionally, experiments showed that overexpression of FCAP33 leads to longer cilia. The qPCR experiments confirmed the MS and IF results, that FCAP33 is generally low abundant in IMCD3 cells, as FCAP33 has a Ct value of 31 compared to the GAPDH, which is high abundant (Ct 19) (Data not shown). However, a comparison of relative expression levels of an abundant or well-known ciliary protein, normalized to GAPDH, would be important for further abundance analysis.

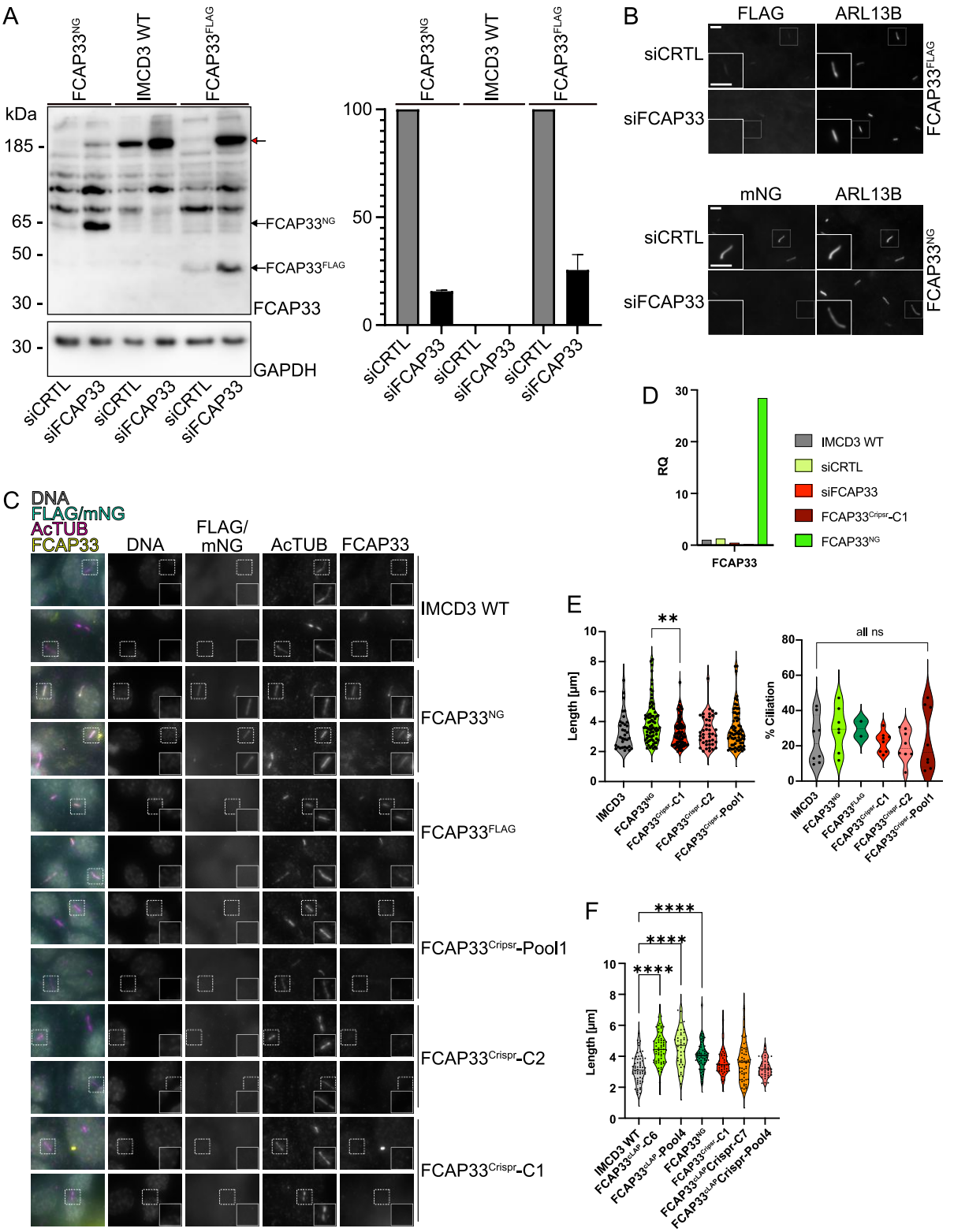

Figure 4: FCAP33 is expressed at low levels in IMCD3 cells and overexpression might influence primary cilium length

(A) Western Blot of FCAP33 KD in different cell lines. Cell lines were treated with control siRNA (siCRTL) or siRNA against FCAP33 (siFCAP33). 75 µg precipitated protein was loaded. Endogenous FCAP33 (IMCD3 WT) not detectable on WB. Tagged variants are detectable (black arrows) and downregulated. Quantification of the signals on the right side. Normalization to GAPDH. WB and quantification done by S. Tarrah.

(B) Downregulation of FCAP33 by using siFCAP33 or control siCRTL shown by IF using tagged cell lines. IF performed by S. Tarrah. (C) IF images with staining of endogenous FCAP33 to compare WT, with overexpression and FCAP33 Crispr cell lines, targeting Exon2. (D) qPCR performed in duplicates to detect mRNA levels. Exon 4/5/6 were amplified (Qiagen Primer) in qPCR. WT has low levels, KD and KO reduced (E) Analysis of cilium length using CiliaQ and ARL13b as cilium marker. Analysis of the ciliation rate to compare effect of different expression levels of FCAP33 on ciliation rate and cilium length. (F) Manual Fiji Analysis of AcTUB length of different cell lines with different FCAP33 expression levels.

Confirmation of low expression levels and characterization of FCAP33Crsipr-C1

From the previous experiments it was known that FCAP33 levels in IMCD3 cells are low. We tested whether directly taking up cells in SDS Sample buffer with DTT would help to efficiently solubilize FCAP33. Cells from one 15-cm cell culture dish were directly resuspended in 200 µl 1x Laemmli buffer + 100 mM DTT. After sample preparation, 10 µl were loaded and run on an SDS-gel and subsequently used for WB. IMCD3 WT cells were compared to the FCAP33-overexpressing cell lines FCAP33^{cLAP}-Pool4 and -C6, FCAP33^{NG}, to the Crispr clone FCAP33^{Crsipr}-C1 and two Crispr rescue cell lines (FCAP33^{cLAP}Crispr-Pool4 and -C7). Only in the overexpressing and the Crispr rescue cell lines FCAP33 could be detected by the FCAP33 antibody (Figure 5 A, left, expected size at 65 kDa) and confirmed by GFP staining (Figure 5 A, right). There was no clear signal for endogenous FCAP33 in IMCD3 WT cells. The indicated bands (Figure 5 A, pink stars) between 30 and 50 kDa could reflect the endogenous FCAP33 as they are less strong in FCAP33-Crispr cells. Nevertheless, differences in signal intensities and FCAP33 levels are still hard to predict, as protein amounts could not be equalized with this method. Overexpressing FCAP33 facilitates detection of FCAP33 on WB (Figure 5 A). Next, different solubilization buffers were compared (RIP-Y and SB). The milder solubilization buffer (SB) was used for previous experiments and the comparison to the RIP-Y (R) solubilized samples did not show differences in WB detection of tagged FCAP33 (Figure 5 B). There might be a specific signal for the endogenous FCAP33 (pink star) in the RIP-Y solubilized samples. We could confirm that high amounts of FCAP33 are needed for efficient detection of the protein on WB level.

To validate the generated FCAP33-Crispr Clone 1 and to perform an additional specificity test, endogenous FCAP33 was purified from cells doing an immunoprecipitation (IP) assay. The FCAP33 antibody was coupled to an Agarose and cell lysates were incubated on the bead material. After washing off all unbound proteins from the beads (FT), competitive elution was performed by using the FCAP33 peptide that was used to generate the FCAP33 antibody (Figure 5 C). IMCD3 WT cells, IMCD3 FCAP33^{FLAG} expressing cells and HEK293T cells

were used as positive controls for the antibody and the IP. SDS-Gel electrophoresis was done with samples of the Input (I), the Flow-Through (FT), the two competitive Elution steps (E) and the SDS-Elution. This was followed by Western Blot (WB) for further analysis using (Figure 5 C). Total protein staining of the membrane showed a specific band in the first elution (1. E), second elution (2. E) and SDS-Elution around the size of 40 kDa in IMCD3 WT and HEK293T cells. From previous experiments it was known that FCAP33 potentially runs at a higher molecular weight than 30 kDa (Figure 4 + M. Sc. Students S. Tarrah, S. Ehr). In affition to bands at the expected size another band at a higher molecular weight (~ 80-90 kDa) can be seen in IMCD3 WT and HEK293T cells. In the first elution a weak band is detected in the FCAP33^{Crispr} cells in the total protein stain (Figure 5 D, Total protein stain, upper panel). However, this band was not detected by antibody staining for FCAP33 (Figure 5 D, bottom panel). Staining the membrane with FCAP33 antibody showed different bands in the elution samples (1.E, 2. E, SDS) of IMCD3 WT cells and HEK293T cells, which are different between the cell lines but seem to be specific as they are not detected in IMCD3 FCAP33^{Crispr}-C1 cells (Figure 5 C, bottom panel). The FLAG-tagged FCAP33 could not be detected in the eluate samples, whereas the input (I) sample of FCAP33-FLAG shows an additional band at 40 kDa when compared to the other cell lines (Figure 5 C, bottom panel, FCAP33, Input samples second lane). The strong signals that were detected in the SDS-Eluates are likely caused by washing off the agarose coupled antibody. From previous studies (S.Tarrah) it was known that the detection of endogenous FCAP33 was easier using the HRP-WB system (Western blot). To further analyze the samples conducted in this experiment, an HRP-Blot was done. Detection of FCAP33 in HEK293T and IMCD3 Eluates was confirmed, but there was also a slight signal in FCAP33^{Crsipr}-C1 cells detected (Figure 5 E). This signal can also be seen in the first Elution of the total protein stain stained membrane (Figure 5 D, top panel, Total Protein Stain). Looking at the input samples shows a pattern with a lot of bands potentially being unspecific as they can be seen in the WT control as well. There were different higher molecular weight bands (Figure 5 E, marked with pink stars) between 80-115 kD, that seemed specific to FCAP33 and are around double the size of the potential FCAP33 bands around 40 kDa. In the SDS-Samples bands at around 185 kDa are visible (Figure 5 D, marked with pink stars). All additional indicated bands fit the size of the high molecular weight bands seen before in Figure 4.

In summary, we could show that FCAP33 is expressed at low levels in WT cells. Therefore, it is rather difficult to detect it in IF and WB experiments in WT cells. Specifically purifying endogenous FCAP33, showed, that IMCD3 WT and HEK293T cells do express the protein

(also confirmed by qPCR for IMCD3 cells) and that FCAP33^{Crsipr}-C1 has a strong reduction of the protein. This could further be confirmed by testing different lysis buffers as well as loading

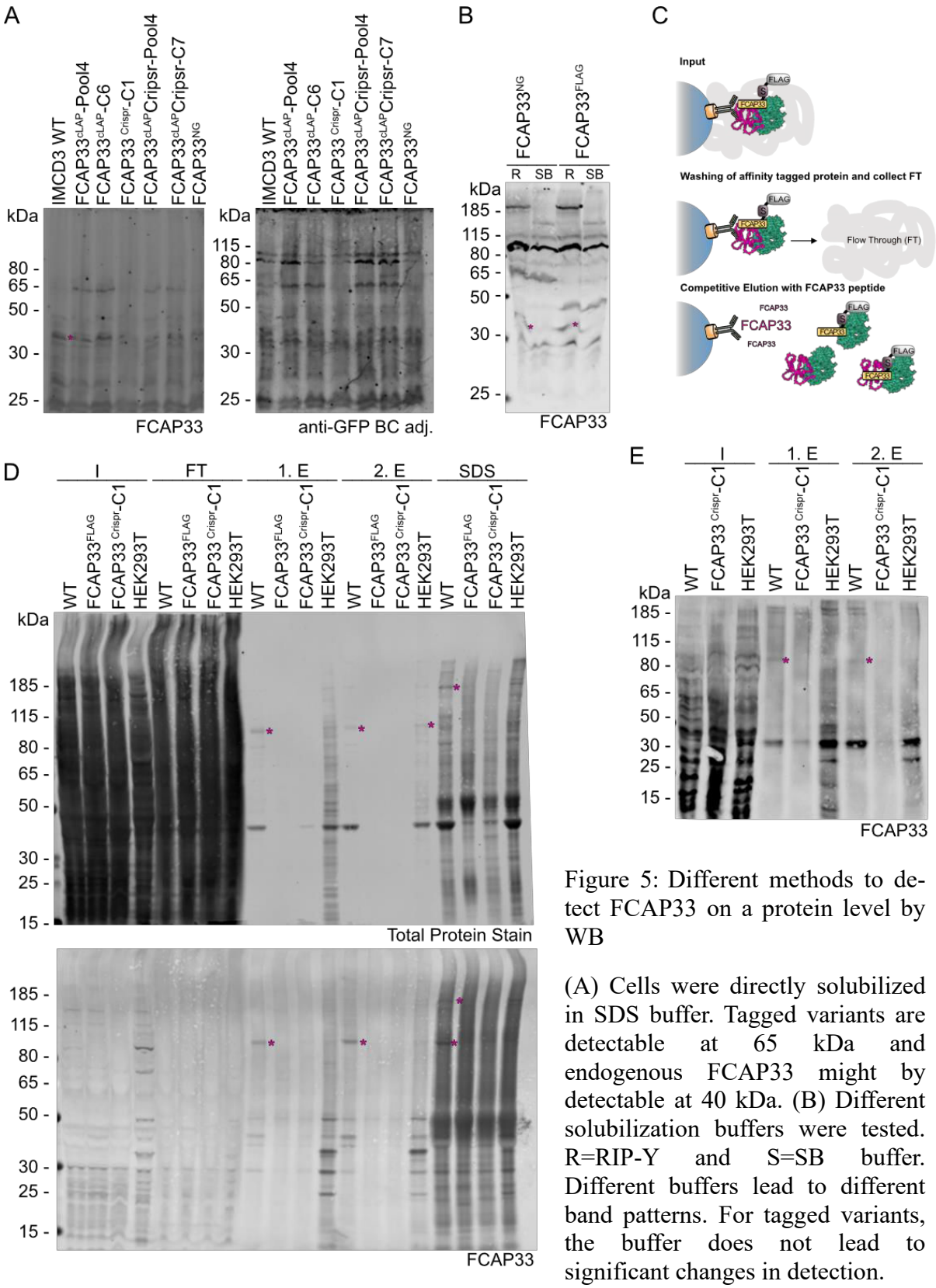

Figure 5: Different methods to detect FCAP33 on a protein level by WB

(A) Cells were directly solubilized in SDS buffer. Tagged variants are detectable at 65 kDa and endogenous FCAP33 might by detectable at 40 kDa. (B) Different solubilization buffers were tested. R=RIP-Y and S=SB buffer. Different buffers lead to different band patterns. For tagged variants, the buffer does not lead to significant changes in detection.

(C) Scheme of IP: Whole cell lysates are incubated with the beads (Input). After binding, beads are washed to remove unspecific interactions. Elution was done competitively with FCAP33 peptide. (D) WB of IP samples on nitrocellulose. Total protein stain and FCAP33 staining show specific FCAP33 elution in IMCD3 and HEK293T cells. Pink stars indicate specific high molecular weight bands. (E) WB of IP samples using HRP system. Clear elution of FCAP33 in WT cells and weak elution signal in FCAP33 Crispr cells.

high concentrated protein samples on WB (Figure 5 A and B). Loading 200 µg total protein of the overexpressing cell lines, $FCAP33^{NG}$ and $FCAP33^{FLAG}$, lead to the detection of the protein on a protein-level. It is likely that the band around 40 kDa reflects the endogenous protein, as it is weaker in the Crispr rescue cell lines (Figure 5 A) and weaker in the pull down assay (Figure 5 D).

BLAST predictions on Uniprot, using the peptide sequence, that was used for antibody generation (YVKLAKQGGRPDLLKHFAPG) did not show any predicted alignment to other *Mus musculus* proteins. The peptide sequence aligns to multiple FCAP33 sequences among different species and to MDM1 in *Marmots*. Checking for potential binding to the *Mus musculus* MDM1 did not show any potential alignment. This indicates that the higher molecular weight bands occurring with the FCAP33 antibody are most likely present due to oligomeric states of the protein. The $FCAP33^{Crsipr}$-C1 was created by targeting early bases of Exon 4. The antibody targets basepairs of Exon 2. This could explain that in the Crispr cell line FCAP33 can still be eluted after IP using the FCAP33 antibody because the N-terminal half of the protein, including Exon 2 is likely to be still expressed.

FCAP33 is predicted an unstable protein and cannot be stabilized by blocking of the proteasome

It is possible that endogenous FCAP33 is not detectable because it is degraded quickly in IMCD3 cells. According to the Expasy ProtParam tool, $FCAP33^{cLAP}$ has an estimated half-life of 30 hours *in vitro*. Furthermore, FCAP33 has an instability index of 45.38. FCAP33 without the GFP has the same estimated half-life but an instability index of 61.05. Indexes higher than 40 classify the protein as unstable. GFP alone has an index of 29.06 and is therefore a stable protein (https://web.expasy.org/protparam/). This explains why $FCAP33^{cLAP}$ has a lower instability index, and could explain why it may be more stable. Additionally, the GFP tagged version is overexpressed. To investigate whether FCAP33 is degraded quickly, we tested if blocking the proteasome leads prevents FCAP33 from being degraded and resulting into the detection of endgenous FCAP33 in IF or WB experiments. MG132 is a proteasome inhibitor (Sun et al., 2006) that was tested on IMCD3 WT cells. Different concentrations of MG132 were added for 3 h to serum-starved IMCD3 WT cells seeded for IF. Acetylated tubulin (AcTUB) was used as cilia marker and the FCAP33 antibody to check the presence of FCAP33 upon MG132 treatment. Compared to the DMSO controls, there were clear condensate-like structures visible at the ciliary base, stained by the FCAP33 antibody (Figure 6 A). Interestingly, MG132 treatment did only lead to FCAP33 „accumulations“ at the ciliary base

but not to a signal within primary cilia. As these FCAP33 accumulations lay within the nucleus region, the overall FCAP33 signal within the nucleus region swas analyzed. As expected, FCAP33 signals were lower in the DMSO controls when compared to the MG132 treated cells (Figure 6 B). Efficient MG132 treatment was additionaly tested on the protein expression levels. If blocking of the proteasome was efficient, cells should have more polyubiquitinated proteins as ubiquitinated proteins cannot be degraded anymore (Sun et al., 2006). This can be detected in cell lysates by Western Blot analysis using an antibody (FK2) against polyubiquitinated proteins. In the different cell lines (IMCD3 WT, FCAP33^{NG} and FCAP33^{Crsipr}-C1) MG132 treated samples showed a stronger FK2 signal compared to the DMSO control (Figure 6 C, left). However, testing the same samples for FCAP33 expression did not show any specific signal for FCAP33 in these cell lysates (Figure 6 C, right). To rule out that the dected FCAP33 accumulations at the ciliary base localize within the nucleus and were not solubilized, the "nuclear fraction" was resuspended in SDS-Sample buffer and analyzed on WB as well. There are bands at 80 kDa and 55 kDa that are different between WT, FCAP33^{Crispr}-C1 and FCAP33^{cLAP}, but the sizes do not refer to the expected protein size of 33 kDa for FCAP33 and there is no difference between MG132 and CRTL samples (Figure 6 D). Overall, the MG132 treatment did not lead to the detection of FCAP33 in primary cilia of IMCD3 WT in IF. Additionally, it did not improve the detection of FCAP33 in WB experiments.

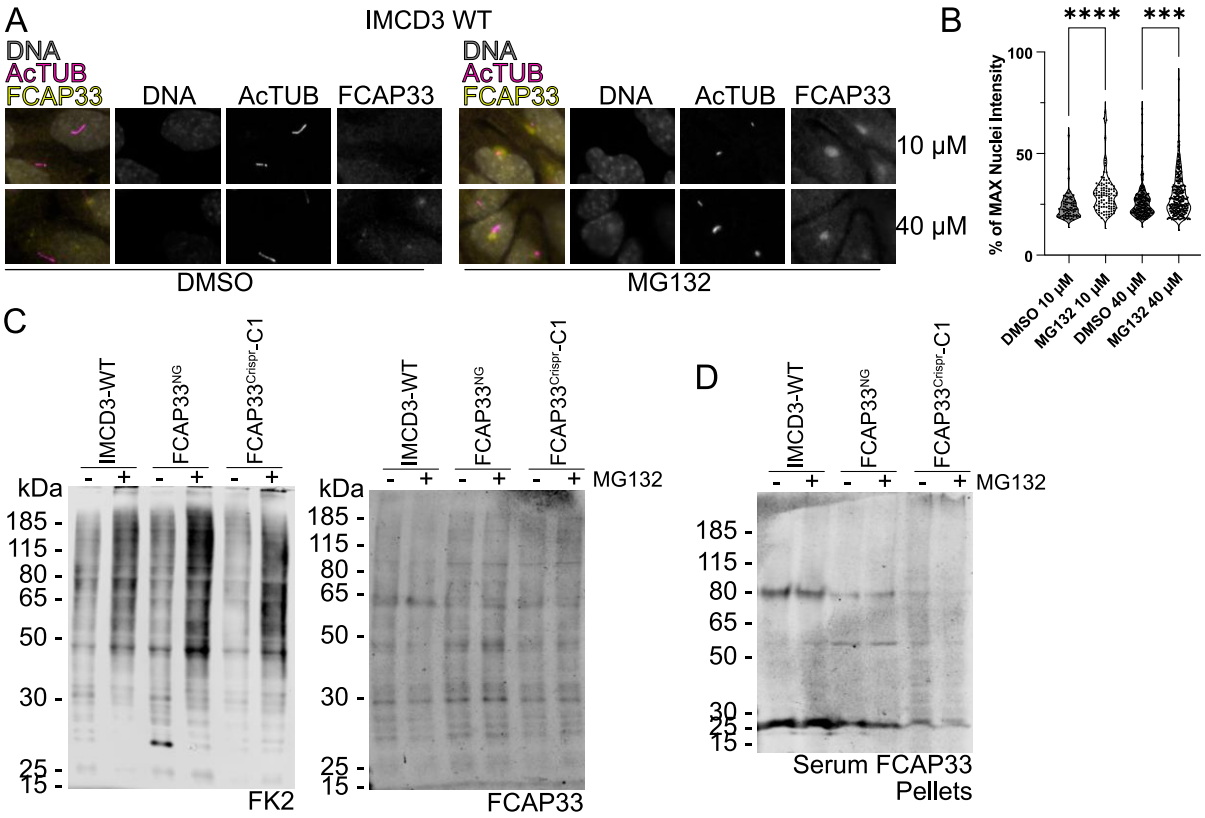

Figure 6: Low levels of FCAP33 are not due to proteasomal degradation

(A) IF experiments to test the influence of proteasome blocking. Treatment of starved cells with different amounts of MG132. Fixed samples were stained with FCAP33 and AcTUB as cilium/tubulin marker. Nuclei were stained with the DNA stain Hoechst. (B) Quantification of nulear signals of FCAP33. (C) WB of the cell lines treated with 40 µM MG132 or DMSO as control. FK2 detects polyubiquitination to confirm efficient MG132 reatement (left). WB of the same samples with FCAP33 antibody. MG132 treatment does not lead to stabilized/specific siignals of FCAP33 compared to the untreated control. (D) Pellet fractions of samples from (C) plus/minus MG132 treatment.

These experiments showed, that the (ciliary) detection limitations of FCAP33 in IMCD3 WT cells is not due to FCAP33 being an unstable protein, but rather to the low expression levels of the protein.

FCAP33 localizes to basal bodies and centrioles

Inhibiting protein degradation did not lead to detectable levels of FCAP33 in IMCD3 WT cells using western blot (WB) or immunofluorescence (IF) analysis. Knowing that FCAP33 was found in the primary cilium proteome and that overexpression overcomes the problem of detection limits we still aimed to figure out a possible way to confirm its localization in IMCD3 WT cells. Different microtubule (MT) and cilia linked structures: BB, axoneme and centrioles are not similarly accessible to antibody staining (Figure 7 A). It is known that some cellular structures e.g. (BB) and centrioles are better accessible for antibody staining upon methanol fixation compared to PFA fixation (Figure 7 B). Especially for microtubule (MT)-based structures, buffers and protocols are adapted for better antibody staining (Shan-rong-Shi et al., 1996; Hua and Ferland, 2017; Danchenko et al., 2019). The core structure of the ciliary axoneme and midbodies are microtubules. In both of the structures we detected overexpressed FCAP33. FCAP33 also co-localized with different tubulin modifications and midbody proteins. Dissecting whether different permeabilization and fixation methods would indeed lead to efficient immunofluorescence (IF) staining in WT cells, I tested different protocols (Figure 7 A and B). IF experiments performed before were done with the standard protocol, if not stated differently. Fixing cells with PFA is sufficient for cilia-membrane proteins and spindle but not always for axonemal proteins of primary cilia (Hua and Ferland, 2017) **(**Figure 7 B). When IMCD3 WT cells were fixed for 10 min with 4% PFA at room temperature (RT) and subsequently followed by the standard IF staining protocol, a lot of midbody structures were detected by staining for acetylated tubulin (AcTUB) (Figure 7 D). Cells seemed to be less ciliated, which is likely due to inefficient staining of primary cilia with AcTUB, compared to

the standard staining combining PFA and methanol (MeOH) (Figure 2, Figure 3). Staining with FCAP33 did show a dispersed cytosolic staining but no signals overlapping with AcTUB positive structures. In FCAP33^{cLAP} expressing cells the AcTUB staining showed a similar pattern like WT cells, having more midbody structures stained than primary cilia (Figure 7 D). The GFP signals co-localize with almost all midbodies stained by AcTUB (Figure 7 D). Additionally, primary cilia could be detected in the GFP channel, even though not being stained by AcTUB. In addition to WT cells and overexpressing cells a set of newly generated Crispr Cas 9 mediated potential knockouts (KO) (done by Lea K. Sanwald) were included in the experiment. Crispr clones were sequenced and analyzed as before using TIDE and sequence alignment, and the most promising clones were selected. For all the Crispr clones tested, FCAP33^{Crsipr}-C4, FCAP33^{Crsipr}-C6 and FCAP33^{Crsipr}-C7, there were again mostly midbodies stained by AcTUB (Figure 7 D). In FCAP33^{Crsipr}-C6 and -C4 cells, spindle structures were detected (Figure 7 D, indicated by pink arrows). These structures of dividing cells also showed stronger FCAP33 signals (Figure 7 D, indicated by pink arrows). This effect might also be observed in WT cells (Figure 7 D). As observed in WT cells there was no overlap of FCAP33 staining with midbody staining by AcTUB. It is known from literature (e.g. for CSPP1 (Hua and Ferland, 2017)) that centrosomal immunolabeling also depends on the permeabilization methods. Fixing cells with MeOH makes the centrosome, a more tightly packed MT structure, better accessible to antibody penetration. The same is also true for some axonemal proteins and basal body proteins (Hua and Ferland, 2017) (Figure 7 B). IMCD3 WT cells as well as FCAP33^{cLAP}, FCAP33^{Crsipr}-C4, FCAP33^{Crsipr}-C6 and FCAP33^{Crsipr}-C7 were fixed for 10 min with ice cold MeOH at -20 °C (Figure 7 E). Primary cilia were successfully stained by AcTUB. Interestingly, almost every primary cilium had puncta-like staining for FCAP33. Some cells were associated with two distinct signals for FCAP33, where only one was associated with the primary cilium (Figure 7 E). The second specific signal could be the daughter centriole. This is very likely as in some cases the second FCAP33 signal is closely located to the primary cilium associated basal signal in terms of space (Figure 7 E). Since a centriolar marker is absent in this immunofluorescence experiment, the spatial localization can only be inferred speculatively. Looking at FCAP33^{cLAP}, FCAP33 also localizes to the base of primary cilia stained with AcTUB, but also within the primary cilia. FCAP33 staining within primary cilia appears to be weaker, when compared to the basal signal, potentially reflecting less dense protein localization along the axoneme. Strikingly, in all Crispr cell lines there was a clear FCAP33 signal at the ciliary base (Figure 7 E). However, within the primary cilium it did not seem that FCAP33 localization could be detected in IMCD3 WT and FCAP33 Crispr cells.

Taken together, PFA fixation was not sufficient for centriolar and BB staining using the FCAP33 antibody. Methanol fixation reveals a basal signal in IMCD3 WT cells and FCAP33-Crispr cells. Last, I tested the so-called antigen retrieval (Antigen retrieval) to even enhance the accessibility of binding sites for antibodies to densely packed structures (Shan-rong-Shi et al., 1996) compared to MeOH only (Figure 7 C). This method uses a heating step and harsh buffer conditions using 5% Urea to open up protein structures for better antibody penetration. Vice versa it is possible that antibody binding could be hampered, such that epitope binding is not possible due to a too strong disruption of the protein structure. This could also lead to a higher chance of unspecific binding. For FCAP33, antigen retrieval led to basal body (BB), centriole, primary cilia and spindle staining by using AcTUB (Figure 7 F). These are all MT-based structures. Co-staining with AcTUB revealed that almost all centriole and BB structures were positive for FCAP33 in IMCD3 WT cells (Figure 7 F, WT). Signals were much weaker and harder to detect than AcTUB, but in some cases even primary cilia were FCAP33 positive. FCAP33 did also co-localize with centriolar staining by AcTUB at the spindle, but only very weakly with spindle microtubules themselves (Figure 7 F). The same results but with stronger signals could be observed for FCAP33^{cLAP} cells. FCAP33^{Crsipr}-C6 and FCAP33^{Crsipr}-C7 showed a similar localization profile of FCAP33 as seen for the MeOH fixed cells, co-localizing with the ciliary base. In FCAP33^{Crsipr}-C4 cells, there was even a FCAP33-signal within primary cilia visible (Figure 7 F). Overall, different fixation and permeabilization methods changed the localization pattern of FCAP33 in different IMCD3 cell lines. Using different techniques strikingly revealed that FCAP33 seems to localize to the BB and centrioles in all cell lines tested, even in FCAP33 Crispr cell lines. Only in midbodies and primary cilia, the localization of FCAP33 seemed to be dependent on the expression levels of the protein, localizing more prominently to midbodies and cilia in the overexpressing cell line (FCAP33^{cLAP}). This leads to different possible assumptions: 1. FCAP33 localizes to centrioles and BB structures. Together with primary cilia and the midbody localization this leads to the hypothesis that FCAP33 associates to different MT-based structures within IMCD3 cells 2. there might still be FCAP33 expression in the different FCAP33-Crispr clones tested, which can still be recognized by the antibody.

In the following parts of the work, different experiments were conducted to determine whether FCAP33 is a microtubule-based protein and unravel its potential role.

To test the second theory, the binding of the antibody was checked in silico. Sequence alignment of the antibody peptide sequence showed (YVKLAKQGGRPDLLKHFAPG) that

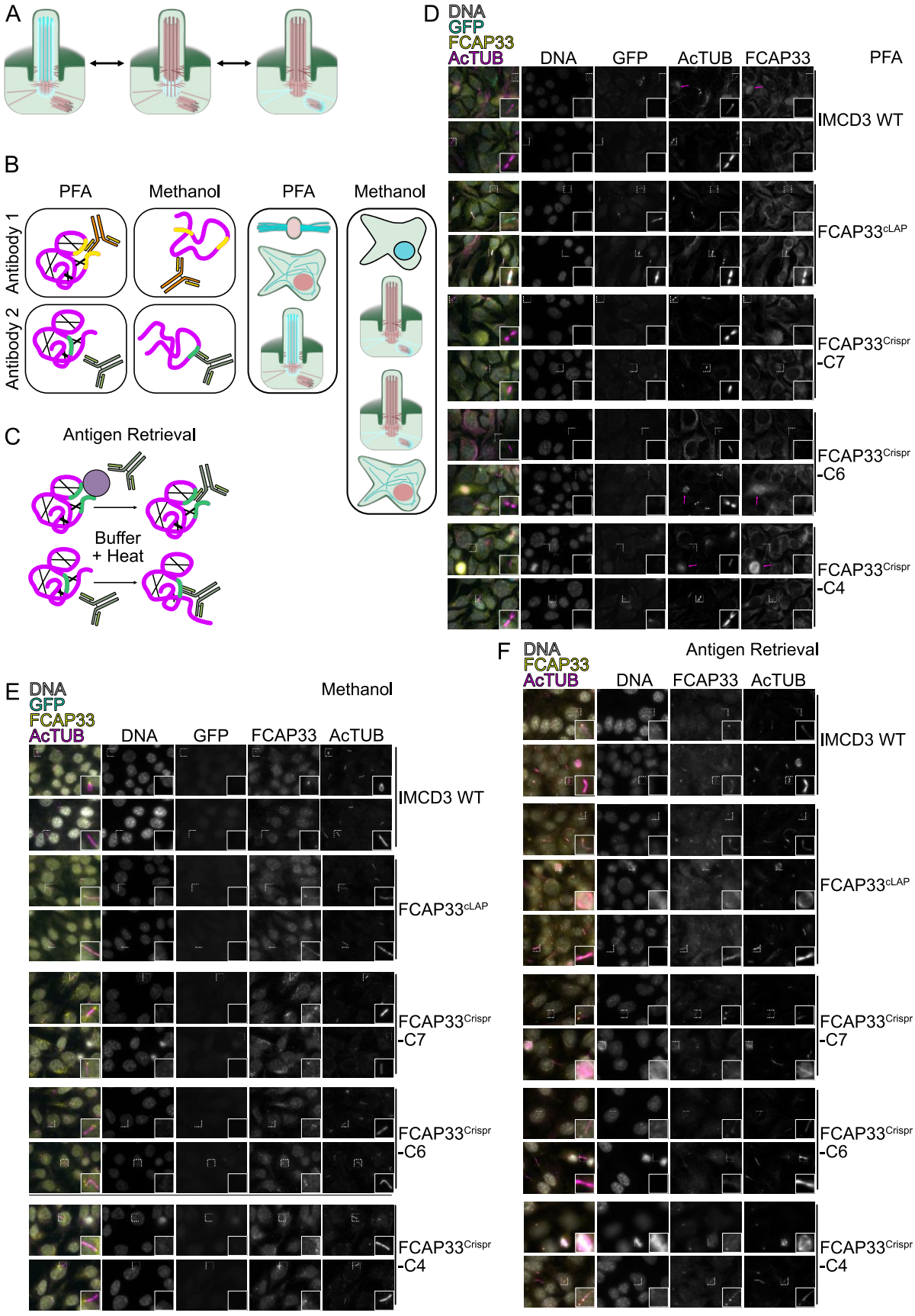

Figure 7: Different methods for fixation and permeabilization reveal additional localization of FCAP33 to basal bodies (BB)and centrioles

(A) Scheme highlighting the axoneme, BB and centrioles to show, that the staining of these structures can depend on permeabilization and fixation methods.

(B) Scheme of accessibility of epitopes to different antibodies. Antibody 1 binds specifically after crosslinking with PFA but not Methanol (MeOH). Antibody 2 cannot bind the epitope after PFA crosslinking, but binding is simplified when the protein structures is opened up by MeOH. (C) Scheme of Antigen Retrieval. Heating and Urea buffer (Methods) allow removal of components potentially blocking the epitope for antibody binding. Or partially opening up/loosening the protein structure. (D) IF of cells fixed with PFA. Hoechst staining for DNA, GFP autofluorescence for GFP tagged FCAP33, AcTUB as cilia and tubulin marker, and FCAP33. (E) IF of cells fixed with MeOH. Hoechst staining for DNA, GFP autofluorescence for GFP tagged FCAP33, AcTUB as cilia and tubulin marker, and FCAP33. (F) IF of cells fixed with MeOH and subjected to Antigen Retrieval. Hoechst staining for DNA, GFP autofluorescence for GFP tagged FCAP33, AcTUB as cilia and tubulin marker.

the antibody indeed binds to the N-terminal part of the protein. The epitope is encoded on Exon2 and Exon3. When Exon 4 is targeted for Crispr Cas9 mediated KO, the N-terminal part, where the antibody binds should still be expressed. FCAP33 only consists of 7 exons, which would also mean that more than half of the protein would still be expressed in these cells. Regarding this, the detection of FCAP33 at centriole and cilia base structures is likely due to a specific antibody binding to the N-terminal part of the protein. It also implies that only knocking out the C-terminal half of the protein is not enough to disrupt its localization to MT-based structures. Vice versa, targeting Exon 2 may potentially lead to non-functional protein within the cells.

FCAP33 associates with axonemal microtubules

We investigated whether FCAP33 is associated to the primary cilium axoneme, the microtubule (MT) core of the primary cilium. Therefore, we performed a membrane removal assay. Ciliated cells were de-permeabilized such that the cellular membrane gets removed. This leads to the removal of the ciliary membrane and therefore sets all proteins free, that localize to the ciliary membrane or the ciliary lumen. To induce de-permeabilization of the cellular membrane, cells were seeded for immunofluorescence (IF) according to the standard protocol and serum-starved to induce ciliation. After starving cells, cells were treated for 30 s or 60 s with 0.5% triton in PHEM buffer (Nachury et al., 2007; Larkins et al., 2011). PHEM buffer is commonly used for microtubule staining as it helps conserving MT structures (Hua and Ferland, 2017; Danchenko et al., 2019). To control the integrity of axonemal MTs control cells where either fixed directly with PFA, or after 30 s or 60 s treatment with PHEM buffer only. To check for efficient removal of the ciliary membrane, cells were stained for the ciliary membrane protein ADP-ribosylation factor like protein 13b (ARL13b) (Figure 8 A). In IMCD3 WT and FCAP33^{cLAP} cells, the efficient removal is shown by the missing ARL13b staining

(Figure 8 A, Figure 8 C). For quantification, acetylated tubulin (AcTUB) was used as a cilia marker to measure intensities of ARL13b, FCAP33 or AcTUB itself. ARL13b levels were most significantly reduced in IMCD3 WT cells after treatment for 60 s with triton compared to the buffer control (Figure 8 D). For imaging, settings were adjusted to the WT PFA control and the same settings were used for all different treatments. In contrast to the removal of membranous ARL13b, the axonemal AcTUB should not be removed upon triton treatment and can be taken as another positive control. Acetylation occurs at lysine 40 (K 40) in the inner site of the MTs within the primary cilium axoneme (Shida et al., 2010) and should therefore not be negatively affected by the removal of the ciliary membrane. Measuring AcTUB levels in IMCD3 WT and FCAP33^{cLAP} expressing cells, showed an increase in AcTUB intensities after triton treatment compared to its respective PHEM control and to the PFA control (Figure 8 D + E). This effect is also represented by the IF images, in which it is clearly visible that AcTUB staining is stronger after triton treatment (Figure 8 A + B). This increase in AcTUB could be caused by a better accessibility of the antibody to the acetylation site upon removal of the ciliary membrane. The goal of this experiment was to investigate if FCAP33 does bind to MTs, more specifically to axoneme in primary cilia. If FCAP33 is an axonemal protein it should reflect a similar behavior as AcTUB and not be removed by de-permeabilization of the cellular membrane. Looking at IF images of FCAP33^{cLAP} cells it does indeed look like triton treatment leads to brighter signals after immunolabeling (Figure 8 B). In IMCD3 WT cells a slight staining of FCAP33 in primary cilia is visible, which we cannot see in the respective PHEM treated controls (Figure 8 B). Quantifying the signals did only show a statistically significant increase after 60 s triton treatment. For overexpressing cells (FCAP33^{cLAP}), the quantification and the statistical analysis reflect what was observed in IF images. Treating the cells for 60 s with triton led to a significant increase in FCAP33 intensities, resembling AcTUB (Figure 8 D+E). This shows that, as hypothesized, FCAP33 binds to the axoneme of primary cilia and shows higher accessibility to the anti-FCAP33 antibody after triton treatment. The increase in FCAP33 intensity even shows that endogenous FCAP33 potentially does not localize to the ciliary lumen but associates directly to MTs. Lumen FCAP33 would be lost after triton treatment and should therefore not lead to increased intensities compared to the control. In FCAP33^{cLAP} expressing cells, the tagged FCAP33 can also be visualized by GFP. Therefore, GFP levels were also analyzed by using the AcTUB mask of primary cilia. This analysis shows that GFP levels decreased (Figure 8 E). This indicates that there is a portion of GFP tagged FCAP33, that is either lumenal which could also be due to overexpression, or that the triton treatment dissociates a portion of GFP-tagged FCAP33. Taken together, FCAP33 localizes and binds to

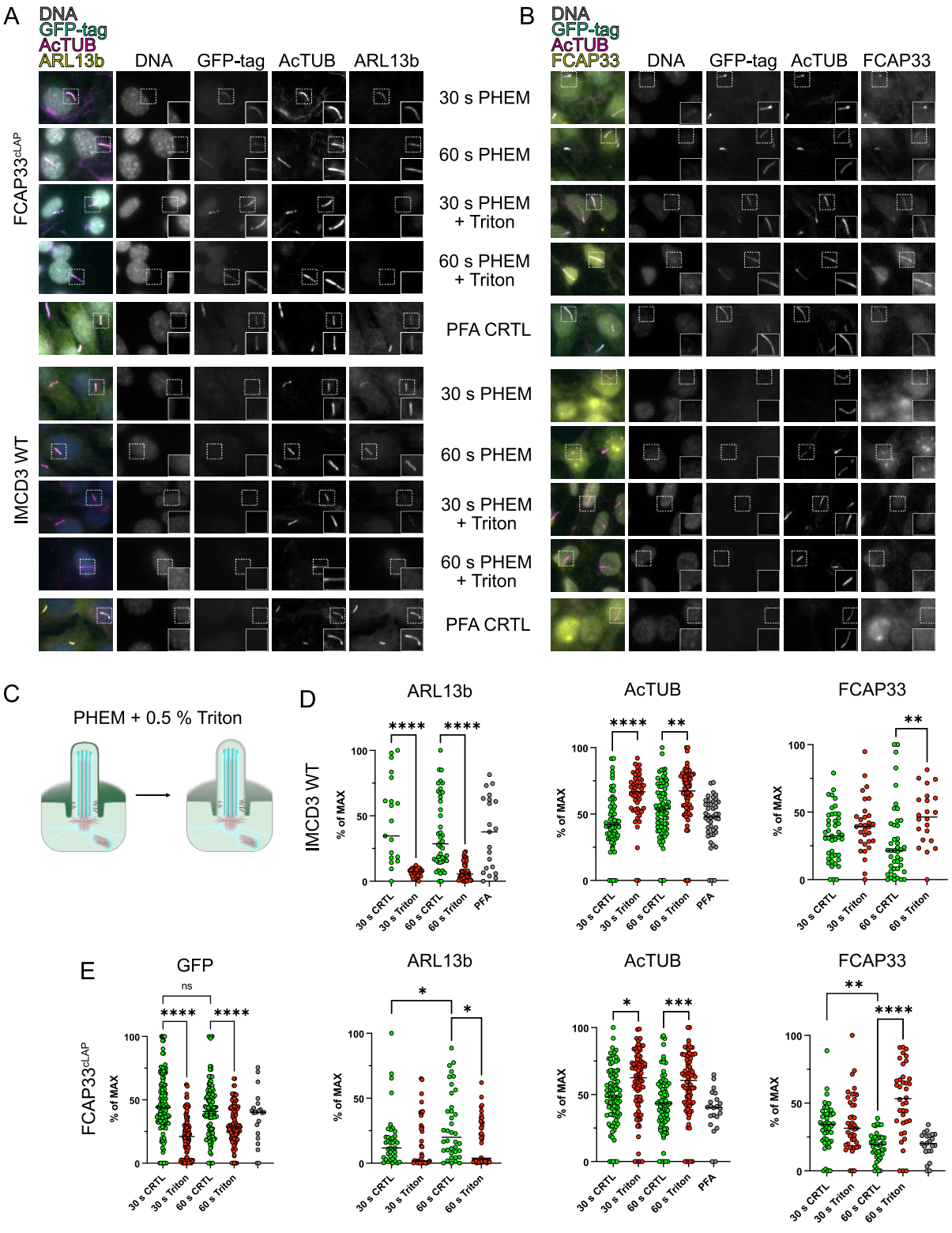

Figure 8: Demembranation of primary cilia reveals axonemal association of FCAP33

Demembranation assay performed together with M. Sc, student S. Ehr. IF of FCAP33^{LAP} cells (upper panel) and IMCD3 WT cells (bottom panel) after treatment for 30s or 30s with PHEM + 0,5% Triton or PHEM only. This was followed by PFE fixation and IF staining. PFA CRTL was fixed directly before PHEM treatment. (A) Staining for AcTUB as axoneme marker and ARL13b as ciliary membrane marker. Triton treatment leads to removal of ARL13b.

GFP to visualize FCAP3^{cLAP}. (B) Staining for AcTUB as axoneme marker and FCAP33. GFP to visualize FCAP3^{cLAP}. (C) Scheme of triton treatment. (D) Manual analysis of intensities within the cilium using AcTUB as marker and measuring intensities within AcTUB mask. Quantification of ARL13b, AcTUB and FCAP33 signals in IMCD3 WT cells. (E) Quantification of GFP, ARL13b, AcTUB and FCAP33 signals in FCAP33^{cLAP} cells. Quantification was done manually in Fiji with AcTUB as cilia mask and intensities were measured within this mask. 2 Images of 2 independent experiments were used. Normalization to highest intensity in each condition and each cell line to represent % of maximum. Multiple-comparison ONE-WAY ANOVA test was done in GraphPad Prsim. PFA control only done in one of two experiments.

the axoneme in primary cilia and endogenous FCAP33 is better accessible after removal of the ciliary membrane. The overexpression in FCAP33^{cLAP} cells leads to a stronger increase in FCAP33 intensities, compared to IMCD3 WT, even though some of the FCAP33^{cLAP} seems to be lost after triton treatment.

Axoneme localization is independent of acetylation

The similarities between AcTUB and FCAP33 in the previous assay could be due to similar roles in the primary cilium. To assess if they interact or are co-dependent on each other we investigated if FCAP33 still localizes to primary cilia if acetylation is not present anymore. To this end, I used a cell line where the alpha tubulin acetyltransferase 1 (aTAT1) was knocked out by Crispr Cas 9 in mouse embryonic fibroblasts (MEFs), referred to as aTAT1$^{-/-}$ (Aguilar et al., 2014) and transfected these cells with FCAP33^{FLAG}. The αTAT1$^{-/-}$ cell line can form primary cilia when ciliation is induced by starvation, but not all cilia are acetylated anymore. Acetylation is needed to stabilize the axoneme, but it is not needed for cilium formation (Shida et al., 2010). The KO used here, is only partial as there is a large population of cilia still being positive for AcTUB staining (Aguilar et al., 2014). This allows us to compare cilia being acetylated versus cilia not being acetylated. In the first test, IMCD3 WT cells and αTAT1$^{-/-}$ were transiently transfected with FCAP33^{FLAG}. Performing IF with these cells, AcTUB and FLAG staining showed that FCAP33^{FLAG} localizes to several MT-based structures like midbodies (stained by AcTUB and FLAG), the microtubule network (stained by FLAG and partially AcTUB) and primary cilia, stained by ARL13b and overlapping with FLAG staining and for some cilia with AcTUB (Figure 9 A). Generating stable cell lines, transfecting αTAT1$^{-/-}$ or IMCD3 WT cells allowed to specifically look into cilia localization of FCAP33 in the αTAT1-KO background and to compare to the IMCD3 WT cells. Using the FCAP33^{FLAG} construct allowed for FLAG detection of FCAP33 in primary cilia (Figure 9 B). Therefore, standard IF was performed on ciliated cells (Figure 9 B) and FLAG signal was quantified using

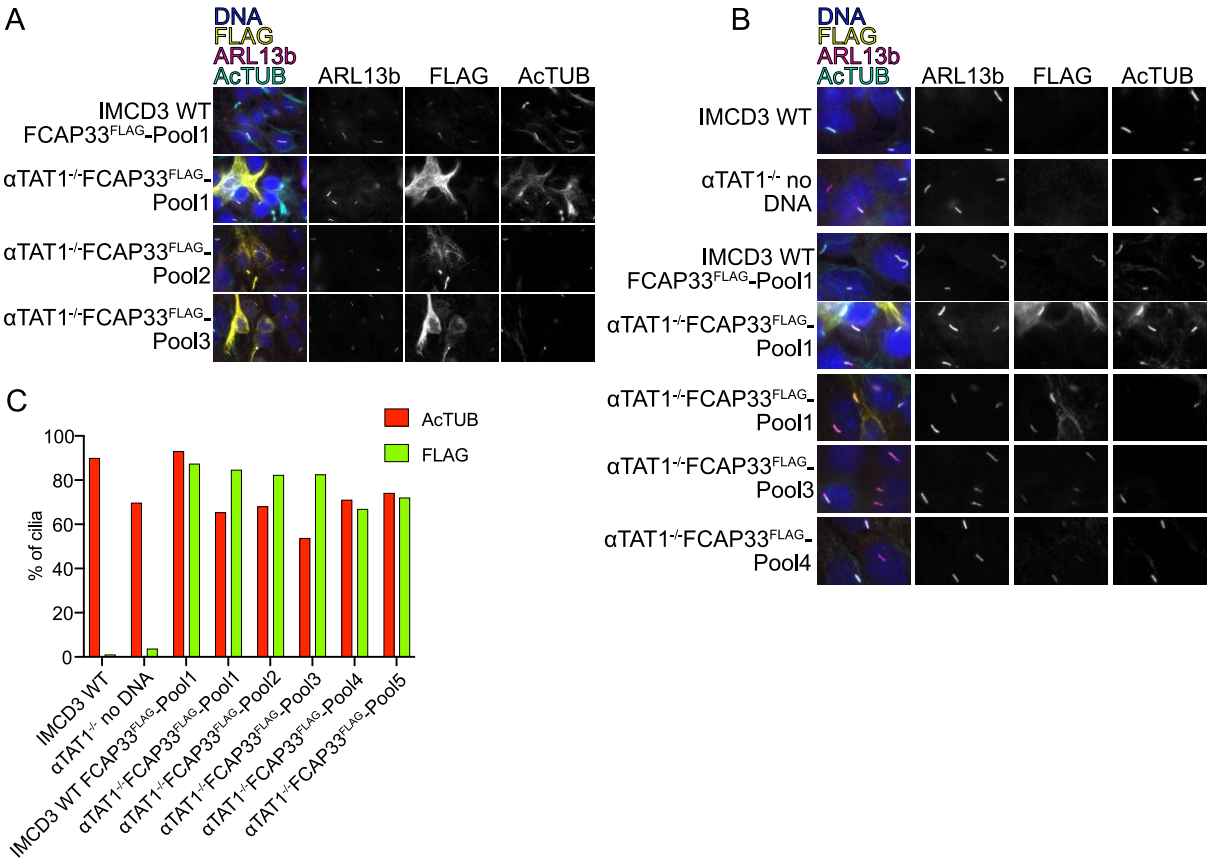

Figure 9: FCAP33 can localize to primary cilia depleted of acetylation

(A) FCAP33^{FLAG} IMCD3 WT cells or aTAT1Crsipr cells were transiently transfected with FCAP33^{FLAG}. Staining for ARL13b as cilia marker and AcTUB for acetylated tubulin. FLAG staining to visualize FCAP33^{FLAG}. (B) IMCD3 WT cells or aTAT1^{Crsipr} cells were stably transfected with FCAP33^{FLAG}. Representative images. Staining for ARL13b as cilia marker and AcTUB for acetylated tubulin. FLAG staining to visualize FCAP33 (C) CiliaQ was used to quantify AcTUB and FLAG signals in primary cilia of different cell lines, with ARL13b as cilia marker.

CiliaQ and ARL13b as cilia marker. IMCD3 WT cells and αTAT1$^{-/-}$ were both efficiently transfected, with a significant increase in FLAG signal compared to the control which reflects unspecific backgrounds signals by FLAG staining (Figure 9 C, green).

The same analysis was done for AcTUB, which shows that αTAT1$^{-/-}$ only is a partial KO as a lot of cilia still are AcTUB positive. Overexpressing FCAP33 in these and WT cilia does not impact AcTUB levls (Figure 9 C). αTAT1$^{-/-}$FCAP33^{FLAG} -Pool1, -Pool2, and -Pool3 have more cilia being FLAG positive, than AcTUB positive, indicating that AcTUB localization is not necessary for FCAP33 to localize to primary cilia. From IF it is clearly visible that FCAP33-FLAG localizes to cilia depleted from AcTUB and e.g. αTAT1$^{-/-}$FCAP33^{FLAG}-Pool3 has the lowest FCAP33 levels but higher AcTUB levels than pool 5 which has more FCAP33 (Figure 9 C).

FCAP33 clearly associates to axonemal MTs, specifically localizing to the axoneme but this association is independent of acetylation of axonemal MTs.

FCAP33 is a static component in primary cilia

The association of FCAP33 to the axoneme could imply that FCAP33 does have a function in axonemal transport of proteins into and out of the cilium. To sense and transmit signals, primary cilia constantly change their protein content mediated by IFT (intra-flagellar transport) proteins that shuttle their cargoes along the axoneme (Nakayama and Katoh, 2018; Nachury and Mick, 2019). A potential role of FCAP33 could be an involvement in this trafficking process. To address this question, I performed live cell imaging using FRAP (fluorescence recovery after photobleaching) to evaluate if FCAP33 is a mobile component within the primary cilium. These experiments were performed with FCAP33^{NG} and FCAP33^{cLAP} cell lines, using the green fluorescence at 488 nm of either the GFP (cLAP) or the neon green. Upon photobleaching the green, fluorescence recovery was monitored by imaging between 5 min to 10 min. As positive control an IMCD3 cell line stably expressing a NG tagged somatostatin receptor 3 (SSTR3) was used. It is known from literature and shown here, that SSTR3, a membrane localized receptor, recovers quickly after photobleaching because it is re shuttled into the primary cilium (Ye et al., 2013) (Figure 10 A, B, C). Micrographs of a representative cilium (Figure 10 A, bottom lane) show that SSTR3 is shuttled into the cilium within seconds. This was shown in multiple cilia (Figure 10 C) and is also visible in the kymograph (Figure 10 B), which represents the cilium shown in Figure 10 A. Following recovery after photobleaching when half-cilium FRAP was performed in FCAP33^{NG} cells, there was only very little recovery after a long recovery time (minutes) (Figure 10 A, B, C). The kymograph represent that FCAP33 does recover. Especially in a short time frame as for SSTR3 (seconds) there is no recovery visible for FACP33 (Figure 10 C). Even a long time frame (Figure 10 A) does not seem to show a shuttling or movement of FCAP33 into the cilium (Figure 10 A). To investigate if there is indeed no recovery of FCAP33 in the primary cilium, even over a longer time course, FRAP experiments were performed and compared between FCAP33^{NG} and FCAP33^{cLAP}, two cell lines expressing FCAP33 to a different extent. Cilium and midbody crops show representative images of the FRAP experiments. The intensity line plots show the FCAP33 signals along the representative cilium or midbody. The green line always represents the intensity before the bleach event, the red line represents the intensity after the bleaching event, and the recovery (orange) reflects the intensity at the end of the respective time-course imaging.

Bleaching half of the cilium, either tip or base did not lead to a remarkable recovery in FCAP33^{NG} cells (lower overexpression) (Figure 10 D and E). Bleaching the stem body region partially and parts of the midbody arms led to a recovery in the stem region of the midbody (Figure 10 D and E). The line plot of the bleached stem body (Figure 10 D row 3), shows clear recovery in the middle region (orange line, third panel) with the middle peak being higher after recovery (orange) compared to bleaching (red). Further investigation of the line plot reveals that the signals in the non-bleached arm regions (left peak and right peak) decrease after bleaching (orange), compared to the stem (figure 10 D row 3). This could indicate that the leftover pool of FCAP33 in these midbody regions shuttles into the bleached region. Bleaching the stem and the arms more strongly, led to almost no recovery in the NG signal (bottom row, Figure 10 D and E). Combining several cilia and midbodies and analyzing their recovery, shows that there is only a slight recovery in cilia (Figure 10 F) and there might be more turnover in midbodies (Figure 10 G).

Performing the same experiments with FCAP33^{cLAP} cells led to similar results. The recovery was slightly stronger compared to FCAP33^{NG} cells (Figure 10 H-K), but the overexpression in this cell line is even higher than in FCAP33^{NG} cells. Especially in midbodies the recovery was stronger (Figure 10 H bottom rows + line plots and Figure 10 K) upon higher FCAP33 expression. The line plot in Figure 10 H, lane 3 confirms the theory, that the bleached pool is "filled up" with the nonbleached portion of FCAP33, represented by a decrease in FCAP33 non-bleached regions after recovery but an increase in the bleached part (Figure 10 H + I, row 3). Interestingly, this effect is again less pronounced for one of the represented midbodies (Figure 10 H and I, bottom lane). Combining several cilia and midbodies and analyzing their recovery shows that there is potentially more recovery in cilia of FCAP33^{cLAP} cells (Figure 10 J) compared to FCAP33^{NG}. The turnover in midbodies (Figure 10 K) also seems to be higher. This high error bars show that the difference between different parts of the midbody and different midbodies are quite strong. In summary, FCAP33 does not seem to be a dynamic component in primary cilia and shows some mobility in most of the midbodies.

Moreover, both cell lines overexpress FCAP33, which means that endogenous FCAP33 would preferentially not recover at all. When the whole cilium was photobleached, there was almost no recovery (Figure 10 L-M).

To recapitulate, FCAP33 in primary cilia is a rather static component and therefore not involved in direct ciliary trafficking of proteins. This depends on the expression levels. Higher overexpression leads to higher recovery, potentially reflecting no recovery in the low expressing IMCD3 WT cells. In midbodies it might depend on the photobleached pool and it

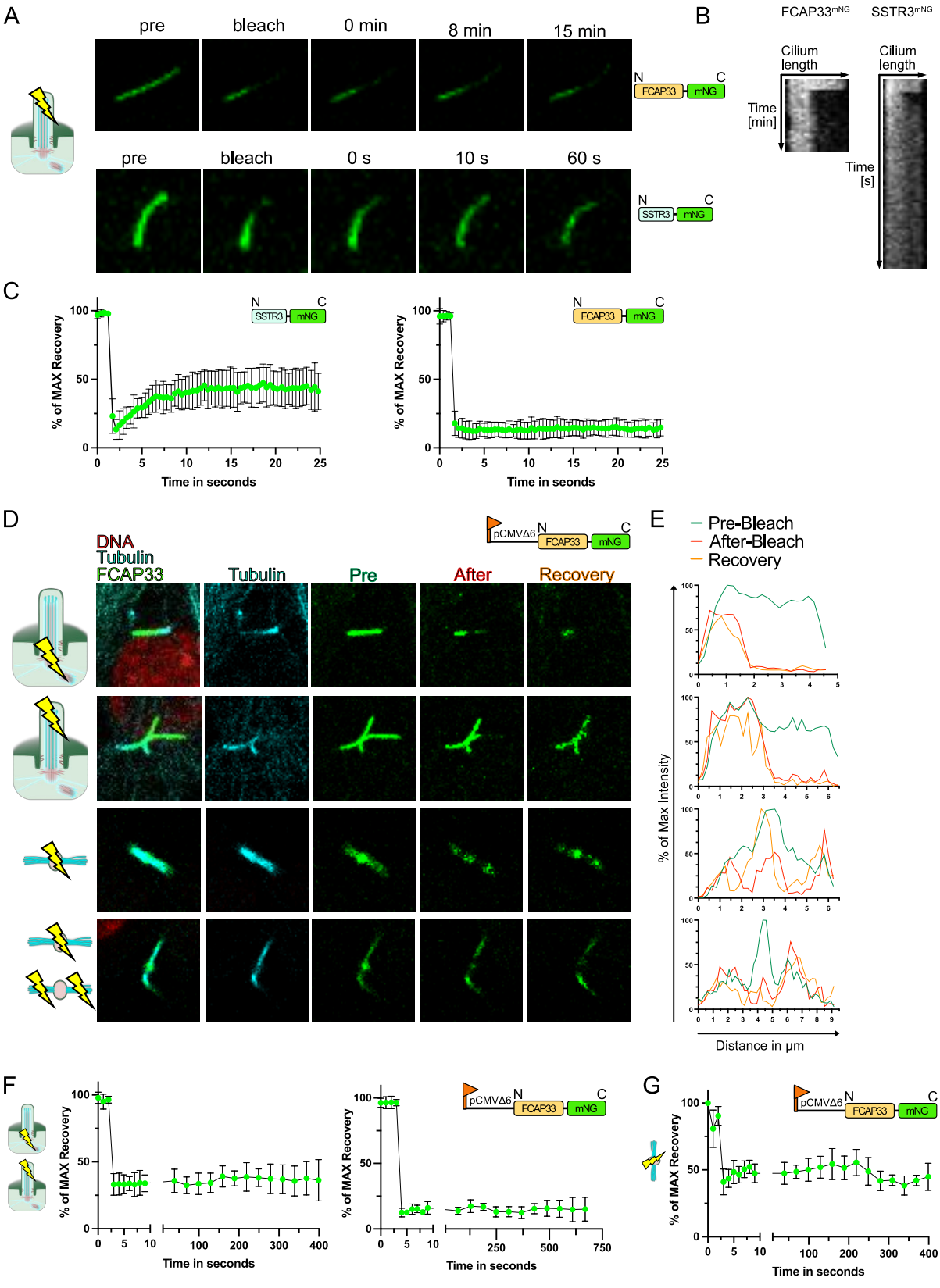
A
pre
bleach
0 min
8 min
15 min
N
C
FCAP33
mNG
pre
bleach
0 s
10 s
60 s
SSTR3
B
FCAP33mNG
SSTR3mNG
Cilium length
Time [min]
Time [s]
C
% of MAX Recovery
Time in seconds
D
DNA
Tubulin
FCAP33
Tubulin
Pre
After
Recovery
pCMVΔ6
E
Pre-Bleach
After-Bleach
Recovery
% of Max Intensity
Distance in µm
F
G

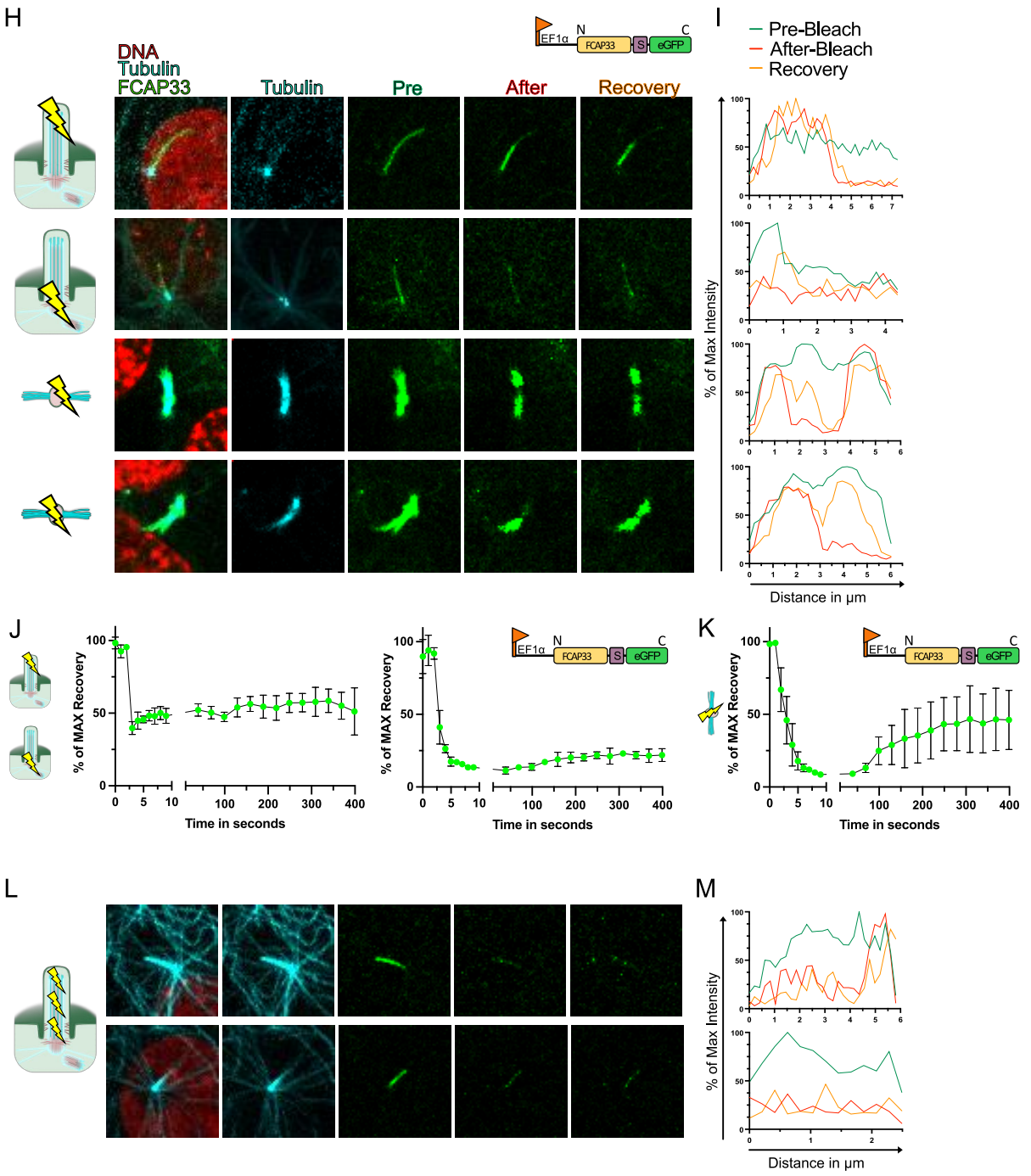

Figure 10: The recovery of FCAP33 after photobleaching is less in primary cilia than in midbodies and depends on the expression levels

(A) Representative cilia crops of FCAP33^{NG} and the control cell line SSTR3^{NG}. Half-cilium FRAP of SSTR3 or FCAP33. (B) Representative Kymographs of the cilia shown in A. Kymographs represent intensities of the single frames taken along the primary cilium at the y axis. The x axis shows the cilium length. (C) Recovery after photobleaching is plotted over time. Left graph shows the mean recovery of 8 SSTR3^{NG} cilia over time with standard deviation. Right graph shows the mean recovery of 11 FCAP33^{NG} cilia over time with standard deviation. (D + H) Representative crops of cilia that were photobleached. First lane, half-cilium FRAP cilium tip. Second lane, half cilium FRAP, cilium base. Third lane, stem body FRAP. Fourth lane, FRAP of midbody arm.

(E+H+M) Line plots representing the intensity profile of FCAP33^{NG} along the cilium or the midbody before bleaching, after bleaching and after recovery. In case of cilia, 0 represents the ciliary base. (F) Recovery after photobleaching is plotted over time. Left graph shows the mean recovery of 10 FCAP33^{NG} cilia over time with standard deviation. Right graph shows the mean recovery of 6 FCAP33^{NG} cilia over a longer time with standard deviation. (G) Recovery after photobleaching is plotted over time. Graph shows the mean recovery of 4 FCAP33^{NG} midbody measurements over time with standard deviation. Three out of four measurements are from one midbody (arms and whole). (J) Recovery after photobleaching is plotted over time. Left graph shows the mean recovery of 6 FCAP33^{cLAP} cilia over time with standard deviation. Right graph shows the mean recovery of 3 FCAP33^{cLAP} cilia over time with standard deviation. (K) Recovery after photobleaching is plotted over time. Graph shows the mean recovery of 3 FCAP33^{cLAP} midbody measurements over time with standard deviation. Two out of four measurements are from one midbody (arms and stem). (L) Representative crops of cilia that were photobleached. Both lanes, full cilium FRAP was aimed. Top lane, some Tip signal left, bottom lane full bleach. All FRAP experiments were done with a confocal microscope at RT. All Line plots and recovery plots are represented as % of the MAX reflecting the % of the highest intensity set to 100% (before bleaching). SPY DNA 555 Probe and SPY tubulin 647 to show nucleus and tubulin in living cells and to determine cilium orientation

depends again on expression levels. Recovery seems stronger in the stem and might potentially be refilled by the fraction in the arms.

FCAP33 colocalizes with AcTUB but shows spotted patterns

We determined that FCAP33 is associated to the axoneme in primary cilia. To further dissect its role, we sought to investigate the localization of FCAP33 with higher resolution. To this end I performed expansion microscopy (ExM) to specify the localization of the protein on microtubules (MTs) in IMCD3 cells. Cell lines with different expression levels of the protein were investigated: IMCD3 WT cells, IMCD3^{cLAP} (higher expression) and IMCD3^{ALFA} (lower expression). IMCD3^{ALFA} stably expresses FCAP33 tagged with the ALFA tagged under the weakl expression of the truncated CMV promotor compared to the higher expression of FCAP33^{cLAP} cells, where FCAP33 is expressed under the non-truncated EF1 alpha promotor. The ALFA tag is a small helix that allows very specific detection by the use of specific ALFA antibodies directed to a small peptide sequence of the helix (Götzke et al., 2019).

Expansion of midbodies in IMCD3 WT and ALFA-tagged cells (Figure 11 A, D) confirmed the localization of FCAP33 at midbody structures showing a puncta pattern co-localizing with AcTUB positive MTs (Figure 11 A, D). IMCD3 WT and FCAP33^{ALFA} also showed specific localization of FCAP33 to the stem body region of the expanded midbody structure (Figure 7 A, D). Line plots of normalized (% of MAX) and absolute fluorescence intensities (FI) of depicted regions of interest (ROIs, lines) were used for co-localization analysis of FCAP33 and

AcTUB and indirectly for the expression levels. These line-plots reflect the co-localization of FCAP33 and AcTUB and the puncta-like pattern in midbodies (Figure 10 A, D).

Imaging of expanded primary cilia in IMCD3 WT cells shows localization of FCAP33 along the axoneme in a spotted pattern (Figure 11 B). At the base of the primary cilium the distance of the microtubules stained by AcTUB is greater and gets more and more narrow towards the tip. This is since the base of the centriole consists of MT triplets and has a bigger lumen than compared to the tip of the cilium. Towards the tip the axoneme has almost no lumen anymore and MTs start to end at different length (Satir and Christensen, 2007; Conkar and Firat-Karalar, 2021). This can be appreciated by AcTUB staining of the expanded samples, with the ciliary base reflecting "separated" MTs, whereas towards the tips the axoneme gets thinner and looks like one MT with the accessible resolution of imaging (Figure 11). In IMCD3 WT cells FCAP33 seems to co-localize on the MT tubules as the FCAP33 signal co-localizes with the separated MTs at the bottom of the primary cilium (Figure 11 B). Additionally, a slight signal of FCAP33 can be estimated at centrioles marked by Centrin and AcTUB. In contrast to Centrin (cyan, BB and Centriole) which is localized to the lumen of the centrioles, FCAP33 seems to decorate the acetylated MTs (Figure 11 B). Line profiles show two peaks for AcTUB at the BB and the Centriole as expected. FCAP33 peaks (yellow) are either at a similar position or more outside from AcTUB (magenta) peaks (Figure 11 B). Even though Centrin sometimes shows several peaks (cyan) they are rather inside of the AcTUB peaks (Figure 11 B). This co-localization is even stronger detected in FCAP33^{cLAP} (Figure 11 C). FCAP33 clearly decorates the acetylated MTs, also at the BB and the centrioles. Line plots of BB1, BB2 and Centriole 1 (Figure 11 C) show similar patterns as before (Figure 11 B). Only at the position of the Centriole 2, more towards the distal end of the centriole, FCAP33 seems more localized to the inner side of the MTs (Figure 11 C). TheFCAP33 antibody had a high background signal in IMCD3 WT and FCAP33^{cLAP} cells. Therefore, the ALFA tagged cell line was tested, to achieve more specific FCAP33 staining by the ALFA antibody. Primary cilia showed a clear co-localization of FCAP33^{ALFA} with AcTUB in a puncta-like pattern (Figure 11 E). Looking at a centriole from the top view in the ALFA-tagged cell line confirms a co-localization with AcTUB at centrioles but not with Centrin at the lumen (Figure 11 E + G). In the merged images colocalizing AcTUB and FCAP33^{ALFA} is hardly visible, due to weak ALFA signals. Single channel projections clearly show the ALFA signal at the ring like structure (Figure 11 E + G). This reflects the low levels of the protein. Looking at IMCD3 WT cells and even at the FCAP33^{cLAP} overexpressing cells, FCAP33 levels at the axoneme and centrioles are generally lower than compared to AcTUB. Only at the spotted regions FCAP33 peaks strongly,

represented by the line plots (Figure 11 B + C) which goes hand in hand with the detection of low levels of FCAP33 in IMCD3 cells, previously described in this work. The ciliary line plots

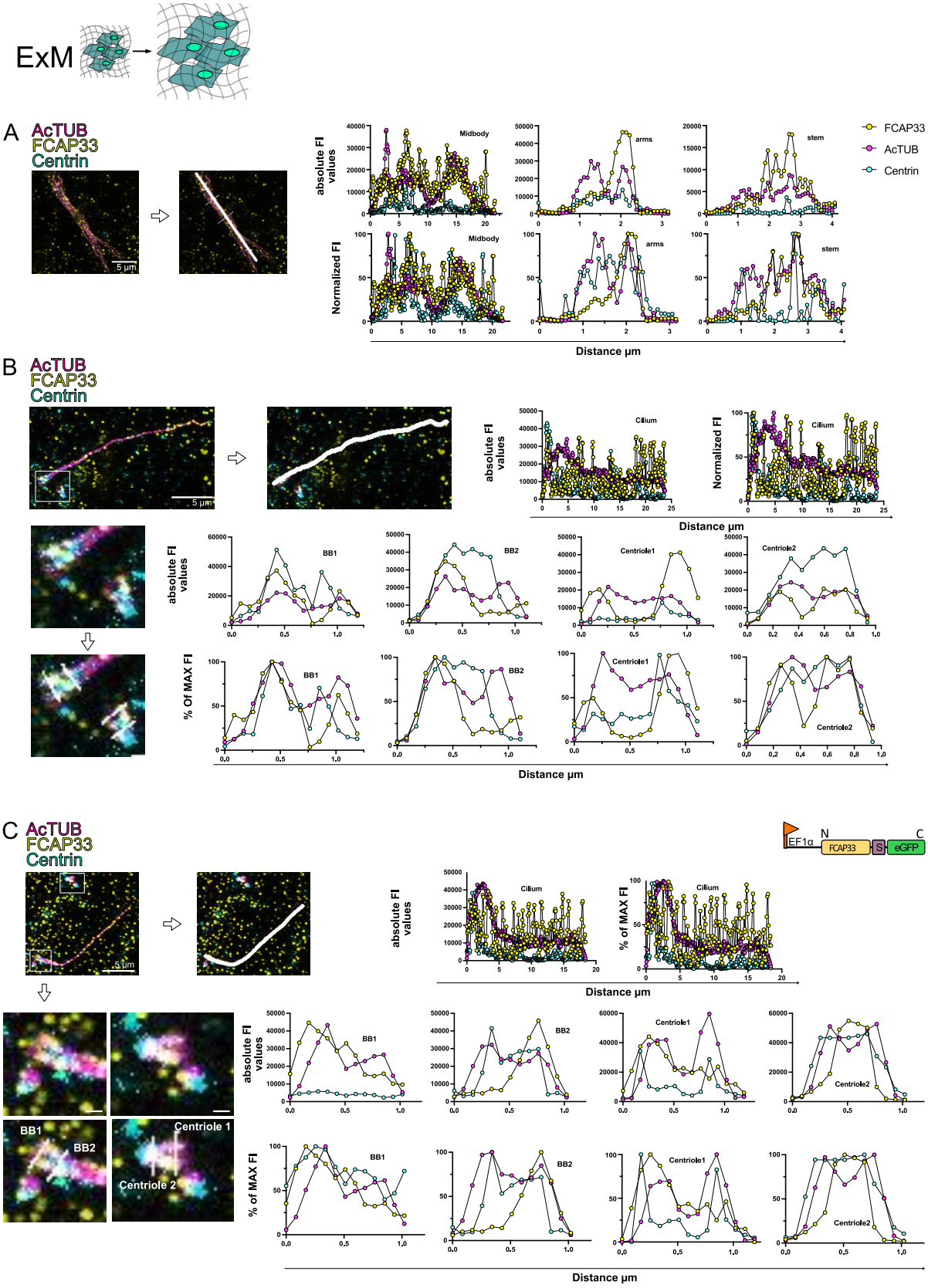

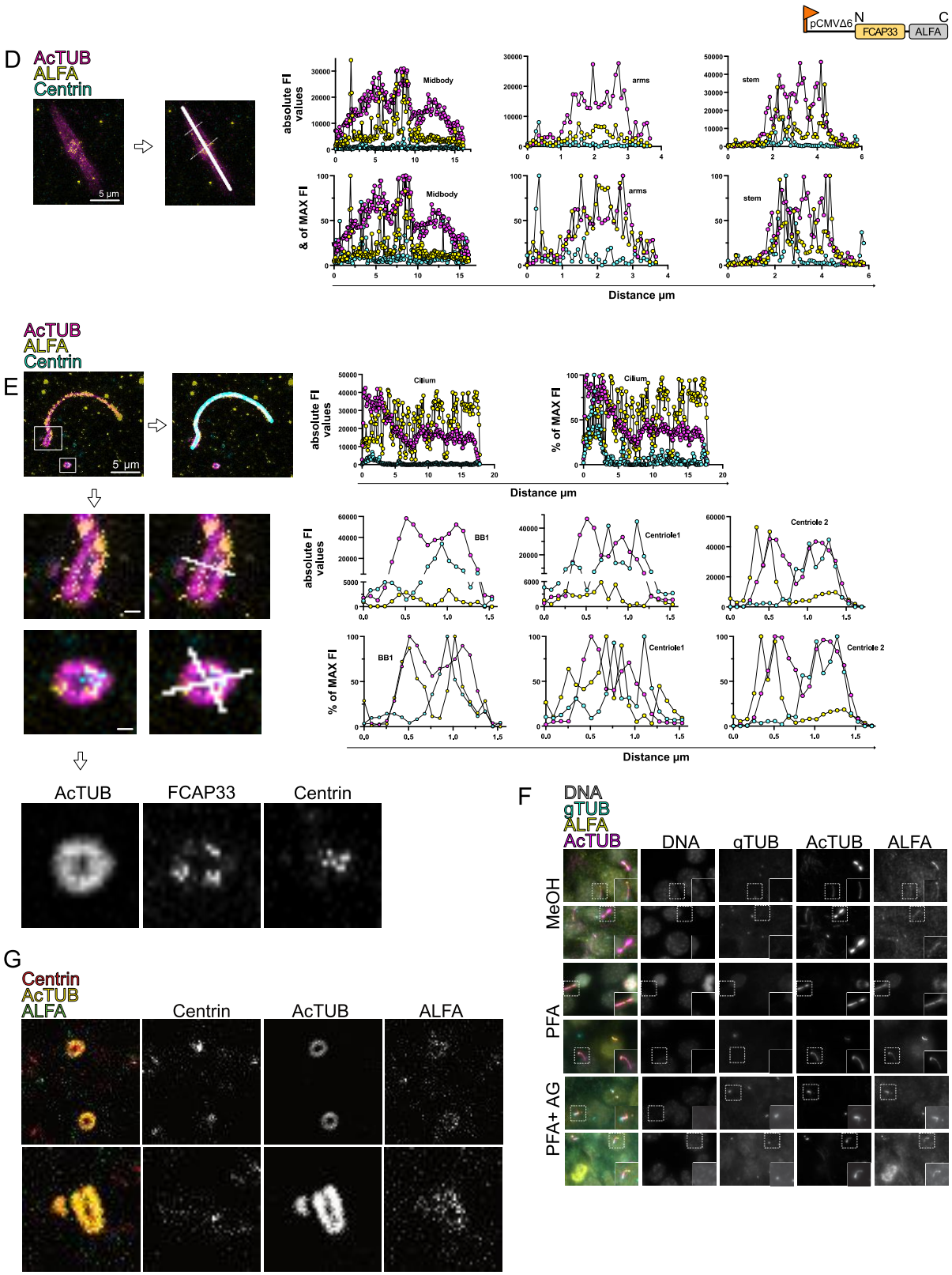

Figure 11: FCAP33 co-localizes with AcTUB in a spotted like manner and shows different pools in IF

(A-E) ExM of different cell lines. Cells were stained for AcTUB (magenta/yellow), Centrin as centriole and base marker (cyan/red), FCAP33 (yellow) and ALFA (yello/green). Imaging with LSM900 using SR Airy Scan mode. Expansion factor 4x. Lines indicate regions used for line plots of absolute fluorescence intensities (FI) of AcTUB; Centrin and FCAP33.

Relative values (% of MAX) in respective channel to analyze potential co-localization of FCAP33, AcTUB and Centrin. White lines in micrographs show ROIs used for co-localization analysis. (A) Midbody in IMCD3 WT cells. Spotted FCAP33 distribution. Stem shows mor FCAP33 than AcTUB. (B) Primary cilium of IMCD3 WT cells. Spotted distribution of FCAP33 with enriched levels at ciliary TIP. BB and Centriole show FCAP33 spots with some of them overlapping with AcTUB. (C) Cilium and Centriole of highly over-expressing FCAP33^{cLAP} cells. Cilium shows puncta pattern. FCAP33 co-localizes with AcTUB in cilium and localizes to BB and Centriole. Partial co-localization at Centriole and BB. (D) Midbody of FCAP33^{ALFA} with lower over-expression. Specific FCAP33 stembody signal. (E) Cilium and Centriole of FCAP33^{ALFA} with lower over-expression. FCAP33 along AcTUB in spotted manner. BB and Centriole localization. (F) IF experiments with FCAP33^{ALFA} cells. Gamma tubulin (gTUB) staining as BB and centriole marker. AcTUB for cilia and midbodies and ALFA staining for FCAP33. ALFA staining shows different ciliary pools of FCAP33 (base, tip and along cilium) and centriole staining. (G) Centriole and BB of FCAP33^{ALFA} with lower over-expression. FCAP33 along AcTUB in spotted manner. BB and Centriole localization.

show a spotted pattern for all different cell lines tested, independent of the expression levels (Figure 11 B, C, E). Expansion microscopy confirmed the proposed localization of FCAP33 to the axoneme of primary cilia but also to midbodies and centrioles.

FCAP33 seemed to be present at much lower levels than the axonemal core protein AcTUB, even in overexpressing cells and FCAP33 was always decorating MTs in a puncta pattern. This pattern was not observed before, when looking at highly overexpressed levels of FCAP33 in standard IF experiments. To test if this pattern can also be confirmed in standard immunofluorescence (IF), the ALFA-tagged and lower expressing cell line was used for IF. Different fixation methods were compared to check for centriolar, and ciliary FCAP33 localization (Figure 11 F).

Indeed, looking at ALFA-staining in these cells, showed a slightly more puncta pattern of the ALFA signal along primary cilia (Figure 11 F). Centriole localization as well as midbody localization was confirmed again under all conditions. In addition, we can see spindle staining again (Figure 11 F, PFA). Antigen retrieval was only efficient when cells were PFA fixed prior to retrieval treatment. Taking the results of all fixation methods and cells with different expression levels together, FCAP33 was confirmed to localize to MTs of the primary cilium axoneme, the centriole, the midbodies and to a very weak extent to spindles.

Staining with gamma tubulin (gTUB) marked the base and the centrioles. Interestingly, some FCAP33^{ALFA} cilia showed a stronger signal at the ciliary tip on the axonemal site distal of the gamma tubulin staining. This was also detected in FCAP33^{NG} cells (Figure 3 A). In conclusion, FCAP33 has an additional base and a ciliary tip pool, which could be dependent on FCAP33 expression levels or cilia status.

Short versions of FCAP33 are not sufficient for proper localization to MT based structures

Microtubule binding proteins can have a MT binding domain but do not necessarily need to. Some of these proteins are even classified by their domains (Fisher et al., 2008). Other microtubule associated proteins (MAPs) or microtubule inner binding proteins (MIPs) have a higher affinity due to their charge, amino acid content, or else (Janke, 2014; Bodakuntla et al., 2019). *In silico* analysis of FCAP33 did not reveal any specific MT binding domain. The charge of the protein is also rather neutral, with a slightly higher number of positively charged amino acids (see section "*In silico* analysis"). A positively charged protein could indicate better binding affinity to MTs as these are generally negatively charged (Bodakuntla et al., 2019). To test if FCAP33 has such a domain, or a specific part of the protein with higher affinity to MTs, truncated versions of the proteins were designed and tagged by a LAP tag (see before).

These constructs either encoded the N-terminal half of the protein ($FCAP33_{1\text{-}167}$) or the C-terminal half ($FCAP33_{168\text{-}288}$). Stable cell lines were created as described, using IMCD3 FlipIn cells. Consequently, the cell lines stably express $FCAP33_{1\text{-}167}$-cLAP/ $FCAP33_{168\text{-}288}$-cLAP in addition to the endogenous full-length FCAP33. In previous experiments, where IMCD3 cells were transfected with the same short versions of FCAP33 tagged to a neongreen tag, $FCAP33^{NG}$ did not localize to primary cilia or midbodies (Data not shown here). In these experiments, cells were usually fixed with PFA prior to MeOH fixation, which was shown to not make the centriolar pool of FCAP33 detectable. To confirm these results, we created cell lines (together with M. Sc. Student S. Ehr) using LAP-tagged truncation variants. We created stable IMCD3 WT cells with $FCAP33^{1\text{-}167}$-cLAP or $FCAP33^{168\text{-}288}$-cLAP. Both variants did not localize to cilia or midbodies, confirming the previous results and that the lack of detection of NG-tagged variants was not due to detection limits (Figure 12 A). Cells were either PFA fixed (Figure 12 A, right panel) prior to MeOH fixation or only MeOH fixed (Figure 12 A, left panel). The PFA fixation led to different GFP "background" signals, being higher in the C-terminal truncation. Only MeOH fixing cells enabled base and centriole staining (Figure 12 A, left). As expected in IMCD3 WT and $FCAP33^{cLAP}$ cells, base and centriole signal was detected upon FCAP33 staining but also in all other cell lines expressing either N-term or C-term (Figure 12 A, left MeOH). Antigen retrieval showed a strong base and centriole signal colocalizing with the AcTUB staining in both variants (Figure 12 B). The ciliary base signal was independent of the expressed short version of FCAP33. This means that the localization of endogenous FCAP33 was not hampered by the overexpression of the truncations.

To screen for a potential phenotype caused by the expression of truncated versions of FCAP33 in IMCD3 cells, IF experiments were performed and cilium length was measured for different clones and pools, using CiliaQ (Figure 12 C). These were compared to IMCD3 WT, $FCAP33^{cLAP}$, as well as were $FCAP33^{Crsipr}$-C4, $FCAP33^{Crsipr}$-C6 and $FCAP33^{Crsipr}$-C7. Analysis of cilia length of the truncations within two different experiments showed varying lengths. Strikingly, different clones for the N-terminal variants showed shorter cilia overall, with C10 being significantly shorter in two independent experiments. $FCAP33^{cLAP}$ length is similar to WT in the first set of measurements but not in the repeated experiment (Figure 12 C). This is because there are a few extremely long cilia, leading to a higher mean than compared to the first experiment. It can be appreciated that overexpressing FCAP33 elongates primary cilia. This was already shown in previous experiments (Figure 4, Figure 2). Regarding cilium length analysis, this represents the high diversity in cilia length especially for the overexpression of full-length FCAP33-cLAP. To further compare the short FCAP33 variants to the Crispr clones, WT and $FCAP33^{cLAP}$ cells, one clone and one pool were picked for each truncation and cilium length was analysis was repeated (Figure 12 C, right). Clone 10 of $FCAP33^{1-167}$-cLAP showed shorter cilia again, even though not being significant when compared to WT. This is not true for the pooled cell line, Pool1. Due to the fact that three independent clones of the N-terminal part did show the same shortening effect (Figure 12 C, left), clonal effects can be ruled out. The results indicate a general effect on ciliary length upon N-terminal overexpression. $FCAP33^{cLAP}$ has WT like cilia length again even though the population shows a different distribution of long cilia versus short cilia again. The expression of the C-terminus leads again to heterogenous cilium length and does not lead to significant changes in cilium length, compared to WT. There are indeed some long cilia as seen for the full-length population and the variance in length is more spread when compared to the N-terminus (Figure 12 C). The same images taken, were used to analyze the ciliation rates. Interestingly, the ciliation rates of clones of the N-terminal truncations were significantly lower than in WT cells (Figure 12 D). Clone 10 showed less cilia in both experiments.

In summary, cilia seem longer when overexpressing FCAP33 in its full-length version. Overexpressing FCAP33 C-terminal variant does not seem to impact the cilium length, which is also true for the different Crispr clones that may still expressing the N-terminal part of the protein. Overexpressing the FCAP33 N-terminal variant does lead to shorter cilia, proposing a dominant negative effect on cilium length.

Short versions of FCAP33 are not sufficient for cilium or midbody localization of the protein in IMCD3 cells. Next, I tested whether transiently transfecting the short versions shows

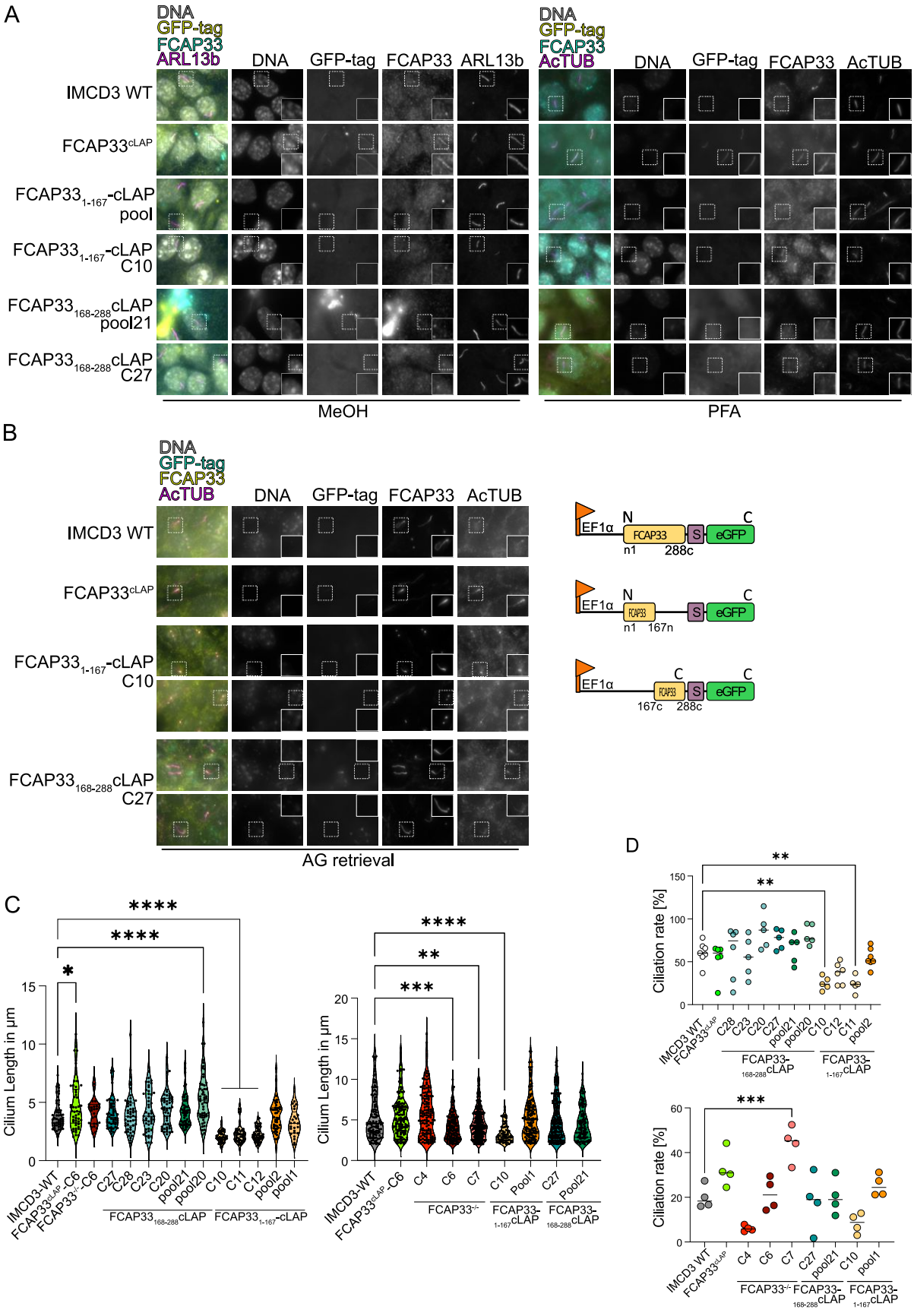
A
DNA
GFP-tag
FCAP33
ARL13b
DNA
GFP-tag
FCAP33
ARL13b
DNA
GFP-tag
FCAP33
AcTUB
DNA
GFP-tag
FCAP33
AcTUB
IMCD3 WT
FCAP33cLAP
FCAP33168-288cLAP pool21
FCAP33168-288cLAP C27
FCAP331-167-cLAP pool
FCAP331-167-cLAP C10
MeOH
PFA
B
DNA
GFP-tag
FCAP33
AcTUB
DNA
GFP-tag
FCAP33
AcTUB
IMCD3 WT
FCAP33cLAP
FCAP331-167-cLAP C10
FCAP33168-288cLAP C27
AG retrieval
EF1α
N
C
FCAP33
S
eGFP
n1
288c
EF1α
N
C
FCAP33
S
eGFP
n1
167n
EF1α
C
C
FCAP33
S
eGFP
167c
288c
C
****
****
*
Cilium Length in µm
15
10
5
0
IMCD3-WT
FCAP33cLAP-C6
FCAP33-/--C6
C27
C28
C23
C20
pool21
pool20
C10
C11
C12
pool2
pool1
FCAP33168-288cLAP
FCAP331-167-cLAP
****
****
**
***
Cilium Length in µm
20
15
10
5
0
IMCD3-WT
FCAP33cLAP-C6
C4
C6
C7
C10
Pool1
C27
Pool21
FCAP33-/-
FCAP33-1-167cLAP
FCAP33-168-288cLAP
D
**
**
Ciliation rate [%]
150
100
50
0
IMCD3 WT
FCAP33cLAP
C28
C23
C20
C27
pool21
pool20
C10
C12
C11
pool2
FCAP33-168-288cLAP
FCAP33-1-167cLAP
***
Ciliation rate [%]
60
40
20
0
IMCD3 WT
FCAP33cLAP
C4
C6
C7
C27
pool21
C10
pool1
FCAP33-/-
FCAP33-168-288cLAP
FCAP33-1-167cLAP

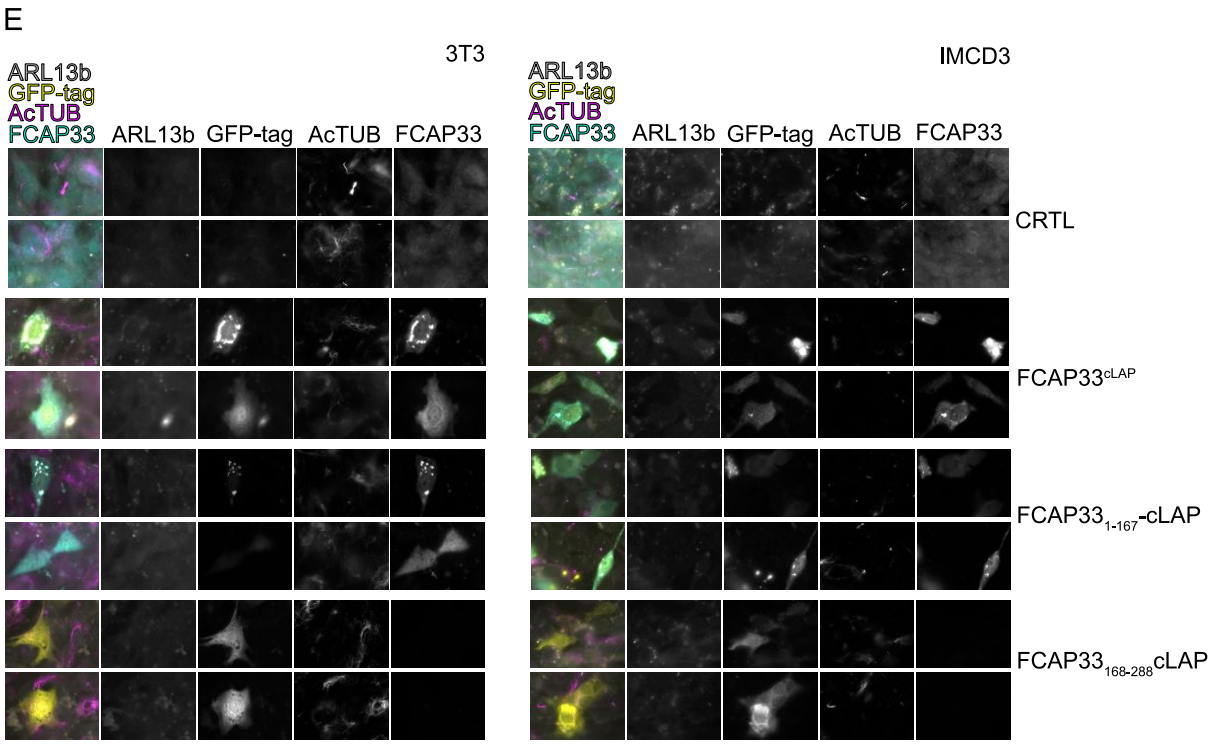

Figure 12: Short versions of FCAP33 do not localize to the primary cilium or midbodies

IF experiments of starved cells of truncated versions of FCAP33. LAP tagged N-terminal part (FCAP33$_{1\text{-}167}$-cLAP) and the C-terminal part (FCAP33$_{168\text{-}288}$-cLAP) are stably expressed in IMCD3 WT cells. Hoechst staining for DNA, GFP fluorescence for tagged FCAP33, FCAP33 staining and AcTUB as cilia and midbody marker. (A) Comparison of MeOH fixation (left) and PFA fixation (right). (B) Antigen retrieval with MeOH fixation. (C) Cilium length was measured, using CiliaQ and ARL13b as cilia marker in two independent experiments. Comparison of different clones and pools of cell lines stably expressing the truncated versions of FCAP33. (D) Ciliation rates were defined with automated Fiji analysis. Same images were used, as for analysis of the cilium length. (E) IF experiments of starved cells after transient transfection of IMCD3 WT and 3T3 WT cells with short versions of FCAP33^{cLAP}. ARL13b and AcTUB as cilium marker, GFP fluorescence for LAP tag and FCAP33 antibody staining.

different localization in IMCD3 and 3T3 cells. Transient transfection allows a temporary and fast transfection of cells but not the stable integration into the genome. Both cell lines used in these experiments are mouse cell lines (Chong et al., 2021). Transient transfection of FCAP33^{cLAP} in IMCD3 cells showed various localizations of the protein. For the IF experiment, cells were starved after transfection. Even though primary cilia could not be detected, strong GFP signals were detected within the cell body overlapping with the antibody staining for FCAP33. In 3T3 cells a similar result as seen for IMCD3 cells was obtained when transfecting the cells with the full-length protein (Figure 12 E). Transient transfection with the N-terminus showed a similar result in both cell lines. GFP-signals co-localizing with FCAP33 were detected within the cell body in an aggregate-like pattern similar to the full-length version

(Figure 12 E). For the C-terminus the localization of FCAP33 after transient transfection seems to be different. The C-terminus shows a rather uniform signal throughout the whole cell body, but no puncta-like or aggregate-like structures (Figure 12 E). For none of the ciliated cells, there was GFP or FCAP33 signal within the cilium region. The control cells showed intact ciliation but only in rare cases FCAP33 was detected at the ciliary base in IMCD3 cells. In 3T3s there was no clear FCAP33 signal detectable (Figure 12 E). FCAP33^{cLAP} and C-terminal variants did not show significant differences, compared to WT cells. The FCAP33 Crispr cell lines had a heterogenous ciliation rate pattern.

In conclusion, truncated variants of the protein are not sufficient for FCAP33 to localize to cilia or midbodies. This is independent of having the N-terminal half or the C-terminal half. Both short versions of the protein are not detectable in cilia or midbodies in IF. Especially in the overexpressing LAP-tagged cell lines, the C-terminus seemed to be stronger expressed (higher GFP background in IF), but the N-terminus might still localize to basal bodies and centrioles in IMCD3 WT cells.

N- and C-terminal fragments of FCAP33 show different expression levels and mediate different functions

To validate the expression of the truncated variants of FCAP33 and to further characterize these truncations, LAP-tagged truncations and the full-length FACP33 were isolated and enriched from cell lysates using immunoprecipitation (IP). IP experiments were performed by S. Ehr by using anti-GFP agarose beads (Figure 13 A). I performed further analysis of the samples by performing SDS-Page followed by western blot (WB) under reducing and non-reducing sample conditions.

The benefit of the LAP tag is, that elution of GFP tagged proteins is performed by protease cleavage and only the small S-tag is still tagged to the protein of interest. For studying potential interactions or functions of the protein it is important to either work with endogenously tagged protein or to work with a construct which reflects the endogenous protein as good as possible. As a huge tag like GFP could impact possible interactions, the ability to cleave it off allows to study interactions in a more physiological way. Another benefit of the S-tag is that it should be present in all samples, before and after cleaving off the GFP, and could therefore be used to detect it on WB in all samples. To analyze the IP samples, input (I), the unbound material called flow-through (FT), the Elution (E) after cleavage with the HRV3C protease and the SDS-Elution (SDS) were analyzed. FCAP33^{cLAP}, FCAP33$_{1\text{-}167}$-cLAP, FCAP33$_{168\text{-}288}$-cLAP and an

IMCD3 WT control were used for the IP experiment. A scheme of the IP is depicted in Figure 13 A. The WB performed after IP sample collection, was decorated with anti S-tag antibody to detect all samples at once. Interestingly, only for the elution samples of FCAP33$_{168-288}$-cLAP there was a specific band detectable that ran at the expected size (Figure 13 C). The lack of detection in the other elution samples could be caused by the inaccessibility of the S-tag in the other constructs, for example due to protein folding or inefficient elution. The lack of detection in the input samples could be due to too low FCAP33-cLAP levels in these samples. To check for both options, first, the input samples were tested by using the GFP antibody. The GFP detection confirmed the expression of all different constructs indicated by specific GFP bands at the expected band sizes for the non-cleaved constructs (Figure 13 B). Band intensities were not quantified but there was an obvious difference in the expression of FCAP33$_{1-167}$-cLAP compared to N-terminus and full-length (FL). The stronger expression of the C-terminus goes hand in hand with the higher GFP background in IF experiments (Figure 12). Additionally, this construct was the only one showing a double band like pattern. The GFP-WB (Figure 13 B) confirmed that all constructs are expressed and detectable in the samples but not accessible for the S-tag antibody before cleavage by the HRV3C protease. Input samples were also checked by staining the membrane with anti-FCAP33 antibody (Figure 13 E). As the antibody only detects the N-terminus of the protein, the C-terminus should not be detected. This was confirmed (Figure 13 E) by the lack of a specific band in the FCAP33$_{168-288}$-cLAP samples. This result additionally reflects the specificity of the antibody discussed at the beginning of this work. To test whether in the elution the S-tag signal is missing due to inefficient unfolding of the protein structure, the reducing agent DTT (+DTT) was added to the samples. Theoretically, samples containing SDS-Sample buffer (Bhuyan, 2010) and heating them up to 95 °C should already lead to unfolding. For strong di-sulfide bonds or other interactions reducing conditions in the sample buffer are needed to completely unfold the protein structure and make it accessible for antibody binding (Mishra et al., 2017). Reducing (+DTT) and non-reducing (-DTT) samples were compared after staining for the S-tag. Adding DTT led to the detection of very weak signals in Elution and SDS samples of FCAP33$_{168-288}$-cLAP but not for the +DTT FL construct. The C-terminus was detected as seen before in the -DTT samples. As the S-tag antibody was not sufficient to analyze the samples of the IP experiments, -DTT and +DTT membranes were redecorated with anti-FCAP33 antibody. As expected, the FL and the N-terminal variant were detected in input, eluate and SDS samples, but not in the C-terminal variant. It was striking that for FCAP33 in the eluate and SDS -DTT samples, bands were detectable at a higher molecular weight, meaning that oligomers which were not unfolded

without reducing conditions were detected (Figure 13 D). In the input samples these complexes were not visible, which could be due to detection limits or due to the GFP tag that might impact such strong oligomerization. Adding DTT efficiently removed the oligomers, as no higher molecular weight bands were detectable anymore with the FCAP33 antibody (Figure 13 D). These oligomers refer to the same size, slightly above 80 kDa as the bands seen for the endogenous protein (Figure 4, Figure 5). In conclusion, this suggests that FCAP33 can form an oligomeric state that is depleted under reducing conditions. This is true for the full-length and the N-terminal protein, but for the C-terminus this effect was not detected upon staining with the S-tag antibody.

During tests to express FCAP33-GST in *Escherichia coli (E. coli)*, I always obtained very low expression of the FL protein with different conditions, compared to controls (Data not shown). Therefore, we were wondering whether FCAP33 might potentially be toxic to *E.coli* and whether expression of the disordered C-terminus might be the reason for a low expression.

To test if the C-terminus might be unstable in *E.coli* and potentially mammalian cells, we co-operated with Monika Lerner (Group of Prof. Dr. Bianca Schrul, PZMS, Homburg) to perform an *in vitro* translation assay. Rabbit reticulocyte lysate can be used as a mammalian cell-free system for the expression of proteins (Pelham and Jackson, 1976). This allows the expression of proteins that would be toxic *in vivo*. The analysis of the protein samples collected after synthesis showed that in a cell free system FCAP33 full-length and C-terminus are expressed and detected by GFP (Figure 13 F). As antibody control, stored input samples generated in previous experiments (Figure 13 B-D) were loaded together with the reticulocyte generated samples on a SDS-Gel for WB analysis. GFP detection on the WB showed that in IVT samples the C-terminus seemed to be lower expressed than FL. This is in contrast with input samples of the IP, where the C-terminus again showed a stronger signal than FL and N-terminal variants. Taking this together, different properties of the N-terminus and the C-terminus of the protein are likely, shown by the lack of proper axonemal and midbody MT association in IMCD3 cells, different expression levels and types after stable, and transient transfection as well as potential oligomerization properties.

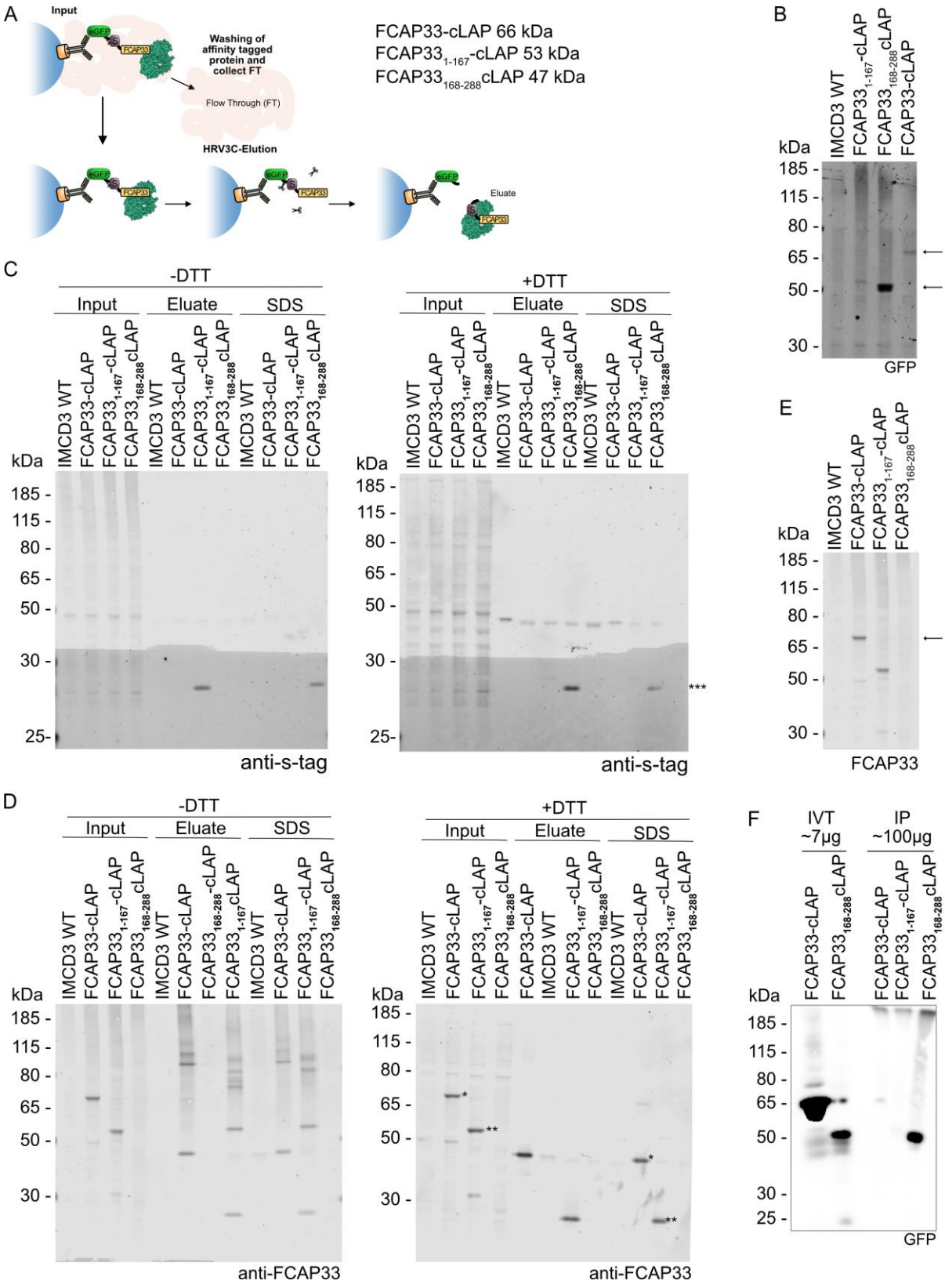

Figure 13: FCAP33 C-terminal variant shows higher expression levels and N-terminus is involved in SDS-resistant oligomer formation

(A) Scheme of GFP pull down assay. Protease cleavage allows elution of proteins bound to the GFP column. The S-tag remains after cleavage. (B) Input samples are run on an SDS-Gel and transferred to nitrocellulose. GFP detection to confirm expression of all FCAP33 variants.

100 µg protein loaded, in 1x SDS 1x Laemmli + DTT boiled 95 °C. (C+D) IP samples are run on an SDS-Gel and transferred to nitrocellulose. S-tag detection (C) and FCAP33 (D) in 1x SDS 1x Laemmli and boiled at 95 °C. +DTT and -DTT sample comparison (E) Input samples were run on an SDS-Gel and transferred to nitrocellulose. FCAP33 detection to confirm expression of FL and N-term FCAP33 variants. 100 µg protein loaded, in 1x SDS 1x Laemmli + DTT boiled 95 °C. (F) Comparison of samples from in-vitro translation assay (IVT) to input samples from IP. HRP blot detecting GFP.

FCAP33 binds to MT in vitro

The different experiments using the truncated versions of FCAP33 revealed that the FL protein is needed for localization to primary cilia and midbodies. Therefore, I hypothesized that the full-length protein is needed for proper microtubule (MT) association and the N- or C-terminal half of the protein is not sufficient for MT binding. To dive deeper into the microtubule binding properties of FCAP33, various tests were run to express FCAP33 tagged to a GST or to a His tag in *E.coli*. Testing different buffers, temperatures, inductions and lysis methods did not lead to yields of purified FCAP33 that were high and pure enough to perform *in vitro* microtubule binding and polymerization assays with purified FCAP33 (Data not shown). To overcome this challenge and get more insight into the MT binding properties of FCAP33 we teamed up with the Lab of Jun.-Prof. Lauta Aradilla Zapata (née Schaedel) at the University in Saarbrücken. The PhD student Dyuthi Sreekumar performed a previously published (Jijumon et al., 2022) lysate-based assay where HEK293T cells were transiently transfected with the FCAP33^{cLAP} constructs. The soluble fraction containing the tagged protein of interest is further subjected to GMPCPP seeds (MT-seeds). Growing MT seeds and the protein of interest can be followed by TIRF microscopy or imaged at steady state after MT formation and potential binding of the protein (Figure 14 A) (Jijumon et al., 2022). Additionally, this allows to use the same plasmid DNA constructs as used for generating stable cell lines in the previous experiments. Adding the soluble fraction of FCAP33^{cLAP}-HEK293T cells to the MT-seeds showed binding of full-length (FL) FCAP33 to the MT-seeds and to the growing MT-lattice, confirming binding of FCAP33 to microtubules in vitro (Figure 14 B, left).

Performing the same experiments with FCAP33$_{1-167}$-cLAP-HEK293T showed binding of the N-terminus to the microtubule lattice (Figure 14 B, middle). The binding to the MT-seeds seemed comparable to the binding of the FCAP33 FL. FCAP33$_{168-288}$-cLAP-HEK293T had generally a high signal to noise ratio and binding seemed weaker (Figure 14 B, right). The ExM experiments showed that the localization of FCAP33 at BB and centrioles overlapped with the staining for AcTUB. Additionally, the behavior of FCAP33 in the demembranation assay was similar to that of acetylated tubulin. However, these results do not allow to differentiate if

FCAP33 is a MAP or if it might even be a MIP. In Figure 14 B it seemed that FCAP33 shows less binding to MT seeds than to growing MTs, which could be a hint for FCAP33 binding to inner MTs. To test this, MTs were pre-formed and the FCAP33 lysate was added afterwards. If FCAP33 is an inner-binding protein, it should bind less to preformed MTs, as inner sites of the MTs are less accessible. The binding of all three versions to preformed MTs (Figure 14 C) did not differ to the binding seen for growing MTs (Figure 14 B). Therefore, FCAP33 does not seem to exclusively bind to the inner site of MTs. Generally, it can be noticed that all three variants bind in a spotted manner along the MTs but the C-terminus seems to form less intense spots. This is also reflected by the line profiles along a MT shown in Figure 14 D. Absolute fluorescence intensity plots of FCAP33-FL and FCAP33 N-terminus show a similar pattern: heterogenous distribution with many maxima and minima. The C-terminus of FCAP33 shows fewer and smaller minima and maxima (Figure 14 D, cyan). In the lysate-based assay, protein amounts are controlled by measuring and adjusting the protein concentration of the whole cell lysate. Next, cell lysates were diluted with non-expressing HEK293T cell lysate to investigate if MT binding of FCAP33 is dose-dependent MTs (Figure 14 E). Again, binding of the C-terminus to MTs (Figure 14 E, right) is less than the binding of FCAP33 FL and N-terminus to MTs (Figure 14 E, left and middle). As a control, we compared FCAP33 also to PRC1 a co-localizing midbody protein. PRC1 shows a more uniform distribution, with much smaller peaks (Figure 14 F + G). In summary, it can be appreciated that full-length and N-terminal FCAP33 show a stronger affinity to MTs than the C-terminal half of FCAP33. The binding pattern seems to be more spotted along the MTs in these versions of FCAP33. Binding affinity does not depend on the concentration and FCAP33 binds similarly to pre-formed MT than to growing MT indicating that it is rather a MAP than a MIP.

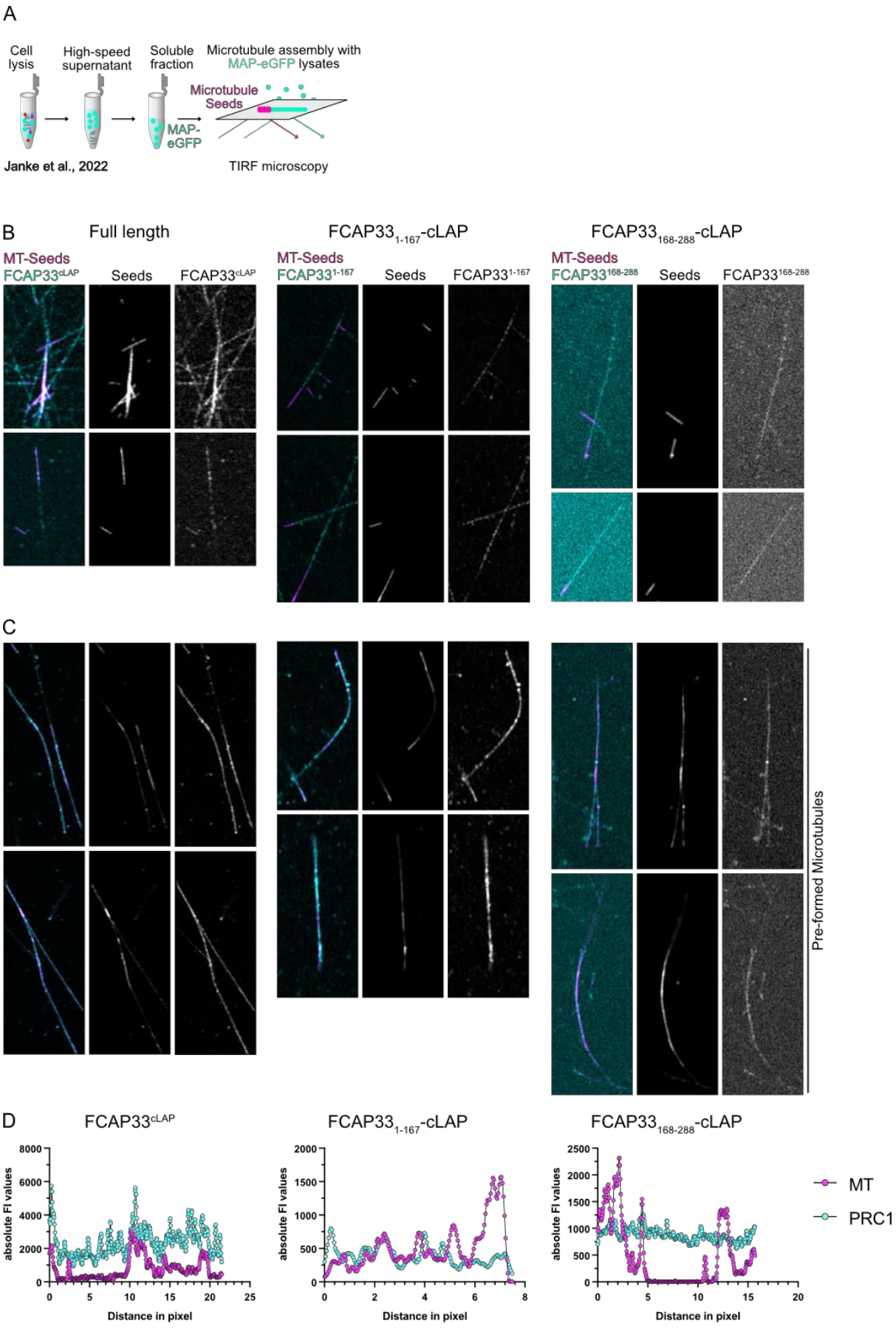
A
Cell lysis
High-speed supernatant
Soluble fraction
Microtubule assembly with MAP-eGFP lysates
Microtubule Seeds
MAP-eGFP
Janke et al., 2022
TIRF microscopy
B
Full length
FCAP33$_{1-167}$-cLAP
FCAP33$_{168-288}$-cLAP
MT-Seeds
FCAP33^{cLAP}
Seeds
FCAP33^{cLAP}
MT-Seeds
FCAP33$^{1-167}$
Seeds
FCAP33$^{1-167}$
MT-Seeds
FCAP33$^{168-288}$
Seeds
FCAP33$^{168-288}$
C
Pre-formed Microtubules
D
FCAP33^{cLAP}
FCAP33$_{1-167}$-cLAP
FCAP33$_{168-288}$-cLAP
absolute FI values
Distance in pixel
MT
PRC1

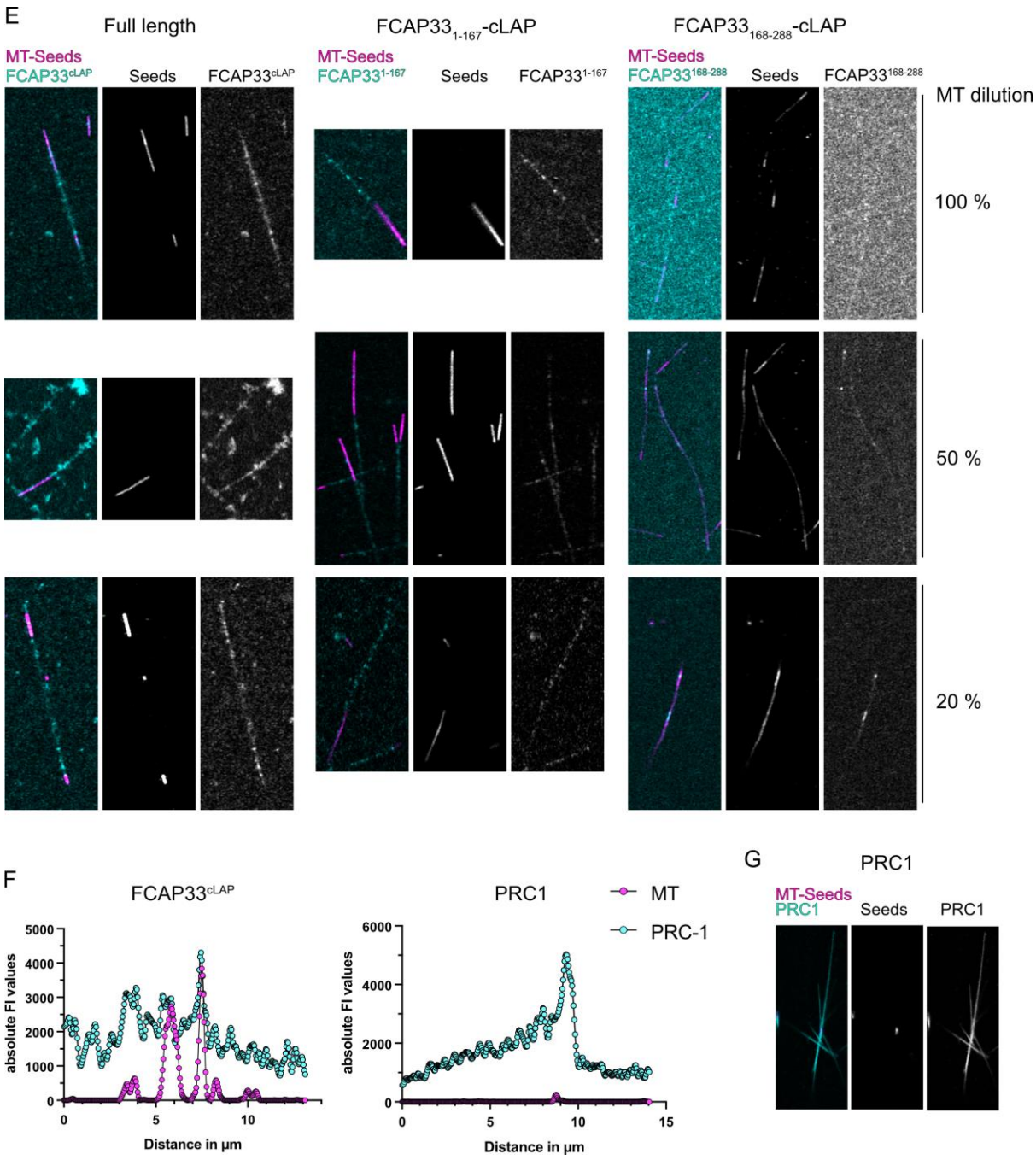

Figure 14: Full-length and N-terminal FCAP33 bind to microtubules with higher affinity, independent of MT status

(A) Scheme of MT-binding assay, adapted from (Jijumon et al., 2022). (B) FCAP33^{cLAP} (cyan) FL (left) and truncations (middle, right) added to rhodamine labeled (magenta) growing MT seeds. Steady-state images. C-term FCAP33$_{167-288}$-cLAP binding is weaker than FL and N-term. (C) FCAP33^{cLAP} (cyan) FL (left) and truncations (middle, right) added to rhodamine labeled (magenta) pre-formed MT seeds. Steady-state images. C-term FCAP33$_{167-288}$-cLAP binding is weaker than FL and N-term. (D) Line-Plot of microtubules. Absolute intensity values of respective channel. Comparison of FL FCAP33 to the truncated versions of FCAP33. Analysis done with preformed MTs. (E) Dilution assay. FCAP33 lysate was diluted with non-expressing cell lysate. FCAP33^{cLAP} (cyan) FL (left) and truncations (middle, right) added to rhodamine labeled (magenta) pre-formed MT seeds. Steady-state images.

C-term FCAP33$_{167-288}$-cLAP binding is weaker than FL and N-term. Binding seems independent of FCAP33 concentration in all three cases. (E) Line-Plot of microtubules. Absolute intensity values of respective channel. Comparison of FL FCAP33 to a control protein PRC-1. FCAP33 profile seems more heterogenous along a MT (more maxima and minima with higher differences). (G) PRC1 (cyan) added to rhodamine labeled (magenta) growing MT seeds. Steady-state images conducted with LSM900.

FCAP33 is potentially important for cell survival

Various experiments showed that FCAP33 localizes to different MT-based structures and cannot be detected anymore at some of these (cilia, midbodies) after depletion of FCAP33 using siRNA or CRISPR Cas 9 mediated gene KO targeting Exon 4. Indeed, it was shown that FCAP33 still seemed to be present at low levels in these Crispr clones (WB) but was not able to localize to midbodies or throughout the whole cilium. FCAP33 localization in the Crispr clones targeting Exon 4 was rather restricted to the centriole and the basal body in most cases. This could either be due to low levels, or due to a truncated leftover of the protein. Several experiments showed that the antibody still detects FCAP33 in theses Crispr clones (C1, C4, C6 and C7). It was also demonstrated that the antibody can specifically bind to the N-terminus of the protein (WB experiments Figure 13). Analysis of sequenced gDNA using benchling and TIDE looked promising for the tested Crispr cell lines. Manually reanalyzing the sequence results revealed that Crispr clone C1, C6 and C7 were heterogenous and still had a WT copy. Only C4 had no WT copy, but a one-base pair insertion that led to a frameshift in the downstream sequence. Therefore, the signals detected in different IF experiments with the Crispr clones: FCAP33^{Crsipr}-C1, FCAP33^{Crsipr}-C6 and FCAP33^{Crsipr}-C7 probably reflect low FCAP33 levels and/or truncated versions. FCAP33^{Crsipr}-C4 should reflect a N-terminal truncation. Regarding these results, it is questionable whether targeting Exon 4 leads to efficient KO of the protein.

To investigate whether it is impossible to completely knock out FCAP33 without leading to cell death and if targeting an earlier Exon leads to the lack of FCAP33 at basal bodies and centrioles, A. Prasai performed another Crispr Cas 9 mediated KO experiment, targeting Exon 2 of FCAP33. There were several cell clones recovering and growing after sorting single cells efficiently transfected with the Crispr plasmid. First, I analyzed the genomic DNA by sequencing, performing sequence alignments and TIDE analysis.

This analysis revealed that from eleven clones FCAP33^{Crsipr}-C10 to FCAP33^{Crsipr}-C20 and FCAP33^{Crsipr}-C22 and four pools FCAP33^{Crsipr}-Pool 1-1, FCAP33^{Crsipr}-Pool 1-2, FCAP33^{Crsipr}-Pool 2-1 and FCAP33^{Crsipr}-Pool 2-2 only 4 clones are potential KOs with high confidence R

values higher than 0.9 and potential deletions and insertions in TIDE analysis. All the other clones with a high confidence value and with over 90% probability of not having a deletion or insertion only contained the WT copy. Alignments of the sequences showed a 100 % similarity of all clones except of the 4 mentioned clones: C12, C16, C16 and C22. Even though several gDNA sequencing experiments were performed, I was not able to fully resolve the sequence around the region of Crispr target sequence. Except for C22, that is likely to still have a WT copy. To find out if the mentioned clones were potential KOs, IF experiments were performed (Figure 15). To identify whether the basal pool of FCAP33 is still visible after FCAP33 staining, cells were fixed with MeOH. IMCD3WT, FCAP33^{Crsipr}-C7 and FCAP33^{Crsipr}-C4 confirmed the basal staining of FCAP33 that was demonstrated before (Figure 15 A). There was no clear difference between the newly generated Crispr clones C12 and C16 compared to the WT control. Especially C16 seemed to have a stronger basal FCAP33 signal than IMCD3 WT. Only C22 might have an absent FCAP33 basal stain. C19 also showed FCAP33 basal staining, but to a weaker extent (Figure 15 A), when compared to WT. These results were confirmed in several images in a second IF experiment (not shown here). Again, MeOH fixation was compared to a combined PFA and MeOH staining (Figure 15 B). Surprisingly, this comparison revealed that FCAP33 could be detected within primary cilia of the Crispr clones and the WT cells in the PFA condition, similar to the FCAP33^{cLAP} control (Figure 15 B). Cilium length and ciliation rates were quantified from different experiments. In a first set, all Crispr clones were analyzed. Theoretically, all clones and pools that contained the WT sequence copy should reflect the IMCD3 WT and only the potential Crispr KOs C12, C16 and C19 should have an expected phenotype. When measuring cilium length using CiliaQ (Figure 15 C), there were no significant changes of the Crispr clones compared to the other cell lines and to the WT after performing a multiple comparison using one-way ANOVA. The violin plots show that the cell lines vary a lot in cilium length and in some cases only a few cilia were measured, e.g C11, Pool 2-1 and C20. Analyzing ciliation rates confirmed that C11, Pool 2-1 and C20 had low ciliation rates (Figure 15 D). C12, C16, C22 and the Exon 4 targeted Crispr clone C4 showed higher ciliation rates in these images/cells compared to the WT control. Both analyses were repeated with the images of Figure 15, B. C12 showed again a higher ciliation rate compared to WT (Figure 15 F), but the effects of C16 and C22 could not be reproduced. Instead, cilium length analysis now revealed significant differences for C12, C16 and C22 (Figure 15 E) that

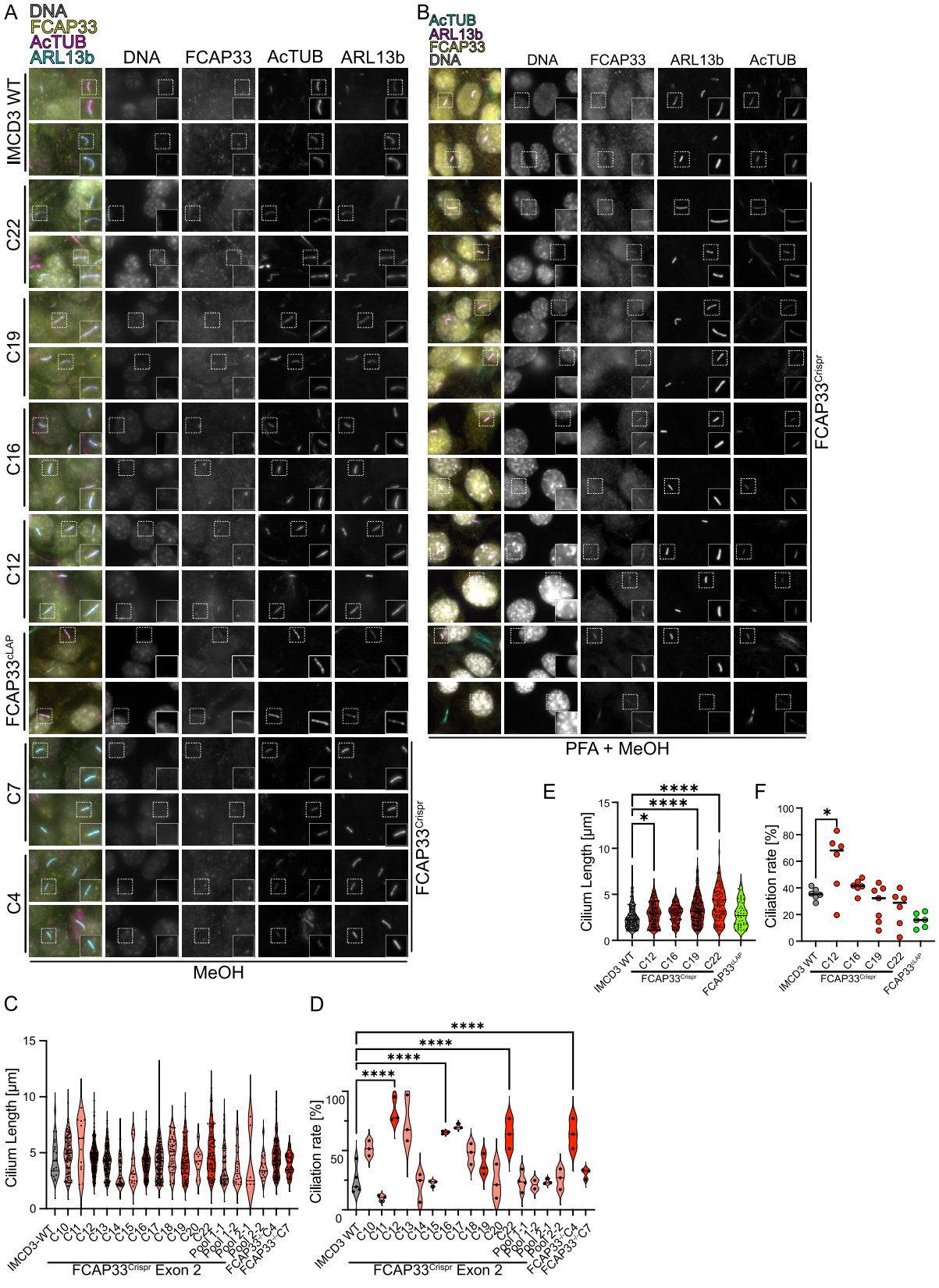

Figure 15: Targeting Exon 2 to knockout FCAP33 does not lead to a full ablation of FCAP33

(A) + (B) IF of different new Crispr cell lines, IMCD3 WT and FCAP33^{cLAP}. Hoechst to stain DNA. FCAP33 staining, AcTUB as cilia and MT marker, ARL13b as cilia marker.

(A) Cells were methanol fixed. (B) Cells were PFA fixed prior to MeOH fixation. (C) + (E) Cilium length was analyzed using CiliaQ and ARL13b as cilia marker. (D) + (F) Ciliation rate was quantified using Fiji and an automated makro counting nuclei and ARL13b structures as cilia.

were not significant before (Figure 15 C). Violin plots (Figure 15 C) of the cilium length indicate that there are indeed some longer cilia, when compared to IMCD3 WT. In summary, it is still under debate if we can efficiently knockout FCAP33, targeting Exon 2. It might not be possible because the cells need FCAP33 to survive. Regarding the IF images it is unlikely that we were able to fully KO FCAP33. Nevertheless, there might be some effect on the cilium length in the tested clones and additionally on the ciliation rate in C12. It cannot be ruled out that sorting cells might cause these effects.

Decreased FCAP33 expression shows delayed entry into mitotic phase

The depletion of FCAP33 by targeting Exon 4 or Exon 2 did not lead to a clear phenotype like non-ciliated cells or the disruption of other cellular structures. The localization of FCAP33 to the cilium, the midbody and weakly to the spindle in tagged cell lines, suggests its involvement in the cell cycle process. To check if the cell growth or division behavior is different in FCAP33 Crispr cells or in overexpressing cells compared to endogenous FCAP33 levels, impedance measurements were performed in parallel to the experiments described in this work before. The impedance is measured by seeding cells in a well plate covered with electrodes and measuring electron flow (Luong et al., 2021). The impedance increases due to thicker cells, larger cells or more cells (Figure 16 A). The cell index (CI), which is unitless, is depicted in the graphs. It is calculated by (impedance at time point n – impedance in the absence of cells)/nominal impedance value (Luong et al., 2021). These values are minimum-maximum normalized using GraphPad.

In a first set of experiments the growth of FCAP33^{Crsipr}-C1 was compared to FCAP33^{NG} and IMCD3 WT cells. Cells were seeded in triplicates for all experiments. Different cell numbers were tested to investigate which cell number is suitable for a growth assay of a one-week duration of cell growth. The seeding of 5000 cells was the best cell number to see an increase in impedance reaching a plateau towards the end of measurements. These tests all had in common that always the FCAP33^{Crsipr}-C1 had a delay in growth or cell division compared to WT (Figure 16 B). Interestingly IMCD3 WT cells had the highest CI throughout the whole measurement and FCAP33^{NG} was between Crispr-C1 and WT cells in the first experiment (Figure 16 B). Combining three different experiments (Figure 16 C) confirmed the delay of

the FCAP33^{Crsipr}-C1cell line. FCAP33^{NG} overall appears to have highest CI before reaching the plateau. Over these multiple experiments IMCD3 WT shows a CI curve between FCAP33^{Crsipr}-C1and FCAP33 overexpression (Figure 16 C). To additionally test different cell lines including other cell lines overexpressing FCAP33 or different control cell lines, repetitions of this experiment were performed. Knock down of FCAP33 using siRNA showed a similar behavior than FCAP33^{Crsipr}-C1, supporting the hypothesis that reduced levels of FCAP33 in IMCD3 cells have an impact on cell growth or cell division (Figure 16 D). The siCRTL had a similiar CI curve than IMCD3 WT (Figure 16 D). FCAP33^{cLAP}, that strongly overexpresses FCAP33, had higher CI values during the whole period of measurements until reaching the plateau as well as the rescued cell line FCAP33^{res} (Figure 16 D). It is of note, that the rescue was created by using FCAP33^{Crsipr}-C1 potentially still expressing (parts of) FCAP33. The Crispr rescue cell line (FCAP33^{cLAP}Crispr) likely still leads to a strong FCAP33 overexpression. Regarding the qRT-PCR experiments, revealing a 30 fold overexpression of FCAP33^{NG}, (Figure 4) it is very likely that even a rescue strongly overexpresses the protein (Figure 16 D). To validate the findings, that FCAP33 Crispr clones, as well as KD and overexpression of FCAP33, do lead to different growth behaviors according to CI measurements, KD experiments were repeated and FCAP33^{Crsipr}-C4 and FCAP33^{Crsipr}-C6 were added to the analysis (Figure 16 F). FCAP33^{cLAP} was the overexpressing control in this set of experiments. The standard clone FCAP33^{cLAP}-C6 and a second clone FCAP33^{cLAP}-C8 were tested as heterogeneity control. All Crispr cell lines and the KD (Figure 16 F, red lines) had lower CI values during the whole experiment, when compared to WT. This confirmed the previous results and the impedance measurement as a tool to look into phenotypic differences between cell lines. The siCRTL curve was between IMCD3 WT and IMCD3 FCAP33 Crispr cell lines (Figure 16 F). siCRTL cells were treated with a scrambeled siRNA and transfection reagents which can always impact lead to off-target effects (Stepanenko and Heng, 2017). In the overexpressing cell lines, FCAP33^{cLAP}-C6 showed a comparable growth behavior than siCRTL as CI values were also between IMCD3 WT and FCAP33 Crispr cells. FCAP33^{cLAP}-C8 had the highest CI values. Generally, the effects of reduced FCAP33 were confirmed and overexpressing FCAP33 did lead to varying CI curves in this replicate experiment (Figure 16 F). The effect of varying CI curves was also seen for FCAP33^{NG} before (Figure 16 B + C). The general tendency of higher CI values in FCAP33 overexpressing cells lines was also confirmed in Figure 16 E. Interestingly, two independent IMCD3 cell lines were tested in this experiment. They do express different constructs in the FlipIn locus but should not have any growth effects. Both of them, show lower CI values. Lastly, FCAP33^{Crsipr}-C22 which did not seem to have

basal signal was compared to FCAP33^{Crsipr}-C4, FCAP33^{Crsipr}-C6, FCAP33^{Crsipr}-C7, IMCD3 WT and FCAP33^{cLAP} (Figure 16 G). At the point of this experiment, it was not known that the sequencing of C22 revealed that C22 still contains a FCAP33 WT copy. Nevertheless, it is possible, that potentially reduced or impaired endogenous FCAP33 could impair impedance in this cell lines as seen for FCAP33^{Crsipr}-C1. Additionally, Clone 10 of FCAP33$^{1-167}$-cLAP was tested, as there was a dominant negative effect on cilium length of the N-terminus (Figure 12). Clone 27 of FCAP33$^{168-288}$-cLAP was also included. Interestingly, FCAP33^{Crsipr}-C6 that already had higher CI tendencies before (Figure 16 G) now seems to even have an opposite growth effect, which could be due to experimental faults. For FCAP33^{Crsipr}-C4 and FCAP33^{Crsipr}-C7 it was reproduced that CI curves were lower than compared to IMCD3 WT (Figure 16 F). FCAP33^{Crsipr}-C22 showed opposite effects having higher CI values than IMCD3 WT and FCAP33$_{168-288}$-cLAP. The C-terminal variant had low CI values until 91 hours but then showed higher cell index values. For the last set of experiments, it has to be considered that for the WT there was only a single measurement and not a triplicate (Figure 16 G). To compare high levels of FCAP33 versus low levels and the truncations, this experiment is still sufficient. For the Exon 4 targeted Crispr cell lines FCAP33^{Crsipr}-C1, FCAP33^{Crsipr}-C4 and FCAP33^{Crsipr}-C7 as well as for FCAP33 knock down, the growth behavior seemed different when compared to IMCD3 WT in different experiments. There is a delay in cell growth/division in comparison to IMCD3 WT and siCRTL cells, especially during the first days, more precisely between day 3-4. The overexpressing cell lines vary more than the Crispr clones and KD cells mentioned. For most of the cases, the overexpression cell lines do not have a delay in growth behavior within the first 1-4 days than reduced levels of FCAP33 seem to cause. However, CI curves exhibit a variable patterm but with a tendency if higher CI values for FCAP33 overexpression. Of note, FCAP33^{Crsipr}-C6 does have different behaviors than the other Exon 4 targeted Crispr clones. C6 has a more WT like behavior in Figure 16 F and this is even stronger in Figure 16 G. This observed phenomenon is also true for the Exon 2 targeted FCAP33^{Crsipr}-C22. Overexpressing short versions seem to have a strong phenotype for the N-terminal variant, but this was not reproduced. To sum up, even though there is a high variability and heterogeneity in the impedance measurements, it was shown that reduced FCAP33 levels lead to a growth delay in the initial growth phase of IMCD3 cells in long-term experiments indicating a retention of the cells in S-phase. This is consistent with results of cell cycle experiments (Figure 17 C) for FCAP33^{Crispr}C4, where more cell are retained in S-phase compared to WT.

IMCD3 cells overexpressing FCAP33 react differently on MT interfering drugs than IMCD3 WT cells

In addition to observe cells while growing and dividing, cells were also treated with the microtubule interfering drugs paclitaxel and nocodazole. Paclitaxel or Taxol binds to beta tubulin by a specific binding site and stabilizes microtubules by inducing polymerization (J. DE MEY and G. GEUENS, R. NUYDENS, R. WILLEBRORDS, 1981; Orr et al., 2003). Nocodazole interferes with polymerization most likely by binding to tubulin dimers and therefore inhibiting polymer assembly in a reversible manner (Lee et al., 1980; Ann Jordan et al., 1992; Vasquez et al., 1997). Both treatments can lead to mitotic arrest. If reduced FCAP33 has a stabilizing effect on MTs, overexpression of FCAP33 should end in a higher resistance to MT interfering drugs and cells reduced in FCAP33 levels should have stronger phenotypes upon drug treatment.

MT interfering drugs resistance was first measured using a viability assay (Figure 16 H). The Presto Blue Viability assay is a fluorescence plate reader format assay to measure cell viability. Resazurin, a blue dye, is reduced in a metabolic active, viable, cell to fluorescent resorufin. Viable cells harbor a reducing environment and therefore fulfill this reaction leading to a high resorufin fluorescence that can be measured (Lall et al., 2013). Different concentrations of Taxol and Nocodazole were added to IMCD3 WT, FCAP33^{Crsipr}-C1 and FCAP33^{NG} cells, for 24 hours. After 24 hours of drug incubation, cells were incubated with the PrestoBlueViability reagent (according to the manufacturers protocol) and released into fresh medium again. The release was measured after 25 min (Figure 16 I) and after 24 hours (Figure 16 J) to see the impact on the drug treatment over recovery time. The graphs represent “metabolic activity” of the cells. This is calculated by the % of reduction, meaning the reduction from resazurin to resorufin. If cells are more viable or metabolically active, the reduction should be stronger than in cells that are less viable or less metabolically active. For the Nocodazole treatment and 25 min recovery, IMCD3 WT cells seemed to have the highest activity over FCAP33^{NG} and Crispr cell lines for all different drug concentrations (Figure 16 I, left). For the Paclitaxel treatment, FCAP33^{NG} cells were more active with no or low drug treatment (0 and 5 nM), when compared to WT and Nocodazole treatment. For higher concentrations of Taxol (25 nM, 50nM 200 nM), similar effects as for the Nocodazole treatment can be appreciated (Figure 16 I, right).

The 24 hours of recovery show a more random pattern for both treatments. Except for 0 nM and 80 nM Nocodazole, WT cells show again the highest activity (Figure 16 J, left). But different to the effects seen before, FCAP33 Crispr cells seem to be more active than NG tagged

cells for some treatments (330 nM, 165 nM, 40 nM) (Figure 16 J, left). Only 20 nM Nocodazole treatment has the same long-term effect on cells as compared to 25 min of recovery. For the Paclitaxel treatment high concentrations, 200 nM and 100 nM had the most severe effect on FCAP33^{NG} cells and the least severe effect on FCAP33^{Crsipr}-C1 cells (Figure 16 J, right). 0 nM and 5 nM Taxol has similar 24 h recovery effects as seen for 25 min of recovery. This is also true for 50 nM Taxol. Only the 25 nM Taxol condition has a changed effect, affecting FCAP33^{NG} the strongest, when compared to the 25 min recovery (Figure 16 J, right).

Generally, the short recovery time point reflects the spontaneous effect of the MT drug on the cells, where WT cells seem to have a less affected viability than NG-tagged cells and FCAP33 Crispr cells (Figure 16 I). The "long-term" effect on viability after 24 hours shows a more random pattern, with increasing effects on the viability upon increasing nocodazole concentrations and potentially also for Taxol concentrations higher than 25 nM.

To investigate the effects of MT affecting drugs even for higher concentrations and longer time frames, impedance measurements were performed again. For Taxol, 50 nM and 1 µM (Liebmann et al., 1993) was tested and for nocodazole 24 nM and 1 µM (Vasquez et al., 1997). The drugs were added to the cells on the day of seeding and starting the impedance measurements. During the measurements no drug was added to the cells again. Interestingly, IMCD3 WT and FCAP33^{Crispr}-C1 cells showed a very similar CI curve upon either Nocodazole or Taxol treatment. For the Taxol treated cells, until 43 hours, there was no big difference in the CI values between the high and the low concentrated Taxol for IMCD3 and FCAP33 Crispr cells (Figure 16 K, right). For FCAP33^{NG} CI values were generally much lower until 113-127 hours and the difference between high and low concentrated Taxol was bigger, with even lower CI for low Taxol amounts (Figure 16 K, right). IMCD3 WT cells reached a plateau-like state after 43 hours until 115-169 hours, followed by continuously decreasing CI values. FCAP33^{NG} cells had a growing CI for a much longer time, compared to IMCD3 WT and FCAP33^{Crispr}-C1 only reaching a peak after 183 hours. This plateau for FCAP33^{NG} was reached slightly faster after treatment with a higher Taxol concentration (Figure 16 K, right). For all cell lines, the CI increases faster with higher Taxol levels until it peaks. After reaching the plateau, CI values decrease faster for higher Taxol levels than for lower Taxol levels. A decreasing CI appears due to less surface on the electrodes covered with cells. This is caused by detaching cells due to cell death. Reasons could be if the cells get too dense and start to detach or programmed cell death due to drug treatment (Luong et al., 2021). For the Nocodazole treated cell, the same effects as for Taxol, comparing high concentrated and low drug concentrations could be observed. After reaching a plateau CI values decrease again, even more prominently for the

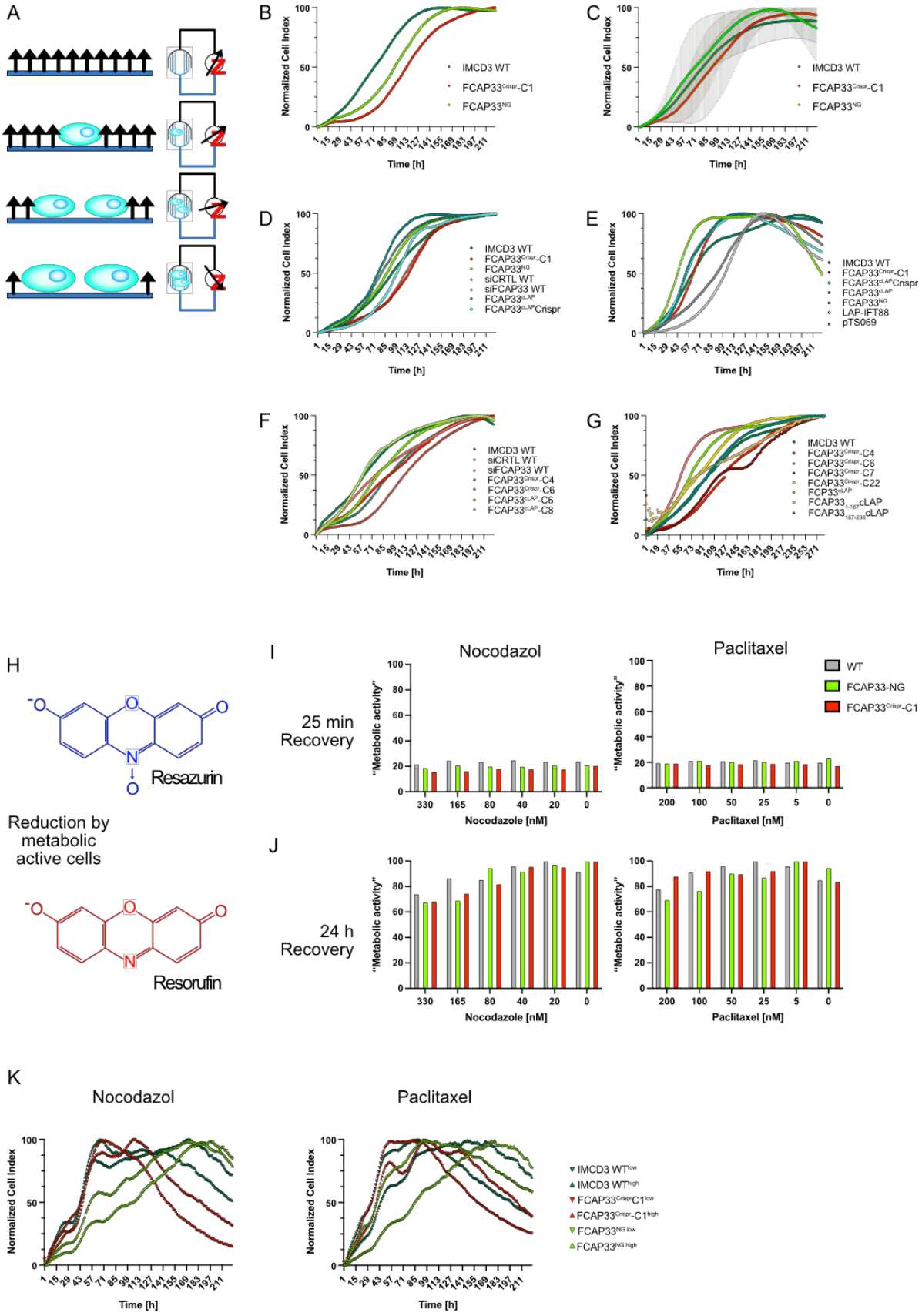

Figure 16: Different levels of FCAP33 in IMCD3 cells impair the growth behavior and the long-term effects after MT drug treatment

(A) Scheme of ExCelligence system measuring impedance. Impedance is impaired by different factors like: cell number, cell thickness or cell death. The impedance is represented as the Normalized Cell Index (see methods). (B)+ (C) Impedance measurement of IMCD3 WT, FCAP33^{NG} (high expression) and FCAP33^{Crsipr}-C1 (low expression). (B) Single experiment. (C) Means of three different experiments. (D) Impedance measurement of IMCD3 WT, FCAP33^{NG} (high expression) and FCAP33^{Crsipr}-C1 (low expression), FCAP33 KD (siFCAP33) and KD control (siCRTL), FCAP33^{cLAP} (strong overexpression) and FCAP33^{cLAP}Crispr (lower overexpression). (E) Impedance measurement of IMCD3 WT, FCAP33^{NG} (high expression) and FCAP33^{Crsipr}-C1 (low expression), FCAP33^{cLAP} (strong overexpression) and FCAP33^{cLAP}Crispr (lower overexpression) and two independent IMCD3 cell lines: IFT88 and pTS069. (F) Impedance measurement of IMCD3 WT, FCAP33^{Crsipr}-C4 and -C6 (low expression), FCAP33 KD (siFCAP33) and KD control (siCRTL), two different clones of FCAP33^{cLAP} (strong overexpression). (G) Impedance measurement of IMCD3 WT, FCAP33^{Crsipr}-C4, -C6, -C7, -C22 (low expression), FCAP33^{cLAP} (strong overexpression) and the truncated versions of FCAP33cLAP: FCAP33$_{1-167}$cLAP and FCAP33$_{168-288}$cLAP. (H) Scheme of Cell Viability assay. Metabolic active cells reduce Resazurin to Resofurin. This shift can be measured with a plate reader. (I) + (J) IMCD3 WT, FCAP33^{NG} and FCAP33^{Crsipr}-C1 were treated with different concentrations of Nocodazole and Paclitaxel for 24 hours and released for (I) 25 min or (J)24 hours. The metabolic activity is represented as % of maximum with the maximum set to 100%. (K) Low concentrations (Paclitaxel 50 nM, Nocodazole 24 nM) and high concentrations (1 µM for Paclitaxel and Nocodazole) were added to cells at the start of the impedance measurements. IMCD3 WT, FCAP33^{NG} (high expression) and FCAP33^{Crsipr}-C1 (low expression) are compared.

high Nocodazole treatment. A similar pattern can be observed for the FCAP33^{Crsipr}-C1 but the plateau seems shorter only reaching 99 Nocodazole can be seen (Figure 16 K, left). First CI increases faster with higher Nocodazole, until a peak is reached. The CI decreases slower for low concentrated nocodazole treatment. For FCAP33^{Crisipr}-C1, peak CI values are again reached between 43-71 hours (for lower nocodazole). IMCD3 WT reaches its plateau later than with Taxol. For FCAP33^{NG} the peak CI values are reached earlier for the cells treated with lower nocodazole, but for the higher concentrations the CI curve looks similar to the taxol treatment (Figure 16 K, left). The lower concentrations of both drugs differ slightly with Nocodazole being higher, probably explaining the differences compared to the low Taxol treatment. The 24 h recovery in the viability assay with high drug treatment shows similar effects on the cells than the first time points in the impedance measurements.

In summary, short-term effects of MT interfering drugs are only little, whereas long-term effects seem more prominent. Cells overexpressing FCAP33 (FCAP33^{NG}) are less impaired in its long-term growth behavior when interfering with the MT network, shown by the delayed reach of the CI plateau reflecting a longer life span. Also, the entry into the mitotic arrest phase, represented by decreasing CI values, is reached much later in FCAP33^{NG} cells when compared to IMCD3 WT or FCAP33-Crispr cells.

FCAP33 does not exhibit severe cell cycle effect

To investigate if the differences in growth behavior are caused by aberrant cell morphology or cell size, bright field images of the different cell lines were collected. Looking at brightfield images and phalloidin staining did not show any obvious changes in morphology for most cell lines (Figure 17 A + B). Only FCAP33$_{1-167}$-cLAP shows a different morphology with projections different from the other IMCD3 cell lines (Figure 17 A, right panel). In siFCAP33 and siCRTL treated cells there are some larger structures, likely from the transfection reagents (Figure 17 A). Next, I collaborated with PD Dr. D. Alansary to perform cytometry assays. This is a perfect method to study cell cycle and cell sizes at the same time. In the cell culture, FCAP33 Crispr cell lines or FCAP33 overexpressing cell lines, did not seem to have any clear growth phenotype (Figure 17 A + B). Nevertheless, impedance measurements hinted to some differences in growth behavior, but it cannot be distinguished between bigger, thicker or more cells, meaning more mitosis events. For cytometry experiments (Figure 17 C + D), cells were starved 24 h prior to fixation and DNA was stained using Hoechst. Serum starvation should lead to ciliation with most cells entering the G0/G1 phase. Surprisingly, only around 60 % of the cells entered G0/G1 for all the different cell lines tested (Figure 17 C).

FCAP33^{Crsipr}-C4 had the highest number of cells being in S-Phase in two different experiments and more cells in S-Phase than in G2/M Phase. IMCD3 WT, FCAP33^{Crsipr}-C6, FCAP33^{Crsipr}-C7, siCRTL, FCAP33^{cLAP}-C6 and FCAP33^{cLAP}-C8 had less percentage of cells in S phase than in G2/M phase (Figure 17 C, bottom). KD using siFCAP33, showed similar results than for FCAP33^{Crsipr}-C4 but was only performed once, like siCRTL, FCAP33^{cLAP}-C6 and FCAP33^{cLAP}-C8 (Figure 17 C). Generally, it seems that even though cells were serum starved and therefore theoretically synchronized, IMCD3 cells were not equally synchronized between the different cell lines at all. Next, the area of the cells measured by cytometry was checked. In both sets of experiments, IMCD3 WT had much bigger cells than FCAP33^{Crsipr}-C4 and FCAP33^{Crsipr}-C7, whereas FCAP33^{Crsipr}-C6 had a cell population that resembled strongly to WT. The bigger cells of FCAP33^{Crsipr}-C6 could explain, why the impedance measurements of this clone differed from the two other clones. The overexpressing cell lines expressing the LAP tagged FCAP33 had sizes similar to IMCD3 WT and siCRTL. Knocking down FCAP33 led to smaller cells as seen for FCAP33^{Crsipr}-C4 and FCAP33^{Crsipr}-C7. As the KD effect could not be reproduced in a second experiment, only representative images for the Crispr cell lines of two experiments are shown (Figure 17 D).

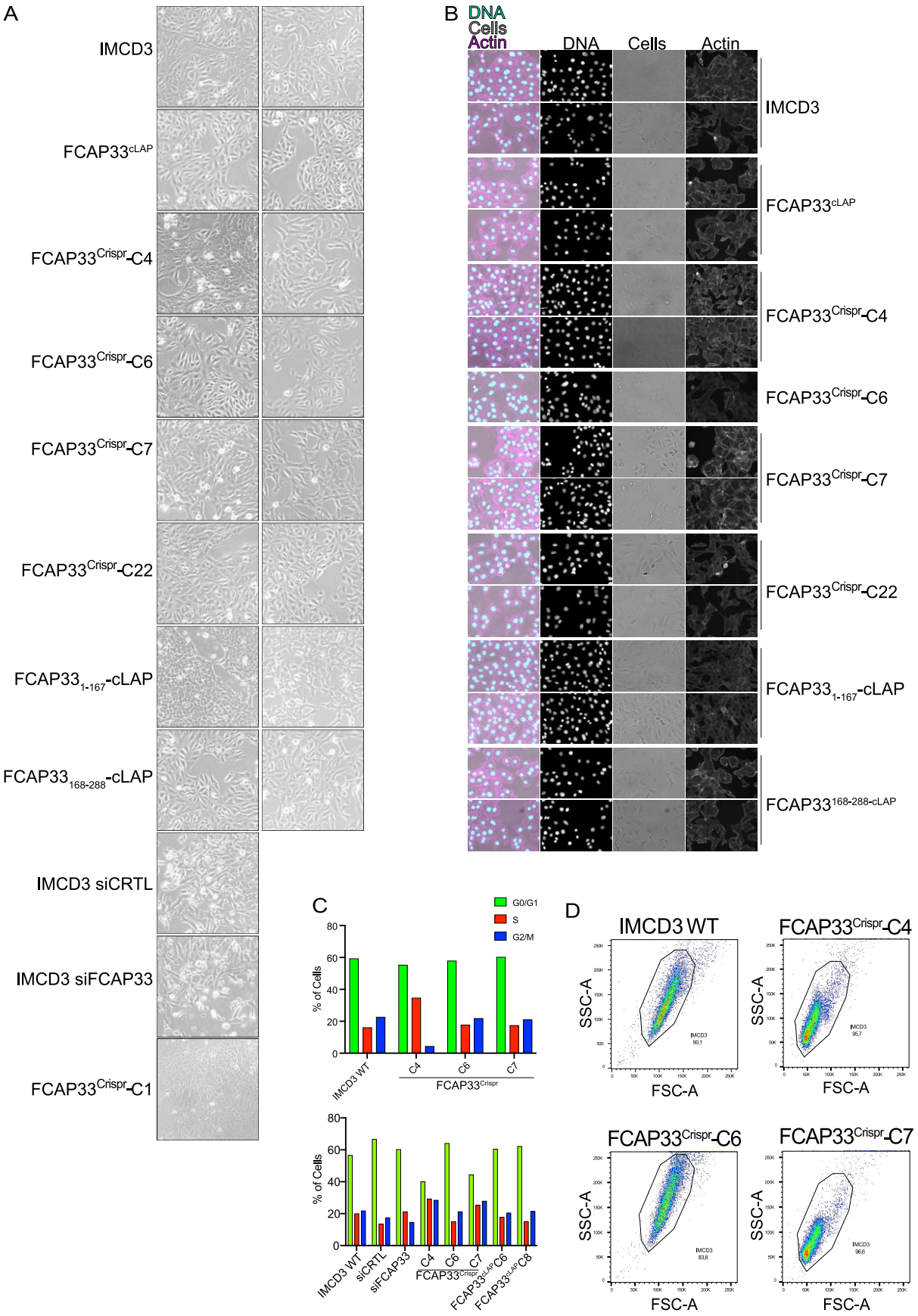

Figure 17: Cell morphology does not show a severe phenotype upon FCAP33 depletion

(A) Light microscopy images from different cell lines in culture on the day of splitting. (B) Phalloidin staining for Actin skeleton, bright field images (cells) and Hoechst staining. (C + D) Flow cytometry analysis of different cell lines. (C) Cells were stained with Hoechst for cell cycle analysis. Two independent experiments. Representation of different cell cycle staged of different cell lines. (D) Cell populations shown in SSC-A (side scatter) and FSC-A (forward scatter) to represent the cell size.

Using cytometry, it revealed size differences in cell lines with reduced FCAP33 levels. Additionally, the Crispr Clone 4, that led to a frameshift and therefore potentially to a shorter version of FCAP33 showed more cells being in S-phase in two experiments, indicating a delayed entry into M-phase and supporting the findings described before (Figure 16).

3D cyst formation is impaired when FCAP33 is overexpressed or reduced

To further analyze potential effects on gene and protein function when FCAP33 is impaired, we made use of a 3D cell culture assay. IMCD3 cells are epithelial cells of the inner-medullary collecting duct. *In vivo*, these epithelial cells have a tightly organized architecture and apicobasal polarity (Giles et al., 2014). To understand if FCAP33 reductions phenotypically changes the cells architecture, these cells can be used for an IMCD3 cyst formation model. Subjected to Matrigel, IMCD3 cells can form spheroids with a hollow lumen and primary cilia pointing towards the inside of the lumen, similar to the *in vivo* situation in the collecting duct (Giles et al., 2014). These would be called a cyst. If FCAP33 is indeed involved in cell cycle progression and MT association, it could be possible that tissue organization is impaired when FCAP33 is absent.

Lea Sanwald performed the 3D spheroid culture assay with IMCD3 WT cells and FCAP33^{Crsipr}-C1 as well as subsequent staining and immunofluorescence experiments using an epifluorescence microscope Leica DMi8 (Figure 18 A). In two independent experiments, IMCD3 WT cells mostly formed spheroids with a hollow lumen stained by the tight junction protein or zonular occludens protein ZO-1 (Giles et al., 2014; Buckley and St Johnston, 2022). The β-catenin staining serves as marker for apical adheres/basolateral membranes and is expected at the surface of the spheroid if apical-basal polarity was induced efficiently (Figure 18 A+B). ARL13B serves as ciliary marker (Giles et al., 2014; Buckley and St Johnston, 2022) and stained cilia pointing towards the lumen. For FCAP33^{Crsipr}-C1 cells only very few spheroids had a lumen stained by a clear ZO-1 outline (Figure 18, bottom panel). Some spheroids had small lumen-like structures (Figure 18 A, bottom panel, row 2), but these spheroids and all other spheroids did not show specific β-catenin staining at the apical site of

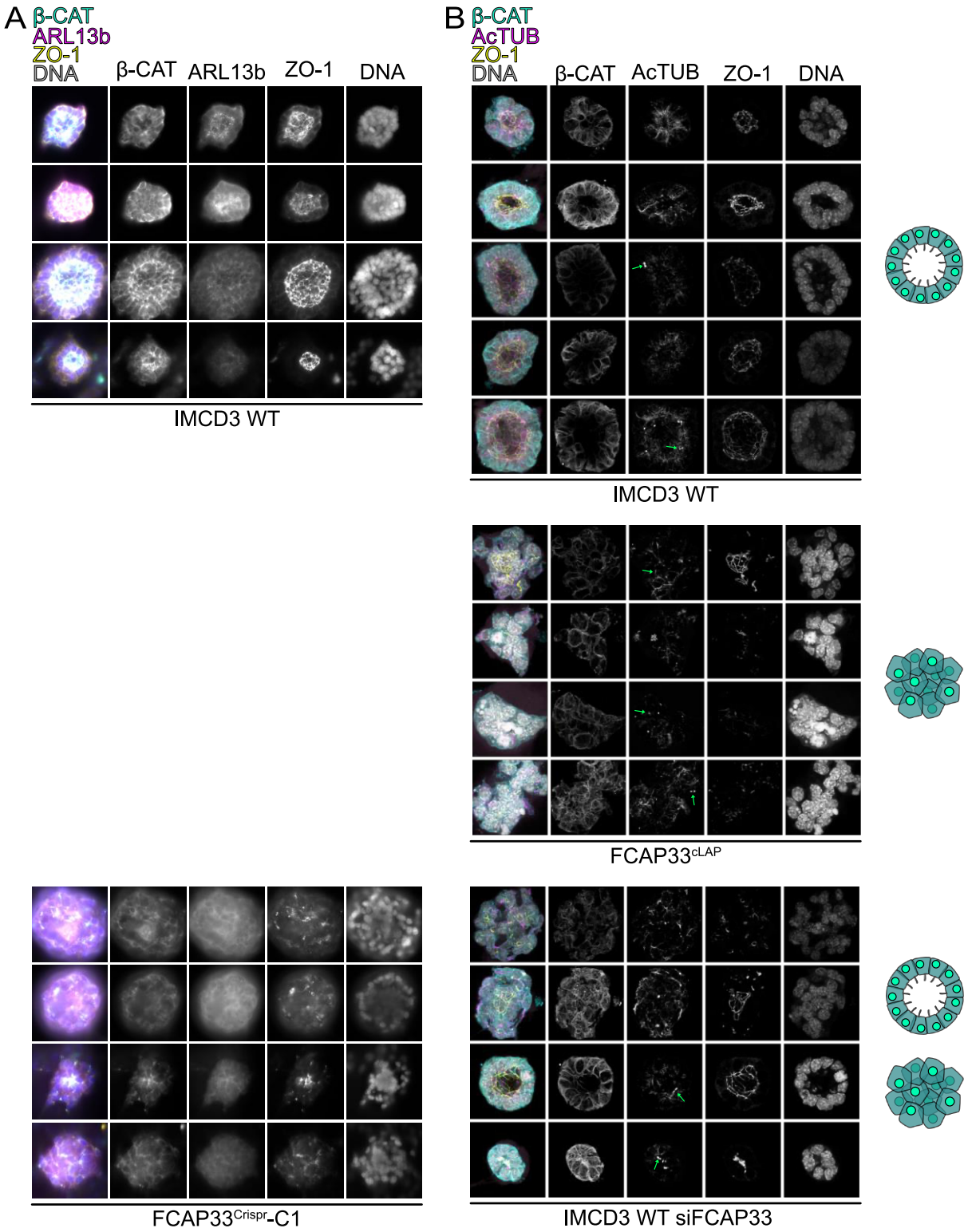

Figure 18: Depletion or overexpression of FCAP33 leads to impaired cyst formation in IMCD3 cells

3D cyst formation assay after Giles et al. Hoechst staining for DNA, ZO-1 staining as tight junctions' marker, ß-CAT (beta catenin) for basolateral membranes as apical-basal polarity marker, ARL13b/AcTUB as cilia marker at AcTUB as MT marker. (A) Epifluorescence microscope images (Leica DMi8) of IMCD3 WT and FCAP33 Crispr cells forming cysts and spheroids. (B) Duplicate experiment with IMCD3 WT cells, FCAP33^{cLAP} (overexpressing) cells, and FCAP33 knockdown (siFCAP33) cells.

the spheroid but rather throughout the whole clump like structure. To investigate whether this was a clonal effect of FCAP33^{Crsipr}-C1 and to overcome the problem that FCAP33^{Crsipr}-C1was one of the Crispr clones where Exon 4 was targeted, we followed the protocol of Giles et al using siRNA to knock down FCAP33. I performed staining and imaging with the LSM900 with Airy Scan to obtain high resolution (SR) images. Similarly to the results obtained with the FCAP33^{Crsipr}-C1 cell line, reducing FCAP33 by siFCAP33 (KD) also resulted in most of the spheroids not forming a lumen (Figure 18 B, bottom). IMCD3 WT cells nicely formed small cysts with a hollow lumen. For FCAP33^{cLAP}, the overexpressing cell line, spheroids were mostly big and clumpy, not forming a lumen and not having characteristic β-catenin staining or ZO-1 (like KD) staining in contrast to WT cells (Figure 18 B). Most surprisingly, cilia (ARL13b or AcTUB) staining successfully stained primary cilia in IMCD3 WT cells in both individual experiments (Figure 18 A+B top), whereas ARL13b positive cilia-like structures were absent in FCAP33^{Crsipr}-C1 (Figure 18, bottom). This in in contrast to culturing these cells in 2D, where primary cilia are efficiently formed. In Figure 18 B, AcTUB was used as a ciliary marker. It is harder to distinguish cilia from other MT-based structures, as acetylated tubulin does not only mark cilia and therefore makes it difficult to dissect if the absence of cilia can be confirmed. Staining with AcTUB showed that some of the cysts or spheroids had midbody structures, indicated by green arrows. To see if the number of midbodies is different between WT, FCAP33^{cLAP}, and FCAP33 KD, the number of midbody events per cyst/spheroids was counted: FCAP33^{cLAP} only formed clumpy spheroids with 1,1 midbody structures per clump. Knockdown showed 0,4 midbodies per structure, only found in properly formed cysts but not in the spheroids and IMCD3 WT had 0,7 midbodies per structure, mixed between nice cysts and more clumpy cysts. This means, that the number of midbodies correlates with the levels of FCAP33 expression.

Reducing FCAP33 levels or disrupting FCAP33 seems to lead to a polarization or signaling defect impairing 3D cyst formation.

Mass spectrometry analysis reveals potential interaction partner and shared hits with ciliary and or flemmingosome and centriole proteome

At the beginning of this project, we first aimed to find interaction partners of FCAP33 by performing co-immuno precipitation assays (CoIP). The aim of a CoIP setup is to pull on a protein via affinity chromatography under native conditions such that interaction partners would still bind to the protein of interest. Soft washing and eluting (pulling down) the protein further allows to isolate protein complexes in the elution fraction.

These samples can be assessed in native or SDS-electrophoresis and analyzed by western blot (WB). At this time point, it was known that FCAP33 localizes to primary cilia and midbodies and that it colocalizes with different tubulins such as alpha and beta tubulin as well as some midbody proteins like PRC1 and MKLP1. Shanli S. Tarrah performed CoIP assays using the FCAP33^{FLAG} cell line.

We checked if we were able to pull down the ciliary transport proteins IFT88 and IFT20, and bTUB which localize to the ciliary axoneme but also to other tubulin structures. Neither of these potential candidates did co-elute, when pulling down FCAP33^{FLAG} (Figure 19A). It is not known if FCAP33 directly interacts with other MT associated proteins or if interactions are transient. Additionally, if there is an interaction complex, how the stoichiometry between FCAP33 and component "X" may be, remains unclear. To overcome these limitations, we moved on with optimizing IP assays for further MS analysis. S. Ehr optimized the CoIP setup using the FCAP33^{cLAP} cell line: FCAP33^{cLAP} and potential interaction partners were isolated from whole cell lysates, using anti-GFP beads. FCAP33^{cLAP} pull-down was performed as described and depicted (Figure 19 B1 and B2) either following a single-step or two-step purification protocol. IMCD3 WT cells were used to check for unspecific binding of proteins to the GFP-beads after two-step purification using GFP- and S-peptide purification. The first MS experiment was performed by M. Sc. student S. Ehr and the samples were further analyzed by MS analysis (MS facility, PZMS, Homburg, Dr. Claudia Fecher-Trost). The FCAP33^{cLAP} cell line overexpresses FCAP33. For MT associated proteins, it is known that overexpression can lead to MT stabilizing, bundling and polymerization phenotypes (Nguyen et al., 1997; Saffin et al., 2005; Tiryaki et al., 2022). Therefore, I compared the FCAP33^{cLAP} cell line to the FCAP33^{ALFA} cell line, which exhibits lower expression of the FCAP33 protein. Samples were analyzed by SDS-PAGE and WB (Figure 19 C). The ALFA-IP was performed using the anti-ALFA beads followed by single-step competitive elution using the ALFA-peptide (Figure 19 B, bottom). For comparison of FCAP33^{ALFA} and FCAP33^{cLAP}, FCAP33^{cLAP} was also subjected to single-step purification (Figure 19 B1). The pull-down of FCAP33^{cLAP} and FCAP33^{ALFA} was confirmed by WB (Figure 19 C). FCAP33 and ALFA detections show efficient elution of FCAP33^{cLAP} and FCAP33^{ALFA} in the elution (E) fractions. As negative controls the same cell lines were used, but the GFP-tagged FCAP33 was subjected to the ALFA beads and *vice versa*. The protein amount used for MS in this experiment was 4x lower (4 mg of protein, starting concentration 3 mg/ml, Elution 122.5 mg/ml) than compared to the MS experiment performed before by S.Ehr (15.7 mg starting concentration 10.9 mg/ml, Elution 523 mg/ml).

MS results were analyzed and compared setting the same thresholds for each different list of MS hits. Lists were filtered for more than 2 peptide counts and a spectral count higher than 2. The fold change was calculated and only proteins with a 2-fold enrichment were considered as specific and used for comparison of the datasets. This led to a total detection of 197 proteins in the MS experiment performed by S. Ehr (1 FCAP33^{cLAP}), 232 proteins for the FCAP33^{cLAP} (2) and to a detection of 288 proteins for FCAP33^{ALFA} (3). The three datasets shared 59 common proteins (Figure 19 D) which are represented in a clustered STRING network (Figure 19 E). DBSCAN Clusters were done with STRINGdb. String networks were done using the STRINGdb open software program. STRINGdb was also used for the GO term analysis of the involvement of the detected hits in biological processes (Figure 19 F). With the 59 common hits (Table 13) a GO term analysis for cellular components were done and sorted for their false discovery rate (FDR) from low FDR values (more significant) to higher FDR values and from a higher gene count to a lower gene count (up to down) (Figure 19 G). The cellular components Myelin sheath, Postsynaptic density and Synapse (gray) can be seen as unspecific in this cell type. Interestingly, some of the hits are linked to microtubules and cytoskeletal fiber, according to GO term analysis. In addition, there is a link to the Chaperone complex, Supramolecular fibers, the ribonucleoprotein complex and membrane rafts (Figure 19 G).

FCAP33 localizes to the primary cilium, the midbody and centrioles. Therefore, the 59 hits were checked for their overlap to the iAPEX ciliary proteome (Sroka et al., 2025), the Flemmingosome (Addi et al., 2020), the centriole proteome (Carden et al., 2023) and the CCDC66 proteome (Deretic et al., 2024). The Flemming body is the midbody remnant that is leftover after cell division and therefore can be isolated. For comparison the open-source database https://flemmingsome.pasteur.cloud/ was used (Addi et al., 2020). Hits, that were present in at least 2 other datasets are listed in the table in Figure 19 H. Interestingly, 4 of them refer to two clusters of the common 59 hits for FCAP33 (Figure 19 F). Ywhaz and Ywhab were linked to the Tubulin/FtsZ family, C-terminal domain cluster. This includes proteins that are important for the formation and the integrity of the cytoskeleton. FtsZ is a tubulin homolog involved in cell division in bacteria, and the C-terminal domain of these proteins usually plays an important role for protein interaction (Buske and Levin, 2012). Tuba1a and Tubb5 were linked to the cluster of FOXO transcription factors. There could be several reasons for this link, with one being that these are core MT components and FOXO transcription factors need to be shuttled in the cell from the nucleus to the cytoplasm by using MTs (Lasick et al., 2023). With these 15 hits (Figure 19 H) a GO term analysis for cellular components (Figure 19 I) and molecular function (Figure 19 J) was done. Synapse (Figure 19 I, gray) can be excluded as

cellular component due to non-specificity for IMCD3 cells. Most links can be drawn to complex formation linked GO terms (Ribonucleoprotein complex, Supramolecular complex, Protein containing complex). Additionally, some genes are linked to cell junctions and membrane rafts, and the cell leading edge. Interestingly the leading edge goes hand in hand with the GO term for Ruffle function. This is not listed here as the gene count was only 3. Also not listed with 3 gene counts is the ribosomal subunit with all three small ribosomal subunit proteins (Rps20, 14, 19). Regarding GO term analysis for the molecular function of the 15 common genes, there is a strong involvement in binding properties: Protein Kinase-, Protein domain-, RNA-, Enzyme- and protein binding. The strongest signal was linked to the GO enrichment in structural molecule activity (Figure 19 J).

Ywhab and Ywhaz belong to the family of 14-3-3 proteins and encode the protein 14-3-3 protein beta/alpha (Protein kinase C inhibitor protein 1) or zelta/delta. The adaptor proteins usually bind partners by recognizing a phosphoserine or phosphothreonine motif, which leads to a modulation of a potential binding partner (Gardino and Yaffe, 2011; Pennington et al., 2018). Ywhab acts on cyclin D, SRPK2 and negatively regulates signaling cascades that mediate activation of MAP kinases (Jang et al., 2009; Douglas et al., 2010). Ywhaz acts on the TFEB transcription factor and indirectly on lammelipodia and ruffle formation (STRING by similarity: ENSP00000379287, YWHAZ). 14-3-3 was also described to be involved in formation of the Centralspindlin complex during central spindle formation. 14-3-3 inhibits via its action on CDK1 the Centralspindlin complex, which is active once released from 14-3-3. 14-3-3 is also an important factor for the completion of constriction at the end of cytokinesis (Fededa and Gerlich, 2012). Ywhab and Ywhaz match with most of the binding-associated GO terms: Enzyme binding, Protein domain specific binding, Identical protein binding, Protein binding and Ywhaz also in Protein kinase binding. Another prominent hit, potentially involved in many functions is Iqgap1, which plays a role in regulating the actin cytoskeleton. IQGAP1 has an MT and F-actin binding domain (Hoeprich et al., 2022). The dissection of the mammalian midbody proteome also showed its localization to the midbody structure (Skop et al., 2004). Iqgap1 also binds to CDC42 (Hart et al., 1996) and is linked to almost all GO terms except of: Structural molecule activity and identical protein binding. Vdac1 is a non-selective voltage-gated ion channel found in the outer mitochondrial membrane and the plasma membrane (Camara et al., 2017). In GO term analysis Vdac1is linked to protein binding, kinase binding and protein kinase binding. In primary cilia it seems to negatively regulate cilia in cancer cells by slowing down disassembly (Dutta et al., 2023). Tuba1a is the detyrosinated tubulin alpha-1A chain and a major component of MTs (STRING: ENSMUSP00000094778,

Tuba1a). It was also found in primary cilia of RPE cells (human protein atlas) as well as MTs. Tubb5 is part of the tubulin beta 5 chain and also a major component of MTs. Both tubulins are also linked to most of the GO terms, RNA binding and protein kinase binding excluded.

Table 13: ID mapping of shared 59 hits between three MS datasets of FCAP33

Entry	Protein names/ Description
P11499	Heat shock protein HSP 90-beta (Heat shock 84 kDa) (HSP 84) (HSP84) (Tumor-specific transplantation 84 kDa antigen) (TSTA)
P99024	Tubulin beta-5 chain
P61979	Heterogeneous nuclear ribonucleoprotein K (hnRNP K)
P68254	14-3-3 protein theta (14-3-3 protein tau)
Q91YQ5	Dolichyl-diphosphooligosaccharide--protein glycosyltransferase subunit 1 (Dolichyl diphosphooligosaccharide--protein glycosyltransferase 67 kDa subunit) (Ribophorin I) (RPN-I) (Ribophorin-1)
P68372	Tubulin beta-4B chain (Tubulin beta-2C chain)
P14869	Large ribosomal subunit protein uL10 (60S acidic ribosomal protein P0) (60S ribosomal protein L10E)
Q5SS90	Uncharacterized protein C7orf57 homolog
P68369	Tubulin alpha-1A chain (EC 3.6.5.-) (Alpha-tubulin 1) (Alpha-tubulin isotype M-alpha-1) (Tubulin alpha-1 chain) [Cleaved into: Detyrosinated tubulin alpha-1A chain]
Q9CQV8	14-3-3 protein beta/alpha (Protein kinase C inhibitor protein 1) (KCIP-1) [Cleaved into: 14-3-3 protein beta/alpha, N-terminally processed]
Q60634	Flotillin-2 (Epidermal surface antigen) (ESA) (Membrane component chromosome 17 surface marker 1 homolog)
P11679	Keratin, type II cytoskeletal 8 (Cytokeratin endo A) (Cytokeratin-8) (CK-8) (Keratin-8) (K8) (Type-II keratin Kb8)
Q8QZY1	Eukaryotic translation initiation factor 3 subunit L (eIF3l) (66 kDa tyrosine-rich heat shock protein) (67 kDa polymerase-associated factor) (Eukaryotic translation initiation factor 3 subunit 6-interacting protein) (Eukaryotic translation initiation factor 3 subunit E-interacting protein) (HSP-66Y) (PAF67)
P60710	Actin, cytoplasmic 1 (Beta-actin) (EC 3.6.4.-) [Cleaved into: Actin, cytoplasmic 1, N-terminally processed]
P05064	Fructose-bisphosphate aldolase A (EC 4.1.2.13) (Aldolase 1) (Muscle-type aldolase)
P04104	Keratin, type II cytoskeletal 1 (67 kDa cytokeratin) (Cytokeratin-1) (CK-1) (Keratin-1) (K1) (Type-II keratin Kb1)
P80317	T-complex protein 1 subunit zeta (TCP-1-zeta) (CCT-zeta-1)
P62889	Large ribosomal subunit protein eL30 (60S ribosomal protein L30)
P56480	ATP synthase subunit beta, mitochondrial (EC 7.1.2.2) (ATP synthase F1 subunit beta)
Q8VDN2	Sodium/potassium-transporting ATPase subunit alpha-1 (Na(+)/K(+) ATPase alpha-1 subunit) (EC 7.2.2.13) (Sodium pump subunit alpha-1)
P80313	T-complex protein 1 subunit eta (TCP-1-eta) (CCT-eta)
P80318	T-complex protein 1 subunit gamma (TCP-1-gamma) (CCT-gamma) (Matricin) (mTRiC-P5)
P42932	T-complex protein 1 subunit theta (TCP-1-theta) (CCT-theta)
P14148	Large ribosomal subunit protein uL30 (60S ribosomal protein L7)

Q8VED5	Keratin, type II cytoskeletal 79 (Cytokeratin-79) (CK-79) (Keratin-79) (K79) (Type-II keratin Kb38)
Q6IFX2	Keratin, type I cytoskeletal 42 (Cytokeratin-42) (CK-42) (Keratin-17n) (Keratin-42) (K42) (Type I keratin Ka22)
Q8VEM8	Solute carrier family 25 member 3 (Phosphate carrier protein, mitochondrial) (Phosphate transport protein) (PTP)
P62984	Ubiquitin-ribosomal protein eL40 fusion protein (Ubiquitin A-52 residue ribosomal protein fusion product 1) [Cleaved into: Ubiquitin; Large ribosomal subunit protein eL40 (60S ribosomal protein L40) (CEP52)]
Q60932	Non-selective voltage-gated ion channel VDAC1 (Outer mitochondrial membrane protein porin 1) (Plasmalemmal porin) (Voltage-dependent anion-selective channel protein 1) (VDAC-1) (mVDAC1) (Voltage-dependent anion-selective channel protein 5) (VDAC-5) (mVDAC5)
P67778	Prohibitin 1 (B-cell receptor-associated protein 32) (BAP 32)
Q91VR2	ATP synthase subunit gamma, mitochondrial (ATP synthase F1 subunit gamma) (F-ATPase gamma subunit)
P80314	T-complex protein 1 subunit beta (TCP-1-beta) (CCT-beta)
P62960	Y-box-binding protein 1 (YB-1) (CCAAT-binding transcription factor I subunit A) (CBF-A) (DNA-binding protein B) (DBPB) (Enhancer factor I subunit A) (EFI-A) (Nuclease-sensitive element-binding protein 1) (Y-box transcription factor)
P62908	Small ribosomal subunit protein uS3 (EC 4.2.99.18) (40S ribosomal protein S3)
Q03265	ATP synthase subunit alpha, mitochondrial (ATP synthase F1 subunit alpha)
O35129	Prohibitin-2 (B-cell receptor-associated protein BAP37) (Repressor of estrogen receptor activity)
Q6NXH9	Keratin, type II cytoskeletal 73 (Cytokeratin-73) (CK-73) (Keratin-73) (K73) (Type II inner root sheath-specific keratin-K6irs3) (Type-II keratin Kb36)
P62264	Small ribosomal subunit protein uS11 (40S ribosomal protein S14)
P16858	Glyceraldehyde-3-phosphate dehydrogenase (GAPDH) (EC 1.2.1.12) (Peptidyl-cysteine S-nitrosylase GAPDH) (EC 2.6.99.-)
Q8BFR5	Elongation factor Tu, mitochondrial
Q9QXS1	Plectin (PCN) (PLTN) (Plectin-1) (Plectin-6)
P09103	Protein disulfide-isomerase (PDI) (EC 5.3.4.1) (Cellular thyroid hormone-binding protein) (Endoplasmic reticulum resident protein 59) (ER protein 59) (ERp59) (Prolyl 4-hydroxylase subunit beta) (p55)
Q9CZX8	Small ribosomal subunit protein eS19 (40S ribosomal protein S19)
P23927	Alpha-crystallin B chain (Alpha(B)-crystallin) (P23)
P63101	14-3-3 protein zeta/delta (Protein kinase C inhibitor protein 1) (KCIP-1) (SEZ-2)
Q9JKF1	Ras GTPase-activating-like protein IQGAP1
P60867	Small ribosomal subunit protein uS10 (40S ribosomal protein S20)
P80315	T-complex protein 1 subunit delta (TCP-1-delta) (A45) (CCT-delta)
Q6IFZ6	Keratin, type II cytoskeletal 1b (Cytokeratin-1B) (CK-1B) (Embryonic type II keratin-1) (Keratin-77) (K77) (Type-II keratin Kb39)
Q9Z0X1	Apoptosis-inducing factor 1, mitochondrial (EC 1.6.99.-) (Programmed cell death protein 8)
P63038	60 kDa heat shock protein, mitochondrial (EC 5.6.1.7) (60 kDa chaperonin) (Chaperonin 60) (CPN60) (HSP-65) (Heat shock protein 60) (HSP-60) (Hsp60) (Mitochondrial matrix protein P1)
P80316	T-complex protein 1 subunit epsilon (TCP-1-epsilon) (CCT-epsilon)
P63017	Heat shock cognate 71 kDa protein (EC 3.6.4.10) (Heat shock 70 kDa protein 8)
P10126	Elongation factor 1-alpha 1 (EF-1-alpha-1) (EC 3.6.5.-) (Elongation factor Tu) (EF-Tu) (Eukaryotic elongation factor 1 A-1) (eEF1A-1)

Q61937	Nucleophosmin (NPM) (Nucleolar phosphoprotein B23) (Nucleolar protein NO38) (Numatrin)
P07356	Annexin A2 (Annexin II) (Annexin-2) (Calpactin I heavy chain) (Calpactin-1 heavy chain) (Chromobindin-8) (Lipocortin II) (Placental anticoagulant protein IV) (PAP-IV) (Protein I) (p36)
P29341	Polyadenylate-binding protein 1 (PABP-1) (Poly(A)-binding protein 1)
P11983	T-complex protein 1 subunit alpha (TCP-1-alpha) (CCT-alpha) (Tailless complex polypeptide 1A) (TCP-1-A)(Tailless complex polypeptide 1B) (TCP-1-B)

Pabpc1 is an mRNA binding protein (GeneID 26982) and therefore only linked to RNA and protein binding, whereas Hsp90ab1as a chaperone is linked to all GO terms except of structural molecular activity. Additionally, several ribosomal associated proteins were found in the 15 common hits (Rpl7, Rps20, Rps14 and Rps19) with Rps19 being involved in several GO terms, but Rps14 and 19 only in RNA binding and Structural molecule activity. See Table 13.

Taken together, MS analysis revealed a common set of 59 proteins between two different cell lines expressing FCAP33 at different levels. These shared 15 hits with the overlapping proteome of the centrioles, CCDC66 and the Flemming body as well as the primary cilium proteome of IMCD3s. In addition to Ywhaz and Ywhab of the 14-3-3 protein family, Ywhaq was also found in the FCAP33 proteome. Three tubulin family proteins were found in all 3 datasets, that potentially link FCAP33 to its tubulin association and maybe the actin cytoskeleton. Additionally, there are strong hints for its link to the cell cycle via a 14-3-3/CDK1association. The FCAP33 proteome also has a big group of CCT complex proteins (Figure 19 E), also found recently in the WDR62 (a centriole and CDK2 linked protein (Kodani et al., 2015)) proteome (Morris et al., 2024) as well as in the midbody proteome (Skop et al., 2004). In the midbody proteome these were excluded as contamination. Ribosomal and 14-3-3 hits are also highly abundant in the Flemmingosome proteome.

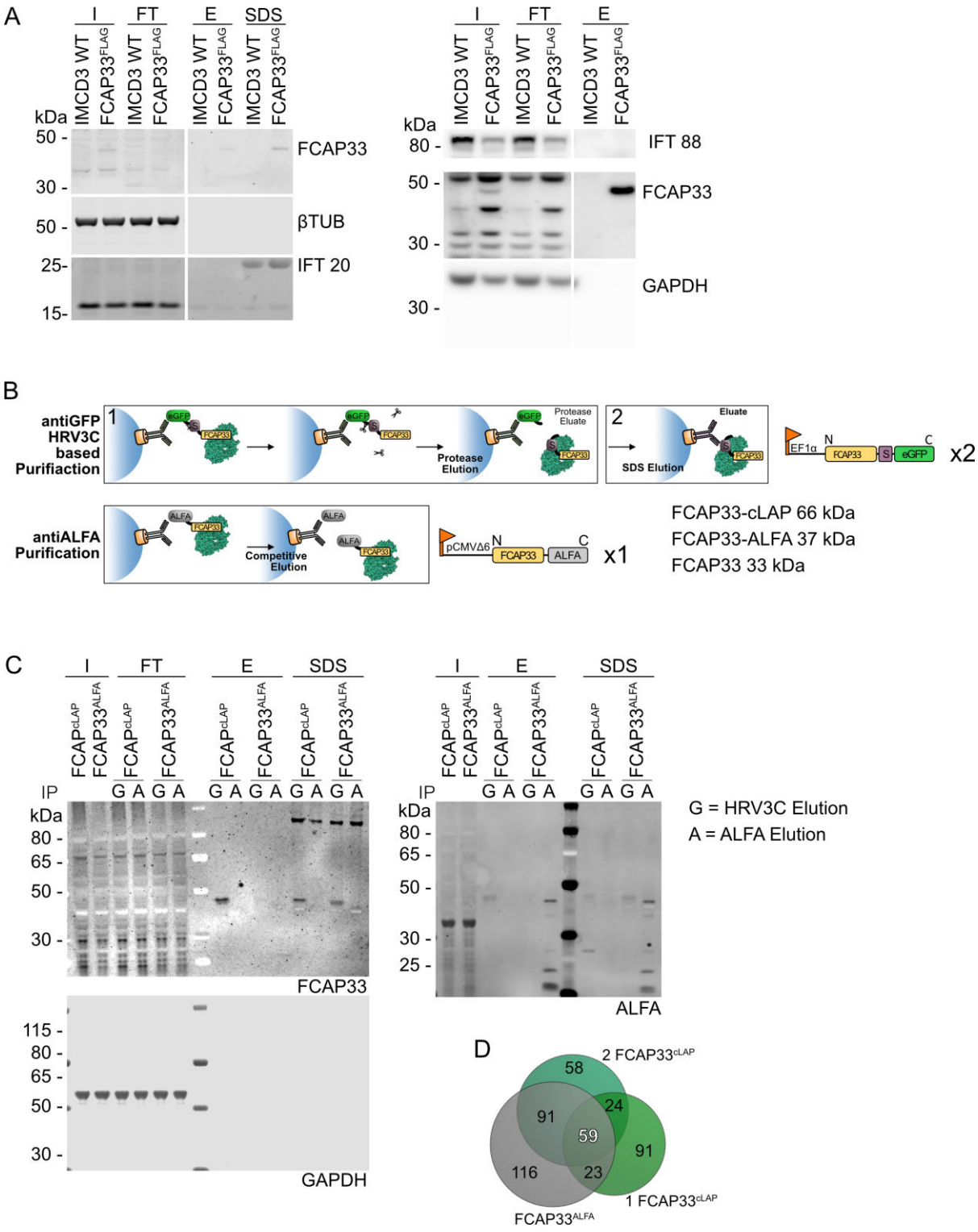
A
I
FT
E
SDS
IMCD3 WT
FCAP33FLAG
kDa
50 -
30 -
FCAP33
βTUB
IFT 20
25-
15-
IFT 88
GAPDH
B
antiGFP HRV3C based Purifiaction
Protease Elution
SDS Elution
Eluate
EF1α
FCAP33
eGFP
x2
antiALFA Purification
Competitive Elution
pCMVΔ6
ALFA
x1
FCAP33-cLAP 66 kDa
FCAP33-ALFA 37 kDa
FCAP33 33 kDa
C
IP
G A G A G A G A G A
FCAPcLAP
FCAP33ALFA
80 -
65 -
50 -
25 -
115 -
ALFA
G = HRV3C Elution
A = ALFA Elution
D
2 FCAP33cLAP
1 FCAP33cLAP
FCAP33ALFA
58
91
24
59
91
116
23

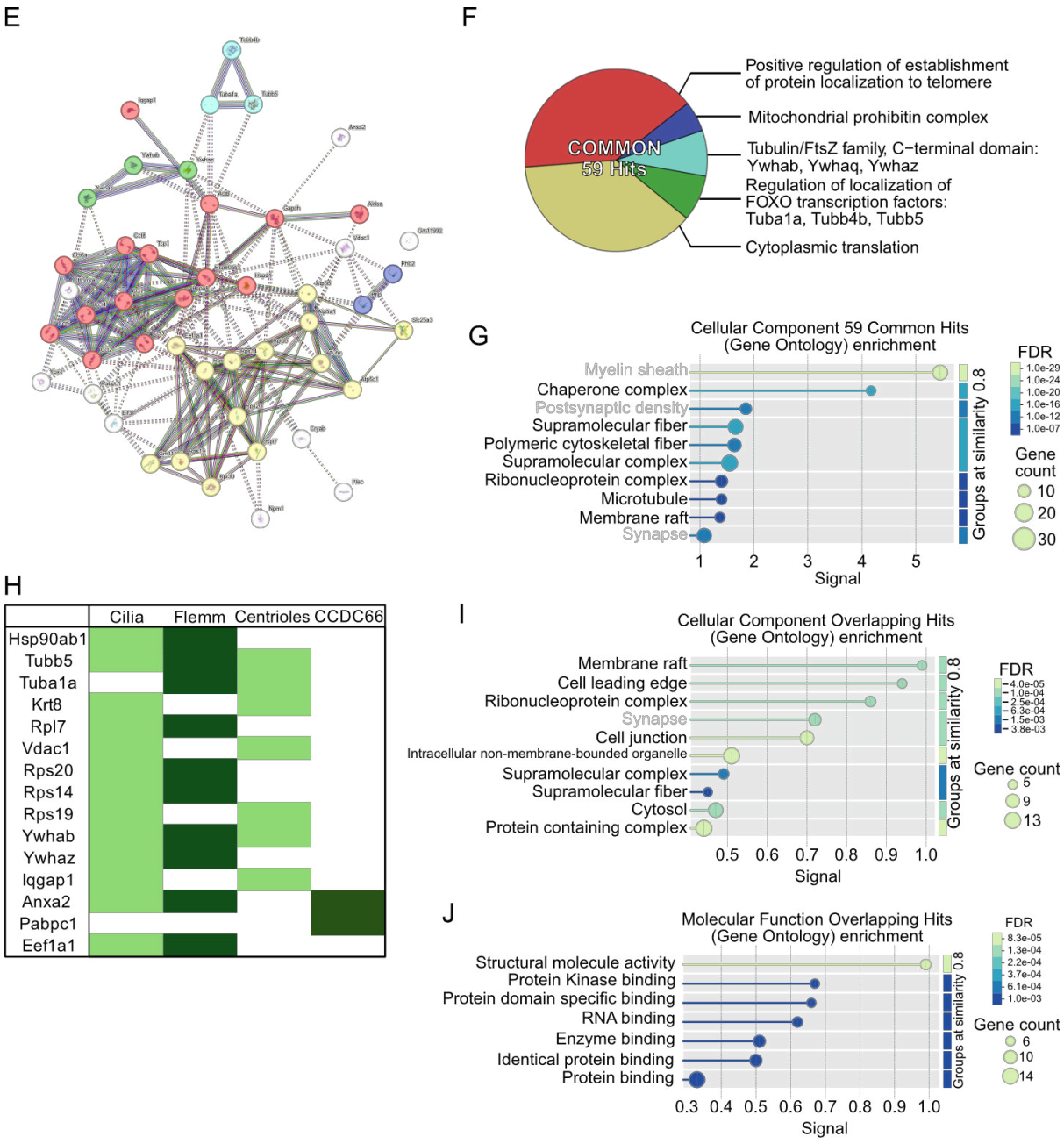

Figure 19: Proteomic Analysis of FCAP33 reveals possible interactions partners previously linked to cilia, centrioles and midbodies

(A) FLAG IP of FCAP33. WB of Input (I), Flow Through (FT) and Eluate (E) samples. Left: decorations of FCAP33, IFT20 and beta tubulin (bTUB). Right: decoration of IFT88, FCAP33 and GAPDH. (B) Scheme of IP setups. 1 FCAP33^{cLAP}: FCAP33 was purified and isolated with interaction partners in a single purification step using the HRV3C Elution. 2 FCAP33^{cLAP}: FCAP33 was purified and isolated with interaction partners in a double purification step. HRV3C Elution was followed by S-Agarose purification, SDS-Elution. FCAP33^{ALFA} was competitively eluted with ALFA peptides using ALFA PE selector. (C) Representative WBs of ALFA-IP and 1 FCAP33^{cLAP} single purification. G=HRV3C Elution and A=ALFA Elution (details see methods). FCAP33 and ALFA staining shows Elution of the protein in the MS samples.

(D) VENN diagram showing the overlap of the MS hits between the three different FCAP33 sample preparations. Only hits with more than 2 peptide counts and a 2-fold enrichment were taken (details see methods). (E)+(F) STRINGdb cluster analysis of 59 common hits of 3 datasets using DBSCAN with Epsilon 3. (G) STRINGdb analysis of 59 common hits of Cellular components with FDR 0.5 and similarity 0.8. (H) Table showing overlapping hits with proteome of Cilia (iAPEX), Flemmingosome, Centrioles, CCDC66. (I) STRINGdb analysis of selected hits of 59 common hits that have at least 2 identical hits in the proteome of Cilia (iAPEX), Flemm(ingosome), Centrioles, CCDC66. Analysis of (I) Cellular Components and (J) Molecular Function of these overlapping hits with FDR 0.5 and similarity 0.8 and a gene count of 5.

In silico analysis of FCAP33

At the beginning of this study FCAP33 was an unknown protein and protein databases did not contain information about FCAP33 except of the AlphaFold predicted structure of FCAP33 (Figure 20 A). During the course of this study, we identified FCAP33 as a microtubule-associated protein (MAP). Our findings suggest that its distinct domains are likely to fulfill different functions, and that FCAP33 is not actively involved in the transport of ciliary proteins. However, the precise molecular function of FCAP33 remains undefined. To address this and to place the mass spectrometry results in a more informative context, I subsequently performed additional *in silico* analyses and database searches.

Predicted expression of FCAP33 in ciliated tissues

Regarding tissue expression prediction in humans, FCAP33 is predicted to be expressed in the brain (confirmed by protein expression and RNA expression, Human Protein Atlas, https://www.proteinatlas.org/), mainly in the Choroid plexus and in the respiratory system and in the bronchus in males and females. Additionally, in female tissues it is highly expressed, where it is most abundant in the fallopian tube tissue. In males, it is also expressed in the testis, only confirmed by RNA expression. Recently, multiple immunofluorescence assays showed co-localization of FCAP33 with the staining of the cilia axoneme of ciliated cells of the fallopian tube, endometrium, cervix, nasopharynx and the bronchus (Human Protein Atlas, https://www.proteinatlas.org/), supporting the fact that FCAP33 is a cilia protein not even restricted to the primary cilium. Single cell RNA analysis data confirmed the strong expression of FCAP33 in ciliated cells of the lung, the fallopian tube, the endometrium and the bronchus, all being multiciliated organs (Figure 20 B). The Human Protein Atlas also reports that the protein localized to primary cilia, the basal body in RPTEC/TERT1 cells and to the primary

cilia transition zone in serum starved hTERT-RPE1 cells. Especially the antibody staining data from The Human Protein Atlas was not available at the beginning of this project.

Structure and amino acid composition of FCAP33

The human FCAP33 has a size of 32,8 kDa (Uniprot (https://www.uniprot.org/) SignalP, Human Protein Atlas) and has four different splice variants. Two of these variants (C9JQZ6 and J3KQX6) have a signal peptide cleavage site predicted by SignalP (https://services.healthtech.dtu.dk/services/SignalP-4.1/). The full-length protein (isoform 1) has six helixes (3 larger ones and 3 small helixes) predicted by Alphafold v2.3.2. and NetSurfP and a large and disordered tail at the C-terminus (Figure 20 A + C). Database searches for motif predictions or sequence similarity predictions only found motifs based on similarity with low confidence values. The only interesting candidate CFAP77, the cilia and flagella associated protein 77 had an E-value of 0.029, meaning a chance of 2,9% for random incorrect blast result (https://www.genome.jp/tools/motif/). Only for DUF5524, a protein domain of unknown function, has the same predicted sequence, confirmed by other additional search tools: NCBI search (https://www.ncbi.nlm.nih.gov/Structure/cdd/wrpsb.cgi), ScanProsite (https://prosite.expasy.org/scanprosite/), HMMER searches (https://www.ebi.ac.uk/Tools/-hmmer/search/phmmer) and InterPro search (https://www.ebi.ac.uk/interpro/). The search for predicted domains did not show any predicted microtubule binding domain, kinase domain or others. The human FCAP33 protein also has some low complexity regions (LC) regions at the C-terminal half, which is also the more disordered region with lower confidence values in structural prediction. The human and the mouse amino acid sequence show a high sequence similarity including the polar residues (Figure 20 C) at aa 201-205 and 274-291 (*Mus musculus*) and aa 201-207 and 273-295 (*Homo sapiens*). In comparison to human FCAP33, the mouse homolog does not have any splice variants predicted which makes analysis and experiments with the mouse protein more straight forward for first studies of the protein (Uniprot).

The software NetSurfP3.0 from DTU Health Tech (https://services.healthtech.-dtu.dk/services/NetSurfP-3.0/) was used to analyze the surface accessibility, secondary structure, disorder and phi/psi angles of the amino acids in the mouse sequence. This analysis goes hand in hand with the AlphaFold structure predictions. Both show that the N-terminus of the protein has a high probability for a disordered region starting between aa 170 and aa 175. From amino acid 230 until the end of the sequence the relative surface accessibility is overall predicted to be exposed to the surface. Generally, throughout the whole sequence, there are

almost no regions that are predicted to be buried, only for some very small region in the C-terminal part of the protein. The mouse sequence contains 3 larger helixes and 3 small helices. Most of these are located in the C-terminal half of the protein where the probability of disordered regions is much lower (disorder values lower than 0.2) and the surface exposure for most regions as well. All helixes are connected by coiled-coil domains and one single strand at position 60 (Figure 20 C).(Details about the amino acid composition of the protein were obtained using the ProtParam tool of the Expasy Website an open access website of the Swiss Institute of Bioinformatics.)

The *Mus musculus* FCAP33 has a theoretical pI of 8.69. In the last 50 amino acids of the sequence there are 12 negatively charged residues but only 4 positively charged amino acids, leading to a slightly negatively charged C-terminal tail.

The overall charge of the protein is rather neutral or slightly positively charged, with 0.9% more positive amino acids. FCAP33 contains an unusually large number of prolines. There are several predicted phosphoserines, which leads to the Uniprot classification of FCAP33 being a phosphoprotein, also confirmed by predictions using phosphosite.org (https://www.phosphosite.org/proteinAction?id=11712&showAllSites=true) and shown in Figure 2 D. Most of the Serines are also conserved between mouse and human. FCAP33 is therefore predicted to be cilium-associated protein with rather neutral charge and a large, disordered C-terminal tail. Its classification as a phosphoprotein was not known at the beginning of the project.

Summarizing the *in silico* analysis, FCAP33 is strongly expressed in ciliated human tissues, especially in multiciliated organs, where it localizes to the ciliary axoneme. Structural predictions and sequence analysis reveal a largely disordered, partially surface exposed C-terminal region and a phosphoprotein nature, though its precise molecular functions remain to be elucidated. These findings support the classification of FCAP33 as a cilium- and our experimental findings as a MT-associated protein that may interact with the MT via its structurally better-defined N-terminus. The structurally less defined C-terminus may convey functions regulated through phosphorylation. These and other potential functions a dissected in the following discussion.

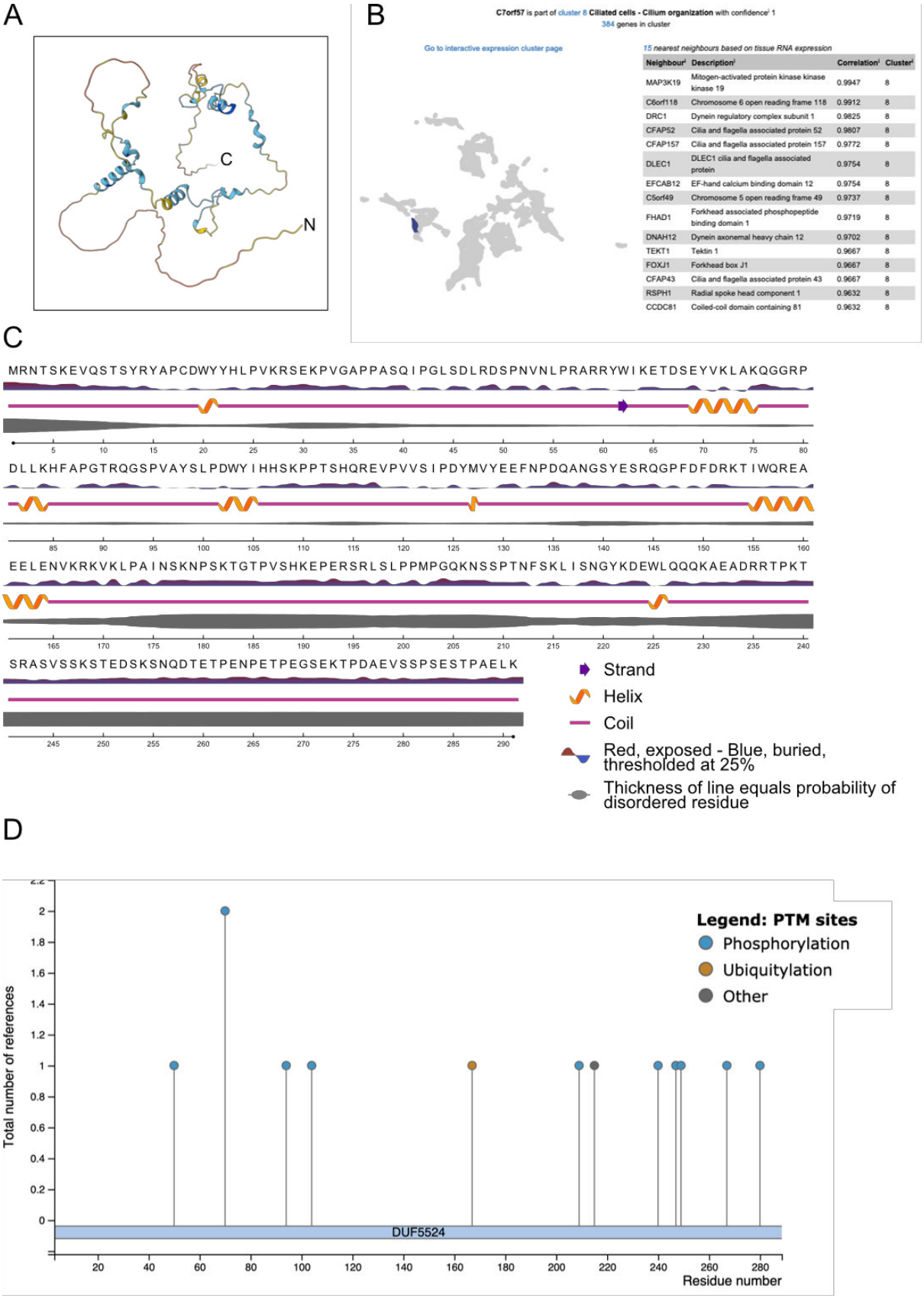

Figure 20: Predicted structure and properties of FCAP33

(A) AlphaFold model of murine FCAP33. Yellow and orange regions: low confidence, blue regions, high confidence. Large, disordered tail at N-terminus.

(B) Table from Human Protein Atlas show nearest neighbors based on tissue RNA expression with the majority being cilium and flagellum associated proteins. (C) NetSurfP prediction showing surface exposure of residues, secondary structure. (D) Prediction of post-translational modifications (PTMs). Potential phosphorylation sites (blue).

Discussion

The primary cilium proteome has been intensively studied in the past years. There have been links to proteins with shared functions in primary cilia, centrioles and microtubules (MTs) (Conkar and Firat-Karalar, 2021). CEP104 (Centrosomal protein of 104 kDa) is a known ciliary protein that localizes to the distal ends of cilia, controlling axonemal integrity, length and stability (Yamazoe et al., 2020a). Now, CEP104 has been described to act in a ciliary tip complex, together with CSPP1 (Centrosomal and spindle pole associated protein 1) to inhibit MT growth and shortening (Frikstad et al., 2019; Ryniawec et al., 2023). Recently, the field of studying MAPs in primary cilia is emerging (Conkar and Firat-Karalar, 2021). For example, the extensive studies of the centriolar protein CCDC66 (Coiled-coil domain containing protein 66) have shown the importance and involvement of many cellular functions of CCDC66, including primary cilia, spindle association and MT functions (Conkar and Firat-Karalar, 2021; Batman et al., 2022; Odabasi et al., 2023). Not only CCDC66, but also ENKD1 (Enkurin domain-containing protein 1) was shown to be a centrosomal and ciliary microtubule-associated protein (MAP) (Tiryaki et al., 2022). CEP290 (Centrosomal protein of 290 kDa), the ciliary, basal body and centriole protein harbors a MT binding domain, which's mutation causes ciliary defects (Drivas et al., 2013). A recent study also showed a non-ciliary MT associated function of Cep290, where Cep290 is described to be responsible for binding to cellular membranes and MTs and regulates focal adhesion in non-ciliated cells (Matsuo et al., 2023). Additionally, there have been links between midbody proteins, midbody remnants and primary cilia. Midbody remnants can migrate to the apical surface of polarized epithelial cells, facilitating the formation of a new primary cilium or having signaling functions (Bernabé-Rubio et al., 2016; Ott, 2016; Labat-de-Hoz et al., 2021).

FCAP33 is a newly found primary cilia protein in IMCD3 cells. It was shown to be a MAP that localizes to primary cilia, centrioles, midbodies and the spindle. In the following discussion, the potential roles and functions of FCAP33 in primary cilia and MT association will be discussed.

A putative role of FCAP33 in axoneme integrity and stability via MT association

In summary we discovered the uncharacterized protein C7orf57 or Gm11992 (mouse) to be a primary cilium protein with MT association which we named FCAP33. FCAP33 is a MAP with a potential stabilizing effect on axonemal microtubules.

We showed that FCAP33 is a microtubule associated protein, demonstrated by its axoneme association (Figure 8) and its MT association in an *in vitro* study (Figure 14). When removing the ciliary membrane, FCAP33 showed a similar behavior like AcTUB, being better accessible for antibody staining after the removal of the ciliary membrane (Figure 8). Nevertheless, direct interaction with acetylated tubulin can be ruled because FCAP33 localizes to primary cilia even when acetylated tubulin is absent (Figure 9). Additionally, it is unlikely that FCAP33 is a MIP as it does associate with preformed MTs in the in vitro setup (Figure 14 B), confirming its function as a MAP. FCAP33 is a non-dynamic protein in primary cilia, even when strongly overexpressed (Figure 10 J), which implies that FCAP33 has rather a scaffold function than any involvement in trafficking. TUBA1a, TUBB4 and TUBB5 which were all found in the FCAP33 proteomic analysis support the microtubule association further. Overexpression of FCAP33 showed that primary cilia tendentiously are longer than WT cells (Figure 4 E and F, Figure 12 C). The overexpression of a short N-terminal variant had a dominant negative effect on cilium length, leading to significantly shorter primary cilia (Figure 12 C).

The protein's localization and its molecular function may be mediated by separate structural domains

FCAP33 does not have a predicted MT binding domain, but short N-terminal or C-terminal halves of FCAP33 did not localize to the primary cilium anymore. The N-terminal half of the protein does induce shortening of primary cilia and lower ciliation rates. Additionally, in an *in vitro* setup the N-terminus seems to have a higher affinity to MTs compared to the C-terminus. Strikingly, both truncated versions did associate with MTs *in vitro* but not *in vivo*. In an IP experiment, we could also show that the N-terminus can form SDS resistant oligomers which are destabilized by DTT (Figure 13 D). This led to the conclusion that the N-terminal half might be more important for binding and interacting with MTs or other binding partners. In FCAP33 Crispr cells, where Exon 4 was targeted and the N-terminus is likely to be still expressed, FCAP33 could be detected at the basal body and centrioles, which would be in agreement with the N-terminal half being the MT interacting part of the protein. The N-terminal half harbors most of the helices except one small helix, whereas the C-terminal truncation is a large,

disordered domain (Figure 2). A reason for a stronger MT interaction of the N-terminus compared to the C-terminus could be due to the N-terminal half being slightly more positively charged. MTs are generally negatively charged, which makes a positively charged protein more likely to bind MTs (Bodakuntla et al., 2019). The C-terminus of FCAP33 has 12 negatively charged but only 3 positively charged amino acid residues, making it rather negatively charged overall. This could be one reason why the affinity to MTs of the C-terminus is lower in the *in vitro* setup, than of the N-terminus of FCAP33. If the N-terminal amino acids 1-167 are responsible for MT interaction, this may also support the hypothesis, that it is responsible for the formation of oligomers (Figure 13). DTT is known to reduce disulfide bonds and is therefore commonly used to fully unfold and solubilize proteins (Mishra et al., 2017). Nevertheless, it was also described that DTT may interact with protein domains not having a cysteine is absent (Alliegro, 2000). The structural predictions of FCAP33 show that there is only one single cysteine at position 18. Indeed, this cysteine sits within the potential oligomerization and interaction domain but for a disulfide bond formation the interface of two cysteines is needed. This would mean that at least two proteins would be needed for the formation of a disulfide bond-based oligomer. Indeed, the oligomers of $FCAP33^{cLAP}$ and $FCAP33_{1-167}$-cLAP are double the size of a single FCAP33 (Figure 13 D). Prediction analysis (Figure 21 A). However, the cysteine at position 18 is not at the interface between the two monomers, making it unlikely to be the interaction site of a potential oligomer formation using the open-source platform GALAXY (Afgan et al., 2018) and "Chimera X" shows a potential interaction, of 2 FCAP33 proteins at the N-terminus

To investigate if oligomerization would be due to the cysteine FCAP33 cysteine mutant experiments should be performed. If, as hypothesized the Crispr clones are still expressing the N-terminal part of the protein, upon targeting of Exon 4 and FCAP33 can still localize to the basal body (BB), this N-terminal region must have the MT interacting sequence of FCAP33. However, this is in contrast to $FCAP33_{1-167}$-cLAP, which was not detectable at the BB or in primary cilia (Figure 12 A) even though it is associated to MTs in a similar manner than FL $FCAP33^{cLAP}$ *in vitro* (Figure 16). There could be several explanations for this: (1) the N-terminal part of FCAP33 is sufficient for MT interaction, but not for proper axoneme association or function. This could be due to a potential post-translational modification (PTM) motif or another motif sitting in the C-terminus and being important for ciliary targeting. Even though this would not explain the lack of $FCAP33_{1-167}$-cLAP at centrioles or BB structures.

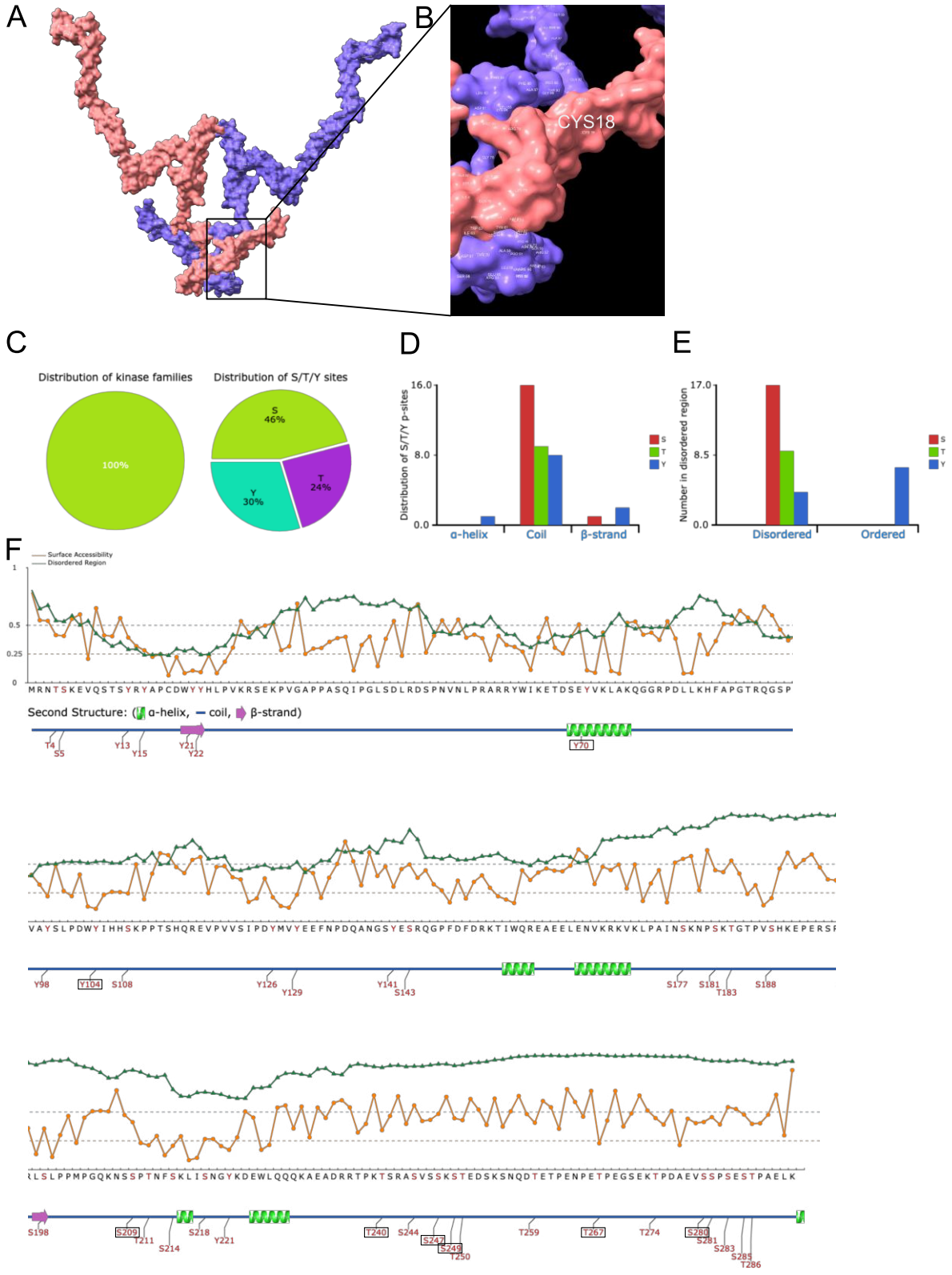

Figure 21: Potential interaction or functional interfaces of FCAP33

(A) Oligomer prediction of two FCAP33 monomers using GALAXY and ChimeraX (B) Cys18 within the oligomer does not lay at the interaction interface directly. (C)-(E) Predicted S, T, Y sites using GPS (group-based prediction system). (F) Disorder propensity (green) and surface accessibility (orange) of the indicated S, T and Y sites.

(2) The interaction is rather based on the structure or folding of FCAP33 and not due to specific modifications. The GFP tag on the short, truncated N-terminal part of FCAP33 could have a structural impact such that MT interaction is abolished, or residues that need to be modified for interaction are not accessible anymore. Even though oligomerization can still take place in this truncation (Figure 15 D). (3) The short version of FCAP33 leads to a diminished activity independent of its localization, when compared to the full-length (FL) version of FCAP33. This diminished activity prevents MTs from growing, which could explain the dominant negative effect of FCAP33$_{1\text{-}167}$-cLAP on cilium length, as the truncated variants are overexpressed. This would also explain the effect, that overexpressing the FL version of FCAP33 leads to an elongation of the axoneme (Figure 4 E and F, Figure 12 C). Theory (1) and (2) are more unlikely due to the lack of localization of the truncated LAP-tagged version in primary cilia, BB or any other MT structures. If the N-terminal part directly interacts with microtubules we would expect to see an interaction *in vivo* and not only the *in vitro* setup, where the interaction of FCAP33$_{1\text{-}167}$-cLAP with MTs was shown (Figure 16). It could, however, be possible that a ciliary targeting mechanism is lacking in FCAP33$_{1\text{-}167}$-cLAP cells, which is not needed for MT association in the *in vitro* situation. Additionally, it may be that the N-terminus does indeed interact with MTs, but that the levels are under the detection limit of our standard IF setup. This would be reasonable as the WB **(**Figure 13) and the IF experiments show (Figure 12), that the C-terminal truncation is much higher expressed, than the N-terminal variant. It might be possible that in cells there is a competition between endogenous FCAP33 and the overexpressed N-terminal variant as shown for the MAPs MAP4 and Tau (Tokuraku et al., 1999; Stamer et al., 2002) before. For the *in vitro* setup, the amount of FCAP33 transfected into HEK293T cells is much higher, and the expression of the protein is much greater than in the IMCD3 cells stably expressing the constructs. Scenario (3) could explain various results seen in this work. Recently, there was a study of TTBK2, which is needed to prime the BB for cilium outgrowth by removing the capping protein CP110 (Benk Vysloužil et al., 2025). This allows the docking of the ciliary vesicles to the mother centriole (basal body) in RPE cells. There was a mutated version of TTBK2, which was lacking the C-terminal BB localization sequence but still having the kinase domain. Both, WT and this short version, were sufficient to support the initial CP110 removal steps important for ciliogenesis, even though the truncation would not localize to the BB anymore. The TTBK2 activity is needed to inhibit the KIF2A basal pool to allow the elongation of the axoneme. The truncated TTBK2 cannot fully inhibit KIF2A leading to its accumulation at the BB. As KIF2A is a negative regulator of axoneme elongation, its accumulation leads to shorter cilia (Benk Vysloužil et al., 2025).

Regarding this study, it could be possible that FCAP33 or its truncated versions function outside of the cilium. This might explain why it was hard to detect direct ciliary interactors, because an interaction could be rather transient and indirect and therefore not stable enough to being pulled down in the CoIP setup. Additionally, for the truncated TTBK2, the phenotypes were similar to the phenotypes observed for the N-terminal truncation of FCAP33. Both short versions show shorter and less cilia even though they do not localize properly. The function of FCAP33 might also be similar to the function of KIF2A or recruit KIF2A. FCAP33 has a lot of serins and was recently classified as phosphoprotein in Uniprot according to the predicted phosphorylation sites (Figure 20**,** Figure 21 C, D, E). This was not known at the beginning of this study, as C7orf57 or Gm11992 was barely included in any studies before. KIF2A has a specific region, where mutating 3 serins into constitutively active serins resulted into decreased localization of KIF2A to the ciliary basal body. This in turn diminished the cilium shortening effect of truncated TTBK2 leading to normal cilium length again (Benk Vysloužil et al., 2025). It is unlikely that FCAP33 fulfills a kinase activity, as such a domain is not predicted and sequence alignments of e.g. the kinase domain of KIF2A did only show minor similarity. Due to prediction analysis, it is likely that FCAP33 is phosphorylated. FCAP33 has many S/T/Y sites with most of them being S sites (Figure 21 E + F). Similarly to KIF2A, the largest population of S sites is located within the most disordered C-terminal region of the protein sequence (Figure 21 F). Additionally, surface accessibility analysis shows (Figure 20 C and Figure 21 F), that the disordered part of the protein is more surface exposed, which would make a possible interaction with kinases or other enzymes and proteins more likely. This might also explain why overexpressing the C-terminal truncation of FCAP33 does not have a dominant negative effect on cilium length. The overexpression of only the functional part might have less of an impact on ciliation, than overexpressing the non-functional part of the protein. If the N-terminus is the interacting/localization domain and the C-terminal part of FCAP33 the domain important for the molecular function via phosphorylation. The N-terminus might still interact with proteins or MTs but due to the lack of functionality it could impair or even block downstream processes. As the affinity of the C-terminus to MTs seems even lower than FL or N-terminal FCAP33, it is possible that the C-terminus alone mis-localizes and is either not functional upon mis-localization or still functional but does not negatively affect endogenous FCAP33. It is possible, that phosphorylation can only occur at the base of the cilium and therefore the “mistargeted” C-terminus has no dominant effect. If FL FCAP33 is important for axoneme elongation it might play a role in tubulin modification. Therefore, I did some

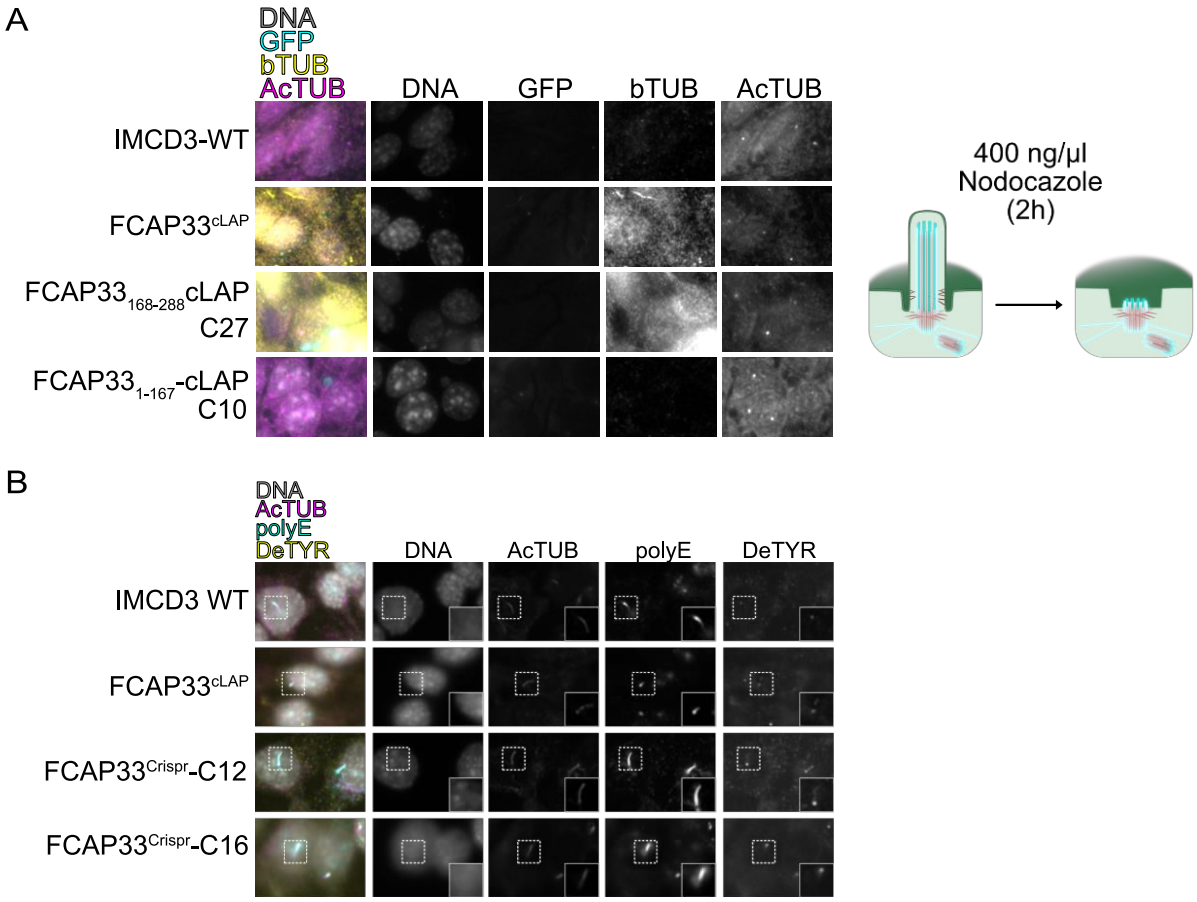

Figure 22: FCAP33 stabilizes MTs and is involved in the regulation of post-translational modifications (PTMs)

(A) Nocodazole induced deciliation by adding nocodazole for two hours to starved cells, prior to fixation. Cells were stained for DNA (Hoechst, gray), beta tubulin (bTUB, yellow) and AcTUB (magenta). (B) IF experiment of starved cells to screen for PTMs. Polyglutamylated tubulin antibody (polyE, cyan) and detyrosinated tubulin antibody (DeTYR, yellow) were used to compare PTMs in WT, overexpression and FCAP33 Crispr Clones. AcTUB as cilia marker (magenta).

preliminary tests to study the effect of FCAP33 on microtubule post-translational modifications (PTMs) and stability. Treating IMCD3 cells with nocodazole leads to disruption of the MT network by binding to tubulin dimers and thus inhibiting tubulin polymer assembly (Vasquez et al., 1997). This leads to deciliation. After treatment of cells with Nocodazole, only ciliary stubs were left. Staining with beta tubulin (bTUB) showed that FCAP33^{cLAP} and FCAP33$_{168-288}$-cLAP had stronger beta tubulin signals. This could indicate stabilization of beta tubulin when overexpressing FL or C-terminal FCAP33, supporting that the C-terminus is the functional part of FCAP33 and might also act outside of the cilium. The N-terminus showed similar intensities of bTUB to WT cells (Figure 22 A). Moreover, I checked different PTM markers in IF by staining with detyrosinated tubulin (DeTYR) and polyglutamylated tubulin (polyE). PTMs of MTs are important for MT stability, to define MAP and motor protein

interaction and to create a specific tubulin code important to define MT functions and processes (Janke, 2014; Conkar and Firat-Karalar, 2021). IMCD3 WT was compared to FCAP33^{cLAP} and FCAP33^{Crsipr}-C16 and FCAP33^{Crsipr}-C12. FCAP33^{Crsipr}-C12 exhibits a ciliation rate that is higher than WT (Figure 15 D and F) but efficient KO could not be confirmed. Comparing polyE and DeTYR in the Cripsr cell lines that potentially have defects in FCAP33 expression, to WT cells and FCAP33 overexpression, shows that deTYR signals in IF seem stronger than in the KO cells. Especially for C12 stronger signals can also be detected for polyE staining (Figure 22 B). However, as signal intensities have not yet been quantified, these observations are currently based on visual assessment. Detyrosinated MTs are resistant to the depolymerizing MT drug nocodazole (Sanyal et al., 2023). This effect could explain the increased ciliation rate of Crispr clone C12 which may be more detyrosinated (Figure 22 B) making it more resistant to depolymerization and therefore deciliation. This would mean that FCAP33 is important for the deciliation process rather than the ciliation process. Or FCAP33 is important to target PTMs, MAPs or enzymes into the primary cilium to thereby regulating ciliation and deciliation. This potential effect was discovered for KIF2A before. The ciliary kinesin protein KIF2A has a MT depolymerizing activity. The MT depolymerizing activity at the mother centriole is important for primary cilium disassembly. KIF2A is phosphorylated by the mitotic kinase PLK1 activating its MT depolymerizing activity. Cells deficient of KIF2A or in a phospho-deficient mutant showed impaired cilium disassembly (Miyamoto et al., 2015).

FCAP33 is a MAP but functionally different from the recently found ciliary MAPs CCDC66 and ENKD1

During this work we showed that there are different pools of FCAP33 within IMCD3 cells, as it localizes to the BB, ciliary axoneme, ciliary tip and centrioles. It could be that these different pools assign different roles to functions as seen for CCDC66. FCAP33 localizes to the axoneme in a spotted manner, like CCDC66 and we were also able to dissect a FCAP33 ciliary tip pool as seen for CCDC66. This could be timely dependent on the ciliation or deciliation status of primary cilia, or different existing pools exist independent of primary cilia. CCDC66 is a ciliary MAP that localizes to the ciliary tip together with CEP104 and CSPP1(Frikstad et al., 2019; Ryniawec et al., 2023) and to the axoneme, where it is immobile, like FCAP33 (Conkar et al., 2019) (Figure 9, Figure 10).

In addition, CCDC66 also localizes to multiple similar structures like FCAP33 such as: midbodies, basal body, centrioles and spindle, but also to the centrosomes and the midzone. The localization of FCAP33 to the spindle seems weaker than compared to CCDC66 and

FCAP33 KD experiments did not show a cytokinesis phenotype (Figure 16, Figure 17), whereas knockdown of CCDC66 led to a variety of defects linked to mitotic and cytokinetic MT structures thus being important for proper cytokinesis (Batman et al., 2022b). Generally, CCDC66 and FCAP33 are both ciliary MAPs and might have comparable roles in terms of having different cellular pools and a multifaceted function. Until today, I could not show an impaired accumulation or increased accumulation of the hedgehog activator smoothened after direct activation with the smoothened agonist (SAG) performing KD or investigating FCAP33 overexpression (Data not shown). This is in contrast to CCDC66, that showed a change in ciliary content upon hedgehog induction in cells depleted of CCDC66 (Odabasi et al., 2023; Deretic et al., 2024). I did not check for the presence or absence of known TZ proteins in FCAP33 depleted cells, but I also could not observe a visual increase in cilium length when knocking down the protein. Generally, the overexpression of FCAP33 did lead to longer cilia, but we could not observe any obvious phenotype in ciliary beta tubulin, polyglutamylated tubulin using GT335 antibody or gamma tubulin staining at the centriole/basal body. However, the preliminary experiment showed that polyE and DeTYR might be less expressed along the axoneme in FCAP33^{cLAP} cells when compared to WT (Figure 22). Therefore, CCDC66 and FCAP33 potentially do not share similar functions, as described effects on mitosis and hedgehog signaling are not in common. Nevertheless, CCDC66 and FCAP33 both interact with MT-based structures. ENKD1 is another recently described ciliary MAP that also localizes to the centrosomes and when overexpressed to the spindle (Tiryaki et al., 2022). This is a similar "phenotype" to what we see in FCAP33^{cLAP} which strongly overexpress FCAP33. In these FCAP33 overexpressing cells, FCAP33 also localizes to the spindle. Upon weaker overexpression (NG and ALFA tagged variants, Figure 12, Figure 3) we were able to detect a faint FCAP33 signal at the spindle. Expansion microscopy of ENKD1 revealed its localization to the centriole wall and the axoneme. It seems that FCAP33 is expressed at lower levels than ENKD1 as ENKD1 signals seem stronger in IF (Tiryaki et al., 2022) but this should be compared within one experiment in the same cell line. In addition, ENKD1 depleted cells had impaired response to hedgehog pathway activation (Tiryaki et al., 2022).

We found a new ciliary MAP that has comparable features to ENKD1 and CCDC66 regarding the localization, which is likely due to their common association with MTs. I could not reveal that FCAP33 regulates ciliary content similarly to ENKD1 and CCDC66 which suggests a distinct function. Furthermore, I could not observe a strong cell cycle or cell division phenotype, which also stands out from CCDC66. Interestingly, both MAPs (ENKD1 and CCDC66) are involved in cilium length regulation, which was also shown for FCAP33.

FCAP33 overexpression leads to heterogenous cilium length, which is generally longer and overexpression of the N-terminus has a negative effect on cilium length.

FCAP33 as a ciliary TIP protein?

There are several known proteins that act at the ciliary tip, such as CEP104 (Centrosomal protein of 104 kDa), EB1/MAPRE1 (End-binding protein1/Microtubule-associated protein RP/EB familiy member 1, NCBI 9606), (EB3/MAPRE3) and DAAM1 (Disheveled-associator of morphogenesis 1) (Kida et al., 2007; Yamazoe et al., 2020a; Wang et al., 2023; Saunders et al., 2025). CEP104 is important for cilium elongation but not cilium formation, as knocking down CEP104 does not lead to cilium loss (Yamazoe et al., 2020). Instead, the TOG-domain, which is the MT interacting domain polymerizes MTs and thus is required for cilium elongation (Frikstad et al., 2019). The localization of CEP104 to the ciliary tip is independent of the end-binding protein EB1 which binds to MT ends in the ciliary axoneme. EB1 is not involved in CP110 (Frikstad et al., 2019) removal and acts independent of CP110. CEP104 is involved for proper ciliary trafficking of Shh components, which is also the link to the combined function of CEP104 with CCDC66 (Frikstad et al., 2019; Yamazoe et al., 2020). EB1 is a MT plus-end tracking (+TIP) protein, together with EB3, which were both shown to be important for cilia formation (Schrøder et al., 2011). Interestingly, the proposed function of EB1 and EB3 on ciliogenesis by Schrøder et al (Schrøder et al., 2011) was not due to the plus end association but through an effect on the basal body or cilium. EB1 and EB3 potentially target MT minus-ends which promotes dynein-mediated trafficking of ciliary precursors to the ciliary base, confirmed by accumulation of ciliary vesicles at the ciliary base upon depletion of EB1 or EB3. EB1/MAPRE1 localizes to the centrosome and BB and DAAM1 to the basal body and vesicles (Kida et al., 2007; Wang et al., 2023). Regarding the localization of FCAP33 to the BB and centriole and its accumulation at the ciliary tip in some cases, suggests a function of FCAP33 at MT ends. Regarding the known ciliary tip candidates, their specific localization to the cilium tip is much more prominent and consistent. A strategy to dissect this function could be to check for similar phenotypes that were associated to known tip proteins such as ciliary vesicles defects, or to dive more into cilium content composition upon hedgehog stimulation of cells. In contrast to FCAP33, CEP104 has a known MT interacting domain (Yamazoe et al., 2020). EB1 and EB3 should be present at a variety of MT structures in the cell (Schrøder et al., 2011). If there is direct interaction, MS analysis should have identified some ciliary tip protein peptides, but there are no hints on direct interaction with the ciliary tip proteins. There could

be transient interaction but structurally and phenotype-wise it is rather unlikely that FCAP33 fulfills a similar role than the mentioned ciliary tip associated proteins.

Actin and Actin-binding proteins in primary cilia

In addition to MT binding proteins there are Actin binding proteins acting or localizing at the primary cilia tip: DAAM1 and Myosin VI. DAAM1 is an actin nucleator, involved in ciliogenesis and affecting the non-canonical Wnt pathway (Wang et al., 2023).

There are not hints for FCAP33 to interact with DAAM1 directly, and the role of the DAAM1 protein is rather undissected. Interestingly, DAAM1 does localize to primary cilia in IMCD3 cells and knockdown of Daam1 in IMCD3 cells, leads to the loss of primary cilia (Corkins et al., 2019). Additionally, it was shown the formin region in DAAM1 is important for proper ciliogenesis (Corkins et al., 2019). FHDC1 a member of the formin family of cytoskeletal remodeling proteins, was also shown to be involved in ciliogenesis. When knocked down FHDC1 inhibits cilium assembly and reduces cilium length but overexpression blocks cilium formation or induces extremely long cilia (Copeland et al., 2018). In contrast to the FHDC1 and DAAM1 phenotype overexpression of KD of FCAP33 did not lead to cilium loss or lower ciliation rates.

In a cyst forming assay, KD of DAAM1 led to the formation of cysts with smaller lumen and without cilia. As shown for Actin, DAAM1 is founc in ciliary vesicles together with IFT88 and ciliary DAAM1 interacted with IFT88 (Corkins et al., 2019). In the last decade the link between actin cytoskeleton and cilia has been investigated and there is clear evidence that the actin skeleton dynamics is important for normal cilia function. F-actins were shown to be important for ciliogenesis (Copeland et al., 2018; Wang et al., 2023), more specifically the docking of the actin cytoskeleton to the basal body (Kohli et al., 2017). This process is required for the myosin mediated transport of pre-ciliary vesicles to initiate ciliogenesis and formation of the ciliary sheath (Albertson et al., 2008; Hoffman and Prekeris, 2022; Wang et al., 2023). F-actin can also act as a negative regulator by blocking the vesicle docking (Wang et al., 2023). F-actin was shown to be polymerized by CDC42 a RHO-family GTPase that is involved in ectocytosis (Wang et al., 2023; Prasai et al., 2025). RHO GTPases generally control actin polymerization (Prasai et al., 2025).

Actin-binding proteins (ABPs) are necessary for proper F-actin morphology. There are Actin capping proteins: CapZ and twinfilin 2, that lead to shorter cilia when knocked down, as well as gelsolin (Wang et al., 2023). The ABPs α-Actinin 1/4, the Arp2/3 complex, and Leucine

zipper protein 1 (LUZP1) can also induce cilium shortening when knocked down but also lengthening when overexpressed (Wang et al., 2023). There are ABPs, that were also detected to be downregulated in certain ciliopathies, showing their potential importance for cilia (Wang et al., 2023). Interestingly, our MS analysis showed that IQGAP1 is a common hit in all three MS datasets and also in the cilia and centriole proteome. It stabilizes CDC42 in a GTP-bound form and has a predicted F-actin binding domain. IQGAP1 is also associated with cytoskeletal proteins but also with actin filaments (Hoeprich et al., 2022). IQGAP1 forms dimers to associate with actin filament sites, it can cap barbed ends, has the ability to form thin actin bundles at stabilizes filaments against polymerization (Hoeprich et al., 2022). In contrast to its presence in primary cilia, the hit in the midbody proteome was also confirmed via IF (Skop et al., 2004). As another common hit of the replicates of FCAP33 MS hits was Actin it would not be unlikely that FCAP33 plays a role as a mediator between the Actin- and the cytoskeleton. Like IQGAP1 that is involved in linking the MT to the actin cytoskeleton, FCAP33 could also be involved in this linking process. We found that FCAP33 is a MAP, as it hast die capability to bind to MTs, but we could not directly co-isolate beta tubulin or acetylated tubulin. We were able to detect tubulin and Actin related hits in MS, which would also fit to the localization of FCAP33 at the midbody like F-actin that is involved in the abscission process (Dema et al., 2018). Its localization at the central part of the midbody also goes hand in hand with a potential interaction with the actomyosin ring. Besides the function of Actin in the final abscission after midbody formation (Andrade and Echard, 2022; Halcrow et al., 2022), midbodies are also linked to the lumen forming process in cyst formation and F-actin is also needed for proper apical lumen formation (Dema et al., 2018). Regarding the discussed role of Actin and ABPs in midbody, cilia and cyst formation, FCAP33 could be novel ABP.

Defective cystogenesis in FCAP3^{3cLAP} cells suggests a role in regulating Actin dynamics

When we performed a cyst formation assay with cells with deficient or overexpressing FCAP33 levels we found that cyst formation was impaired. The FCAP33 overexpressing cell line only formed clumps and KD as well as a truncated version (FCAP33^{Crsipr}-C1) of FCAP33 did form round structures with occurrences of cysts but not properly formed lumen. This means, that FCAP33 must be involved in the formation of a proper apical lumen, either by being a direct factor in the lumen forming process or its involvement in signaling processes.
The beforementioned MT tip protein DAAM1 (Disheveled Associated Activator of Morphogenesis 1) functions through the non-canonical Wnt/PCP Pathway (Kida et al., 2007;

Park et al., 2008; Corkins et al., 2019). In *Xenopus laevis* DAAM1 is important for proper kidney development (Kida et al., 2007). Regarding the cyst formation defect in DAAM1 KD cells, this could be due to its involvement in the PCP pathway and/or due to its function in primary cilia. Even though DAAM1 has an effect on ciliogenesis and it was fond in cilia proteomes (Ishikawa et al., 2012; Sroka et al., 2025) it could not be detected by antibody staining. It might be that the levels of DAAM1 are comparably low to the levels of FCAP33. CDC42 regulates actin polymerization, spindle orientation and exo- and endocytosis of apical endosomes, another necessary process for epithelial cell polarization (Blasky et al., 2015). It was shown that CDC42 depletion leads to the formation of several lumen due to the disruption of mitotic spindle/midbody orientation (Jaffe et al., 2008). Midbody formation is the first symmetry breaking event for polarization and therefore initiates the formation of an apical lumen (Blasky et al., 2015; Farmer, 2022). As we did not follow early stages of cyst formation, we do not have insights whether the spindle orientation in the initiating 3D structure was correct. Jaffe et all states that the midbody positions the abscission site of the first dividing cell which in turn establishes the apical surface. Disruption of Cdc42 leads to misoriented spindles and - midbodies, resulting in multiple, ectopic lumens due to the improper positioning of apical surfaces (Jaffe et al., 2008). Therefore, misalignment of midbodies would lead to the formation of several lumen. In fact, in overexpressing cells (FCAP33^{cLAP}) the DNA stain shows cells that are in a dividing state (lane 2+3 Figure 17 B) as well as several midbodies (more than in WT). It is in contrast to the model by Jaffe et al, that even IMCD3 WT cells do have midbody structures within the cyst structure. Mislocalized leftover midbodies should lead to impaired cyst formation according to Jaffe et al. (Jaffe et al., 2008). I could observe that midbodies in the KD condition are localized more at the apical side of the cyst/clump or within the clumps in overexpressing cells (Figure 18). Besides the importance of MTs, Actin and the midbody for lumen formation in cysts, vesicle trafficking is also essential for epithelial function. Ion channels, junction proteins, receptors, transporters and more, are packed in vesicles and their transport and secretion to the apical or basolateral membrane is important for epithelium function (Blasky et al., 2015; Buckley and St Johnston, 2022). Additionally, vesicles are also important for cilia formation (Nachury et al., 2007) and exocytosis processes are not only involved in tissue organization but also primary cilia formation. Vesicles use the MT network for trafficking (Buckley and St Johnston, 2022). Regarding the likelihood of FCAP33 to transiently mediate or interact with MTs and Actin, it might be possible that FCAP33 is involved in vesicle trafficking or vesicle mediated processes at Actin and MT sites. The dominant-negative effect of the N-terminus could be caused by it being the molecularly non-

functional part of FCAP33 that impairs vesicle trafficking to primary cilia and therefore ciliogenesis is impaired. But it is also possible that the docking of the Actin-cytoskeleton to the BB is partially blocked, which in turn leads to deficient vesicle trafficking to the cilium.
Taken together, the function of FCAP33 as a MAP suggests a function of FCAP33 on MTs. On a molecular level, we could not reveal its function yet, but we were able to show that different parts of the protein might fulfill different functions. The C-terminal half of the protein is likely to act via exposed phosphorylation sites, while the N-terminal half shows higher affinity to MTs potentially being the MT binding site. Comparing literature, looking at lumen formation in 3D and the MS hits it is conceivable that FCAP33 interacts with Actin. Therefore, it is possible that FCAP33 acts as mediator between Actin and MTs. Moreover, FCAP33 induces cilium lengthening which could be explained by effects on both: on Actin and on MTs.

FCAP33 as a putative component of the Centralspindlin complex

If we look at the localization of the tagged FCAP33 within the midbody structure, it can be appreciated that FCAP33 not only localizes to the spindle MT but even more at the midbody arms and specifically at the stem. At the stem body it colocalizes and is surrounded by the core midbody protein MKLP1(Figure 3 D). Centralspindlin is highly concentrated at this region, where the compacted antiparallel MT plus ends come together after furrow ingression between two divided cells. Different to the antiparallel MTs, Centralspindlin forms a ring like structure surrounding the midbody. MKLP1 could also be shown to locate to this ring link structure but it is not known how its transition from MT bundles to the cortical ring is mediated (White and Glotzer, 2012). How this transition takes place would also be unclear for FCAP33 but it shows a similarity in localization to MKLP1. The MS analysis revealed that several proteins of the 14-3-3 protein family were found. The 14-3-3 proteins are phospho-binding proteins regulating a variety of cellular functions (Pennington et al., 2018), including the interaction with the Centralspindlin complex (Douglas et al., 2010; White and Glotzer, 2012). Upon phosphorylation of MKLP1 at S710 the protein 14-3-3 binds Centralspindlin. It does not bind Centralspindlin when MKLP1 is phosphorylated at S708. S708 in MKLP1 is the site which is phosphorylated by Aurora B at the central spindle and midbody which then inhibits the MKLP1 14-3-3 interaction (Guse et al., 2005; Douglas et al., 2010; White and Glotzer, 2012). Aurora B is a serine/threonine-protein kinase of the CPC complex, a key regulator for mitosis. Due to the described localization of FCAP33 at the spindle/midbody and the described functions of 14-3-3 it is possible that 14-3-3 and FCAP33 interact or have similar functions. We found three

members of the 14-3-3 protein family in our MS experiments: Ywhab, Ywhaq and Ywhaz. Ywhab and Ywhaz were also found in the flemmingosome, confirming the role in processing the Centralspindlin complex, and it was found in the cilia proteome. The role of 14-3-3 components in primary cilia was not described so far but could be due to the multifaceted role of 14-3-3 proteins. Together with the fact that FCAP33 has several predicted phosphorylation sites, it is likely that 14-3-3 proteins interact with FCAP33. 14-3-3 prevents Centralspindlin from clustering, when MKLP1 cannot bind to it, which is when S708 is phosphorylated. This allows attachment of MKLP1 to the central spindle. This mechanism regulates Centralspindlin such that MKLP1 only clusters at the spindle and not anywhere else in the cell (Guse et al., 2005). FCAP33 might be involved in such a regulating function or interaction function to localize other proteins or itself to the midbody structure. The function of FCAP33 at the midbody is still not solved, but this could be a mechanism to explain how it is involved in these cellular processes. It could also explain its localization to midbodies and how it might be regulated.

An additional function of FCAP33, other than having a direct function in midbodies or a direct function in primary cilia, could be an indirect signaling function in cilia due to its midbody association.

FCAP33 as a regulator of primary cilia through its involvement in spindle and midbody function

Primary cilia and midbody formation are both tightly linked to the cell cycle. The ciliogenesis of primary cilia needs a controlled MT organization and the delivery of membrane as well as vesicles and proteins (Sorokin, 1968; Nachury et al., 2007; Smith et al., 2011). During cytokinesis, there is tight control of MTs to organize bundles and the cleavage furrow during central spindle organization (Albertson et al., 2008; Hutterer et al., 2009). There are proteins described as being involved in both processes, such as RhoA, BBS6, CP110 (Park et al., 2008; Smith et al., 2011). Smith et al showed, in addition to the known midbody proteins such as PRC1 and MKLP1, which were already extensively discussed beforehand, INCEP and Centriolin localize to basal bodies of multi-ciliated epithelial cells (Smith et al., 2011). They also showed that the proteome of cilia, basal body and midbody have indeed overlapping hits and a gene network also showed PRC1 and MKLP1 to be tightly linked to a cluster of cytokinesis and ciliogenesis, supporting them to be involved in both ciliogenesis and midbody formation. This revealed that the presence for midbody proteins at the BB is not uncommon

and might be a hint for their involvement in ciliogenesis (Smith et al., 2011). FCAP33 was also found to be localized at the ciliary base, even only when the endogenous N-terminal part until Exon 4 was expressed. It was also still detectable at centrioles and very weakly at spindles and midbodies. The similar localization patterns of MKLP1 and PRC1 with FCAP33 (discussed before) could indicate, that FCAP33 belongs to a similar "class of proteins" as MKLP1 and other midbody components found at the ciliary base. Whether this is due to a shared function in vesicle trafficking, MT bundling, or Actin recruitment remains to be investigated.

In addition to this shared function there are studies that describe a potential link between midbodies and primary cilia, even though this potential role is not relevant for all cell types (Bernabé-Rubio et al., 2016; Ott, 2016; Farmer, 2022). It is believed that for kidney epithelial cells, such as IMCD3 cells mostly the extracellular route is used (Sorokin, 1968; Goetz and Anderson, 2010; Garcia-Gonzalo and Reiter, 2012). This process of ciliation requires the docking of the basal body to the cell membrane and only then, cilium formation is initiated (Bernabé-Rubio et al., 2016; Wu et al., 2018; Labat-de-Hoz et al., 2021). After abscission the midbody remnant (MBR) was described in different functions. In polarized epithelial cells, MBR harbor ciliary proteins such as IFT20, IFT88 and Rab8 (Bernabé-Rubio et al., 2016). In a Rab8 dependent fashion, the MBR can move along the apical surface of the cells until reaching the BB (centrosome docked to the membrane). This initiates the formation of a primary cilium (Bernabé-Rubio et al., 2016). There are different proposed mechanisms of the cilium emergence in the alternative route and the evolutionary evolvement of the MBR. The connection between centriole and ciliary vesicles and their hierarchy still remains to be investigated (Sorokin, 1968; Labat-de-Hoz et al., 2021).

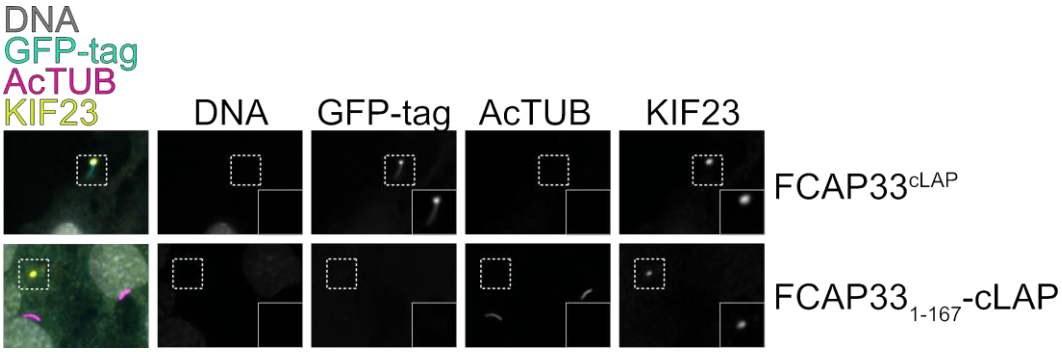

Figure 23: IF of midbody remnants

KIF23/MKLP1 as midbody (MB) and MB remnant marker (yellow), AcTUB as cilia and midbody marker (magenta), GFP tag for FCAP33^{cLAP}. Comparison of N-terminal FCAP33 and FL overexpression.

Indeed, FCAP33^{cLAP} expressing cells FCAP33 localized to the MBR stained by KIF23 (MKLP1). The N-terminus did not localize to these MBR structures as seen for cilia and midbodies (Figure 23).

Outlook

Taken together, we found the unknown protein C7orf57/Gm11992 in the cilium proteome and decided to investigate this unidentified protein which we termed FCAP33. We showed that FCAP33 localizes to midbodies, its remnants, primary cilia, basal bodies, centrioles and the spindle. Due to its localization to multiple MT-based structures and its confirmed microtubule association we can classify FCAP33 as a ciliary MAP. Regarding the discussed topics, such as cyst formation and involvement in ciliation, a mediating function between Actin and MTs could be possible. In addition, FCAP33 is a predicted phosphoprotein and shows links to 14-3-3 protein family members. Therefore, an involvement in the Centralspindlin complex is conceivable and would fit the model of connecting Actin and MTs. We were not able to generate a full FCAP33 KO so far, which made it difficult to screen for potential phenotypes. It does not lead to the collapse of the cell cycle, when reducing or impairing FCAP33, but we found that overexpressing the N-terminus negatively affected either ciliogenesis or disassembly, causing shorter and less cilia. Overexpressing the full-length protein led to longer cilia and the C-terminus did not have any dominant effect. These findings support the conclusion that the more exposed C-terminus of FCAP33, with its potential phosphorylation sites may confer the functional activity and the N-terminus likely mediates microtubule binding. This is further supported by observations in Exon 4 targeted Crispr clones, where the truncated endogenous FCAP33 still localizes to the basal body and to a lesser extent to midbodies. Whether FCAP33's localization FCAP33 to the basal body and the primary cilium is a consequence of its presence at the midbody remnant and its involvement in ciliogenesis, or reflects a broader, multifunctional role remains to be elucidated, e.g. by live imaging of across a cell division cycle.

Knockdown of FCAP33 does not lead to a length or ciliation effect, but it would be interesting to further dissect the ciliary proteomic changes upon for instance hedgehog signaling activation in a KD situation or with expression of the dominant negative truncation. Alongside this, combining expansion and STED microscopy together with electron microscopy could help to dissect its specific localization on MTs. Pull-down assays isolating Actin, MTs or MKLP1

could also be helpful to confirm an interaction. This project opens the possibility of several further investigations while supporting the previously found links between midbody proteins, centrioles and primary cilia. It further shows that studying ciliary MAPs is of importance for the future and a multifaceted role of MAPs between different organelles is likely.

Literature

Addi, C., Presle, A., Frémont, S., Cuvelier, F., Rocancourt, M., Milin, F., et al. (2020). The Flemmingsome reveals an ESCRT-to-membrane coupling via ALIX/syntenin/syndecan-4 required for completion of cytokinesis. *Nat Commun* 11, 1941. doi: 10.1038/s41467-020-15205-z

Afgan, E., Baker, D., Batut, B., van den Beek, M., Bouvier, D., Čech, M., et al. (2018). The Galaxy platform for accessible, reproducible and collaborative biomedical analyses: 2018 update. *Nucleic Acids Research* 46, W537–W544. doi: 10.1093/nar/gky379

Agrawal, N., Dasaradhi, P. V. N., Mohmmed, A., Malhotra, P., Bhatnagar, R. K., and Mukherjee, S. K. (2003). RNA Interference: Biology, Mechanism, and Applications. *Microbiol Mol Biol Rev* 67, 657–685. doi: 10.1128/MMBR.67.4.657-685.2003

Aguilar, A., Becker, L., Tedeschi, T., Heller, S., Iomini, C., and Nachury, M. V. (2014). A-tubulin K40 acetylation is required for contact inhibition of proliferation and cell-substrate adhesion. *Mol Biol Cell* 25, 1854–1866. doi: 10.1091/mbc.E13-10-0609

Akhmanova, A., and Steinmetz, M. O. (2015). Control of microtubule organization and dynamics: two ends in the limelight. *Nat Rev Mol Cell Biol* 16, 711–726. doi: 10.1038/nrm4084

Albertson, R., Cao, J., Hsieh, T., and Sullivan, W. (2008). Vesicles and actin are targeted to the cleavage furrow via furrow microtubules and the central spindle. *The Journal of Cell Biology* 181, 777–790. doi: 10.1083/jcb.200803096

Alliegro, M. C. (2000). Effects of Dithiothreitol on Protein Activity Unrelated to Thiol–Disulfide Exchange: For Consideration in the Analysis of Protein Function with Cleland's Reagent. *Analytical Biochemistry* 282, 102–106. doi: 10.1006/abio.2000.4557

Andrade, V., and Echard, A. (2022). Mechanics and regulation of cytokinetic abscission. *Front. Cell Dev. Biol.* 10, 1046617. doi: 10.3389/fcell.2022.1046617

Ann Jordan, M., Thrower, D., and Wilson, L. (1992). Effects of vinblastine, podophyllotoxin and nocodazole on mitotic spindles : Implications for the role of microtubule dynamics in mitosis. *Journal of Cell Science* 102, 401–416. doi: 10.1242/jcs.102.3.401

Badano, J. L., Mitsuma, N., Beales, P. L., and Katsanis, N. (2006). The Ciliopathies: An Emerging Class of Human Genetic Disorders. *Annu. Rev. Genom. Hum. Genet.* 7, 125–148. doi: 10.1146/annurev.genom.7.080505.115610

Batman, U., Deretic, J., and Firat-Karalar, E. N. (2022). The ciliopathy protein CCDC66 controls mitotic progression and cytokinesis by promoting microtubule nucleation and organization. *PLoS Biol* 20, e3001708. doi: 10.1371/journal.pbio.3001708

Beaudouin, J., Gerlich, D., Daigle, N., Eils, R., and Ellenberg, J. (2002). Nuclear Envelope Breakdown Proceeds by Microtubule-Induced Tearing of the Lamina. *Cell* 108, 83–96. doi: 10.1016/S0092-8674(01)00627-4

Benk Vysloužil, D., Bernatík, O., Lánská, E., Renzová, T., Binó, L., Lacigová, A., et al. (2025). Tau-tubulin kinase 2 restrains microtubule-depolymerizer KIF2A to support primary cilia growth. *Cell Commun Signal* 23, 73. doi: 10.1186/s12964-025-02072-8

Berbari, N. F., O'Connor, A. K., Haycraft, C. J., and Yoder, B. K. (2009). The Primary Cilium as a Complex Signaling Center. *Current Biology* 19, R526–R535. doi: 10.1016/j.cub.2009.05.025

Bernabé-Rubio, M., Andrés, G., Casares-Arias, J., Fernández-Barrera, J., Rangel, L., Reglero-Real, N., et al. (2016). Novel role for the midbody in primary ciliogenesis by polarized epithelial cells. *Journal of Cell Biology* 214, 259–273. doi: 10.1083/jcb.201601020

Bhuyan, A. K. (2010). On the mechanism of SDS-induced protein denaturation. *Biopolymers* 93, 186–199. doi: 10.1002/bip.21318

Blasky, A. J., Mangan, A., and Prekeris, R. (2015). Polarized Protein Transport and Lumen Formation During Epithelial Tissue Morphogenesis. *Annu. Rev. Cell Dev. Biol.* 31, 575–591. doi: 10.1146/annurev-cellbio-100814-125323

Bodakuntla, S., Jijumon, A. S., Janke, C., and Magiera, M. M. (2020). Purification of Tubulin with Controlled Posttranslational Modifications and Isotypes from Limited Sources by Polymerization-Depolymerization Cycles. *JoVE*, 61826. doi: 10.3791/61826

Bodakuntla, S., Jijumon, A. S., Villablanca, C., Gonzalez-Billault, C., and Janke, C. (2019). Microtubule-Associated Proteins: Structuring the Cytoskeleton. *Trends in Cell Biology* 29, 804–819. doi: 10.1016/j.tcb.2019.07.004

Boisvert, F.-M., Van Koningsbruggen, S., Navascués, J., and Lamond, A. I. (2007). The multifunctional nucleolus. *Nat Rev Mol Cell Biol* 8, 574–585. doi: 10.1038/nrm2184

Breslow, D. K., and Holland, A. J. (2019). Mechanism and Regulation of Centriole and Cilium Biogenesis. *Annu. Rev. Biochem.* 88, 691–724. doi: 10.1146/annurev-biochem-013118-111153

Brouhard, G. J., Stear, J. H., Noetzel, T. L., Al-Bassam, J., Kinoshita, K., Harrison, S. C., et al. (2008). XMAP215 Is a Processive Microtubule Polymerase. *Cell* 132, 79–88. doi: 10.1016/j.cell.2007.11.043

Brown, A., and Zhang, R. (2020). Primary Cilia: A Closer Look at the Antenna of Cells. *Current Biology* 30, R1494–R1496. doi: 10.1016/j.cub.2020.10.084

Buckley, C. E., and St Johnston, D. (2022). Apical–basal polarity and the control of epithelial form and function. *Nat Rev Mol Cell Biol* 23, 559–577. doi: 10.1038/s41580-022-00465-y

Burnette, W. N. (1981). "Western Blotting": Electrophoretic transfer of proteins from sodium dodecyl sulfate-polyacrylamide gels to unmodified nitrocellulose and radiographic

detection with antibody and radioiodinated protein A. *Analytical Biochemistry* 112, 195–203. doi: 10.1016/0003-2697(81)90281-5

Buske, P. J., and Levin, P. A. (2012). Extreme C Terminus of Bacterial Cytoskeletal Protein FtsZ Plays Fundamental Role in Assembly Independent of Modulatory Proteins. *Journal of Biological Chemistry* 287, 10945–10957. doi: 10.1074/jbc.M111.330324

Camara, A. K. S., Zhou, Y., Wen, P.-C., Tajkhorshid, E., and Kwok, W.-M. (2017). Mitochondrial VDAC1: A Key Gatekeeper as Potential Therapeutic Target. *Front Physiol* 8, 460. doi: 10.3389/fphys.2017.00460

Carden, S., Vitiello, E., Rosa E Silva, I., Holder, J., Quarantotti, V., Kishore, K., et al. (2023). Proteomic profiling of centrosomes across multiple mammalian cell and tissue types by an affinity capture method. *Developmental Cell* 58, 2393-2410.e9. doi: 10.1016/j.devcel.2023.09.008

Cheeseman, I. M., and Desai, A. (2008). Molecular architecture of the kinetochore–microtubule interface. *Nat Rev Mol Cell Biol* 9, 33–46. doi: 10.1038/nrm2310

Chen, H. Y., Kelley, R. A., Li, T., and Swaroop, A. (2020). Primary cilia biogenesis and associated retinal ciliopathies. *Seminars in Cell & Developmental Biology*, S1084952119301673. doi: 10.1016/j.semcdb.2020.07.013

Chong, Z. X., Yeap, S. K., and Ho, W. Y. (2021). Transfection types, methods and strategies: a technical review. *PeerJ* 9, e11165. doi: 10.7717/peerj.11165

Cleary, J. M., and Hancock, W. O. (2021). Molecular mechanisms underlying microtubule growth dynamics. *Current Biology* 31, R560–R573. doi: 10.1016/j.cub.2021.02.035

Conkar, D., and Firat-Karalar, E. N. (2021). Microtubule-associated proteins and emerging links to primary cilium structure, assembly, maintenance, and disassembly. *The FEBS Journal* 288, 786–798. doi: 10.1111/febs.15473

Copeland, S. J., McRae, A., Guarguaglini, G., Trinkle-Mulcahy, L., and Copeland, J. W. (2018). Actin-dependent regulation of cilia length by the inverted formin FHDC1. *MBoC* 29, 1611–1627. doi: 10.1091/mbc.E18-02-0088

Corkins, M. E., Krneta-Stankic, V., Kloc, M., McCrea, P. D., Gladden, A. B., and Miller, R. K. (2019a). Divergent roles of the Wnt/PCP Formin Daam1 in renal ciliogenesis. *PLoS ONE* 14, e0221698. doi: 10.1371/journal.pone.0221698

Corkins, M. E., Krneta-Stankic, V., Kloc, M., McCrea, P. D., Gladden, A. B., and Miller, R. K. (2019b). Divergent roles of the Wnt/PCP Formin Daam1 in renal ciliogenesis. *PLoS ONE* 14, e0221698. doi: 10.1371/journal.pone.0221698

Danchenko, M., Csaderova, L., Fournier, P. E., and Sekeyova, Z. (2019). Optimized fixation of actin filaments for improved indirect immunofluorescence staining of rickettsiae. *BMC Res Notes* 12, 657. doi: 10.1186/s13104-019-4699-9

Dawe, H. R., Smith, U. M., Cullinane, A. R., Gerrelli, D., Cox, P., Badano, J. L., et al. (2007). The Meckel–Gruber Syndrome proteins MKS1 and meckelin interact and are

required for primary cilium formation. *Human Molecular Genetics* 16, 173–186. doi: 10.1093/hmg/ddl459

Debec, A., Sullivan, W., and Bettencourt-Dias, M. (2010). Centrioles: active players or passengers during mitosis? *Cell. Mol. Life Sci.* 67, 2173–2194. doi: 10.1007/s00018-010-0323-9

Dema, A., Macaluso, F., Sgrò, F., Berto, G. E., Bianchi, F. T., Chiotto, A. A., et al. (2018). Citron kinase-dependent F-actin maintenance at midbody secondary ingression sites mediates abscission. *Journal of Cell Science* 131, jcs209080. doi: 10.1242/jcs.209080

Deretic, J., Cengiz-Emek, S., Seyrek, E., and Firat-Karalar, E. N. (2024). Ccdc66 regulates primary cilium stability, disassembly and signaling important for epithelial organization. doi: 10.1101/2024.06.16.599243

Desai, A., and Mitchison, T. J. (1997). MICROTUBULE POLYMERIZATION DYNAMICS. *Annu. Rev. Cell Dev. Biol.* 13, 83–117. doi: 10.1146/annurev.cellbio.13.1.83

Diener, C., Hart, M., Fecher-Trost, C., Knittel, J., Rheinheimer, S., Meyer, M. R., et al. (2023). Outside the limit: questioning the distance restrictions for cooperative miRNA binding sites. *Cell Mol Biol Lett* 28, 8. doi: 10.1186/s11658-023-00421-4

Douglas, M. E., Davies, T., Joseph, N., and Mishima, M. (2010). Aurora B and 14-3-3 Coordinately Regulate Clustering of Centralspindlin during Cytokinesis. *Current Biology* 20, 927–933. doi: 10.1016/j.cub.2010.03.055

Drivas, T. G., Holzbaur, E. L. F., and Bennett, J. (2013). Disruption of CEP290 microtubule/membrane-binding domains causes retinal degeneration. *J. Clin. Invest.* 123, 4525–4539. doi: 10.1172/JCI69448

Dutta, A., Halder, P., Gayen, A., Mukherjee, A., Mukherjee, C., and Majumder, S. (2023). Increase in primary cilia number and length upon VDAC1 depletion contributes to attenuated proliferation of cancer cells. *Experimental Cell Research* 429, 113671. doi: 10.1016/j.yexcr.2023.113671

Eggenschwiler, J. T., and Anderson, K. V. (2007). Cilia and Developmental Signaling. *Annu. Rev. Cell Dev. Biol.* 23, 345–373. doi: 10.1146/annurev.cellbio.23.090506.123249

Elbashir, S. M., Harborth, J., Lendeckel, W., Yalcin, A., Weber, K., and Tuschl, T. (2001). Duplexes of 21-nucleotide RNAs mediate RNA interference in cultured mammalian cells. *Nature* 411, 494–498. doi: 10.1038/35078107

Farmer, T. (2022). New signaling kid on the block: the role of the postmitotic midbody in polarity, stemness, and proliferation. *MBoC* 33, pe2. doi: 10.1091/mbc.E21-06-0288

Fededa, J. P., and Gerlich, D. W. (2012). Molecular control of animal cell cytokinesis. *Nat Cell Biol* 14, 440–447. doi: 10.1038/ncb2482

Fisher, K. H., Deane, C. M., and Wakefield, J. G. (2008). The functional domain grouping of microtubule associated proteins. *Commun Integr Biol* 1, 47–50. doi: 10.4161/cib.1.1.6795

Fırat-Karalar, E. N., and Stearns, T. (2014). The centriole duplication cycle. *Phil. Trans. R. Soc. B* 369, 20130460. doi: 10.1098/rstb.2013.0460

Frikstad, K.-A. M., Molinari, E., Thoresen, M., Ramsbottom, S. A., Hughes, F., Letteboer, S. J. F., et al. (2019). A CEP104-CSPP1 Complex Is Required for Formation of Primary Cilia Competent in Hedgehog Signaling. *Cell Reports* 28, 1907-1922.e6. doi: 10.1016/j.celrep.2019.07.025

Fu, J., Hagan, I. M., and Glover, D. M. (2015). The centrosome and its duplication cycle. *Cold Spring Harb Perspect Biol* 7, a015800. doi: 10.1101/cshperspect.a015800

Gadadhar, S., Bodakuntla, S., Natarajan, K., and Janke, C. (2017). The tubulin code at a glance. *Journal of Cell Science* 130, 1347–1353. doi: 10.1242/jcs.199471

Gambarotto, D., Hamel, V., and Guichard, P. (2021). "Ultrastructure expansion microscopy (U-ExM)," in *Methods in Cell Biology*, (Elsevier), 57–81. doi: 10.1016/bs.mcb.2020.05.006

Garcia-Gonzalo, F. R., and Reiter, J. F. (2012). Scoring a backstage pass: Mechanisms of ciliogenesis and ciliary access. *Journal of Cell Biology* 197, 697–709. doi: 10.1083/jcb.201111146

Garcia-Gonzalo, F. R., and Reiter, J. F. (2017). Open Sesame: How Transition Fibers and the Transition Zone Control Ciliary Composition. *Cold Spring Harb Perspect Biol* 9, a028134. doi: 10.1101/cshperspect.a028134

Gardino, A. K., and Yaffe, M. B. (2011). 14-3-3 proteins as signaling integration points for cell cycle control and apoptosis. *Seminars in Cell & Developmental Biology* 22, 688–695. doi: 10.1016/j.semcdb.2011.09.008

Gerdes, J. M., Christou-Savina, S., Xiong, Y., Moede, T., Moruzzi, N., Karlsson-Edlund, P., et al. (2014). Ciliary dysfunction impairs beta-cell insulin secretion and promotes development of type 2 diabetes in rodents. *Nat Commun* 5, 5308. doi: 10.1038/ncomms6308

Gibbons, I. R. (1961). THE RELATIONSHIP BETWEEN THE FINE STRUCTURE AND DIRECTION OF BEAT IN GILL CILIA OF A LAMELLIBRANCH MOLLUSC. *The Journal of Cell Biology* 11, 179–205. doi: 10.1083/jcb.11.1.179

Giles, R. H., Ajzenberg, H., and Jackson, P. K. (2014). 3D spheroid model of mIMCD3 cells for studying ciliopathies and renal epithelial disorders. *Nat Protoc* 9, 2725–2731. doi: 10.1038/nprot.2014.181

Glotzer, M. (2001). Animal Cell Cytokinesis. *Annu. Rev. Cell Dev. Biol.* 17, 351–386. doi: 10.1146/annurev.cellbio.17.1.351

Goetz, S. C., and Anderson, K. V. (2010). The primary cilium: a signalling centre during vertebrate development. *Nat Rev Genet* 11, 331–344. doi: 10.1038/nrg2774

Götzke, H., Kilisch, M., Martínez-Carranza, M., Sograte-Idrissi, S., Rajavel, A., Schlichthaerle, T., et al. (2019). The ALFA-tag is a highly versatile tool for

nanobody-based bioscience applications. *Nat Commun* 10, 4403. doi: 10.1038/s41467-019-12301-7

Gromley, A., Yeaman, C., Rosa, J., Redick, S., Chen, C.-T., Mirabelle, S., et al. (2005). Centriolin Anchoring of Exocyst and SNARE Complexes at the Midbody Is Required for Secretory-Vesicle-Mediated Abscission. *Cell* 123, 75–87. doi: 10.1016/j.cell.2005.07.027

Guse, A., Mishima, M., and Glotzer, M. (2005). Phosphorylation of ZEN-4/MKLP1 by Aurora B Regulates Completion of Cytokinesis. *Current Biology* 15, 778–786. doi: 10.1016/j.cub.2005.03.041

Halcrow, E. F. J., Mazza, R., Diversi, A., Enright, A., and D'Avino, P. P. (2022). Midbody Proteins Display Distinct Dynamics during Cytokinesis. *Cells* 11, 3337. doi: 10.3390/cells11213337

Han, Y.-G., and Alvarez-Buylla, A. (2010). Role of primary cilia in brain development and cancer. *Current Opinion in Neurobiology* 20, 58–67. doi: 10.1016/j.conb.2009.12.002

Haren, L., Remy, M.-H., Bazin, I., Callebaut, I., Wright, M., and Merdes, A. (2006). NEDD1-dependent recruitment of the γ-tubulin ring complex to the centrosome is necessary for centriole duplication and spindle assembly. *The Journal of Cell Biology* 172, 505–515. doi: 10.1083/jcb.200510028

Hart, M. J., Callow, M. G., Souza, B., and Polakis, P. (1996). IQGAP1, a calmodulin-binding protein with a rasGAP-related domain, is a potential effector for cdc42Hs. *EMBO J* 15, 2997–3005.

He, M., Agbu, S., and Anderson, K. V. (2017). Microtubule Motors Drive Hedgehog Signaling in Primary Cilia. *Trends in Cell Biology* 27, 110–125. doi: 10.1016/j.tcb.2016.09.010

Hildebrandt, F., Benzing, T., and Katsanis, N. (2011). Ciliopathies. *N Engl J Med* 364, 1533–1543. doi: 10.1056/NEJMra1010172

Hoeprich, G. J., Sinclair, A. N., Shekhar, S., and Goode, B. L. (2022). Single-molecule imaging of IQGAP1 regulating actin filament dynamics. *MBoC* 33, ar2. doi: 10.1091/mbc.E21-04-0211

Hoffman, H. K., and Prekeris, R. (2022). Roles of the actin cytoskeleton in ciliogenesis. *Journal of Cell Science* 135, jcs259030. doi: 10.1242/jcs.259030

Hua, K., and Ferland, R. J. (2017). Fixation methods can differentially affect ciliary protein immunolabeling. *Cilia* 6, 5. doi: 10.1186/s13630-017-0045-9

Hutterer, A., Glotzer, M., and Mishima, M. (2009). Clustering of Centralspindlin Is Essential for Its Accumulation to the Central Spindle and the Midbody. *Current Biology* 19, 2043–2049. doi: 10.1016/j.cub.2009.10.050

Inoué, S., and Salmon, E. D. (1995). Force Generation by Microtubule Assembly/Disassembly in Mitosis and Related Movements. *MBoC* 6, 1619–1640. doi: 10.1091/mbc.6.12.1619

Ishikawa, H., Thompson, J., Yates, J. R., and Marshall, W. F. (2012). Proteomic analysis of mammalian primary cilia. *Curr Biol* 22, 414–419. doi: 10.1016/j.cub.2012.01.031

Izawa, I., Goto, H., Kasahara, K., and Inagaki, M. (2015). Current topics of functional links between primary cilia and cell cycle. *Cilia* 4, 12. doi: 10.1186/s13630-015-0021-1

J. DE MEY, M. D. B., and G. GEUENS, R. NUYDENS, R. WILLEBRORDS, (1981). Taxol induces the assembly of free microtubules in living cells and blocks the organizing capacity of the centrosomes and kinetochores. *Proc. Natl Acad. Sci. USA* Vol. 78, 5608-5612,.

Jaffe, A. B., Kaji, N., Durgan, J., and Hall, A. (2008). Cdc42 controls spindle orientation to position the apical surface during epithelial morphogenesis. *The Journal of Cell Biology* 183, 625–633. doi: 10.1083/jcb.200807121

Jang, S.-W., Liu, X., Fu, H., Rees, H., Yepes, M., Levey, A., et al. (2009). Interaction of Akt-phosphorylated SRPK2 with 14-3-3 Mediates Cell Cycle and Cell Death in Neurons. *Journal of Biological Chemistry* 284, 24512–24525. doi: 10.1074/jbc.M109.026237

Janke, C. (2014). The tubulin code: Molecular components, readout mechanisms, and functions. *Journal of Cell Biology* 206, 461–472. doi: 10.1083/jcb.201406055

Jijumon, A. S., Bodakuntla, S., Genova, M., Bangera, M., Sackett, V., Besse, L., et al. (2022). Lysate-based pipeline to characterize microtubule-associated proteins uncovers unique microtubule behaviours. *Nat Cell Biol* 24, 253–267. doi: 10.1038/s41556-021-00825-4

Jin, H., White, S. R., Shida, T., Schulz, S., Aguiar, M., Gygi, S. P., et al. (2010). The Conserved Bardet-Biedl Syndrome Proteins Assemble a Coat that Traffics Membrane Proteins to Cilia. *Cell* 141, 1208–1219. doi: 10.1016/j.cell.2010.05.015

Joukov, V., and De Nicolo, A. (2019). The Centrosome and the Primary Cilium: The Yin and Yang of a Hybrid Organelle. *Cells* 8, 701. doi: 10.3390/cells8070701

Kerssemakers, J. W. J., Laura Munteanu, E., Laan, L., Noetzel, T. L., Janson, M. E., and Dogterom, M. (2006). Assembly dynamics of microtubules at molecular resolution. *Nature* 442, 709–712. doi: 10.1038/nature04928

Khodjakov, A., Cole, R. W., Oakley, B. R., and Rieder, C. L. (2000). Centrosome-independent mitotic spindle formation in vertebrates. *Current Biology* 10, 59–67. doi: 10.1016/S0960-9822(99)00276-6

Kida, Y. S., Sato, T., Miyasaka, K. Y., Suto, A., and Ogura, T. (2007). Daam1 regulates the endocytosis of EphB during the convergent extension of the zebrafish notochord. *Proc. Natl. Acad. Sci. U.S.A.* 104, 6708–6713. doi: 10.1073/pnas.0608946104

Kobayashi, T., and Dynlacht, B. D. (2011). Regulating the transition from centriole to basal body. *Journal of Cell Biology* 193, 435–444. doi: 10.1083/jcb.201101005

Kodani, A., Yu, T. W., Johnson, J. R., Jayaraman, D., Johnson, T. L., Al-Gazali, L., et al. (2015). Centriolar satellites assemble centrosomal microcephaly proteins to recruit CDK2 and promote centriole duplication. *eLife* 4, e07519. doi: 10.7554/eLife.07519

Kohli, P., Höhne, M., Jüngst, C., Bertsch, S., Ebert, L. K., Schauss, A. C., et al. (2017). The ciliary membrane-associated proteome reveals actin-binding proteins as key components of cilia. *EMBO Reports* 18, 1521–1535. doi: 10.15252/embr.201643846

Kozminski, K. G., Johnson, K. A., Forscher, P., and Rosenbaum, J. L. (1993). A motility in the eukaryotic flagellum unrelated to flagellar beating. *Proc. Natl. Acad. Sci. U.S.A.* 90, 5519–5523. doi: 10.1073/pnas.90.12.5519

Labat-de-Hoz, L., Rubio-Ramos, A., Casares-Arias, J., Bernabé-Rubio, M., Correas, I., and Alonso, M. A. (2021). A Model for Primary Cilium Biogenesis by Polarized Epithelial Cells: Role of the Midbody Remnant and Associated Specialized Membranes. *Front. Cell Dev. Biol.* 8, 622918. doi: 10.3389/fcell.2020.622918

Lall, N., Henley-Smith, C. J., De Canha, M. N., Oosthuizen, C. B., and Berrington, D. (2013). Viability Reagent, PrestoBlue, in Comparison with Other Available Reagents, Utilized in Cytotoxicity and Antimicrobial Assays. *International Journal of Microbiology* 2013, 1–5. doi: 10.1155/2013/420601

Larkins, C. E., Aviles, G. D. G., East, M. P., Kahn, R. A., and Caspary, T. (2011). Arl13b regulates ciliogenesis and the dynamic localization of Shh signaling proteins. *MBoC* 22, 4694–4703. doi: 10.1091/mbc.e10-12-0994

Lasick, K. A., Jose, E., Samayoa, A. M., Shanks, L., Pond, K. W., Thorne, C. A., et al. (2023). FOXO nuclear shuttling dynamics are stimulus-dependent and correspond with cell fate. *MBoC* 34, ar21. doi: 10.1091/mbc.E22-05-0193

Lee, J. C., Field, D. J., and Lee, L. L. Y. (1980). Effects of nocodazole on structures of calf brain tubulin. *Biochemistry* 19, 6209–6215. doi: 10.1021/bi00567a041

Liebmann, J., Cook, J., Lipschultz, C., Teague, D., Fisher, J., and Mitchell, J. (1993). Cytotoxic studies of paclitaxel (Taxol®) in human tumour cell lines. *Br J Cancer* 68, 1104–1109. doi: 10.1038/bjc.1993.488

Luong, A., Cerignoli, F., Abassi, Y., Heisterkamp, N., and Abdel-Azim, H. (2021). Analysis of acute lymphoblastic leukemia drug sensitivity by changes in impedance via stromal cell adherence. *PLoS ONE* 16, e0258140. doi: 10.1371/journal.pone.0258140

Ma, Y., He, J., Li, S., Yao, D., Huang, C., Wu, J., et al. (2023). Structural insight into the intraflagellar transport complex IFT-A and its assembly in the anterograde IFT train. *Nat Commun* 14, 1506. doi: 10.1038/s41467-023-37208-2

Matsuo, K., Nakajima, Y., Shigeta, M., Kobayashi, D., Sakaki, S., Inoue, S., et al. (2023). Ciliary protein CEP290 regulates focal adhesion via microtubule system in non-ciliated cells[1]. doi: 10.1101/2023.04.02.535304

May, E. A., Sroka, T. J., and Mick, D. U. (2021). Phosphorylation and Ubiquitylation Regulate Protein Trafficking, Signaling, and the Biogenesis of Primary Cilia. *Front. Cell Dev. Biol.* 9, 664279. doi: 10.3389/fcell.2021.664279

May-Simera, H. L., Wan, Q., Jha, B. S., Hartford, J., Khristov, V., Dejene, R., et al. (2018). Primary Cilium-Mediated Retinal Pigment Epithelium Maturation Is Disrupted in Ciliopathy Patient Cells. *Cell Reports* 22, 189–205. doi: 10.1016/j.celrep.2017.12.038

Meunier, S., and Vernos, I. (2016). Acentrosomal Microtubule Assembly in Mitosis: The Where, When, and How. *Trends in Cell Biology* 26, 80–87. doi: 10.1016/j.tcb.2015.09.001

Mick, D. U., Rodrigues, R. B., Leib, R. D., Adams, C. M., Chien, A. S., Gygi, S. P., et al. (2015). Proteomics of Primary Cilia by Proximity Labeling. *Developmental Cell* 35, 497–512. doi: 10.1016/j.devcel.2015.10.015

Mill, P., Christensen, S. T., and Pedersen, L. B. (2023). Primary cilia as dynamic and diverse signalling hubs in development and disease. *Nat Rev Genet* 24, 421–441. doi: 10.1038/s41576-023-00587-9

Mishra, M., Tiwari, S., and Gomes, A. V. (2017). Protein purification and analysis: next generation Western blotting techniques. *Expert Review of Proteomics* 14, 1037–1053. doi: 10.1080/14789450.2017.1388167

Mitchell, D. R. (2007). "The Evolution of Eukaryotic Cilia and Flagella as Motile and Sensory Organelles," in *Eukaryotic Membranes and Cytoskeleton*, (New York, NY: Springer New York), 130–140. doi: 10.1007/978-0-387-74021-8_11

Miyamoto, T., Hosoba, K., Ochiai, H., Royba, E., Izumi, H., Sakuma, T., et al. (2015). The Microtubule-Depolymerizing Activity of a Mitotic Kinesin Protein KIF2A Drives Primary Cilia Disassembly Coupled with Cell Proliferation. *Cell Reports* 10, 664–673. doi: 10.1016/j.celrep.2015.01.003

Morita, E., Sandrin, V., Chung, H.-Y., Morham, S. G., Gygi, S. P., Rodesch, C. K., et al. (2007). Human ESCRT and ALIX proteins interact with proteins of the midbody and function in cytokinesis. *EMBO J* 26, 4215–4227. doi: 10.1038/sj.emboj.7601850

Morris, M. J., Yeap, Y. Y., Chen, C., Millard, S. S., Pagan, J. K., and Ng, D. C. H. (2024). The microcephaly protein WDR62 regulates cellular purine metabolism through the HSP70/HSP90 chaperone machinery. doi: 10.1101/2024.07.01.601630

Nachury, M. V., Loktev, A. V., Zhang, Q., Westlake, C. J., Peränen, J., Merdes, A., et al. (2007). A Core Complex of BBS Proteins Cooperates with the GTPase Rab8 to Promote Ciliary Membrane Biogenesis. *Cell* 129, 1201–1213. doi: 10.1016/j.cell.2007.03.053

Nachury, M. V., and Mick, D. U. (2019). Establishing and regulating the composition of cilia for signal transduction. *Nat Rev Mol Cell Biol* 20, 389–405. doi: 10.1038/s41580-019-0116-4

Nachury, M. V., Seeley, E. S., and Jin, H. (2010). Trafficking to the Ciliary Membrane: How to Get Across the Periciliary Diffusion Barrier? *Annu. Rev. Cell Dev. Biol.* 26, 59–87. doi: 10.1146/annurev.cellbio.042308.113337

Nager, A. R., Goldstein, J. S., Herranz-Pérez, V., Portran, D., Ye, F., Garcia-Verdugo, J. M., et al. (2017). An Actin Network Dispatches Ciliary GPCRs into Extracellular Vesicles to Modulate Signaling. *Cell* 168, 252-263.e14. doi: 10.1016/j.cell.2016.11.036

Nakayama, K., and Katoh, Y. (2018). Ciliary protein trafficking mediated by IFT and BBSome complexes with the aid of kinesin-2 and dynein-2 motors. *The Journal of Biochemistry* 163, 155–164. doi: 10.1093/jb/mvx087

Nguyen, H.-L., Chari, S., Gruber, D., Lue, C.-M., Chapin, S. J., and Bulinski, J. C. (1997). Overexpression of full- or partial-length MAP4 stabilizes microtubules and alters cell growth. *Journal of Cell Science* 110, 281–294. doi: 10.1242/jcs.110.2.281

Nicastro, D., Schwartz, C., Pierson, J., Gaudette, R., Porter, M. E., and McIntosh, J. R. (2006). The Molecular Architecture of Axonemes Revealed by Cryoelectron Tomography. *Science* 313, 944–948. doi: 10.1126/science.1128618

Nigg, E. A., and Holland, A. J. (2018). Once and only once: mechanisms of centriole duplication and their deregulation in disease. *Nat Rev Mol Cell Biol* 19, 297–312. doi: 10.1038/nrm.2017.127

Nigg, E. A., and Stearns, T. (2011). The centrosome cycle: Centriole biogenesis, duplication and inherent asymmetries. *Nat Cell Biol* 13, 1154–1160. doi: 10.1038/ncb2345

Odabasi, E., Conkar, D., Deretic, J., Batman, U., Frikstad, K.-A. M., Patzke, S., et al. (2023). CCDC66 regulates primary cilium length and signaling via interactions with transition zone and axonemal proteins. *Journal of Cell Science* 136, jcs260327. doi: 10.1242/jcs.260327

Orr, G. A., Verdier-Pinard, P., McDaid, H., and Horwitz, S. B. (2003). Mechanisms of Taxol resistance related to microtubules. *Oncogene* 22, 7280–7295. doi: 10.1038/sj.onc.1206934

Ott, C. M. (2016). Midbody remnant licenses primary cilia formation in epithelial cells. *Journal of Cell Biology* 214, 237–239. doi: 10.1083/jcb.201607046

Otto, E. A., Schermer, B., Obara, T., O'Toole, J. F., Hiller, K. S., Mueller, A. M., et al. (2003). Mutations in INVS encoding inversin cause nephronophthisis type 2, linking renal cystic disease to the function of primary cilia and left-right axis determination. *Nat Genet* 34, 413–420. doi: 10.1038/ng1217

Park, T. J., Mitchell, B. J., Abitua, P. B., Kintner, C., and Wallingford, J. B. (2008). Dishevelled controls apical docking and planar polarization of basal bodies in ciliated epithelial cells. *Nat Genet* 40, 871–879. doi: 10.1038/ng.104

Pazour, G. J., and Witman, G. B. (2003). The vertebrate primary cilium is a sensory organelle. *Current Opinion in Cell Biology* 15, 105–110. doi: 10.1016/S0955-0674(02)00012-1

Pedersen, L. B., and Rosenbaum, J. L. (2008). "Chapter Two Intraflagellar Transport (IFT)," in *Current Topics in Developmental Biology*, (Elsevier), 23–61. doi: 10.1016/S0070-2153(08)00802-8

Pedersen, L. B., Schrøder, J. M., Satir, P., and Christensen, S. T. (2012). "The Ciliary Cytoskeleton," in *Comprehensive Physiology*, ed. Y. S. Prakash (Wiley), 779–803. doi: 10.1002/cphy.c110043

Pelham, H. R. B., and Jackson, R. J. (1976). An Efficient mRNA-Dependent Translation System from Reticulocyte Lysates. *European Journal of Biochemistry* 67, 247–256. doi: 10.1111/j.1432-1033.1976.tb10656.x

Pennington, K., Chan, T., Torres, M., and Andersen, J. (2018). The dynamic and stress-adaptive signaling hub of 14-3-3: emerging mechanisms of regulation and context-dependent protein–protein interactions. *Oncogene* 37, 5587–5604. doi: 10.1038/s41388-018-0348-3

Prasai, A., Ivashchenko, O., Maskova, K., Bykova, S., Schmidt Cernohorska, M., Stepanek, O., et al. (2025). BBSome-deficient cells activate intraciliary CDC42 to trigger actin-dependent ciliary ectocytosis. *EMBO Rep* 26, 36–60. doi: 10.1038/s44319-024-00326-z

Prosser, S. L., and Pelletier, L. (2017). Mitotic spindle assembly in animal cells: a fine balancing act. *Nat Rev Mol Cell Biol* 18, 187–201. doi: 10.1038/nrm.2016.162

Ran, F. A., Hsu, P. D., Wright, J., Agarwala, V., Scott, D. A., and Zhang, F. (2013). Genome engineering using the CRISPR-Cas9 system. *Nat Protoc* 8, 2281–2308. doi: 10.1038/nprot.2013.143

Reiter, J. F., Blacque, O. E., and Leroux, M. R. (2012). The base of the cilium: roles for transition fibres and the transition zone in ciliary formation, maintenance and compartmentalization. *EMBO Reports* 13, 608–618. doi: 10.1038/embor.2012.73

Reiter, J. F., and Leroux, M. R. (2017). Genes and molecular pathways underpinning ciliopathies. *Nat Rev Mol Cell Biol* 18, 533–547. doi: 10.1038/nrm.2017.60

Rosenbaum, J. L., and Witman, G. B. (2002). Intraflagellar transport. *Nat Rev Mol Cell Biol* 3, 813–825. doi: 10.1038/nrm952

Ryniawec, J. M., Hannaford, M. R., Zibrat, M. E., Fagerstrom, C. J., Galletta, B. J., Aguirre, S. E., et al. (2023). Cep104 is a component of the centriole distal tip complex that regulates centriole growth and contributes to Drosophila spermiogenesis. *Current Biology* 33, 4202-4216.e9. doi: 10.1016/j.cub.2023.08.075

Saffin, J.-M., Venoux, M., Prigent, C., Espeut, J., Poulat, F., Giorgi, D., et al. (2005). ASAP, a human microtubule-associated protein required for bipolar spindle assembly and cytokinesis. *Proc. Natl. Acad. Sci. U.S.A.* 102, 11302–11307. doi: 10.1073/pnas.0500964102

Sang, L., Miller, J. J., Corbit, K. C., Giles, R. H., Brauer, M. J., Otto, E. A., et al. (2011). Mapping the NPHP-JBTS-MKS Protein Network Reveals Ciliopathy Disease Genes and Pathways. *Cell* 145, 513–528. doi: 10.1016/j.cell.2011.04.019

Sanyal, C., Pietsch, N., Ramirez Rios, S., Peris, L., Carrier, L., and Moutin, M.-J. (2023). The detyrosination/re-tyrosination cycle of tubulin and its role and dysfunction in neurons and cardiomyocytes. *Seminars in Cell & Developmental Biology* 137, 46–62. doi: 10.1016/j.semcdb.2021.12.006

Satir, P., and Christensen, S. T. (2007). Overview of Structure and Function of Mammalian Cilia. *Annu. Rev. Physiol.* 69, 377–400. doi: 10.1146/annurev.physiol.69.040705.141236

Saunders, H. A. J., Van Den Berg, C. M., Hoogebeen, R. A., Schweizer, D., Stecker, K. E., Roepman, R., et al. (2025). A network of interacting ciliary tip proteins with opposing activities imparts slow and processive microtubule growth. *Nat Struct Mol Biol*. doi: 10.1038/s41594-025-01483-y

Schöckel, L., Möckel, M., Mayer, B., Boos, D., and Stemmann, O. (2011). Cleavage of cohesin rings coordinates the separation of centrioles and chromatids. *Nat Cell Biol* 13, 966–972. doi: 10.1038/ncb2280

Schrøder, J. M., Larsen, J., Komarova, Y., Akhmanova, A., Thorsteinsson, R. I., Grigoriev, I., et al. (2011). EB1 and EB3 promote cilia biogenesis by several centrosome-related mechanisms. *Journal of Cell Science* 124, 2539–2551. doi: 10.1242/jcs.085852

Seeley, E. S., and Nachury, M. V. (2010). The perennial organelle: assembly and disassembly of the primary cilium. *Journal of Cell Science* 123, 511–518. doi: 10.1242/jcs.061093

Shan-rong-Shi, Cote, R. J., Young, L., Imam, S. A., and Taylor, C. R. (1996). Use of pH 9.5 Tris-HCI Buffer Containing 5% Urea for Antigen Retrieval Immunohistochemistry. *Biotechnic & Histochemistry* 71, 190–196. doi: 10.3109/10520299609117158

Shida, T., Cueva, J. G., Xu, Z., Goodman, M. B., and Nachury, M. V. (2010). The major α-tubulin K40 acetyltransferase αTAT1 promotes rapid ciliogenesis and efficient mechanosensation. *Proc. Natl. Acad. Sci. U.S.A.* 107, 21517–21522. doi: 10.1073/pnas.1013728107

Singla, V., and Reiter, J. F. (2006). The Primary Cilium as the Cell's Antenna: Signaling at a Sensory Organelle. *Science* 313, 629–633. doi: 10.1126/science.1124534

Skop, A. R., Liu, H., Yates, J., Meyer, B. J., and Heald, R. (2004). Dissection of the Mammalian Midbody Proteome Reveals Conserved Cytokinesis Mechanisms. *Science* 305, 61–66. doi: 10.1126/science.1097931

Smith, K. R., Kieserman, E. K., Wang, P. I., Basten, S. G., Giles, R. H., Marcotte, E. M., et al. (2011). A role for central spindle proteins in cilia structure and function. *Cytoskeleton* 68, 112–124. doi: 10.1002/cm.20498

Smith, P. K., Krohn, R. I., Hermanson, G. T., Mallia, A. K., Gartner, F. H., Provenzano, M. D., et al. (1985). Measurement of protein using bicinchoninic acid. *Analytical Biochemistry* 150, 76–85. doi: 10.1016/0003-2697(85)90442-7

Sorokin, S. P. (1968). Reconstructions of centriole formation and ciliogenesis in mammalian lungs. *Journal of Cell Science* 3, 207–230. doi: 10.1242/jcs.3.2.207

Sroka, T. J., Sanwald, L. K., Prasai, A., Hoeren, J., Von Der Malsburg, K., Chaumet, V., et al. (2025). iAPEX: Improved APEX-based proximity labeling for subcellular proteomics using an enzymatic reaction cascade. doi: 10.1101/2025.01.10.632381

Stamer, K., Vogel, R., Thies, E., Mandelkow, E., and Mandelkow, E.-M. (2002). Tau blocks traffic of organelles, neurofilaments, and APP vesicles in neurons and enhances oxidative stress. *The Journal of Cell Biology* 156, 1051–1063. doi: 10.1083/jcb.200108057

Stepanek, L., and Pigino, G. (2016). Microtubule doublets are double-track railways for intraflagellar transport trains. *Science* 352, 721–724. doi: 10.1126/science.aaf4594

Stepanenko, A. A., and Heng, H. H. (2017). Transient and stable vector transfection: Pitfalls, off-target effects, artifacts. *Mutation Research/Reviews in Mutation Research* 773, 91–103. doi: 10.1016/j.mrrev.2017.05.002

Sun, F., Anantharam, V., Zhang, D., Latchoumycandane, C., Kanthasamy, A., and Kanthasamy, A. G. (2006). Proteasome inhibitor MG-132 induces dopaminergic degeneration in cell culture and animal models. *NeuroToxicology* 27, 807–815. doi: 10.1016/j.neuro.2006.06.006

Szczesny, R. J., Kowalska, K., Klosowska-Kosicka, K., Chlebowski, A., Owczarek, E. P., Warkocki, Z., et al. (2018). Versatile approach for functional analysis of human proteins and efficient stable cell line generation using FLP-mediated recombination system. *PLoS ONE* 13, e0194887. doi: 10.1371/journal.pone.0194887

Tanos, B. E., Yang, H.-J., Soni, R., Wang, W.-J., Macaluso, F. P., Asara, J. M., et al. (2013). Centriole distal appendages promote membrane docking, leading to cilia initiation. *Genes Dev.* 27, 163–168. doi: 10.1101/gad.207043.112

Tiryaki, F., Deretic, J., and Firat-Karalar, E. N. (2022). ENKD1 is a centrosomal and ciliary microtubule-associated protein important for primary cilium content regulation. *The FEBS Journal*, febs.16367. doi: 10.1111/febs.16367

Tokuraku, K., Katsuki, M., Matui, T., Kuroya, T., and Kotani, S. (1999). Microtubule-binding property of microtubule-associated protein 2 differs from that of microtubule-associated protein 4 and tau. *European Journal of Biochemistry* 264, 996–1001. doi: 10.1046/j.1432-1327.1999.00710.x

Towbin, H., Staehelin, T., and Gordon, J. (1979). Electrophoretic transfer of proteins from polyacrylamide gels to nitrocellulose sheets: procedure and some applications. *Proc. Natl. Acad. Sci. U.S.A.* 76, 4350–4354. doi: 10.1073/pnas.76.9.4350

Vale, R. D. (2003). The Molecular Motor Toolbox for Intracellular Transport. *Cell* 112, 467–480. doi: 10.1016/S0092-8674(03)00111-9

Vasquez, R. J., Howell, B., Yvon, A. M., Wadsworth, P., and Cassimeris, L. (1997). Effects of nocodazole on structures of calf brain tubulin. *MBoC* 8, 973–985. doi: 10.1091/mbc.8.6.973

Vázquez-Novelle, M. D., and Petronczki, M. (2010). Relocation of the Chromosomal Passenger Complex Prevents Mitotic Checkpoint Engagement at Anaphase. *Current Biology* 20, 1402–1407. doi: 10.1016/j.cub.2010.06.036

Wang, J. T., and Stearns, T. (2017). The ABCs of Centriole Architecture: The Form and Function of Triplet Microtubules. *Cold Spring Harb Symp Quant Biol* 82, 145–155. doi: 10.1101/sqb.2017.82.034496

Wang, S., Wang, X., Pan, C., Liu, Y., Lei, M., Guo, X., et al. (2023). Functions of actin-binding proteins in cilia structure remodeling and signaling. *Biology of the Cell* 115, e202300026. doi: 10.1111/boc.202300026

Weisenberg, R. C., Broisy, G. G., and Taylor, E. William. (1968). Colchicine-binding protein of mammalian brain and its relation to microtubules. *Biochemistry* 7, 4466–4479. doi: 10.1021/bi00852a043

Wheway, G., Nazlamova, L., and Hancock, J. T. (2018). Signaling through the Primary Cilium. *Front. Cell Dev. Biol.* 6, 8. doi: 10.3389/fcell.2018.00008

White, E. A., and Glotzer, M. (2012). Centralspindlin: At the heart of cytokinesis. *Cytoskeleton* 69, 882–892. doi: 10.1002/cm.21065

Wu, C.-T., Chen, H.-Y., and Tang, T. K. (2018). Myosin-Va is required for preciliary vesicle transportation to the mother centriole during ciliogenesis. *Nat Cell Biol* 20, 175–185. doi: 10.1038/s41556-017-0018-7

Yamazoe, T., Nagai, T., Umeda, S., Sugaya, Y., and Mizuno, K. (2020a). Roles of TOG and jelly-roll domains of centrosomal protein CEP104 in its functions in cilium elongation and Hedgehog signaling. *Journal of Biological Chemistry* 295, 14723–14736. doi: 10.1074/jbc.RA120.013334

Yamazoe, T., Nagai, T., Umeda, S., Sugaya, Y., and Mizuno, K. (2020b). Roles of TOG and jelly-roll domains of centrosomal protein CEP104 in its functions in cilium elongation and Hedgehog signaling. *Journal of Biological Chemistry* 295, 14723–14736. doi: 10.1074/jbc.RA120.013334

Ye, F., Breslow, D. K., Koslover, E. F., Spakowitz, A. J., Nelson, W. J., and Nachury, M. V. (2013). Single molecule imaging reveals a major role for diffusion in the exploration of ciliary space by signaling receptors. *eLife* 2, e00654. doi: 10.7554/eLife.00654

Aus datenschutzrechtlichen Gründen wird der Lebenslauf in der elektronischen Fassung der Dissertation nicht veröffentlicht.